THE UNIVERSITY OF
WARWICK

University of Warwick institutional repository: http://go.warwick.ac.uk/wrap

A Thesis Submitted for the Degree of PhD at the University of Warwick

http://go.warwick.ac.uk/wrap/49184

This thesis is made available online and is protected by original copyright.

Please scroll down to view the document itself.

Please refer to the repository record for this item for information to help you to cite it. Our policy information is available from the repository home page.

Characterisation of Pneumococcal Peptidoglycan Cross-linking Enzymology

Jennifer Shepherd B. Sc. (Hons.)

A thesis submitted in partial fulfilment of the requirements for the degree of

Doctor of Philosophy

The University of Warwick
School of Life Sciences

September 2011

Contents

Figures and Tables

Chapter 1: Introduction

Chapter 2: Materials and methods

Chapter 4: Characterisation of Divalent Metal Ion Binding to the MurM protein from *Streptococcus pneumoniae* using Isothermal Titration Calorimetry (ITC)

Chapter 5: Kinetic Characterisation of MurM from penicillin-resistant (159) and penicillin-sensitive (R6 and Pn16) strains of *Streptococcus pneumoniae*

Chapter 6: Towards an X-ray crystal structure of the MurM protein from *Streptococcus pneumoniae*

Acknowledgements

Firstly, I would like to thank my supervisors Dr David Roper and Professor Chris Dowson and the University of Warwick Postgraduate Research Fellowship scheme for giving me the opportunity to work on a project that has been both stimulating and challenging. In particular, I wish to thank Dr David Roper for his continuous support, patience and encouragement throughout the project.

I would also like to thank Anita Catherwood for teaching me how to synthesise Lipid II and for providing me with this valuable reagent. Thank you to Dr Ken Flint for the generous offer to proof read this thesis and for the valuable discussions concerning metalloproteins. Furthermore I wish to thank Dr Adrian Lloyd for insightful discussions about the project and Professor Vilmos Fulop for the processing of X-ray crystallography data. Thanks to the Molecular Biology Service in the School of Life Sciences, University of Warwick for DNA sequencing analysis and to everyone in media prep and wash up for ensuring that there was always a ready supply of LB and autoclaved flasks in the lab.

Many thanks to all members of the structural biology group for providing a friendly atmosphere which has made Warwick such an enjoyable place to work. I would also like to thank all of my friends and family for their support. A special thanks to my Grandad Jack who was always interested in my work but who sadly passed away only a short time before being able to read this. I dedicate this thesis to his memory.

Declaration

I hereby declare that the research submitted in this thesis was conducted by myself under the supervision of Dr David Roper and Professor Chris Dowson at the School of Life Sciences, University of Warwick. Where work has been contributed by other individuals, it has been specifically stated in the text.

No part of this work has previously been submitted to be considered for a degree or other qualification. All sources of information have been acknowledged in the form of references.

Summary

Despite the introduction of penicillin, infections caused by *Streptococcus pneumoniae* are associated with significant morbidity and mortality. As a result, there is an urgent need for successful identification of new drug targets within the organism. This thesis focuses on characterisation of MurM, which initiates the synthesis of branched muropeptides within pneumococcal peptidoglycan. MurM and MurN generate either alanyl-alanine or seryl-alanine appendages on the stem peptide lysine of Lipid II, ultimately resulting in indirect cross-linkage of the cell wall. Inactivation of *murMN* causes a reversion to penicillin sensitivity in penicillin-resistant strains. However, elucidation of the relationship between MurM activity and penicillin-resistance is complicated by some penicillin-sensitive strains, including R6, having an unusually high proportion of indirect cross-linkage in their cell wall. Therefore, $MurM_{R6}$ has been kinetically characterised with Lipid II, Ala-$tRNA^{Ala}$ and Ser-$tRNA^{Ser}$ for comparison to $MurM_{Pn16}$ (penicillin-sensitive) and $MurM_{159}$ (penicillin-resistant). These results confirmed that $MurM_{159}$ is more catalytically active than $MurM_{Pn16.}$ However, in the presence of Ser-$tRNA^{Ser}$, the catalytic activity of $MurM_{R6}$ approaches that of $MurM_{159}$. Stimulation of MurM by cardiolipin indicates the potential role of pneumococcal membrane phospholipid composition in the regulation of this enzyme.

Assessment of MurM substrate specificity was made using misaminoacylated Ser-$tRNA^{Ala}$. Results indicate that Ser-$tRNA^{Ala}$ is used more efficiently by MurM providing a link between peptidoglycan biosynthesis and the fidelity of protein synthesis in *S. pneumoniae*. A 2'-amino minihelix analogue of Ala-$tRNA^{Ala}$ inhibits MurM with an IC_{50} of 0.5 µM demonstrating specific acceptance of the amino acid from the 2' hydroxyl of the terminal adenine of the tRNA substrate. Crystallisation of MurM in the presence of zinc and subsequent characterisation of its metal-ion binding properties by kinetic analysis, isothermal titration calorimetry and bioinformatics-informed site-directed mutagenesis have identified that this enzyme is zinc-dependent. In combination, these findings have far-reaching implications for future drug design.

Abbreviations

3D	three dimensional
Å	angstroms
A_{595nm}	absorbance at wavelength 595 nm
A^{76}	terminal adenine of tRNA
aa-PGSs	aminoacyl-phosphatidylglycerol synthases
ADP	adenosine diphosphate
AI	protein expression by auto-induction
AIDS	acquired immune deficiency syndrome
AlaRS	alanyl-tRNA synthetase
APS	ammonium persulphate
ATP	adenosine triphosphate
bp	base pairs
BSA	bovine serum albumin
C55-P	undecaprenylphosphate
C55-PP	undecaprenylpyrophosphate
$CaCl_2$	calcium chloride
cal	calories
CD	circular dichroism
CHAPS	3-[(3-cholamidopropyl)dimethylammonio]-1-propanesulphonate
cpm	counts per minute
C-terminus	carboxy-terminus
Da	dalton
DEAE sephacel	diethylaminoethyl-sephacel resin
DMSO	dimethyl-sulphoxide
DNA	deoxyribonucleic acid
DTT	dithiothreitol
ε	epsilon
E. coli	*Escherichia coli*
E. faecalis	*Enterococcus faecalis*

E. faecium	*Enterococcus faecium*
Edn	edition
EDTA	ethylenediaminetetraacetic acid
EF-Tu	elongation factor thermo unstable
et al.	*Et alia* (and others)
eV	electron volt
FAD	flavin adenine dinucleotide (oxidised)
$FADH_2$	flavin adenine dinucleotide (reduced)
G	grams
GDP	guanosine diphosphate
GlcNAc	N-acetylglucosamine
GRASP	Graphical Representation and Analysis of Structural Properties
H	hours
$[H^3]$	used to designate amino acids labelled with tritium
HEPES	4-(2-hydroxyethyl)-1-piperazineethanesulphonic acid
HIC	hydrophobic interaction chromatography
HIV	Human Immunodeficiency Virus
IC_{50}	the half maximal inhibitory concentration
IDT	Integrated DNA Technologies
IMAC	immobilised metal ion affinity chromatography
IPTG	isopropylthiogalactoside
ITC	isotheral titration calorimetry
Kb	kilobases
k_{cat}	turnover number
KCl	potassium chloride
K_d	dissociation constant
kDa	kilo-dalton
k_m	Michaelis constant
k_m/k_{cat}	catalytic efficiency index
L	litre
LB	Luria-Bertani medium

LII	Lipid II
M	molar (grams per litre)
M. flavus	*Micrococcus flavus*
M. jannaschii	*Methanococcus jannaschii*
MES	2-(*N*-morpholino)ethanesulphonic acid
meso-Dap	meso-diaminopimelic acid
mg	milli-gram
Mg^{2+}	magnesium ions
$MgCl_2$	magnesium chloride
$MgSO_4$	magnesium sulphate
MIC	minimum inhibitory concentration
min	minutes
mL	milli-litre
mM	milli-molar
MOPS	3-(N-morpholino)propanesulphonic acid
MPa	mega-pascal
mPa	milli-pascal
MurNAc	N-acetylmuramic acid
n	stoichiometry
NaCl	sodium chloride
$NADP^+$	nicotinamide adenine dinucleotide phosphate (oxidised)
NADPH	nicotinamide adenine dinucleotide phosphate (reduced)
ng	nano-gram
nM	nano-molar
nm	nano-metre
NMT	N-myristoyl transferases
N-terminus	amino-terminus
^oC	degrees Celsius
OD_{600nm}	optical density at wavelength 600 nm
PAGE	polyacrylamide gel electrophoresis
PBPs	penicillin binding proteins

PCR	polymerase chain reaction
PDB	protein data bank
PEG	polyethylene glycol
PEG MME	polyethylene glycol mono-methylether
PEP	phosphoenolpyruvate
pH	$\log_{10}[H^+]$
Pmol	pico-moles
PMSF	phenylmethylsulphonyl fluoride
Psi	pound force per square inch
RNA	ribonucleic acid
RNAP	RNA polymerase
RP-HPLC	reverse phase high performance liquid chromatography
S. aureus	*Staphylococcus aureus*
S. capitis	*Staphylococcus capitis*
S. coelicolor	*Streptomyces coelicolor*
S. pneumoniae	*Streptococcus pneumoniae*
S. simulans	*Staphylococcus simulans*
S. viridifaciens	*Streptomyces viridifaciens*
SDS PAGE	sodium dodecyl sulphate polyacrylamide gel electrophoresis
Sec	seconds
SerRS	seryl-tRNA synthetase
SOC	super optimal broth with catabolite repression
TAE	tris-acetate-EDTA buffer
TBE	tris-borate-EDTA buffer
TCA	trichloroacetic acid
TEMED	tetramethylethylenediamine
TEV	Tobacco Etch Virus protease
ThrRS	threonyl-tRNA synthetase
TLC	thin layer chromatography
Tm	melting temperature
tRNA	transfer ribonucleic acid

TSB	tryptic soy broth
µg	micro-gram
µL	micro-litre
µM	micro-molar
µm	micro-metre
UDP	uridine diphosphate
UMP	uridine monophosphate
USA	United States of America
UV	ultraviolet
V	volts
V_{max}	maximal velocity
(v/v)	volume to volume ratio
Vol	volume
(w/v)	weight to volume ratio
W. viridescens	*Weissella viridescens*
x g	centrifugal force
$Zn(OAc)_2$	zinc acetate
Zn^{2+}	zinc ions
α	alpha
β	beta
ΔH	enthalpy change
ΔS	entropy change

Single letter abbreviations for nucleotides in DNA and RNA:

A	Adenine
C	Cytosine
G	Guanine
T	Thymine
U	Uracil

Single and three letter abbreviations for amino acids

Amino acid	Three letter code	One letter code
Alanine	Ala	A
Arginine	Arg	R
Asparagine	Asn	N
Aspartic acid	Asp	D
Cysteine	Cys	C
Glutamic acid	Glu	E
Glutamine	Gln	Q
Glycine	Gly	G
Histidine	His	H
Isoleucine	Ile	I
Leucine	Leu	L
Lysine	Lys	K
Methionine	Met	M
Phenylalanine	Phe	F
Proline	Pro	P
Serine	Ser	S
Threonine	Thr	T
Tryptophan	Trp	W
Tyrosine	Tyr	Y
Valine	Val	V

Chapter 1

Introduction

1.1. Antibiotic discovery and the development of resistance

Multidrug-resistant bacterial infections represent a major public health burden and contribute significantly to morbidity, mortality, and healthcare costs in both developed and developing countries. In the USA more people die from hospital acquired bacterial infections than HIV (Payne, 2008). It is estimated that the cost of such infections to the USA health care system alone is in excess of $20 billion per annum. Successful treatment of these infections using antibiotics is hindered by the development of tolerance or resistance over time. There is, therefore, an urgent need for new antibiotics, the identification of new antibiotic targets and new antimicrobial strategies to alleviate bacterial infections.

Antibiotics are broadly defined as organic molecules that inhibit microbial growth as a direct result of interaction with specific prokaryotic cell targets. The first successful antimicrobials to be introduced into the clinical setting were the sulphonamides in 1937 with resistant microorganisms first being identified in the late 1930's. This was followed by the introduction of penicillin into the clinical setting in the 1940's. Penicillin was discovered by Alexander Fleming in 1928 and, soon after its discovery, a bacterial mechanism of resistance (β-lactamases) was identified (Davies and Davies, 2010). This is a direct result of the fact that many environmental strains of bacteria act as a reservoir for antibiotic resistance genes

which can often be mobilised and transferred to other strains with high frequency (Allen *et al.*, 2010). A summary of the most commonly used antibiotics and their prokaryotic targets are shown in Table 1.1.

Antibiotic Class	**Example**	**Target**	**Typical spectrum of activity**
β-Lactams	Penicillin	Peptidoglycan biosynthesis	Gram + and -
Aminoglycosides	Gentamicin	Translation (30S ribosomal subunit)	Gram -
Glycopeptides	Vancomycin	Peptidoglycan biosynthesis	Gram +
Tetracyclins	Minocylcine	Translation (30S ribosomal subunit)	Gram + and -
Macrolides	Erythromycin	Translation (50S ribosomal subunit)	Gram +
Lincosamides	Clindamycin	Translation (50S ribosomal subunit)	Gram +
Streptogramines	Synercid	Translation	Gram +
Oxazolidinones	Linezolid	Translation	Gram +
Phenicols	Chloramphenicol	Translation (50S ribosomal subunit)	Gram + and -
Quinolones	Ciprofloxacin	DNA replication (DNA gyrase)	Gram + cocci
Pyrimidines	Trimethoprim	C_1 metabolism	Gram + and -
Sulfonamides	Sulfamethoxazole	C_1 metabolism	Gram + and -
Rifamycins	Rifampin	Transcription (RNA polymerase)	Gram + and -
Lipopeptides	Daptomycin	Cell membrane	Gram +
Cationic peptides	Colistin	Cell membrane	Gram + and -

Table 1.1: Classes, examples and targets of commonly used antibiotics. The most common mechanisms of resistance to these compounds include alteration of the target molecules, blockage of antibiotic entrance into the cell, efflux of antibiotics from the cell and chemical modification or hydrolysis. In reference to the typical spectrum of activity, + refers to Gram-positive bacteria and – refers to Gram-negative bacteria. Adapted from Davies and Davies (2010).

Many bacterial pathogens causing serious life-threatening infections have developed high levels of resistance that span multiple classes of antibiotics. Resistance typically arises as a result of four different mechanisms (i) alterations to the bacterial target,

(ii) antibiotic efflux from the cell, (iii) development of a means of preventing antibiotic entry into the cell in the first place, and (iv) chemical modification or degradation of antibiotic compounds. It is often the case that one or more of these mechanisms can affect a single antibiotic and a collection of these mechanisms within a single bacterial species can result in the emergence of multidrug-resistant pathogens (Morar and Wright, 2010). Significant pathogens that have acquired multidrug resistance in the nosocomial setting are listed in Table 1.2 and include both Gram-positive and Gram-negative organisms. Such superbugs have often acquired multiple mutations that confer high level resistance to the antibiotic classes that they are commonly exposed to as a result of recommended treatment regimes. This can result in reduced options for successful therapeutic care and extended, costly hospitalisations for patients infected with these pathogens.

Prominent bacterial pathogens that have acquired multidrug-resistance	
Gram-positive	**Gram-negative**
Staphylococcus aureus *Staphylococcus epidermidis* *Streptococcus pneumoniae* *Clostridium difficile* *Enterococcus faecium* *Enterococcus faecalis* *Mycobacterium tuberculosis*	*Escherichia coli* *Pseudomonas aeruginosa* *Klebsiella pneumoniae* *Salmonella* spp. *Haemophilus influenzae* *Proteus mirabilis* *Campylobacter jejuni*

Table 1.2: Examples of multidrug-resistant pathogens that are a significant economical and health burden in the nosocomial setting.

Development of resistance towards penicillin and other β-lactam antibiotics has severely hampered the treatment of many bacterial infections including those caused by *Streptococcus pneumoniae* and *Staphylococcus aureus*.

1.2. *Streptococcus pneumoniae*

Streptococcus pneumoniae is a Gram-positive diplococcus that is carried asymptomatically in the nasopharynx of 5-10% of healthy adults and 20-40% of healthy children. The organism is well established as the common causative agent of many community acquired infections including pneumonia, otitis media, meningitis and septicaemia. Pneumococcus was first identified by Klebs in 1875 during the visualisation of pulmonary tissue from patients dying of pneumonia. Successful isolation of the bacterium was first achieved from saliva by both Pasteur in France and Sternberg in the USA in 1881 (Austrian, 1981). Despite the introduction of penicillin in the 1940s, there is still significant morbidity and mortality associated with infections caused by *S. pneumoniae.* This is particularly relevant in the cases of young children, the elderly and people with predisposing medical conditions, such as AIDS. Approximately 5 million fatal cases of pneumococcal pneumonia in children under the age of 5 are reported globally each year. In addition to this, 5 to 7% of the half a million cases of pneumococcal pneumonia reported in the USA every year are fatal (Jedrzejas, 2001). Mortality is largely due to the emergence of multidrug-resistant strains of *S. pneumoniae* which are making infections by the organism increasingly difficult to treat.

The first recorded evidence of the emergence of a penicillin-resistant isolate of *S. pneumoniae* with a minimum inhibitory concentration (MIC) of 0.5 μg mL^{-1} was in 1967 in Papua New Guinea. This was closely followed by an outbreak of pneumococcal infections caused by multidrug-resistant strains in South Africa in 1977. In addition to showing resistance to penicillin, the isolates at the root of this outbreak were also found to be resistant to either chloramphenicol or a combination

of erythromycin, clindamycin, chloramphenicol and tetracycline (Charpentier and Tuomanen, 2000).

By the 1980's, penicillin-resistant isolates of *S. pneumoniae* were being identified on a global scale. At this time, more than 10% of isolates found in Israel, France, Poland, Spain, Hungary, South Africa, New Guinea and the USA showed low or intermediate levels of resistance to penicillin. In all cases, existence of these isolates promoted the emergence of strains showing high levels of resistance. By 1989, 58% of all pneumococcal isolates from children in Hungary showed resistance to penicillin. By the early 1990's some countries, including Iceland, were reporting up to 20% of isolates as being multidrug resistant (Charpentier and Tuomanen, 2000).

1.2.1. Mechanism of chloramphenicol and tetracycline resistance in *Streptococcus pneumoniae*

The first isolate of *S. pneumoniae* showing resistance to chloramphenicol was found in Poland in the 1970's. Chloramphenicol inhibits bacterial growth by targeting the peptidyl-transferase activity of the ribosome and blocking protein synthesis. *S. pneumoniae* can evade the activity of this antibiotic by producing an acetyl-transferase that hydrolyses chloramphenicol to its derivatives, thus preventing association with the 50S subunit of the ribosome. In many cases, the gene encoding this acetyl-transferase (*cat*) is found on a conjugative transposon which can readily transfer between different strains and organisms thus allowing for rapid dissemination of the resistance determinant (Widdowson and Klugman, 1999; Charpentier and Tuomanen, 2000). Chloramphenicol and tetracycline resistance are often found on the same transposon within pneumococcus.

The first tetracycline-resistant pneumococcus was isolated in 1963 from a child that had been diagnosed with meningitis (Holt *et al.*, 1969). Like chloramphenicol, tetracycline blocks bacterial growth by targeting the process of protein synthesis. Tetracycline specifically interacts with the 30S subunit of the ribosome binding either to the acceptor or the peptidyl-donor sites. This interaction prevents amino-acylated tRNA species from accessing the acceptor site. Tetracycline-resistant isolates of pneumococcus have acquired the *tet(M)* and *tet(O)* genes which are typically located on transposons. The way in which Tet(M) and Tet(O) protect the ribosome from tetracycline is not well understood. However, it has been suggested that Tet(M) either promotes the release of tetracycline from the ribosome or modifies tRNA so that interaction with the ribosome is not affected in the presence of the antibiotic (Manavathu *et al.*, 1990; Dantley *et al.*, 1998).

1.2.2. Mechanism of fluoroquinolone resistance in *Streptococcus pneumoniae*

Fluoroquinolones, such as moxifloxacin, were initially introduced into the clinical setting in order to combat infections caused by penicillin-resistant strains of pneumococcus. These antibiotics specifically target DNA gyrase, which is involved in supercoiling of DNA during replication, and topoisomerase IV which is responsible for the segregation of chromosomes. Resistance to fluoroquinolones in pneumococcus has evolved by mutation of the *gyrA*, *gyrB*, *parC* and *parE* genes. In addition to this, some resistant strains have demonstrated the use of an efflux mechanism preventing accumulation of the antibiotic within the cell (Widdowson and Klugman, 1999).

The order of accumulation of mutations in *gyrA* and *parC* is particularly important in determining the overall level of resistance to any specific fluoroquinolone. For example, in order to establish high levels of resistance to ciprofloxacin, *S. pneumoniae* must first acquire mutations in the *parC* gene which confer low levels of resistance. The most common substitutions in this gene include serine-79 to tyrosine or threonine and aspartate-83 to either glycine or alanine. In strains with this genetic background the acquisition of additional mutations in the *gyrA* gene, particularly at serine-83 or glutamate-88, can then lead to high levels of ciprofloxacin resistance (Janoir *et al.*, 1996; Tankovic *et al.*, 1996). Whilst no mutations in *gyrB* have been reported to cause quinolone resistance in clinical isolates of *S. pneumoniae*, mutation of serine-127 to leucine in a laboratory strain was responsible for conferring novobiocin resistance (de la Campa *et al.*, 1997; Charpentier and Tuomanen, 2000).

1.2.3. Mechanism of macrolide resistance in *Streptococcus pneumoniae*

Macrolide antibiotics, such as erythromycin, block protein synthesis by binding in a reversible manner to the peptidyl-donor site on the 50S subunit of the ribosome. The first erythromycin-resistant isolate of pneumococcus was identified in 1967 in Toronto. Two mechanisms of resistance against this antibiotic class exist in *S. pneumoniae*. The first is concerned with the alteration of the 23S rRNA in the peptidyl transferase domain by methylation of an adenine residue. This type of resistance is acquired by conjugative transfer of a transposon encoding the *erm* gene, the product of which is an S-adenosylmethionine-dependent methylase. The second mechanism involves efflux of the antibiotic out of the cell. This is achieved by the product of the *mefE* gene which is a hydrophobic transmembrane protein that forms

an efflux pump driven by the proton motive force (Widdowson and Klugman, 1999; Charpentier and Tuomanen, 2000). Many macrolide-resistant isolates of *S. pneumoniae* also show resistance to penicillin.

1.2.4. Mechanism of diaminopyrimidine and sulphonamide resistance in *Streptococcus pneumoniae*

In many developing countries, the combination of a diaminopyrimidine (Trimethoprim) and a sulphonamide (Sulphamethoxazole) antibiotic is the first course of action for the treatment of infections of the lower respiratory tract (Maskell *et al.*, 1997). Both of these antibiotics affect the synthesis of folic acid with trimethoprim targeting dihydrofolate reductase and sulphamethoxazole targeting dihydropteroate synthetase (Hitchings, 1973). The main mechanism of resistance to trimethoprim by pneumococcus is the acquisition of a single amino acid mutation, isoleucine to leucine, at position 100 in dihydrofolate reductase. Resistance to sulphamethoxazole in pneumococcus involves amino acid duplications within dihydropteroate synthetase (Charpentier and Tuomanen, 2000). The first clinical isolate of pneumococcus showing resistance to this combination of antibiotics was identified in 1972 from a patient suffering with acute bronchitis. More than 90% of sulphamethoxazole resistant isolates of pneumococcus identified in South Africa are also penicillin and chloramphenicol resistant (Adrian and Klugman, 1997).

1.2.5. Mechanism of β-lactam resistance in *Streptococcus pneumoniae*

The mechanism of action of β-lactam antibiotics is based on interference with the biosynthesis of peptidoglycan by covalent binding of the antibiotic to the active site serine residue of penicillin-binding proteins (PBPs). Pneumococcus is known to have

five PBPs that are of high molecular weight (1a, 1b, 2x, 2a and 2b) in addition to one low molecular weight PBP (Hakenbeck *et al.*, 1999). In *S. pneumoniae*, penicillin resistance is conferred by the accumulation of mutations in the transpeptidase domains of PBP 2x, 2b and 1a so that their affinity for the antibiotic is significantly reduced (Grebe and Hakenbeck, 1996; Charpentier and Tuomanen, 2000).

In addition to this, unique alterations in PBPs 1a and 2x have resulted in the emergence of pneumococcal strains with high levels of resistance to a specific class of β-lactam antibiotics known as the cephalosporins (Charpentier and Tuomanen, 2000). In many cases, the genes encoding these PBPs have become mosaic due to the insertion of extended nucleotide sequences that are not of pneumococcal origin. Comparison of these mosaic sequences with the genomes of other commensal strains within the genus *Streptococcus* has indicated that the likely origin of such mutations is horizontal gene transfer between *S. sanguis*, *S. mitis*, *S. oralis* and *S. pneumoniae*. This phenomenon is enhanced by the natural competency of the organism for the uptake of exogenous DNA (Charpentier and Tuomanen, 2000). Insertion of mosaic sequences can alter the active site of PBPs and change the way in which peptidoglycan building blocks are recognised within these bacteria.

S. pneumoniae is unusual in that high level penicillin resistance is a result of a combination of the acquisition of more than one low affinity PBP and the activity of the MurM protein (del Campo *et al.*, 2006). MurM is an aminoacyl-ligase that is responsible for the synthesis of branched structure muropeptides in pneumococcal peptidoglycan and is currently under-exploited as a target for the development of novel antibiotics that could restore the effectiveness of penicillin (Filipe *et al.*, 2000;

Lloyd *et al.*, 2008). The role of MurM and its involvement in penicillin resistance will be discussed further in section 1.4.

1.3. The peptidoglycan biosynthesis pathway

1.3.1. The bacterial cell wall

The year 1884 marked the discovery of a reagent by Hans Christian Joachim Gram that could be used to stain bacterial cells for visualisation under the microscope. Differences in cell wall structure and hence reactivity with the stain allowed for the classification of bacteria as either Gram-positive or Gram-negative (Figure 1.1).

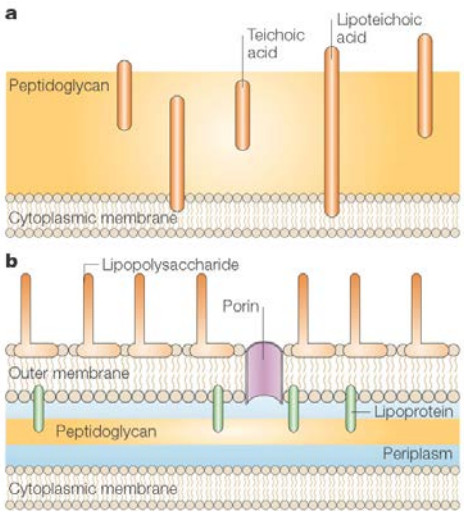

Figure 1.1: Differences in the cell wall structure of (a) Gram-positive and (b) Gram-negative bacteria. The Gram-positive cell wall consists of a thick homogenous layer of peptidoglycan on the outside of the cytoplasmic membrane with teichoic acid molecules embedded in the structure. In contrast to this, the peptidoglycan layer in Gram-negative cells is located in the periplasmic space situated between the cytoplasmic membrane and the outer membrane. The major components of the Gram-negative cell wall are lipopolysaccharide and lipoproteins with less than 10% of the structure being comprised of peptidoglycan. Adapted from Cabeen and Jacobs-Wagner (2005).

In Gram-positive organisms, the peptidoglycan layer coats the outer surface of the cell, is characteristically thick and has a depth of 20 to 80 nm. Approximately 30-70% of the total cell wall is made up entirely of peptidoglycan resulting in retention

of the dye-iodine complex during staining. In contrast to this, the peptidoglycan layer of Gram-negative organisms is much thinner, has a depth of only 2-3 nm and is surrounded by a porous outer membrane resulting in decolourisation after alcohol treatment during the Gram-staining process (Bugg, 1999; Cabeen and Jacobs-Wagner, 2005). In Gram-negative organisms, the peptidoglycan structure is arranged as a monolayer making up less than 10% of the total cell wall. This contrasts sharply with the chemically and structurally diverse multi-layered scaffold produced by Gram-positive organisms (Schleifer and Kandler, 1972). It is important to note that peptidoglycan is unique to prokaryotic cells with only a few members of the Archaea, including *Halobacterium halobium* and a few bacteria, including *Micrococcus morrhuae* and *Chlamydia* species, lacking the structure. This validates the biosynthesis of this layer as an important target for antimicrobial agents.

1.3.2. The structure and function of peptidoglycan

Peptidoglycan, or murein, is an essential structural component of the bacterial cell wall and has two key constituents: the glycan strands and the pentapeptide side chains. In many cases, there are also interstrand peptide cross-links within the structure and these are important in penicillin-resistance and sortase function. The primary function of the peptidoglycan layer is to protect the cell from turgor pressure induced lysis which arises due to the osmotic pressure inside the cell being higher than that of the external medium (Bugg, 1999). The turgor pressure inside Gram-negative and Gram-positive bacterial cells has been estimated at 0.5 mPa and 3 MPa respectively. In addition to this protective role, many Gram-positive bacteria heavily utilise their peptidoglycan as a platform for the anchoring of surface proteins

including virulence factors and adhesins (Macheboeuf *et al.*, 2006; Dramsi *et al.*, 2008).

At the molecular level, the carbohydrate (or glycan strand) backbone of peptidoglycan is common to all bacteria and consists of a β-1,4-linked chain of alternating N-acetylglucosamine (GlcNAc) and N-acetylmuramic acid (MurNAc) residues. This repeating structure is shown in Figure 1.2.

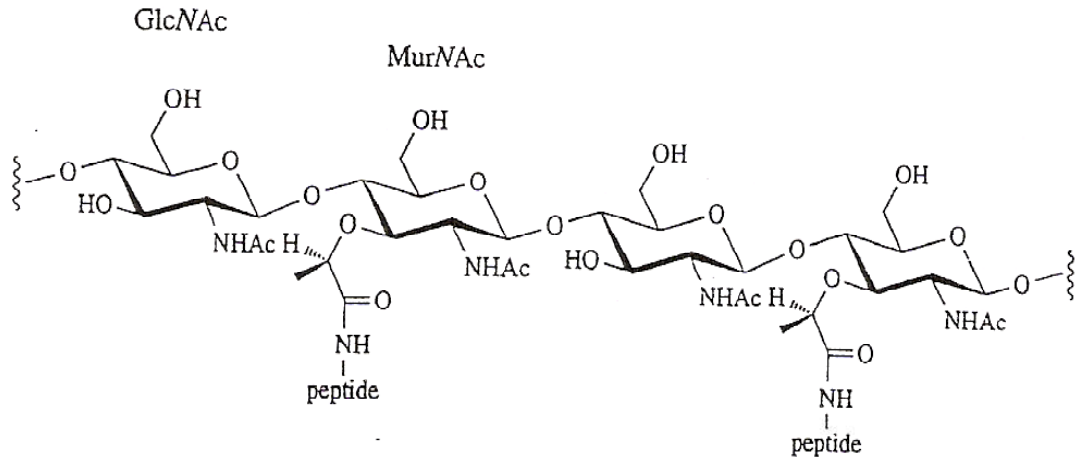

Figure 1.2: Structure of the glycan chains of peptidoglycan. The repeating β-1, 4-linked structure illustrated here is found in the peptidoglycan of all currently examined bacteria with only minor variations. The length of the glycan chain of peptidoglycan has been estimated for various bacterial genera and species. As an example, the glycan chains present in *Staphylococcus aureus* are typically a minimum of 12 and a maximum of 16 disaccharide units long. Adapted from Bugg (1999).

The pentapeptide side chain component of peptidoglycan is attached to the lactyl-ether appendage of MurNAc and is comprised of alternating L- and D-amino acids that are unique to this structure. Pentapeptide side chains have the common structure L-ala-γ-D-glu-X-D-ala-D-ala. Within this structure, X is used to represent an L-amino acid that possesses an amino side chain. In Gram-negative organisms, X is

normally *meso*-diaminopimelic acid (*meso*-DAP) whereas in Gram-positive organisms it is most commonly L-lysine (Bugg, 1999).

In order to keep separate peptidoglycan strands together, a network of interstrand peptide cross-links form between individual pentapeptide side chains. It is the degree of this cross-linking that determines the overall rigidity of the peptidoglycan structure. Typically, Gram-negative bacteria, such as *Escherichia coli*, have a lower level of cross-linking (25-50%) than Gram-positive bacteria (70-90%). The simplest and most common linkage to occur is a direct one between *meso*-DAP and a D-alanine residue located at position four of a second pentapeptide side chain. Such a transpeptidation reaction results in the formation of an amide bond and the release of the terminal D-alanine residue from the second pentapeptide side chain. Examples of organisms in which this simplest type of linkage occurs are *E. coli* and various strains within the genus *Bacillus*, as shown in Figure 1.3.

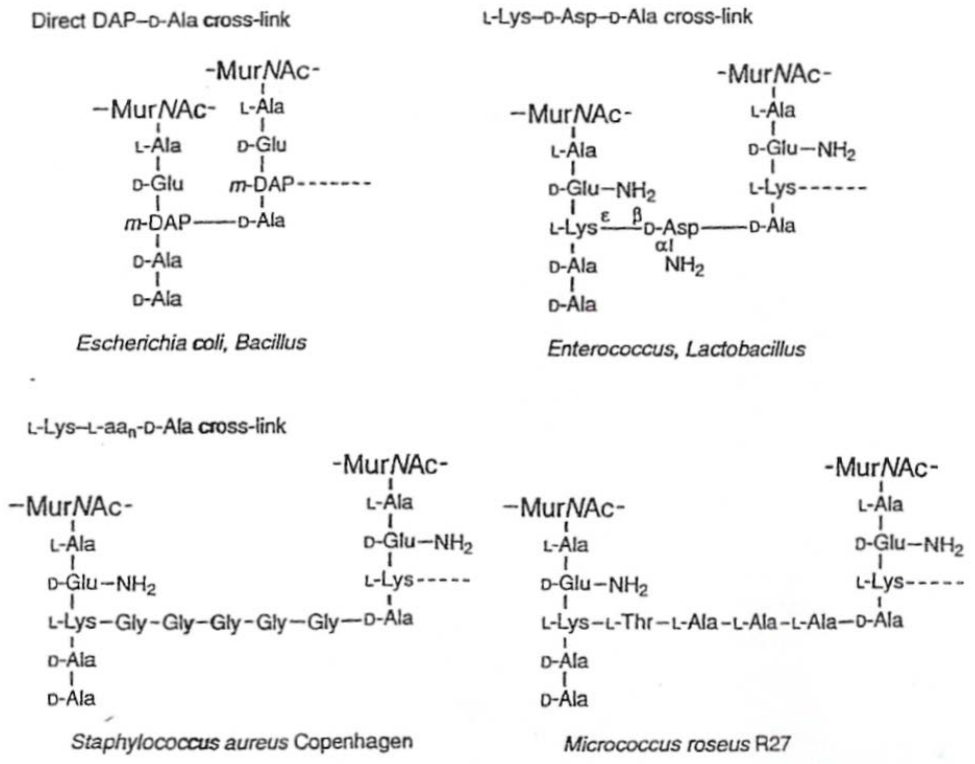

Figure 1.3: Types of peptide cross-links occurring at position 3 of a donor pentapeptide chain. The simplest type of link is direct amide bond formation between *meso*-DAP and D-alanine (top, left). In Gram-positive bacteria, peptide bridge formation via incorporation of L-amino acids or glycine is more common. For example, *Staphylococcus aureus* strain Copenhagen typically utilises five glycine residues in its cross-link (bottom, left) whereas *Micrococcus* species use a combination of L-alanine, L-serine and L-threonine (bottom, right). Taken from Bugg (1999).

However, for bacteria that contain L-lysine at the third position (point X in the pentapeptide structure), there is usually an intervening amino acid chain providing the linkage to the D-alanine residue of the second pentapeptide chain. In such circumstances, the structure of this cross-link is variable. Gram-positive organisms tend to construct the peptide bridge from one to five residues of either an L-amino acid or glycine (Garcia-Bustos *et al.*, 1987; Bugg, 1999). In *S. pneumoniae*, the formation of these cross-links is the result of the activity of the MurM and MurN proteins.

1.3.3. Peptidoglycan biosynthesis

Peptidoglycan biosynthesis follows a pathway of three defined stages that take place in different parts of the cell (Figure 1.4). The primary stages take place in the cytoplasm and initially involve the production of the N-acetylglucosamine-N-acetylmuramyl pentapeptide (Barreteau *et al.*, 2008). The second stage involves the synthesis of lipid linked intermediates on the inner face of the cytoplasmic membrane. It is at this stage that the addition of amino acids involved in indirect cross-linkages occurs in many Gram-positive organisms. After translocation of the phospho-MurNAc-pentapeptide across the cytoplasmic membrane by an undecaprenyl phosphate lipid carrier, mature peptidoglycan is assembled on the cell surface by transpeptidation and transglycosylation (Barreteau *et al.*, 2008; Bouhss *et al.*, 2008). Whilst the main focus of this work is on the lipid linked stages of peptidoglycan biosynthesis, all three stages are discussed below.

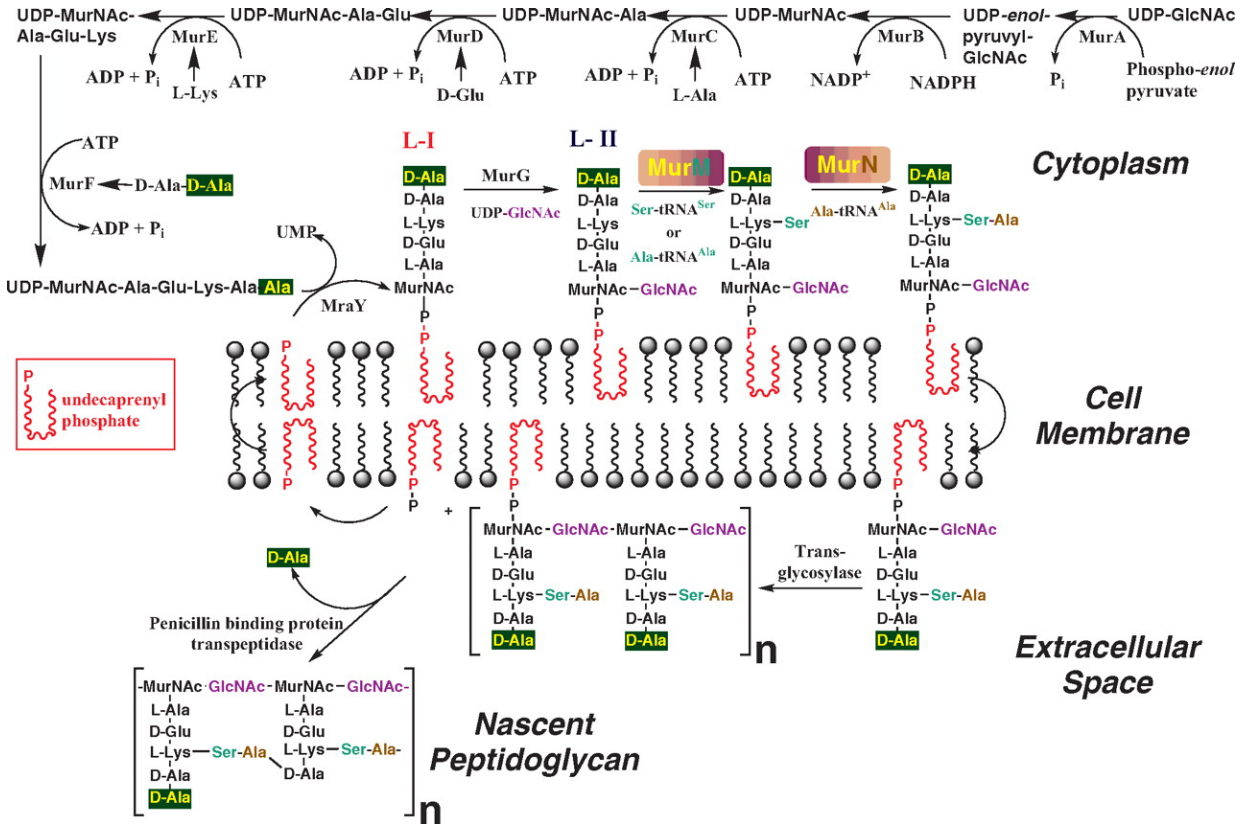

Figure 1.4: Summary of the three stages of peptidoglycan biosynthesis in *Streptococcus pneumoniae*. The cytoplasmic stages are concerned with the production of the N-acetylglucosamine-N-acetylmuramyl pentapeptide by Mur A to F. The lipid-linked stages are catalysed by MraY and MurG generating Lipid II. This structure is further modified at this stage in *Streptococcus pneumoniae* by MurM and MurN. MurM adds either alanine or serine as the first amino acid of the indirect cross-link and MurN invariably adds alanine as the second amino acid of the cross-link. The final, extracellular, stages of peptidoglycan biosynthesis are referred to as transpeptidation and transglycosylation and are carried out by the penicillin-binding proteins (PBPs). Taken from Lloyd *et al.* (2008).

1.3.3.1. The cytoplasmic stages of peptidoglycan biosynthesis

It is possible to separate the cytoplasmic stages of peptidoglycan biosynthesis into three well defined processes: (1) the generation of UDP-GlcNAc from fructose-6-phosphate; (2) the generation of UDP-MurNAc from UDP-GlcNAc and; (3) the addition of the pentapeptide side chain to UDP-MurNAc. These three processes will be discussed below.

1.3.3.1.1. The generation of UDP-GlcNAc from fructose-6-phosphate

The synthesis of UDP-GlcNAc from fructose-6-phosphate is the product of four separate enzymatic activities conferred by the GlmS, GlmM and GlmU proteins. The *glmS* gene encodes an amidotransferase called glucosamine-6-phosphate synthase. GlmS from both *E. coli* and *Thermus thermophilus* have been overexpressed and purified allowing for their characterisation (Badet *et al.*, 1987; Badet-Denisot *et al.*, 1997).

GlmS is a dimeric enzyme which uses glutamine as a source of ammonia in order to convert D-fructose-6-phosphate into D-glucosamine-6-phosphate. This is then converted to glucosamine-1-phosphate by the isomerase, GlmM, as shown in Figure 1.5.

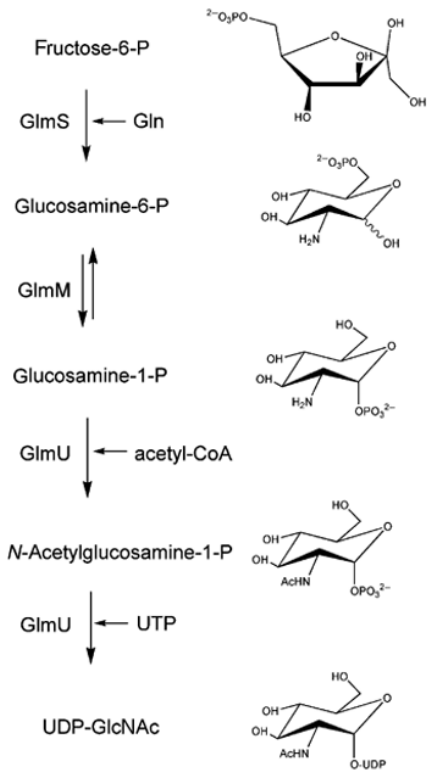

Figure 1.5: Production of UDP-GlcNAc from fructose-6-phosphate in bacteria by the GlmS, GlmM and GlmU enzymes. Adapted from Barreteau *et al.* (2008).

The generation of UDP-GlcNAc from glucosamine-1-phosphate requires the activities of a bifunctional enzyme called GlmU. The C-terminal domain of GlmU is responsible for the first reaction which involves acetylation of glucosamine-1-phosphate using acetyl-CoA. The N-terminal domain of the protein then carries out uridyl-transfer from UDP to N-acetylglucosamine-1-phosphate (Barreteau *et al.*, 2008).

1.3.3.1.2. The generation of UDP-MurNAc from UDP-GlcNAc

The first committed step in the synthesis of peptidoglycan is the conversion of UDP-GlcNAc to UDP-MurNAc by the MurA and MurB enzymes. All of the Mur enzymes involved in peptidoglycan biosynthesis are unique to bacteria and, in addition to this, are highly conserved across various bacterial species. This makes them ideal targets

for the design of novel antibiotics (El Zoeiby *et al.*, 2003). The structures of MurA, MurB, MurD, MurE and MurF are shown in Figure 1.6.

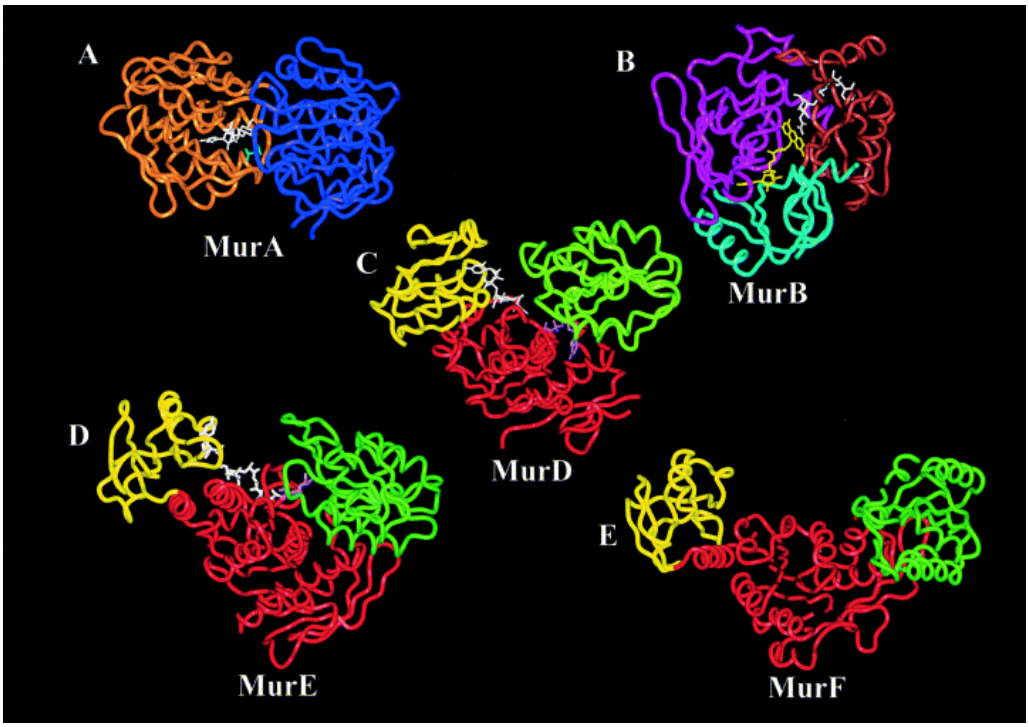

Figure 1.6: The structures of MurA (A), MurB (B), MurD (C), MurE (D) and MurF (E) taken from El Zoeiby *et al.* (2003).
(A) The structure of MurA solved to 1.8 Å (PDB code 1UAE): domain I is shown in orange, domain II is shown in violet, UDP-N-acetylglucosamine is shown in white and fosfomycin is shown in blue (Skarzynski *et al.*, 1996).
(B) The structure of MurB solved to 1.8 Å (PDB code 2MBR): domain I is shown in pink, domain II is shown in blue, domain III is shown in brown, UDP-N-acetylglucosamine enolpyruvate is shown in white and flavin adenine dinucleotide (FAD) is shown in yellow (Benson *et al.*, 1997).
(C) The structure of MurD solved to 1.7 Å (PDB code 2UAG): domain I is shown in yellow, domain II is shown in red, domain III is shown in green, UDP-N-acetylmuramyl-I-alanine is shown in white and the amino acid substrate, D-glutamic acid is shown in rose (Bertrand *et al.*, 1999).
(D) The structure of MurE solved to 2.0 Å (PDB code 1E8C): domain I is shown in yellow, domain II is shown in red, domain III is shown in green, UDP-N-acetylmuramyl dipeptide is shown in white and the amino acid substrate, meso-diaminopimelic acid is shown in rose (Gordon *et al.*, 2001).
(E) The structure of MurF solved to 2.3 Å (PDB code 1GG4): domain I is shown in yellow, domain II is shown in red, domain III is shown in green (Yan *et al.*, 2000).

MurA catalyses the transfer of the enolpyruvate moiety from phosphoenolpyruvate (PEP) to the 3' hydroxyl of UDP-GlcNAc. This generates a phospholactoyl-UDP-GlcNAc tetrahedral intermediate (Figure 1.7, step 1). This type of biochemical reaction using PEP is rare and has only been seen with one other enzyme, AroA, in the shikimic acid pathway (Bugg, 1999; Barreteau *et al.*, 2008). Gram-negative bacteria typically have one copy of *murA* whereas gene duplication has resulted in Gram-positive bacteria, such as *S. pneumoniae*, having two copies of the gene.

MurA is approximately 45 kDa in size comprising 419 amino acids. Structural studies have shown that the protein consists of two globular domains that are kept in contact with each other by a double stranded linker (Figure 1.6). In *E. coli* MurA, domain I comprises residues 22-229 and domain II comprises residues 1-21 and 230-419 (El Zoeiby *et al.*, 2003). Residues of particular importance within the enzyme include lysine-22, which is strictly conserved due to its role in PEP binding, and cysteine-115 which is an active site residue that is essential for product release (Eschenburg *et al.*, 2005).

MurA is the only enzyme within the cytoplasmic stages of peptidoglycan biosynthesis that is actively targeted by an antibiotic approved for use within the clinical setting. Fosfomycin is typically used for the treatment of gastrointestinal and urinary tract infections and competitively inhibits MurA by forming a covalent bond with a cysteine residue adjacent to the active site. Development of resistance to fosfomycin is common. Some bacteria, including *Mycobacterium tuberculosis* and *Chlamydia trachomatis*, are naturally resistant to the antibiotic because they have an aspartate residue instead of a cysteine in the equivalent position. In addition to this,

chromosomal resistance to the antibiotic can arise in three ways: (1) alteration in the L-α-glycerophosphate and glucose-6-phosphate active transport systems thus impairing fosfomycin uptake by the cell; (2) reduction in the affinity of the transferase enzyme for the antibiotic and; (3) increased transcription of *murA* resulting in overproduction of the enzyme. Plasmid-encoded resistance can also result in the ability to modify the antibiotic so that it is no longer effective (El Zoeiby *et al.,* 2003). As a result of this, the development of new antibiotics that can target either MurA or other enzymes within the peptidoglycan biosynthesis pathway is essential.

After the action of MurA, the NADPH-dependent reductase MurB is responsible for catalysing the reduction of the enolpyruvate residue on UDP-GlcNAc to D-lactate giving rise to UDP-MurNAc (Figure 1.7, step 2). MurB is approximately 38 kDa in size, 342 amino acids in length and is comprised of three domains (Figure 1.6). Domains one and two are known to be involved in the binding of flavin adenine dinucleotide (FAD) which is used as a redox intermediate during the two half reactions that are catalysed by the enzyme. Domain three is concerned with substrate binding (El Zoeiby *et al.*, 2003; Barreteau *et al.*, 2008).

Initially, MurB catalyses the reduction of FAD to $FADH_2$ by the transfer of two electrons from NADPH. This results in the release of $NADP^+$ which subsequently allows UDP-GlcNAc-enolpyruvate to bind to the enzyme. The transfer of two electrons from the reduced FAD to the third carbon of the enolpyruvyl group produces an intermediate that can be protonated at the second carbon generating

UDP-MurNAc. Serine-229 is essential for the activity of MurB since it becomes the proton donor in the second half of the reaction (El Zoeiby *et al.*, 2003).

1.3.3.1.3. The addition of the pentapeptide side chain to UDP-MurNAc

The pentapeptide side chain component of the peptidoglycan backbone is assembled in a sequential manner by four essential enzymes that are broadly classified as the Mur ligases (Smith, 2006). The order of addition of amino acids onto the D-lactoyl group of UDP-MurNAc is illustrated in Figure 1.7 and consists of: L-alanine (catalysed by MurC); D-glutamic acid (catalysed by MurD); a diamino acid such as meso-diaminopimelic acid in Gram-negatives and L-lysine in Gram-positives (catalysed by MurE) and finally the dipeptide D-alanine-D-alanine (catalysed by MurF).

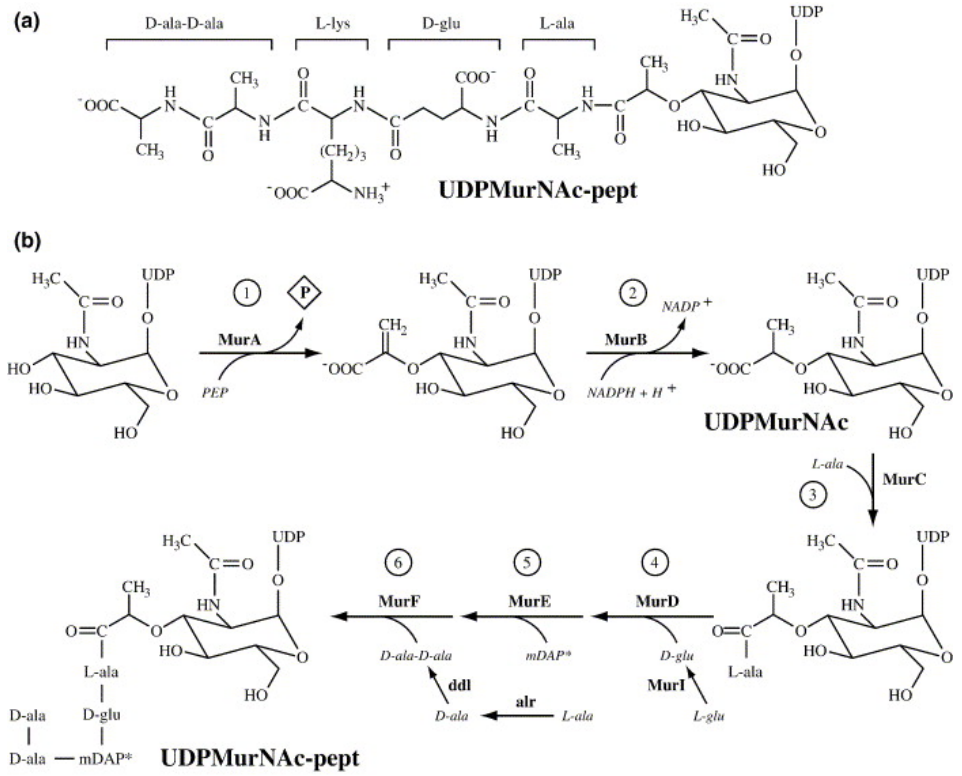

Figure 1.7: Summary of (a) the structure of UDP-MurNAc pentapeptide and (b) the 6 cytoplasmic stages of peptidoglycan biosynthesis carried out by MurA to MurF. Adapted from Smith (2006).

All Mur ligases share the same reaction mechanism catalysing amide or peptide bond formation by activation of the UDP-precursor at the carboxyl group. This is concurrent with the release of ADP and inorganic phosphate from ATP. In addition to this, all the Mur ligases possess a sequence of six conserved amino acids and a consensus sequence that is required for ATP binding. It was this finding that lead to the redefinition of Mur ligases as a new family of enzymes (Bouhss *et al.*, 1997). In addition to MurC, MurD, MurE and MurF which are all involved in peptidoglycan biosynthesis, this family of enzymes also includes folylpoly-γ-L-glutamate synthetase, the C-terminus of cyanophycin synthetase and poly-γ-glutamate synthetase from bacteria within the genus *Bacillus* (Barreteau *et al.*, 2008).

X-ray crystallography experiments have demonstrated that members of the Mur ligase family share the same general three-dimensional structure which can be divided more specifically into three key domains (Figure 1.8). The N-terminal domain is known to be involved in the binding of the UDP-precursor, the middle domain with the binding of ATP and the C-terminal domain is responsible for interactions with the amino acid (Smith, 2006).

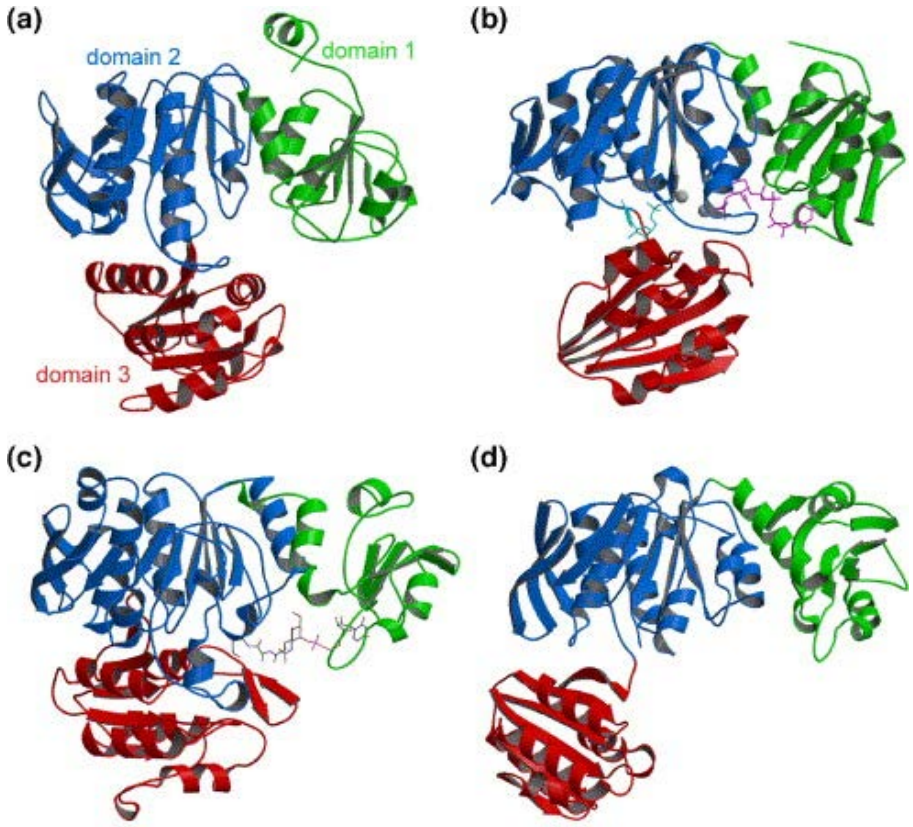

Figure 1.8: The characteristic three domain structures of *Escherichia coli* MurC (a), MurD (b), MurE (c) and MurF (d). Adapted from Smith (2006). Note that the structure of *E. coli* MurC was first solved by Deva *et al*. (2006).

In terms of peptidoglycan biosynthesis, MurC, which is approximately 54 kDa in size and 491 amino acids long, adds the first amino acid of the pentapeptide side chain and this is usually alanine (Schleifer and Kandler, 1972). *E. coli* MurC has been extensively characterised and shown to have a strict preference for L-alanine as opposed to D-alanine which is not recognised as a substrate by the enzyme. The reaction mechanism of MurC is strictly ordered with ATP binding to the enzyme first followed by UDP-MurNAc second and finally L-alanine.

After L-alanine addition, MurD, which is approximately 47 kDa in size and 438 amino acids long, adds the second amino acid of the side chain which is usually D-

glutamic acid. In contrast to the other Mur ligases, MurD is less specific for the UMP moiety of the UDP-precursor and recognises 1-phospho-MurNAc-L-Ala as its substrate. After MurD activity, MurE adds the third amino acid, which is typically *meso*-DAP in Gram-negative bacteria and L-lysine in Gram-positive bacteria. MurE is approximately 53 kDa in size and 495 amino acids long. In almost every case, MurE is highly specific and incorporation of an incorrect amino acid by this enzyme in *E. coli* leads to cell lysis.

The amino acid residues found at positions four and five of the pentapeptide side chain are added together as a dipeptide by MurF. MurF is approximately 47 kDa in size and 452 amino acids long. The most common dipeptide to be added is D-alanine-D-alanine, however vancomycin-resistant strains of bacteria often have D-alanine-D-serine or D-alanine-D-lactate at this position (Healy *et al.*, 2000). MurF is comparable to MurC in that it follows the same ordered reaction mechanism. However, the activity of the enzyme is reliant on the generation of the dipeptide substrate which requires an ATP-dependent ligase called Ddl. The reaction carried out by MurF completes the cytoplasmic stages of peptidoglycan synthesis (Barreteau *et al.*, 2008).

1.3.3.2. The lipid-linked stages of peptidoglycan biosynthesis

The lipid-linked stages of peptidoglycan biosynthesis are carried by MraY and MurG which generate Lipid I and Lipid II respectively (Figure 1.9).

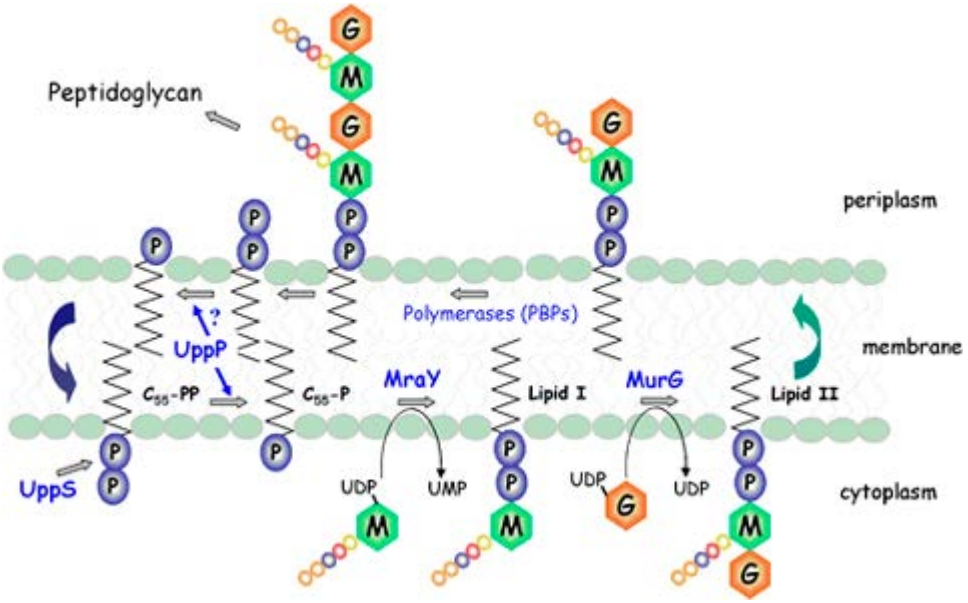

Figure 1.9: Summary of the lipid-linked stages of peptidoglycan biosynthesis. UppS is undecaprenyl-pyrophosphate synthase, UppP is undecaprenyl-pyrophosphate phosphatase, G is GlcNAc, M is MurNac pentapeptide, UDP is uridine diphosphate, UMP is uridine monophosphate, P is phosphate and PBPs are penicillin binding proteins. Taken from Bouhss *et al.* (2008).

MraY is a translocase which catalyses the transfer of UDP-MurNAc pentapeptide to undecaprenyl phosphate (C55-P) producing Lipid I. Orthologues of MraY are found across Gram-positive and Gram-negative bacteria and alignment of these sequences led to the identification of five conserved hydrophilic regions within the protein (Bouhss *et al.*, 1999). The protein is proposed to consist of ten transmembrane helices that join four periplasmic loops and five cytoplasmic sequences. Two proposed catalytic mechanisms for the protein exist. These are shown in Figure 1.10.

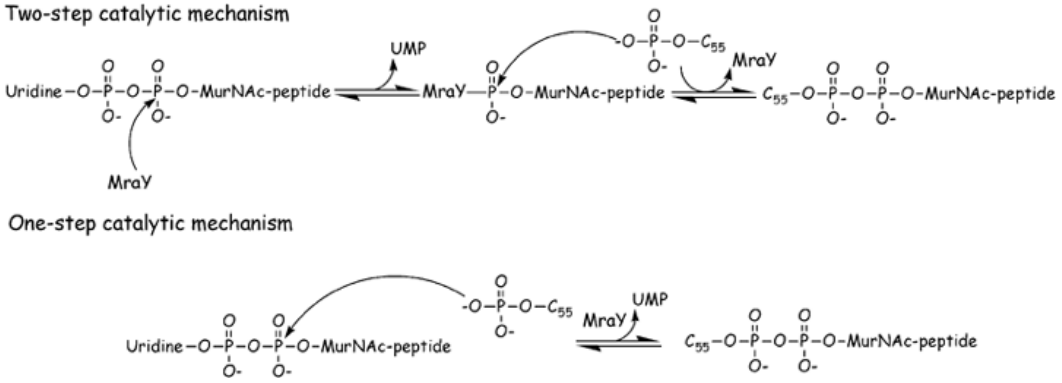

Figure 1.10: Summary of the two proposed catalytic mechanisms of MraY. Taken from Bouhss *et al.* (2008).

The two step catalytic mechanism of MraY was originally proposed by Heydanek *et al.* (1969). However these experiments were heavily criticised due to the fact that they were based on utilisation of a non-purified form of MraY. An alternative single step mechanism has been proposed that generates lipid I by direct attack of the phosphate on C55-P which then attaches to the β-phosphate of UDP-MurNAc pentapeptide. Further investigation is required to establish which of the two mechanisms is correct. Known inhibitors of MraY include various nucleosides, amphomycin and protein E, however, none of these agents are currently clinically approved antibiotics (van Heijenoort, 2007; Bouhss *et al.*, 2008).

Following the activity of MraY, MurG catalyses the transfer of GlcNAc from a UDP-GlcNAc donor molecule to the hydroxyl group on carbon 4 of the MurNAc moiety of lipid I. The end product of this reaction is Lipid II. X-ray crystallography has shown that the N-terminal domain of MurG binds lipid I whereas the C-terminal domain binds UDP-GlcNAc (van Heijenoort, 2007). In addition to this, studies on *E. coli* MurG have demonstrated that the enzyme associates with the cytoplasmic face

of the membrane. This finding is indicative of the fact that the peptidoglycan monomer (Lipid II) is fully assembled prior to its transportation across the cytoplasmic membrane (Bupp and van Heijenoort, 1993).

It is at the Lipid-II intermediate stage that amino acid bridges are added to L-lysine at the third position of the pentapeptide side chain in some Gram-positive organisms. One exception to this rule is seen in the case of *Weissella viridescens* which adds the bridging amino acid to UDP-MurNAc pentapeptide as opposed to Lipid II (Hegde and Blanchard, 2003). These bridges ultimately result in indirect cross-linkage between L-lysine at the third position of one peptidoglycan chain and D-alanine at the fourth position of another. Examples of such amino acid cross-bridges are shown in Table 1.3.

Bacterial species	**Cross-bridge composition**	**Enzyme(s) involved in cross-bridge formation**
Streptococcus pneumoniae	L-Ala-L-Ala or L-Ser-L-Ala	MurMN
Staphylococcus aureus	Gly-Gly-Gly-Gly-Gly	FemXAB
Staphylococcus simulans *Staphylococcus capitis*	Gly-Gly-Ser-Gly-Ser	FemXAB Lif/Epr
Weissella viridescens	L-Ala-L-Ser or L-Ala-L-Ser-L-Ala	FemX and unknown
Enterococcus faecalis	L-Ala-L-Ala	BppA1 and BppA2
Streptomyces coelicolor	Gly	FemX and VanK
Enterococcus faecium	D-Asx	Asl_{fm}

Table 1.3: Summary of amino acid cross bridge formation in Gram-positive organisms leading to indirect cross-linking within the structure of peptidoglycan (Vollmer *et al.*, 2008)

Purification and subsequent characterisation of the branching enzymes listed in Table 1.3 has indicated that they fall into two groups. This grouping is based on whether the enzyme adds Glycine/L-amino acids or D-amino acids to the

pentapeptide side chain. Those enzymes falling in the first group obtain their amino acid substrate from aminoacylated tRNA species and are broadly termed Fem ligases. In contrast to this, enzymes that add D-amino acids are often members of the ATP-grasp family (Vollmer *et al.*, 2008). Whilst the focus of this work is on the MurM protein from *S. pneumoniae*, a detailed discussion of these enzymes can be found in sections 1.4 to 1.10.

Once the synthesis of the phosphor-MurNAc-pentapeptide unit is complete, it must be translocated across the cytoplasmic membrane by a lipid carrier. The exact process by which this is achieved has just been determined with the conclusion that it is performed by the integral membrane protein FtsW (Mohammadi *et al.*, 2011).

1.3.3.3. Assembly of mature peptidoglycan on the cell surface by transpeptidation and transglycosylation

The final stages of peptidoglycan synthesis involve Lipid II polymerisation and cross-linking of this material to form mature peptidoglycan on the outer face of the cytoplasmic membrane. This is achieved by two enzymatic activities: transglycosylation and transpeptidation. Both of these reactions are catalysed by membrane-bound penicillin-binding proteins (PBPs), which are thought to be present in all known bacteria.

PBPs are commonly categorised into two classes: high molecular weight and low molecular weight. The high molecular weight PBPs are further subdivided into Class A and Class B depending on the catalytic activity and structure of the N-terminal

domain. Class A PBPs are bifunctional showing transglycosylase activity at the N-terminus and transpeptidase activity at the C-terminus. Class B PBPs do not have the same activity at their N-terminus and this region of the protein is thought to be involved in the control of cell morphogenesis instead (Sauvage *et al.*, 2008). Most of the low molecular mass PBPs are D-D-carboxypeptidases instead of transpeptidases and catalyse hydrolysis of the terminal D-Ala-D-Ala prior to cross-linkage. The purpose of this activity is not well understood but could be a regulation point for cross-linking via the inactivation of some stem peptides (Buynak, 2007; Lovering *et al.*, 2007).

Transglycosylation is currently underexploited as a target for the design of new antimicrobials. All of the glycosyltransferase domains within characterised PBPs contain five motifs that are conserved. Three of these motifs are located within the catalytic site and encompass two glutamate residues which are essential for enzyme activity. The other two motifs are essential for maintenance of the structure of the glycosyltransferase fold (Gautam *et al.*, 2010).

Transpeptidation occurs in three stages. Firstly, a non-covalent complex is formed between the PBP and the pentapeptide side chain moiety of Lipid II. This achieved by recognition of the terminal D-alanine-D-alanine, in positions four and five of the pentapeptide side chain, by the PBP. Formation of this complex results in the active site serine residue of the PBP attacking a carbon atom on the D-alanine-D-alanine peptide bond resulting in generation of an acyl-enzyme intermediate. This process results in the release of the terminal D-alanine residue from the pentapeptide side chain followed either by hydrolysis or cross-linkage with the peptide side chain

component of another peptidoglycan monomer. There are many antibiotics which target the activity of PBPs and these are summarised in Table 1.4.

Antibiotic class	Compound	Target	Mode of action
β-lactams	Penicillin Carbapenems Cephalosporins Methicillin	Transpeptidase	These antibiotics are analogues of D-Ala-D-Ala and competitively bind to the enzyme
Glycopeptide	Vancomycin Teicoplanin	Transpeptidase, transglycosylase and MurG	Lipid II binding
Semi-synthetic glycopeptides	Oritavancin Dalbavancin Telavancin	Transglycosylase Transglycosylase	Binds to the enzyme causing dimerization Lipid II binding and membrane depolarisation
Glycolipodepsipeptide	Ramoplanin	Transglycosylase and MurG	Lipid I and II binding causing fibril formation
Phosphoglycolipid	Moenomycin	Transglycosylase and MurG	Analogue of Lipid II which competitively binds to the enzyme
Cyclic glycopeptide	Mannopeptimycines	Transglycosylase	Binds to Lipid II at a different site to vancomycin

Table 1.4: Summary of antibiotics developed to target the last stage of peptidoglycan synthesis. This stage is the most over-exploited since there is no requirement for the compounds to cross the cytoplasmic membrane. Adapted from Gautam *et al.* (2010).

In contrast to many other pathogens, β-lactam resistance in *S. pneumoniae* does not occur as a result of the acquisition of plasmid encoded β-lactamases which are able to cleave penicillin directly. Resistance is acquired instead by accumulation of mutations in PBPs so that they no longer have a high affinity for penicillin (see section 1.2.5). In addition to this, knock out of the cross-linking enzyme MurM, causes a reversion to penicillin sensitivity in strains that were previously resistant. One possible explanation for this is given by the knowledge that mutated low-affinity forms of PBP 2x found in penicillin-resistant strains of *S. pneumoniae* have a more open active site which may preferentially bind the branched form of the Lipid II substrate generated by the action of MurM and MurN (Dessen *et al.*, 2001). As a result of this, development of inhibitors towards MurM in *S. pneumoniae* and Fem ligases in other organisms may enable restoration of the potency of one or more of the antibiotics shown in Table 1.4. The role of MurM and other Fem ligases and their potential as targets for the design of novel antibiotics is discussed in more detail in the sections that follow.

1.4. The role of MurM and MurN in *Streptococcus pneumoniae*

The peptidoglycan layer of *S. pneumoniae* is unusual in that it is typically comprised of a combination of both linear and branched muropeptides. The branched muropeptides carry a dipeptide that is comprised of either alanyl-alanine or seryl-alanine which participates in indirect cross-linkage of the cell wall (Fiser *et al.*, 2003). The proteins involved in this process were identified as MurM and MurN which are encoded by the *fibA* and *fibB* (factors important in β-lactam resistance) genes in *S. pneumoniae* respectively (Filipe and Tomasz, 2000; Weber *et al.*, 2000).

Both proteins are of a similar size (approximately 47 kDa) with MurM being 406 amino acids long and MurN being 410 amino acids long.

MurM and MurN are both tRNA-dependent aminoacyl ligases that are part of the Fem ligase family. MurM is 25% identical at the amino acid level to its functional homologue, FemX, found in *S. aureus*. MurN shares 29% amino acid identity to the FemA protein of *S. aureus*. Hybridisation studies have indicated that MurM and MurN are transcribed together as an operon (Filipe and Tomasz, 2000).

Selective inactivation of *murN* results in the synthesis of an unusual peptidoglycan structure in which the branched muropeptide bridge is comprised of only one amino acid. This is indicative of the fact that MurM adds either alanine or serine as the first amino acid of the muropeptide bridge and that this addition is required for the activity of MurN, which invariably adds alanine as the second amino acid of the bridge (Filipe *et al.*, 2000). The roles of MurM and MurN in the synthesis of pneumococcal peptidoglycan are summarised in Figure 1.11.

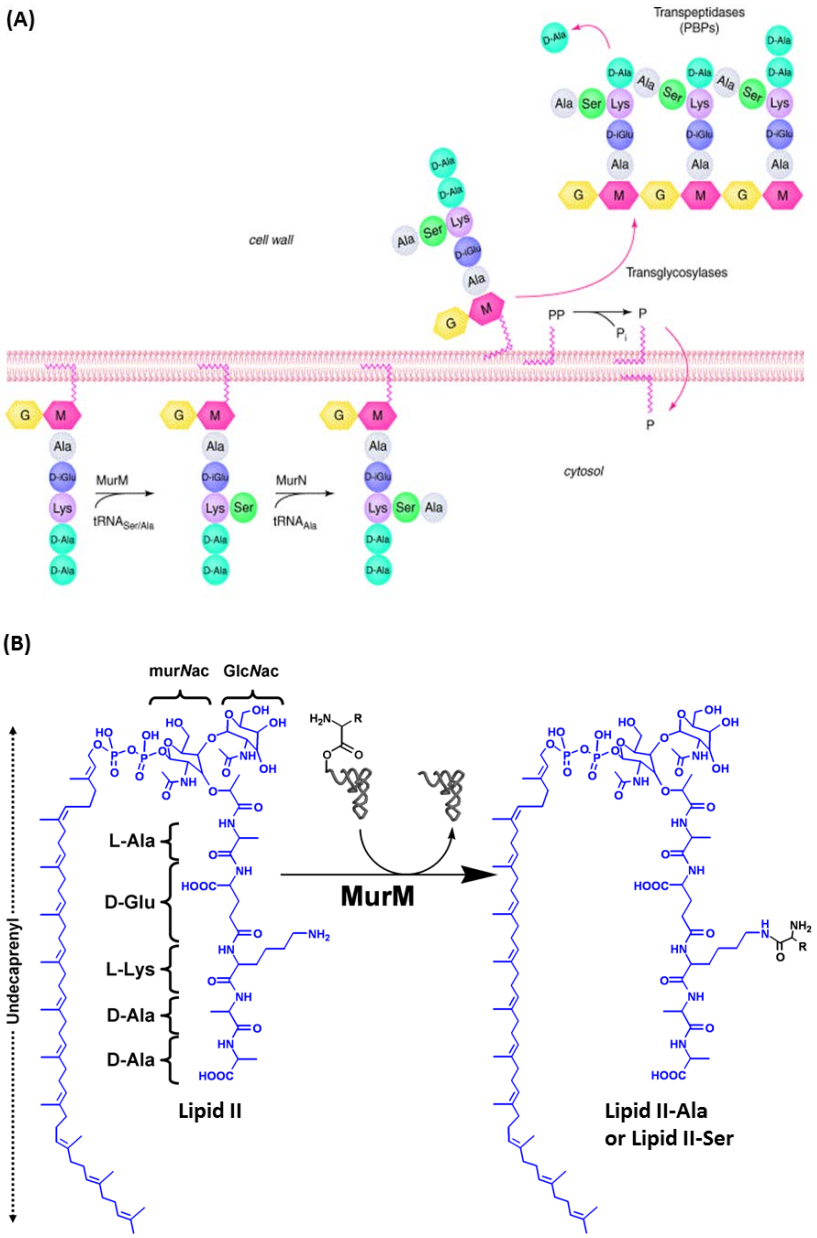

Figure 1.11: (A) The role of MurM and MurN in cell wall branching using Lipid II as substrate. Lipid II is comprised of N-acetylated disaccharide units of glucosamine (yellow hexagon labelled G) and muramic acid (pink hexagon labelled M). The pentapeptide side chain attaches to the muramic acid residues. Lipid II itself is anchored via bactoprenyl pyrophosphate (pink zig-zag line) to the plasma membrane. MurM is an aminoacyl ligase responsible for the addition of either serine or alanine to the cell-wall precursor lysine residue. Taken from Fiser *et al.* (2003). (B) The chemical structure of Lipid II, the substrate for MurM, and Lipid II-Ala/Ser, the product of the MurM catalysed reaction. Note that R is CH_3 in the case of alanine and CH_2OH in the case of serine. Taken from Lloyd *et al.* (2008).

A series of chimeric mutants of MurM from three different strains of *S. pneumoniae* have been used to determine the sequence within the protein that determines the specificity for alanine or serine addition to the epsilon-amino group of the stem peptide lysine. In strain DE1, 77% of muropeptides are branched with MurM showing a preference for alanine. In contrast to this, strains KY17 and R36A both have a preference for serine with 84% and 41% of muropeptides being branched respectively. The region of MurM responsible for amino acid selectivity was determined using a fusion mutant whereby the MurM gene was of strain KY17 origin except for the region between residues 244 and 274, which was of strain DE1 origin. Transformation of this mutant into strain R36A resulted in an alteration in peptidoglycan structure to match that of strain DE1. The overall proportion of branched muropeptides increased to 81% and overall preference was converted from serine to alanine addition. Complete inactivation of MurM was achieved by deletion of the last 10 amino acids at the C-terminus of the protein showing that these residues are essential for catalytic activity (Filipe *et al.*, 2001a).

The substrate for MurM has been determined to be Lipid II as opposed to UDP-MurNAc pentapeptide which is the substrate for the FemX protein in *W. viridescens* (see section 1.6). This was discovered by the addition of vancomycin to a wild-type and a *murM* deletion mutant culture of *S. pneumoniae* strain Pen6 during the exponential growth phase. The accumulated cytoplasmic and lipid-linked precursors were analysed by reverse phase high performance liquid chromatography (RP-HPLC). Only the lipid extract showed a peak consistent with the presence of a pentapeptide carrying the dipeptide cross-bridge added by the activity of the MurM and MurN proteins (Filipe *et al.*, 2001a).

Whilst the *murN* gene appears to be well conserved across different strains of *S. pneumoniae*, the *murM* gene is much more mosaic in sequence particularly in penicillin-resistant strains (see section 1.4.2). For example, the MurM protein in penicillin-resistant strain Pen6 is only 86.5% identical in its amino acid sequence to that of penicillin-sensitive strain R36A. In contrast to this, the MurN proteins from these two strains are 99.3% identical at the amino acid level (Filipe and Tomasz, 2000). The role of both of these proteins in penicillin resistance is discussed below.

1.4.1. The link between MurMN activity and penicillin resistance

In 1990, prior to identification of the *murMN* operon in *S. pneumoniae*, it was observed that a highly penicillin-resistant isolate in South Africa had a highly branched peptidoglycan that could be co-transferred with penicillin resistance to susceptible pneumococci (Zighelboim and Tomasz, 1980; Garcia-Bustos *et al.*, 1988). This finding was suggestive of a link between the abundance of branched muropeptides in the pneumococcal cell wall and penicillin resistance.

Further investigation demonstrated that other pneumococcal strains with high levels of penicillin resistance also had a high proportion of branched muropeptides in their cell wall in comparison to penicillin-sensitive strains. After the identification of the *murMN* operon, these genes were inactivated by insertion duplication mutagenesis in order to investigate the involvement of MurM and MurN in penicillin resistance. It was found that inactivation of this operon had no significant effect on the growth rate, morphology or autolysis rate of pneumococcus suggesting that these genes are not essential for viability. However, major changes in the overall composition of the peptidoglycan layer were seen in both penicillin-sensitive and penicillin-resistant

strains of pneumococcus in a *murMN* inactivation background. In penicillin-resistant strain Pen6, 32.9% of muropeptides within the cell wall are branched. After inactivation of *murMN* in this strain, all branched muropeptides disappeared from the cell wall structure concurrent with a 26.4% increase in the abundance of linear muropeptides. In addition to this, inactivation of *murMN* in this strain also caused a dramatic reduction in the MIC for penicillin from 6 μg mL^{-1} to 0.032 μg mL^{-1}. This effect was also seen in other penicillin-resistant strains of pneumococcus regardless of their genetic background, labelling MurM and MurN as the first major non-PBP determinants of β-lactam resistance within this organism (Filipe and Tomasz, 2000).

Further investigation indicated that inactivation of *murN* alone only caused a 2-fold decrease in the MIC for penicillin (Filipe *et al.*, 2000). In addition to this, deduction of the relationship between MurMN and levels of penicillin resistance has been further complicated by the finding that transformation of a penicillin-sensitive strain (R36A) with the mosaic MurM allele of a penicillin-resistant strain did not prevent the organism from being penicillin-sensitive despite enrichment of the cell wall with branched muropeptides. This suggests that, whilst MurM is necessary for high level resistance to penicillin, it is not sufficient in the absence of low affinity forms of PBPs (Filipe *et al.*, 2002).

In addition to a return to penicillin-sensitivity in strains that were previously resistant, inactivation of *murMN* also results in the generation of pneumococcal strains with increased susceptibility to cell lysis. This effect is pronounced during exposure of the cells to low concentrations of other antibiotics that target peptidoglycan biosynthesis including fosfomycin, vancomycin, D-cycloserine and

nisin. Although not formally proven, this suggests that MurM and MurN might have a key role in a stress response pathway that is concerned with maintaining the biosynthesis of peptidoglycan (Filipe *et al.*, 2002).

In summary, high level β-lactam resistance in *S. pneumoniae* is a complex process whereby the involvement of the *murMN* operon is determined by the presence of mutations either in PBP 1a or in PBPs 2x and 2b. Whilst the *murM* gene is relatively well conserved across penicillin-sensitive pneumococci, a mosaic structure composed of integrated regions of heterologous origin is often seen in penicillin-resistant strains. Often, particular PBP and MurM combinations are preserved which suggests that they may evolve together in specific clones to achieve high level penicillin resistance (Soriano *et al.*, 2008). It is possible that alterations in *murM* are indirectly required for high level penicillin resistance because they help to maintain the necessary changes that have arisen in low affinity PBPs by reducing the overall fitness cost to the cell (Chesnel *et al.*, 2005; del Campo *et al.*, 2006).

1.4.2. Homology models for the structure of MurM and MurN

In 2003, Fiser and others constructed a 3D comparative structural model for MurM based upon the X-ray crystal structure of *S. aureus* FemA (Benson *et al.*, 2002; Fiser *et al.*, 2003). During construction of the 3D model, it was found that MurM had regions of similarity to seryl-tRNA synthetase, N-myristoyl transferases (NMT) and a winged helical DNA protein found in *Methanococcus jannaschii* (Figure 1.12).

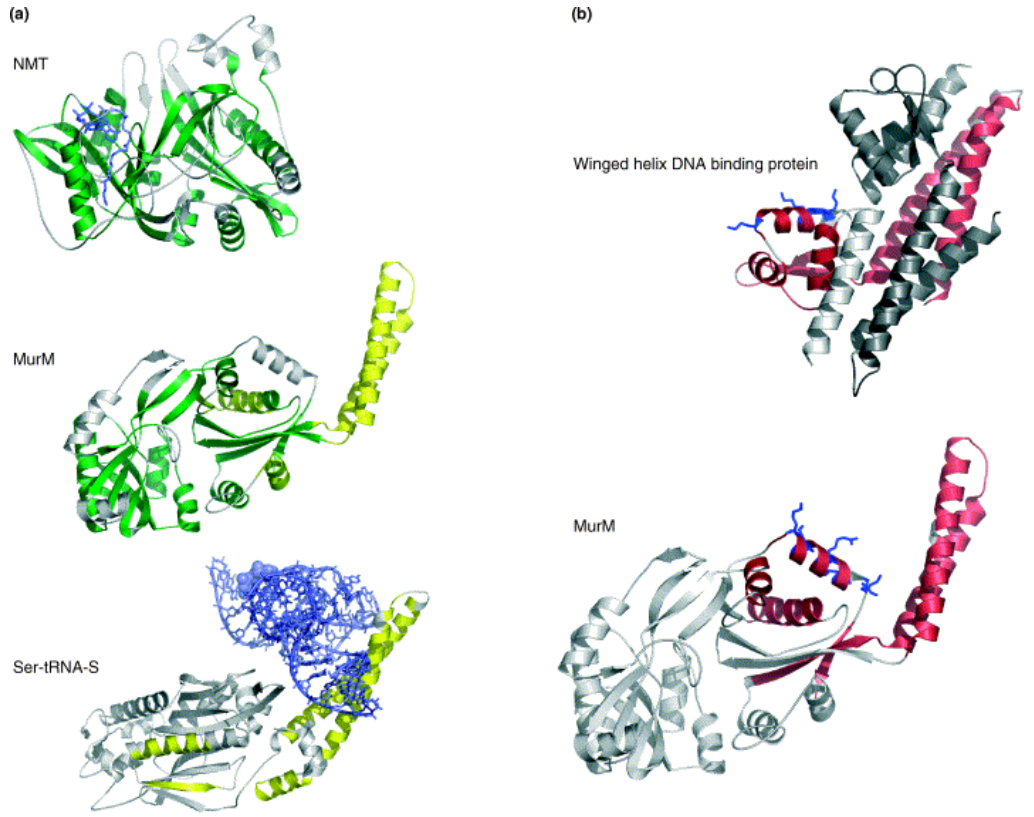

Figure 1.12: Predicted structural similarity between MurM, for which there is currently no crystal structure, N-myristoyl transferase (NMT), Seryl-tRNA synthetase (SerRS) and a winged helical DNA binding protein. (A) Distance matrix alignment prediction of MurM structure based on NMT and Seryl-tRNA synthetase. Regions highlighted in green show similarity between MurM and NMT. Regions highlighted in yellow show similarity between MurM and SerRS. The blue stick models represent bound tRNA and myristoyl CoA in SerRS and NMT respectively. (B) Structural similarity between MurM and a winged helical DNA binding protein from *Methanococcus jannaschii*. Regions in red represent structural features shared between the two enzymes. The lysine and arginine residues predicted to be in the putative DNA recognition helices are represented by blue sticks. Taken from Fiser *et al*. (2003).

According to the proposed 3D homology model, MurM has a structure that is composed of two domains. Domain I is made up of two twisted β-sheet cores that are surrounded by helices. In contrast to this, domain II is a coiled helical arm. Basic sequence comparison between MurM, MurN, FemX and FemA has demonstrated that the C-terminal region of MurM, which contains many conserved lysine and arginine residues, resembles the C-terminal region of FemX more than FemA. This is to be expected since both MurM and FemX have similar biological roles adding the first amino acid of the muropeptide cross bridge in *S. pneumoniae* and *S. aureus* respectively (Fiser *et al.*, 2003). A discussion of the predicted structure of MurM with reference to the three homology models is given below.

1.4.2.1. tRNA synthetases as homology models for MurM

For penicillin-sensitive strains of *S. pneumoniae*, the *murM* gene is highly conserved. However, the *murM* gene of penicillin-resistant isolates tends to be mosaic in the sense that the conserved sequences found in susceptible isolates are combined with divergent sequences of various origins (Fiser *et al.*, 2003). Using the 3D model, comparison of the MurM protein from Kentucky strain and Denver strain, which prefer to add serine and alanine to Lipid II respectively, indicated that most of the differences between the two MurM variants lie within the alpha helical coiled arm structure which is proposed to be involved in the recognition and binding of aminoacyl-tRNA. This correlates well with the finding that the FemX homologue in *W. viridescens* incorporates serine, alanine or glycine onto UDP-MurNAc pentapeptide depending on the availability of the corresponding amino-acyl tRNA species. The apparent lack of amino-acid selectivity with this enzyme appears to parallel the absence of a coiled helical arm domain (Hegde and Shrader, 2001). This

domain is present in the X-ray crystal structure of *S. aureus* FemA and shows structural resemblance to tRNA recognition domains found in tRNA synthetase enzymes (Benson *et al.*, 2002). In MurM, the helical arm is thought to be responsible for amino acid selectivity (Fiser *et al.*, 2003). Many tRNA synthetases have a requirement for divalent metal ions for maintenance of structure and/or recognition of the amino acid substrate (Liu *et al.*, 1993; Sood *et al.*, 1999; Sankaranarayanan *et al.*, 2000). This will be discussed further in chapter 4. The metal ion dependency of MurM and other Fem ligases has yet to be investigated.

1.4.2.2. N-myristoyl transferase (NMT) as a homology model for MurM

Domain I of the predicted MurM model shows significant similarity to the fold found in NMT (Figure 1.12). When taken in conjunction with the fact that both enzymes have a lipid substrate, this is suggestive of the fact that there may also be some functional similarities between the two enzymes (Fiser *et al.*, 2003).

In the case of MurM, the C-terminus of the protein is well conserved between different allelic variants of the enzyme and is essential for catalytic activity. Filipe *et al.* (2001) constructed a series of deletion mutants of the MurM protein from strain KY17 by insertion of premature stop codons during cloning. Upon transformation of these mutants into *S. pneumoniae* strain R36A, it was shown that MurM activity could not be detected when 10 amino acids were removed from the C-terminus of the protein (Filipe *et al.*, 2001a). In NMT, the C-terminus is also indispensible since it is required to reach into the binding site of the enzyme where it donates a carboxyl group so that the reaction can proceed.

Further investigation into the similarity between the MurM model and NMT was carried out by Fiser *et al.* (2003) using GRASP (Graphical Representation and Analysis of Structural Properties) to look for the distribution of electrostatic charges across the protein. The results of this analysis are shown in Figure 1.13 and make a comparison to an equivalent analysis of FemA using the X-ray crystal structure of the protein (PDB code 1LRZ).

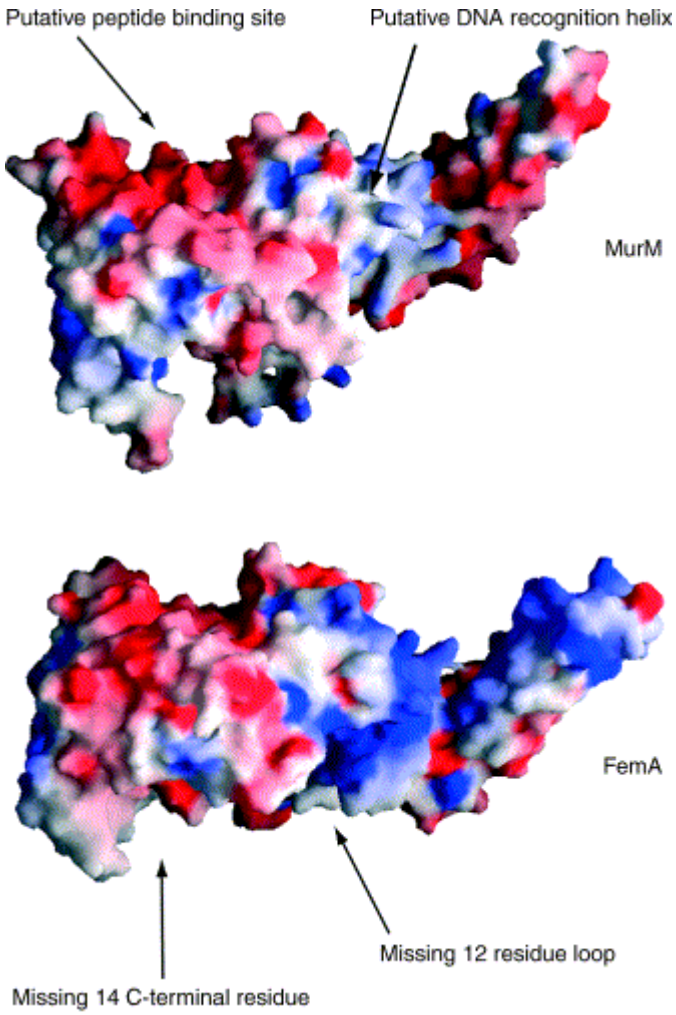

Figure 1.13: GRASP analysis of the MurM model showing distribution of electrostatic charge across the surface of the enzyme. Negatively charged surface patches are shown in red and positively charged surface patches are shown in blue. The putative peptide binding site is located in the vicinity of a negatively charged surface patch. Taken from Fiser *et al.* (2003).

GRASP analysis has shown that there is a negatively charged patch within the MurM model that is similar to that found at the active site of NMT. Within the MurM model, there are seven residues that participate in the formation of this negatively charged patch: E12, E19, E21, E48, D78, D81 and E126. It has been proposed that, should the model of MurM hold true, this area of the protein may participate in the binding of the positively charged lysine residue that is found at the third position of the pentapeptide side chain of Lipid II (Fiser *et al.*, 2003).

The model showing structural similarity between MurM and NMT is also supported by the knowledge that the most conserved segment between MurM and FemA is found between residues 66 and 84. This region is found in the negatively charged surface patch that is proposed to make up the peptide binding site of MurM and it is possible that this applies to FemA as well.

Originally the structure of FemA (Figure 1.14) was described as two repeated histone acetyl transferase domains with the implication that subdomain IA, which is the location of the proposed peptide binding site in the MurM model, is buried and inaccessible (Benson *et al.*, 2002).

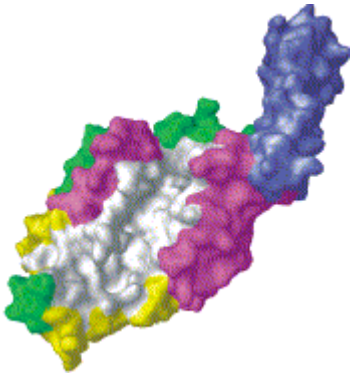

Figure 1.14: The X-ray crystal structure of FemA showing the proposed binding site for Lipid II (PDB code 1LRZ). Domain 1A is highlighted in yellow and comprises residues 1-110, 129-144 and 396-401. Domain 1B is highlighted in magenta and comprises residues 145-166, 189-245 and 308-395. Regions highlighted in green and blue show additional secondary structure elements in domains I and II respectively. Regions highlighted in white are proposed by Benson *et al.* (2002) to be part of the peptide binding site of the enzyme. Adapted from Benson *et al.* (2002).

As shown in Figure 1.14, Benson *et al.* (2002) propose that the only pocket in FemA that would be suitable for binding Lipid II is found across the surface of subdomain 1B. However, whilst the crystal structure was solved to 2.1 Å, there are 14 C-terminal residues as well as a 12 residue loop that could not be located on the electron density map. This could mean that a substantial part of the peptide binding cleft may not be visible and that the actual location of the site could well be within the negatively charged surface patch identified by Fiser *et al.* (2003) in both FemA and the model of MurM.

1.4.2.3. DNA binding proteins as homology models for MurM

The structural homology between the MurM model and a DNA binding protein from *M. jannaschi* has been used by Fiser *et al.* (2003) to hypothesise a possible relationship between MurM and penicillin resistance. The DNA-binding protein in *M. jannaschi* is similar to *E. coli* MarR and *Bacillus subtilis* BmrR, both of which

are transcription factors concerned with the expression of drug transporters (Ray *et al.*, 2003). In addition to this, one of the closet homologues to the protein is RU223 which is found in *S. aureus* where it is essential for high level β-lactam resistance (De Lencastre *et al.*, 1999). Thus it is possible that, by sharing some resemblance to transcription factors, MurM has a regulatory role in response to exposure of *S. pneumoniae* to antibiotics (Fiser *et al.*, 2003).

1.4.3. Kinetic characterisation of MurM

The kinetic activities of two variants of MurM from penicillin-sensitive strain Pn16 and penicillin-resistant strain 159 were characterised *in vitro* for the first time at the University of Warwick by Lloyd *et al*. (2008). At the amino acid level, $MurM_{Pn16}$ and $MurM_{159}$ show 18% divergence and kinetic characterisation was possible due to the ability to produce both the Lipid II and the tRNA substrate in sufficient quantities. UDP-MurNAc pentapeptide synthesis was achieved using purified forms of MurA to F. This was then converted to Lipid I and II using *Micrococcus flavus* membranes as described in Chapter 2. Key positions in the 3D predicted model of MurM where strain variation does and does not occur are shown in Figure 1.15.

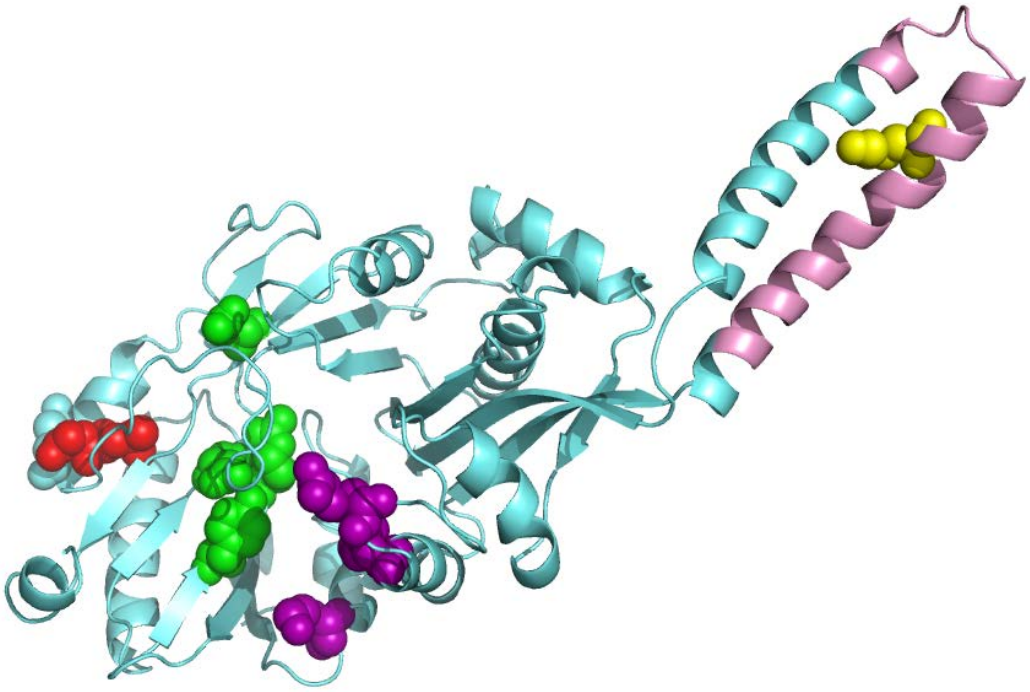

Figure 1.15: Schematic model of MurM based on the X-ray crystal structure of *Staphylococcus aureus* FemA (minus Lipid II and tRNA). Residues highlighted in red are found at positions 134 and 135 and can vary between strains. Residues highlighted in green show the putative catalytic site of the enzyme. Residues highlighted in purple show the putative peptide binding site. Residues highlighted in pink show positions 244-274 which are variable between strains and have been shown to be involved with amino acid selectivity of the enzyme. Position 260 is shown in yellow and is thought to be a key residue in amino acid selectivity with lysine giving rise to alanine addition and threonine giving rise to serine addition.

In the studies undertaken by Lloyd *et al.* (2008), both $MurM_{Pn16}$ and $MurM_{159}$ were cloned into the expression vector pET21b such that they were synthesised with a C-terminal hexa-histidine tag upon expression. Analysis of the peptidoglycan structure from both strains of *S. pneumoniae* demonstrated *in vivo* and, for the first time, *in vitro* that MurM supports the synthesis of the dipeptide bridge found on the Ɛ-amino group of the third lysine on the pentapeptide side chain of branched muropeptides. In addition to this, the proportion of branched muropeptides within the cell wall structure was shown to be consistent with the overall activity of the MurM enzyme in the strain of interest.

$MurM_{159}$ was found to preferentially add alanine to Lipid II whereas $MurM_{Pn16}$ showed a preference for serine addition. This finding is consistent with these enzymes having lysine and threonine at position 260 respectively. The activity of MurM was found to require aminoacylated tRNA species as shown in Table 1.5.

[^{3}H]- Acyl tRNA	**MurM**	**tRNA source**	**Specific activity (nmol.min^{-1}.mg^{-1})**
Alanyl-tRNA^{Ala}	Pn16	Pn16	0.172 ± 0.025
		159	0.175 ± 0.022
	159	Pn16	2.095 ± 0.285
		159	1.942 ± 0.466
Seryl-tRNA^{Ser}	Pn16	Pn16	0.370 ± 0.038
		159	0.247 ± 0.025
	159	Pn16	0.312 ± 0.055
		159	0.281 ± 0.096

Table 1.5: Determination of the activity of $MurM_{Pn16}$ and $MurM_{159}$ with Alanyl-tRNA^{Ala} and Seryl-tRNA^{Ser}. Assays were carried out in the presence of 10 µM Lipid II and 0.45 µM pneumococcal [H^3] Ala-tRNA^{Ala} or Ser-tRNA^{Ser}. Specific activities were calculated from initial rates of time courses usually within the first 3 min of the reaction. Taken from Lloyd *et al*. (2008).

The overall activity of $MurM_{Pn16}$ was shown to be lower in the case of both Ala-tRNA^{Ala} and Ser-tRNA^{Ser} than that of $MurM_{159}$ with Ala-tRNA^{Ala}. Interestingly, $MurM_{159}$ appeared to have a similar specific activity to $MurM_{Pn16}$ when assayed using Ser-tRNA^{Ser} as the co-substrate. From this study, it was also concluded that the differences in the proportion of branched structured muropeptides in the cell wall peptidoglycan of strains Pn16 and 159 was a result of $MurM_{159}$ having a higher catalytic efficiency than $MurM_{Pn16}$ with only a small contribution coming from the effect of tRNA pools within the strains themselves.

In-depth kinetic analysis allowed several key conclusions to be made regarding the two MurM variants:

(i) MurM acts at the lipid linked stages of peptidoglycan biosynthesis;

(ii) the D-alanyl-D-alanine dipeptide found at the fourth and fifth positions of the pentapeptide side chain of Lipid II are not required for the catalytic activity of MurM;

(iii) the GlcNAc moiety of Lipid II is not required for the catalytic activity of MurM;

(iv) carboxylation of the Ɛ-amino group of lysine at the third position in the pentapeptide side chain did not support MurM activity;

(v) Lipid II-alanine can be used as a substrate by MurM which suggests that there is a link between these enzymes and the Fem ligases of *S. aureus* in terms of evolution and;

(vi) MurM is able to interact with its tRNA substrate via recognition of either the acceptor stem or the TψC loop or both of these entities (Lloyd *et al.*, 2008).

In order to complement these studies, a series of phosphonamide transition-state analogues were synthesised as potential inhibitors of MurM by Cressina *et al.* (2007) at the University of Warwick. Design of these inhibitors was based on the hypothesis that the reaction catalysed by MurM is likely to proceed via the formation of a tetrahedral transition state that could be readily mimicked by a phosphonate or phosphonamide group as shown in Figure 1.16 (Cressina *et al.*, 2007; Cressina *et al.*, 2009).

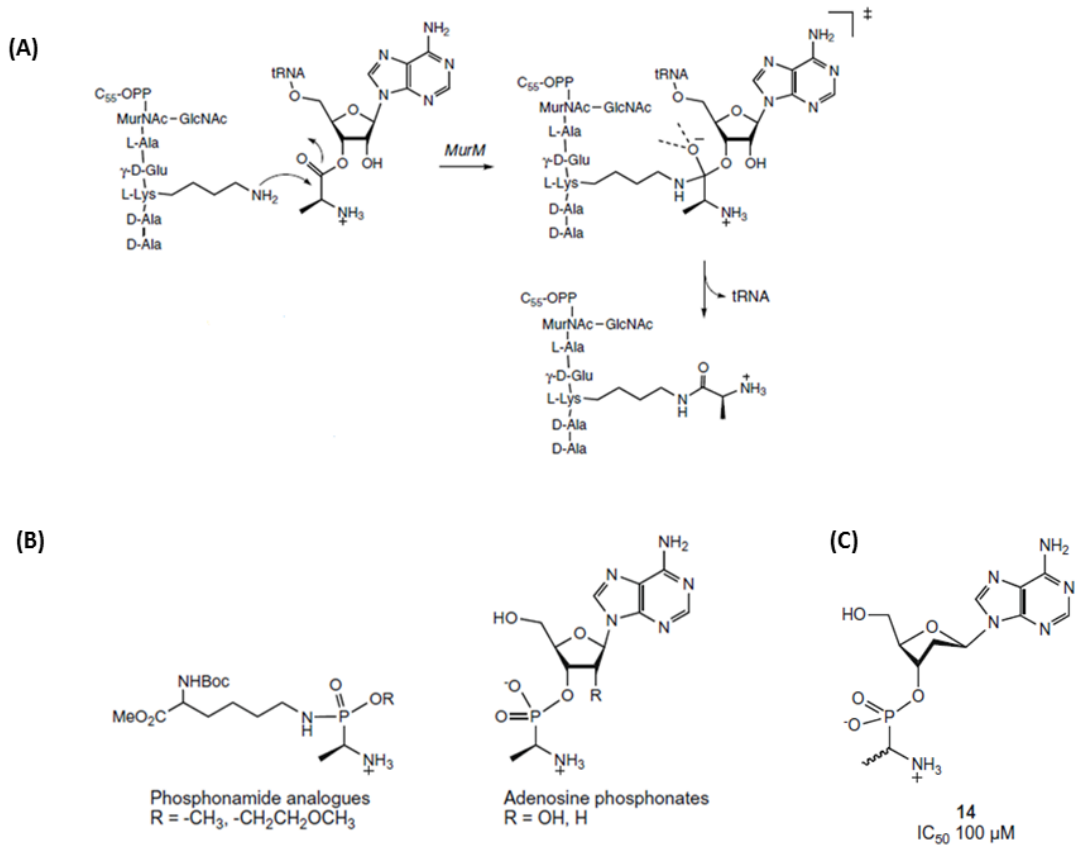

Figure 1.16: Summary showing the mechanism of the MurM-catalysed reaction which is likely to proceed via formation of a tetrahedral transition state (A). This transition state could be readily mimicked by a phosphonate or a phosphonamide group. The structure of the most active inhibitor of MurM synthesised so far is a 2'-deoxyadenosine analogue with an IC_{50} of 100 μM (C). Adapted from Cressina *et al.* (2007) and Cressina *et al.* (2009).

It was found that phosphonamide analogues of the transition state designed to mimic the attack of the lysine at position three of the pentapeptide side chain were not able to cause inhibition of MurM. However, some of the adenosine 3'-phosphonate analogues synthesised in these studies showed some inhibitory activity towards MurM with a 2'-deoxyadenosine analogue (Figure 1.16 C) being the most potent at an IC_{50} of 100 μM (Cressina *et al.*, 2007; Cressina *et al.*, 2009). Success of some of these compounds could lead to promising results in the future in terms of inhibition of enzymes in the Fem ligase family.

1.4.4. Kinetic characterisation of MurN

The MurN proteins from a penicillin-sensitive (Pn16) and a penicillin-resistant (159) strain of *S. pneumoniae* have also been characterised at the University of Warwick by De Pascale *et al*. (2008). In these studies $MurN_{Pn16}$ and $MurN_{159}$ expression could only be achieved by cloning the genes into pBADM-41 allowing for production of MurN fused to maltose binding protein.

Assessment of the kinetic activity of MurN was possible due to the development of a chemical means of synthesising the substrate for the enzyme: Lipid II-Ala or Lipid II-Ser. This methodology was developed by De Pascale *et al*. (2008) and involved synthesis of UDP-MurNAc pentapeptide followed by a chemical coupling reaction using alanine or serine protected at the N-terminus. The product of this reaction was then incubated with *M. flavus* membranes to generate Lipid II as described in chapter 2. Activity assays using this substrate showed that MurN requires Alanyl-$tRNA^{Ala}$ for activity. In addition, both $MurN_{Pn16}$ and $MurN_{159}$ had a catalytic efficiency that was 20-fold higher when presented with Lipid II-Ala compared to Lipid II-Ser. These studies indicated that MurN cannot use Lipid II which confirms that the activity of MurM is required prior to the addition of alanine as the second amino acid of the cross bridge. The kinetic parameters obtained for the two variants of MurN showed no real divergence from each other despite the difference in penicillin sensitivity of the two strains from which they were derived (De Pascale *et al.*, 2008).

1.5. The role of the FemX, A and B proteins in *Staphylococcus aureus*

S. aureus is a well-known human pathogen that is responsible for causing various pathologies including abscesses in several organ tissues and septicaemia (Mazmanian *et al.*, 2001). Cross-linking in the peptidoglycan of this organism requires the formation of a pentaglycine interpeptide bridge via modification of the Lipid II intermediate (Schleifer and Kandler, 1972). Interpeptide bridge formation is now known to be catalysed by the action of the FemX (FhmB), FemA and FemB proteins (whereby Fem stands for factors essential for methicillin resistance) and utilises three tRNA species that have been charged with glycine as shown in Figure 1.17.

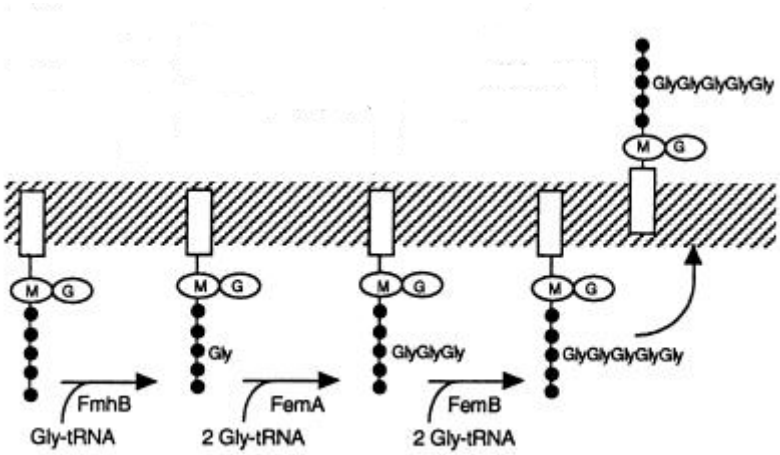

Figure 1.17: The role of the FemX (FmhB), FemA and FemB proteins in the cross-linking of *Staphylococcus aureus* peptidoglycan. All three enzymes require tRNA species that have been aminoacylated with glycine. M = N-acetylmuramic acid and G = N-acetylglucosamine. The black circles represent the pentapeptide side chain. Adapted from Rohrer *et al*. (1999).

Prior to the identification of FemX, FemA and FemB, investigation into the formation of cross-links within the cell wall of *S. aureus* indicated that Glycyl-$tRNA^{Gly}$ was a requirement for the process. As a result, it was initially thought that

the formation of the pentaglycine bridge would require the involvement of the ribosomes. However, this was disproved when it was found that inhibitors of protein synthesis did not affect the process and that the addition of the five glycine residues was sequential with elongation occurring from the amino terminus (Kamiryo and Matsuhashi, 1972; Rohrer and Berger-Bachi, 2003b).

Whilst the identity of the FemX protein remained elusive for some time, knock-out of the *femAB* genes by allelic replacement with *tetK* resulted in the generation of an unusual peptidoglycan structure containing monoglycine bridges. The overall level of cross-linking was severely reduced in the knock-out mutants and complementation with either *femA* or *femAB* resulted in an increase in length of the cross bridge to tri-glycine or tetra-glycine respectively (Stranden *et al.*, 1997). These studies provided the first experimental evidence for the existence of a third protein, now known to be FemX, whose activity was required for the addition of the first glycine residue of the cross bridge.

In addition to this, reduction of transcription from the *femAB* operon via insertion of Tn551 resulted in several significant phenotypes including (i) a reduction in the cell wall glycine content concurrent with a reduction in overall levels of peptidoglycan cross-linking; (ii) a reduction in cell wall turnover; (iii) disruption to cell septum formation; (iv) retarded separation of cells and; (v) loss of methicillin resistance and an increase in sensitivity to β-lactam antibiotics. Further studies investigating selective knock-out of either *femA* or *femB* showed that cells containing such deletions were viable but only because they had acquired a series of complementary mutations necessary for their survival under these circumstances. This suggests that

femAB inactivation is lethal without the acquisition of complementary mutations and that the activity of FemX is essential for cell viability (Ling and Berger-Bachi, 1998).

The true identity of FemX was discovered upon sequencing of the *S. aureus* genome allowing for the identification of three genes; *fmhA, fmhB* and *fmhC,* which show homology to *femA* and *femB*. Of these genes only *fmhA* and *fmhC* could be inactivated without any noticeable changes in phenotype. In contrast, inactivation of *fhmB* was not tolerated making it the likely candidate for FemX (Tschierske *et al.*, 1999).

Confirmation of the role of the protein product of *fhmB* in the synthesis of the pentaglycine bridge was achieved by Rohrer *et al*. (1999). In this study, the promoter for the *fhmB* gene was replaced by the xylose regulon from *Staphylococcus xylosus* enabling glucose-mediated control of transcription from the *fhmB* gene. Upon depletion of FhmB from cells, there was a notable accumulation of peptidoglycan monomers that were not substituted with any glycine residues. This proved the involvement of FhmB, which is now more commonly called FemX, in the addition of the first glycine residue to the pentapeptide side chain of Lipid II. It was also noted that deletion of *femX* resulted in a loss of resistance to methicillin despite the presence of the required low affinity form of PBP2a (Rohrer *et al.,* 1999). This suggests that this PBP requires the presence of the pentaglycine side chain in order to function correctly. It has also been shown that the presence of the pentaglycine bridge is essential for optimum activity of the sortase protein which anchors various

surface proteins including virulence factors to the staphylococcal cell wall (Ton-That *et al.*, 1998).

Additional studies have shown that pentaglycine bridge formation can be reconstructed *in vitro* using purified forms of FemX, FemA, FemB, Glycyl-tRNA synthetase, UDP-MurNAc pentapeptide, Lipid I, Lipid II and a pool of *S. aureus* tRNA (Schneider *et al.*, 2004). Use of the *in vitro* system indicated that the substrates for FemX, FemA and FemB were exclusively Lipid II, Lipid II-Gly and Lipid II-Gly-Gly respectively. It was also shown that all three enzymes were capable of carrying out catalysis independently of each other. It has recently been confirmed that the *S. aureus* genome encodes five $tRNA^{Gly}$ genes, three of which are likely to be directed away from protein synthesis and used as donors for peptidoglycan synthesis. Thus, one proposition is that each of the three Fem enzymes is specific for one of three specific tRNA species (Giannouli *et al.*, 2009).

After the X-ray crystal structure of FemA was solved by Benson *et al*. (2002), it was hypothesised that the protein has a single binding site for the tRNA substrate. This would result in the requirement for an additional tRNA-binding reaction to add the second glycine residue. However, protein-protein interactions have been found to occur between two monomers of FemA, two monomers of FemB and a combination of FemA and FemB. No such interactions were seen in the case of FemX which suggests that it acts as a monomer whilst FemA and FemB act as homodimers. Dimerisation of FemA and FemB would allow two glycine residues to be added to the Lipid II substrate without the need for additional tRNA binding reactions (Rohrer and Berger-Bachi, 2003a). However, more detailed structural studies on the enzyme

with the bound tRNA substrate will provide further insight into the catalytic mechanism of the enzyme.

1.6. The role of Lif and Epr in *Staphylococcus simulans* and *Staphylococcus capitis*

S. simulans and *S. capitis* both produce glycyl-glycine endopeptidases which are able to cleave the pentaglycine bridges that are found in the cell wall of Staphylococci. In order to protect themselves from such enzymes, *S. simulans* produces lysostaphin immunity factor (Lif) and *S. capitis* produces endopeptidase resistance factor (Epr). Lif and Epr are broadly termed FemAB-like factors because they show 41% identity to these enzymes and catalyse the insertion of serine instead of glycine at position three and position five of the pentaglycine bridge respectively. The resulting peptidoglycan structure, which has an interpeptide bridge comprised of alternating serine and glycine, is protected from hydrolysis by the Glycyl-glycine endopeptidases as they are unable to break the peptide bonds between these two residues.

Interestingly, in the background of a *femAB* knock-out, Lif and Epr are not able to extend the monoglycine cross bridge produced by FemX. This suggests that these proteins require FemA and FemB for activity (Ehlert *et al.*, 2000).

1.7. The role of FemX in *Weissella viridescens*

The FemX protein of *W. viridescens* is a well characterised member of the Fem ligase family of non-ribosomal peptidyl-transferases. Like MurM, FemX uses aminoacylated tRNA species to add the first amino acid of an L-alanine-L-serine

cross bridge within the peptidoglycan structure. The second amino acid is added by an unknown enzyme as shown in Figure 1.18. The substrate for *W. viridescens* FemX is the cytoplasmic precursor, UDP-MurNAc pentapeptide. This contrasts with the substrate specificity of many of the other Fem ligases, including MurMN and FemXAB, which either preferentially or exclusively utilise the membrane bound precursor Lipid II (Maillard *et al.*, 2005).

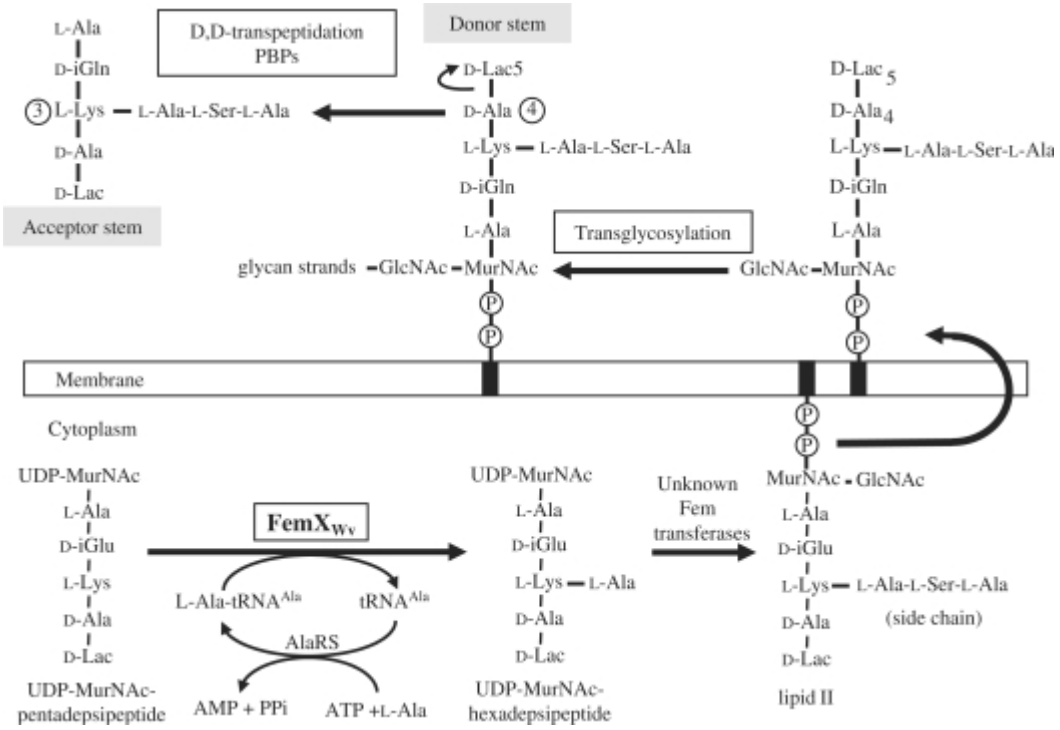

Figure 1.18: Summary of the pathway of peptidoglycan biosynthesis in *Weissella viridescens*. FemX is responsible for the addition of the first residue of the L-ala-L-ser-L-ala cross bridge onto the nucleotide precursor UDP-MurNAc-pentapeptide. This reaction requires Ala-tRNA^{Ala} as a substrate for FemX. Ala-tRNA^{Ala} is generated by the activity of alanyl-tRNA synthetase (AlaRS). Additional unknown Fem transferases add the second (L-ser) and third (L-ala) residues of the side chain. Taken from Fonvielle *et al*. (2009).

A series of kinetic analyses have been carried out *in vitro* on purified FemX from *W. viridescens*. This has demonstrated that the catalytic mechanism of the enzyme is a highly ordered process which proceeds sequentially through four stages. Binding of

UDP-MurNAc to the enzyme is followed by the binding of Alanyl-tRNA^{Ala}. This then results in the transfer of alanine from the tRNA carrier to the epsilon amino group of L-lysine found at the third position of the pentapeptide side chain. Finally the carrier tRNA and the UDP-MurNAc hexapeptide product are released from the enzyme. The aspartate residue found at position 108 within FemX is thought to be a catalytic site residue since mutation to asparagine caused a 230-fold reduction in catalytic efficiency (Hegde and Blanchard, 2003).

The X-ray crystal structure of FemX in the presence and absence of UDP-MurNAc pentapeptide was solved by Biarrotte-sorin *et al*. (2004). FemX consists of two globular domains which are equivalent to each other in terms of structure. These two domains are separated from each other by a cleft which forms the binding site for UDP-MurNAc pentapeptide as shown in Figure 1.19.

Figure 1.19: X-ray crystal structure of *Weissella viridescens* FemX with bound UDP-MurNAc pentapeptide (PDB code 3GKR). The region highlighted in blue shows domain I of the protein (residues 1-145 and 317-335). The region highlighted in magenta represents domain II (residues 146-316). UDP-MurNAc pentapeptide is shown in orange and is mostly in contact with domain one of the protein. Adapted from Biarrotte-Sorin *et al*. (2004).

As shown in Figure 1.19, UDP-MurNAc pentapeptide is bound mostly to the first domain making many polar contacts with the enzyme. The uracil ring found on the UDP-MurNAc moiety of the substrate makes a hydrogen bond with tyrosine-103 and is also stabilised by stacking interactions with phenylalanine at position 70 in FemX. The MurNAc ring appears to be completely exposed to the solvent and only D-glutamate and the terminal D-alanyl-D-alanine dipeptide appear to interact with FemX. Interaction of these pentapeptide side chain residues is through threonine-209 in the case of D-glutamate and through a combination of arginine-211, tyrosine-256 and tyrosine-215 in the case of the terminal D-alanyl-D-alanine (Biarrotte-Sorin *et al.*, 2004).

Site directed mutagenesis of lysine-36 and arginine-211 to methionine has been shown to have a significant detrimental effect on the catalytic activity but not on the structure of FemX. In addition to this, analogues of UDP-MurNAc pentapeptide that either do not have any of the phosphate groups or are missing the terminal D-alanyl-D-alanine dipeptide cannot be utilised as substrate by FemX. Taken together, these two findings have suggested that lysine-36 and arginine-211 are essential in the formation of hydrogen bonds that stabilise the enzyme-substrate complex and enable the reaction to proceed (Maillard *et al.*, 2005).

The major difference between the structure of *S. aureus* FemA and that of *W. viridescens* FemX is the absence of the coiled helical arm structure in the latter. The overall structure of FemX suggests that domain I and II may have distinct roles with the former being concerned with the binding UDP-MurNAc pentapeptide and the latter in tRNA binding. This proposition is supported by the fact that there is a long

positively charged channel running across domain II of FemX which would be able to complement the negatively charged backbone of Alanyl-tRNA^{Ala}.

The interaction between FemX and its tRNA substrate has been partially characterised by modification of both the tRNA and the amino acid moiety of the substrate. These studies have demonstrated that FemX preferentially adds alanine to the third lysine of UDP-MurNAc pentapeptide because it interacts much more unfavourably with L-serine and the acceptor arm of tRNA^{Gly}. *In vitro* activity assays have demonstrated that FemX utilises Ser-tRNA^{Ser} and Gly-tRNA^{Gly} 17 and 38-fold less efficiently than it uses Ala-tRNA^{Ala} as a substrate respectively. Site-directed mutagenesis has shown that the penultimate base pair of tRNA^{Ala}, G^{2}-C^{71}, is an essential identity element for FemX. This is replaced by C^{2}-G^{71} in tRNA^{Gly} species (Villet *et al.*, 2007).

Further investigations into the specificity of the interaction between FemX and its tRNA substrate have recently been carried out by Fonvielle *et al*. (2009 and 2010). Aminoacyl-tRNA synthetases are responsible for transferring amino acid residues from an adenylate species to either the 2' or the 3' position of the terminal nucleotide (A^{76}) of a molecule of tRNA. Upon completion of this process, spontaneous trans-esterification occurs resulting in flipping of the amino acid residue between these two positions.

Prior to these studies, the effect of spontaneous trans-esterification on the recognition of tRNA by members of the Fem ligase family had not been investigated. However, as shown in Figure 1.20, the A site of the ribosome was known to be specific for

tRNA species carrying the amino acid on the 3' hydroxyl group with the 2' hydroxyl group aiding the catalysis of peptide bond formation (Weinger *et al.*, 2004).

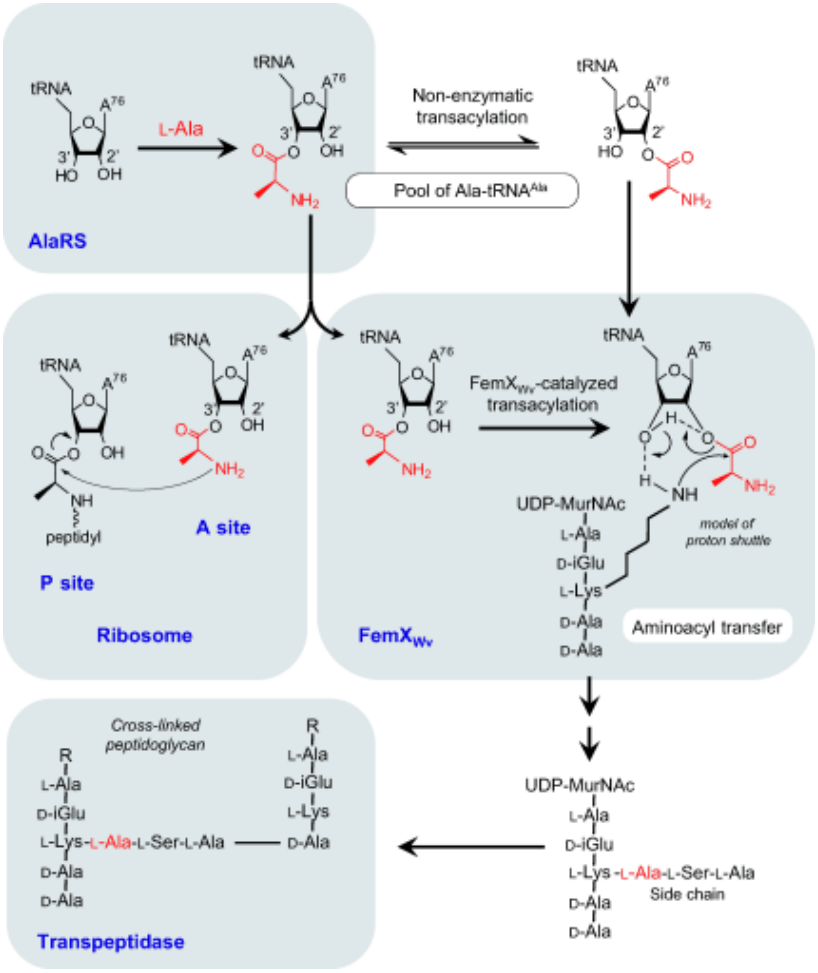

Figure 1.20: Summary of the participation of Ala-tRNA^{Ala} regioisomers aminoacylated on either the 2' or the 3' hydroxyl group in protein and peptidoglycan synthesis. The enzymes catalysing the reactions shown in this diagram are given in blue. FemX is responsible for the transfer of alanine from Ala-tRNA^{Ala} to the side chain of L-lys in UDP-MurNAc pentapeptide. R is used to represent the backbone of peptidoglycan which is comprised of alternating N-acetylglucosamine and *N*-acetylmuramic acid residues. UDP = uridine diphosphate. Taken from Fonvielle *et al.* (2010).

In order to determine the specificity of FemX for the 2' and 3' regioisomers of Ala-tRNA^{Ala}, a series of non-isomerisable analogues, shown in Figure 1.21, were chemically synthesised by Fonvielle *et al.* (2010). In compounds A and B, alanine is

locked at the 2' and 3' hydroxyl group of the terminal adenine residue respectively. Compound C represents the natural substrate for the enzyme whereby alanine can transfer freely between the 2' and 3' hydroxyl of the terminal adenine residue.

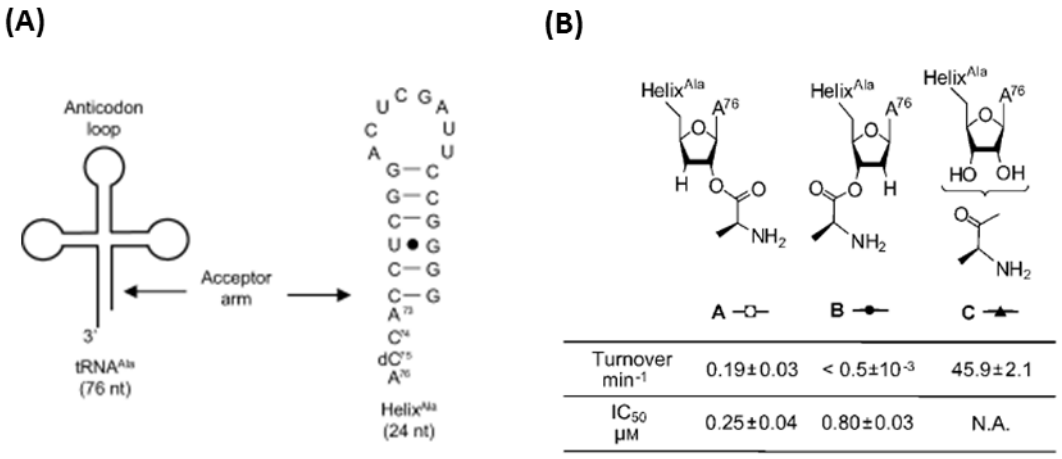

Figure 1.21: Non-isomerisable analogues of Ala-tRNA^{Ala} used by Fonvielle *et al*. (2010) to determine the regio-specificity of *Weissella viridescens* FemX for its tRNA substrate. All analogues consist of the 24-nucleotide acceptor arm helix of tRNA^{Ala} shown in (A) and either a terminal 3′ deoxyadenosine (compound A), a terminal 2′ deoxyadenosine (compound B), or a terminal adenosine residue (compound C) shown in (B). Compounds A, B and C were assayed as substrates (see turnover number) and as inhibitors in the presence of full-length Ala-tRNA^{Ala}. Adapted from Fonvielle *et al*. (2010).

Activity assays demonstrating turnover of compound A, but not of compound B, by *W. viridescens* FemX indicated that the enzyme recognises tRNA^{Ala} that has been aminoacylated on the 2' position of the terminal adenine as its true substrate. Given that alanyl-tRNA synthetase is known to aminoacylate tRNA^{Ala} at the 3' position, these results suggest that FemX first catalyses trans-acetylation of the amino acid to the 2' position of the tRNA molecule prior to its transfer to the third lysine of UDP-MurNAc pentapeptide. Compounds A and B were also tested as inhibitors of FemX using full-length Ala-tRNA^{Ala} as the substrate. Compound B, which was not utilised as a substrate by the enzyme, was shown to cause inhibition with an IC_{50} of 0.8 µM.

This suggests that $tRNA^{Ala}$ species that carry alanine at the 3' position can still bind to FemX even though transfer of the amino acid to UDP-MurNAc pentapeptide is not catalysed from this position. This would enable FemX to sequester the aminoacylated Ala-$tRNA^{Ala}$ species produced by alanyl-tRNA synthetase in competition with the ribosome. Compound A was found to inhibit the enzyme three times more efficiently than compound B clearly indicating that FemX catalyses transfer of the amino acid from the 2' hydroxyl group which then enables release of $tRNA^{Ala}$ from the enzyme (Fonvielle *et al.*, 2009; Fonvielle *et al.*, 2010). The regio-specificity of other Fem ligases for their tRNA substrates has not yet been investigated.

1.8. The role of BppA1 and BppA2 in *Enterococcus faecalis*

The peptidoglycan of *E. faecalis* contains indirect cross-linkages that are comprised of two alanine residues attached to the Ɛ-amino group of L-lysine found at the third position of the pentapeptide side chain of UDP-MurNAc. This process requires alanyl-tRNA synthetase, Alanyl-$tRNA^{Ala}$ and two Fem ligases called BppA1 and BppA2.

BppA1 transfers the first alanine residue of the cross-link to its cytoplasmic substrate, UDP-MurNAc pentapeptide. BppA1 is an orthologue of *S. pneumoniae* MurM and shares 39% sequence identity with this protein. The second amino acid is added by BppA2, which has 38% sequence identity to *S. pneumoniae* MurN. BppA1 and BppA2 are able to function independently of each other such that deletion of *bppA2* causes the generation of a peptidoglycan structure where the indirect cross-bridge is comprised of mono-alanine. Peptidoglycan monomers branched by these incomplete side chains were still accepted as substrates by the PBPs, however,

expression of β-lactam resistance was reduced. This suggests that the low affinity penicillin-binding proteins require the complete L-ala-L-ala bridge for full β-lactam resistance (Bouhss *et al.*, 2002).

1.9. The role of FemX and VanK in *Streptomyces coelicolor*

Streptomyces coelicolor has a series of seven genes within its genome, termed *VanSRJKHAX*, that are required for high-level vancomycin resistance. Within this gene cluster, *vanK* is known to encode a transferase that is a member of the Fem ligase family. In addition to this, *S. coelicolor* also has a second Fem ligase, FemX, which is encoded on a different part of the chromosome and utilises soluble UDP-MurNAc pentapeptide as opposed to Lipid II as a substrate. Both of these proteins are involved with the formation of the mono-glycine branch found within the peptidoglycan of this organism. However, they are functional under different conditions and are thus not active at the same time.

In the absence of vancomycin, FemX, which recognises UDP-MurNAc pentapeptide that terminates in D-alanyl-D-alanine, is active and responsible for the addition of mono-glycine to the third position of the side chain. However, in the presence of vancomycin, a two component regulatory system, VanRS, switches on expression of the vancomycin gene cluster. This results in the VanHAX enzymes terminating the pentapeptide side chain of UDP-MurNAc in D-alanyl-D-lactate instead of D-alanyl-D-alanine thus conferring resistance to the antibiotic. FemX cannot recognise UDP-MurNAc pentapeptide when it terminates in D-alanyl-D-lactate and hence cannot branch the precursor in the presence of vancomycin. Therefore, the activity of FemX is replaced by that of VanK under these conditions as shown in Figure 1.22.

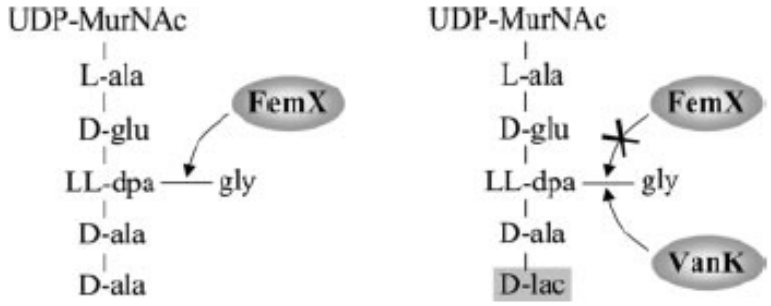

Figure 1.22: The role of FemX and VanK in *Streptomyces coelicolor* in the absence (left) and the presence (right) of vancomycin. Taken from Hong *et al.* (2005).

In wild-type *S. coelicolor* cells that are exposed to vancomycin, the presence of D-lactate containing precursors carrying the mono-glycine branch can be detected. This is not the case in *vanK* knockout mutants. Mutations in *femX* only result in loss of cell viability in the absence of vancomycin further confirming the interchangeable nature of these two enzymes (Hong *et al.*, 2005).

1.10. The role of Asl_{fm} in *Enterococcus faecium*

The peptidoglycan of *Enterococcus faecium* contains D-iso-asparagine on the Ɛ-amino group of the third lysine on the pentapeptide component of UDP-MurNAc pentapeptide. In 1972, it was shown that this reaction was ATP-dependent and involved the activation of D-aspartate as β-aspartyl-phosphate (Staudenbauer and Strominger, 1972; Staudenbauer *et al.*, 1972). However, the enzymes involved in this process were not identified for another 34 years after this study (Bellais *et al.*, 2006).

Reverse genetics identified a gene cluster in *E. faecium* encoding aspartate racemase (Rac_{fm}) and ligase (Asl_{fm}) which, together, are required for the incorporation of D-aspartate onto the side chain of peptidoglycan precursors. The D-aspartate residue

then undergoes amidation on its α-carboxyl group to form the D-iso-asparagine residue that makes the indirect branch within *E. faecium* peptidoglycan as shown in Figure 1.23.

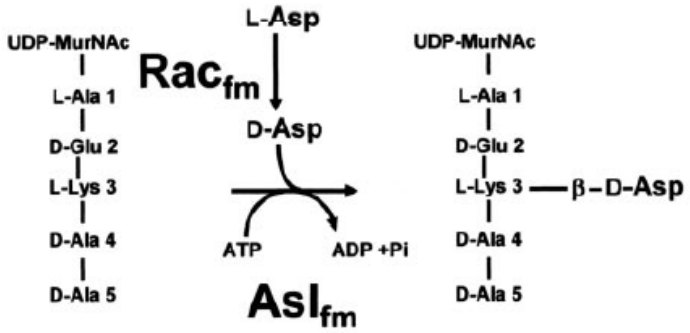

Figure 1.23: Incorporation of D-aspartate by Rac_{fm} and Asl_{fm} onto the epsilon amino group of lysine in *Enterococcus faecium* peptidoglycan. Taken from Bellais *et al*. (2006).

Characterisation has shown that Asl_{fm} is a member of the ATP-grasp family of proteins which encompasses a wide range of enzymes that carry out ATP-dependent carboxylate amine ligations. This enzyme is highly specific and, when expressed in *E. faecalis*, indirect cross bridges in the cell wall structure change in composition from two alanine residues to a single D-aspartate. Genes that are homologous to the Asl_{fm} protein of *E. faecium* have been found in all ten of the genomes of bacteria that are known to produce precursor molecules that contain D-aspartate residues. No such homologues were found in any of the species which generate indirect cross-links in their cell wall peptidoglycan using members of the Fem ligase family. This suggests that D-amino acids are incorporated into peptidoglycan by one closely related family of enzymes that are very specialised in terms of their function (Bellais *et al.*, 2006).

1.11. Other enzymes involved in non-ribosomal peptide synthesis

1.11.1. Protein argininyl and phenylalanyl/leucyl transferases

One mechanism by which protein turnover is regulated in prokaryotic and eukaryotic cells is by application of the N-end rule. This pathway is based on the addition of a single amino acid residue to the N-terminus of a protein which modifies its half-life and ultimately results in targeting for degradation. One mechanism of amino acid extension at the N-terminus of proteins involves transfer from aminoacylated tRNA species. This tRNA-dependent method of regulation of protein turnover can occur in both prokaryotes and eukaryotes via L/F and R transferases respectively. L/F transferases catalyse the transfer of either leucine or phenylalanine to the N-terminal arginine or lysine of the protein that must be targeted for degradation. Whilst the N-termini of these transferases can be considered unique to this family of enzymes, the C-termini shares distinct homology with the Fem ligase family (Francklyn and Minajigi, 2010).

1.11.2. MprF proteins

MprF proteins are virulence factors that control the permeability of the cell wall to cationic antimicrobials by catalysing the aminoacylation of inner membrane lipids. Aminoacylation of membrane lipids adjusts the net negative charge of the membrane bilayer in a manner that is dependent on the aminoacylated tRNA substrate. The most well characterised MprF proteins are the aminoacyl-phosphatidylglycerol synthases (aa-PGSs). These enzymes are broadly distributed across bacteria and transfer amino acids from aminoacylated tRNA molecules to the polar head group of phosphatidylglycerol. The most common amino acid to be transferred is lysine causing an increase in the net positive charge of the cytoplasmic membrane which, in

turn, lowers permeability to cationic molecules including defensins, aminoglycosides, β-lactams and glycopeptides. Recently, aa-PGSs that are able to transfer amino acids other than lysine to phosphatidylglycerol have been discovered. *Clostridium perfringens* and *Pseudomonas aeruginosa* have Ala-PGSs which are able to aminoacylate phosphatidylglycerol with alanine and thus neutralise the overall charge of the membrane. This modification has been shown to enhance the resistance of *P. aeruginosa* to a multitude of negatively-charged β-lactam antibiotics, such as oxacillin and methicillin (Ernst and Peschel, 2011).

1.11.3. VlmA in *Streptomyces viridifaciens*

Streptomyces viridifaciens naturally synthesises valanimycin which is an antibiotic derived from L-valine and L-serine. There are two intermediates in the formation of valanimycin and these are isobutylamine and isobutylhydroxylamine. In order to synthesise this compound, *S. viridifaciens* has a biosynthetic cluster made up of 14 genes. One of the genes in this cluster, *vlmL*, encodes a seryl-tRNA synthetase enzyme which catalyses the transfer of serine from seryl-$tRNA^{Ser}$ to the hydroxyl group of isobutylhydroxylamine. The reaction catalysed by VlmL is essential for the production of valanimycin and this enzyme shares the GNAT fold found in Fem ligases and the L/F and R transferases described in section 1.11.1 (Garg *et al.*, 2008; Aravind *et al.*, 2010).

1.11.4. Cyclodipeptide synthases

Cyclodipeptide synthases are a new class of enzymes that have only recently been defined. These enzymes also utilise aminoacylated tRNA species as a substrate, this time for the production of numerous cyclodipeptides which form the precursors of a

wide range of natural products. However, structurally they show much more homology with tRNA synthetase enzymes than they do with members of the Fem ligase family. One class of cyclodipeptide synthase is AlbC which is commonly involved in secondary metabolite production. Members of the AlbC family are responsible for the synthesis of the antibiotic albonoursin in *Streptomyces noursei* and of the siderophore pulcherriminic acid in *B. subtilis* (Aravind *et al*., 2010; Sauguet *et al*., 2011).

1.12. Aims

The increase in the global prevalence of multidrug-resistant strains of *Streptococcus pneumoniae* is becoming a major concern. Most strains are now resistant to the β-lactam class of antibiotic which targets the final stages of peptidoglycan synthesis. For this reason, there is an urgent need for new drug targets and compounds to alleviate this problem. Given that peptidoglycan is unique to prokaryotic cells, it is still an ideal target for antibiotic design and there is an increasing amount of interest in targeting the enzymes involved in the cytoplasmic and lipid linked stages of peptidoglycan biosynthesis. Currently the MurMN proteins of *S. pneumoniae* and the Fem ligases of other pathogens are under-explored as targets for novel antibiotic design even though their inhibition has the potential to restore the activity of many clinically approved antibiotics including penicillin.

The main objective of this project was to investigate the relationship between levels and types of amino acids used in indirect cross-linking within pneumococcal peptidoglycan across a range of penicillin-resistant and penicillin-sensitive strains. In addition, the secondary aim of this work was to determine how differences between amino acid preference and the proportion of indirect cross-linkages in the cell wall relate to the structure and function of allelic variants of the MurM protein from these strains. The two main aims can be broken down into the following objectives:

1. Cloning, over-expression and purification of the *murM* gene from penicillin-resistant and penicillin-sensitive strains of *S. pneumoniae*. Strain R6 is particularly unusual since it is penicillin-sensitive despite having a relatively high-level of indirect cross-linkage within its

peptidoglycan. Therefore characterisation of the MurM protein from this strain may give a better understanding of the link between MurM activity, the proportion of branched muropeptides in the cell wall and levels of penicillin resistance.

2. Obtaining MurM protein of suitable purity and homogeneity for use in structural studies, including crystallography.

3. Comparing the kinetic activities of different allelic variants of MurM proteins with Lipid II, Ala-tRNA^{Ala} and Ser-tRNA^{Ser}.

4. Identification of amino acids important in conferring relative levels of MurM ligase activity and amino acid selectivity.

It is hoped that extensive characterisation of MurM will allow for a greater understanding of its overall role within *S. pneumoniae* and that this will shed some light onto its relationship to penicillin resistance. Ultimately, a greater understanding of MurM and other Fem ligases will aid successful drug design against these enzymes in the future which could vastly improve the success rate of treatment regimens for a variety of bacterial infections.

Chapter 2

Materials and Methods

2.1. Chemicals, Reagents, Buffers and Growth Media

2.1.1. Chemicals and Reagents

Unless otherwise stated, all chemicals used in this project were supplied by Melford Laboratories Ltd (UK), Fisher Scientific (UK), Fluka (Germany), Acros organics (Belgium), Sigma-Aldrich (USA), MERCK (USA) and Geneflow (UK).

2.1.2. Buffers

All buffers were prepared using MilliQ water and pH was adjusted using a Jenway pH meter calibrated with pH 4.01, 7.01 and 10.01 buffers provided by Hanna Instruments (UK). Solutions used for crystallography were passed through a Ministart 0.2 µM hydrophilic syringe filter provided by Sartorius Stedim Biotech (France) prior to use. Buffers used for tRNA preparation and handling were autoclaved at 15 psi for 20 min at 120^{o}C prior to use.

2.1.3. Bacterial growth and maintenance

All strains of *Escherichia coli* were grown and maintained in Luria-Bertani (LB) medium comprised of 12.5 g Bacto-tryptone, 6.25 g yeast extract and 12.5 g NaCl L^{-1} at pH 7.5. Super optimal broth supplemented with catabolite repression (SOC) medium for cell recovery after heat shock was comprised of 20 g Bacto-tryptone, 5 g Bacto-yeast extract, 0.5 g NaCl, 2.5 mL 1 M KCl and 20 mL 1 M glucose L^{-1} at pH 7.0.

All strains of *Streptococcus pneumoniae* and *Micrococcus flavus* were obtained from the University of Warwick culture collection. Both were grown and maintained in Tryptic Soy Broth (TSB) which consisted of 30 g of dehydrated TSB medium made up to 1 L with MilliQ water.

Auto-induction medium for protein expression was comprised of 20 mL 50 x 5052, 50 mL 20 x NPS and 1 mL of 1 M $MgSO_4$ made up to 1 L with LB (Studier, 2005). 50 x 5052 and 20 x NPS were made up as described in Studier (2005). All of these growth media components were autoclaved at 15 psi for 20 min at 120^{o}C prior to use.

2.2. Cloning and manipulation of DNA

2.2.1. Genomic DNA extraction

For the purposes of DNA extraction, *Streptococcus pneumoniae* strains Pn16, 159 and R6 were plated out on TSB agar to obtain single colonies. Plates were incubated for 2 days at 37^{o}C in an atmosphere comprised of 50% carbon dioxide. For each strain, a single colony was selected and re-cultured until a lawn of cells across 6 TSB plates was obtained. These cells were then resuspended in 1 mL of TSB and processed using the Promega Wizard Genomic DNA Purification Kit following the protocol for isolation of DNA from Gram-positive bacteria. The purified DNA was quantified using a nanodrop spectrophotometer prior to use in PCR. Genomic DNA was extracted from *Staphylococcus aureus* strain Mu50 in the same way.

2.2.2. Amplification of genes using the Polymerase Chain Reaction (PCR)

Standard PCR amplifications were carried out in 50 µL volumes using an Eppendorf mastercycler and either Pfx or Accuprime *Taq* DNA polymerase from Invitrogen. A typical PCR amplification consisted of the components shown in Table 2.1.

PCR using Accuprime *Taq* DNA polymerase	
Component	**Volume (µL)**
10 x Accuprime PCR buffer 2	10.0
Forward primer (10 µM)	2.0
Reverse primer (10 µM)	2.0
Template DNA (10 ng μL^{-1})	2.0
Accuprime *Taq*	0.5
MilliQ water	83.5
PCR using Pfx *Taq* DNA polymerase	
Component	**Volume (µL)**
10 x Pfx amplification buffer	5.0
10 x enhancer solution	5.0
Forward primer (10 µM)	1.0
Reverse primer (10 µM)	1.0
10 mM dNTP mix	1.5
50 mM $MgSO_4$	1.0
Template DNA (10 ng μL^{-1})	2.0
Pfx *Taq*	0.5
MilliQ water	33.0

Table 2.1: Composition of a typical PCR reaction using either Accuprime or Pfx *Taq* DNA polymerases from Invitrogen. Accuprime *Taq* was used in the first instance. Pfx *Taq* was used for difficult PCR reactions since specificity and efficiency of amplification could be improved by the addition of 10 x enhancer.

In each case, a typical PCR amplification was subjected to denaturation at 94^{o}C for 2 min. This was followed by 35 cycles of denaturation at 94^{o}C for 30 sec, annealing at 55-68^{o}C for 30 sec and extension at 68^{o}C for 1 min per kb of DNA. After cycling, a final extension step was carried out at 68^{o}C for 10 min and the reactions were then

held at 4°C. Annealing temperature was varied according to the melting temperature of the primers to maximise the overall yield of PCR product obtained.

All of the primers used in this study were synthesised either by Invitrogen or Integrated DNA Technologies (IDT) and purified by standard de-salting unless otherwise stated. Primer sequences used for cloning and sequencing are shown in Table 2.2.

Primer number	Primer name	Primer sequence (5' to 3')	Incorporated sites
1	R6 and Pn16 MurM forward primer	TTTGCGGGATCCCATATG TACCGTTATCAAATTGGC ATTCC	*Bam*HI and *Nde*I
2	159 MurM forward primer	TTTGCGGGATCCCATATG TATCGTTATCAGCTTGGG AT	*Bam*HI and *Nde*I
3	R6 MurM reverse primer (C-terminal 6 histidine tag)	TTTGCGCTCGAGCTTTCTA TGTTTTTTTCTTAATGTTT TACGG	*Xho*I
4	MurM reverse primer (C-terminal 12 histidine tag)	TTTGCGCTCGAGGTGGTG GTGGTGGTGGTGCTTTCT ATGTTTTTTTCTTAATGTT TTACGG	*Xho*I, hexa-histidine tag not encoded by the vector (HPLC purified)
5	FemA forward primer	TTTGCGGGATCCCATATG AAGTTTACAAATTTAACA GCTAAAG	*Bam*HI and *Nde*I
6	FemA reverse plus TEV site	TTTGCGCTCGAGGCCCTG AAAATACAGGTTTTCAAA AA TTCTGTCTTTAACTTTTTT AAG	*Xho*I, TEV protease recognition site (PAGE purified)

Primer number	Primer name	Primer sequence (5’ to 3’)	Incorporated sites
7	FemA reverse (C-terminal 12 histidine tag)	TTTGCGCTCGAGGTGGTG GTGGTGGTGGTGAAAAAT TCTGTC	*Xho*I, hexa-histidine tag not encoded by the vector (HPLC purified)
8	MurM reverse plus TEV site	TTTGCGCTCGAGGCCCTG AAAATACAGGTTTTCCTTT CTATGTTTTTTTCTTAATG TTTTACGG	*Xho*I, TEV protease recognition site (PAGE purified)
9	T7 RNA polymerase forward primer	TTTGCGGGTGGTCTCCCAT GAACACGATTAACATCGC TAA	*Bsa*I producing *Nco*I compatible ends
10	T7 RNA polymerase reverse primer for cloning into pProExHTa	TTTGCGCTCGAGTTACGC GAACGCGAAGTCCGACTC TAAG	*Xho*I and a stop codon
11	T7 RNA polymerase reverse primer for cloning into pET28a	TTTGCGCTCGAGCGCGAA CGCGAAGTCCGACTCTAA G	*Xho*I
12	FemX forward primer	TTTGCGGGTGGTCTCCCAT GGAAAAGATGCATATCAC TAATCAGG	*Bsa*I producing *Nco*I compatible ends
13	FemX reverse plus TEV site	TTTGCGCTCGAGGCCCTG AAAATACAGGTTTTCTTTT CGTTTTAATTTACGAGAT ATTTTAATTTTAGC	*Xho*I TEV protease recognition site (PAGE purified)
14	FemB forward primer	TTTGCGGGTGGTCTCCCAT GAAATTTACAGAGTTAAC TGTTACC	*Bsa*I producing *Nco*I compatible ends

Primer number	Primer name	Primer sequence (5' to 3')	Incorporated sites
15	FemB reverse plus TEV site	TTTGCGCTCGAGGCCCTGAAAATACAGGTTTTCTTTCTTTAATTTTTTACGTAATTTATCC	*Xho*I TEV protease recognition site (PAGE purified)
16	Glycyl-tRNA synthetase forward primer	TTTGCGGGTGGTCTCCCATGGCAAAAGATATGGATACAATTG	*Bsa*I producing *Nco*I compatible ends
17	Glycyl-tRNA synthetase reverse primer	TTTGCGCTCGAGGAATTTTGTTTTTTCAGTTAAGAAAGC	*Xho*I
18	T7 promoter sequencing primer	TAATACGACTCACTATAGGG	
19	T7 terminator sequencing primer	GCTAGTTATTGCTCAGCGG	
20	pProExHTa vector inserts, forward primer (sequencing)	AGCGGATAACAATTTCACACAGG	
21	pProExHTa vector inserts, reverse primer (sequencing)	CTGCGTTCTGATTTAATCTGTATCAGGC	
22	T7 RNA polymerase middle sequencing primer 1	GTCAAGACTCTGAGACTATCGAACTCGCACC	
23	T7 RNA polymerase middle sequencing primer 2	GCTTACGCTGGCGAAAGGT	

Table 2.2: Primer sequences used for cloning and sequencing of the *murM* genes from *Streptococcus pneumoniae* (strains R6, Pn16 and 159), the *femXAB* and *glycyl-tRNA synthetase* genes from *Staphylococcus aureus* (strain Mu50) and the *T7 RNA polymerase* gene from *Escherichia coli* BL21 Star (DE3).placIRare2 cells. The sequences of all of the primers are given in the 5' to 3' direction. Details of flanking restriction and protease recognition sites added to the genes by the primers have been given. All primers were purified by standard de-salting unless otherwise stated in the incorporated sites column.

2.2.3. Visualisation of DNA

DNA fragments were visualised by 0.8 - 1% (w/v) high melting point agarose (GibcoBRL) gel electrophoresis using 1 x Tris-acetate buffer (TAE). Gels were stained for DNA by adding 5 µL of either 10 mg mL^{-1} ethidium bromide or 1000 x SYBR safe DNA stain (Invitrogen) per 50 mL prior to casting. This enabled DNA to be visualised on a UV transilluminator (Syngene G:Box using Gene-snap software). 1 kb ladder from Fermentas was used as a marker on all gels to enable estimation of the size of all DNA fragments.

2.2.4. Purification of PCR products

The products of PCR amplifications were purified using either the Promega Wizard Prep Kit or the Qiagen PCR clean-up Kit depending on the size of the DNA fragment according to manufacturer's instructions. Restriction digests of PCR products were routinely purified using the same kits.

2.2.5. Restriction digestion of PCR products and vectors

All restriction digests were carried out using enzymes obtained from New England Biolabs (NEB) according to manufacturer's instructions. Restricted PCR products were purified away from the enzymes as described in 2.2.4. Restricted vectors were purified using the Qiagen gel extraction kit.

2.2.6. Quantification of DNA

DNA concentration was obtained by measuring the absorbance ratio at 260/280 nm using a ND-1000 Nano-drop spectrophotometer.

2.2.7. DNA Ligations

T4 DNA ligase (Invitrogen) was used to ligate restricted PCR products into similarly restricted vectors according to manufacturer's instructions. A typical ligation consisted of PCR product and vector at a 10:1 molar ratio. Ligations were left at room temperature for at least 4 h prior to transformation of 2 µL of the DNA into *E. coli* Top10 cells.

2.2.8. Preparation and transformation of chemically-competent *Escherichia coli* cells

Chemically-competent *E. coli* cells were prepared using an adapted version of the rubidium chloride protocol developed by Hanahan *et al*. (1985). A 2.5 mL starter culture was grown at 37^{o}C for 16 h and then used to inoculate 250 mL of LB supplemented with 20 mM $MgSO_4$. Once the cells had reached an OD_{600nm} of 0.4, they were centrifuged at 4^{o}C in a Beckman JA-14 rotor at 4,500 x *g* for 5 min. The cell pellet was resuspended in 100 mL of TFB 1 (30 mM potassium acetate, 10 mM calcium chloride, 50 mM manganese chloride, 100 mM rubidium chloride, 15% glycerol pH 5.8). After incubation on ice for 5 min, the cells were centrifuged as before and the pellet was resuspended in 10 mL of TFB2 (10 mM MOPS, 75 mM calcium chloride, 10 mM rubidium chloride, 15% glycerol pH 6.5). Cells were incubated on ice for 1 h and then aliquots of 50 µL per tube were made and snap frozen in liquid nitrogen prior to storage at -80^{o}C.

Prior to transformation, an aliquot of cells was thawed on ice. Then 1 - 4 µL of plasmid DNA or ligation reaction was added to the cell aliquot which was subsequently incubated on ice for 30 min. Cells were heat shocked by incubation at

42^{o}C for 30 sec and then immediately placed back on ice for 2 min prior to the addition of 300 µL of SOC medium. Recovery from heat shock was initiated by incubation at 37^{o}C in a shaking incubator (200 rpm) for 1 h. Transformants were plated out in 50 - 100 µL aliquots on LB agar plates supplemented with the appropriate selective antibiotics and incubated for 20 h at 37^{o}C.

2.2.9. Site-directed mutagenesis by PCR

Mutagenesis of single amino acid residues to alanine was carried out using Stratagene's Quikchange methodology and Pfu Ultra DNA polymerase. Primers were designed to be approximately 30 bases in length with the desired mutation in the middle (Table 2.3). Where possible the GC content of each primer set was kept above 40% with the forward and the reverse primer designed to anneal to the same sequence on opposite strands of the template plasmid. Dimethyl-sulphoxide (DMSO) was added to a final concentration of 2.5% when the overall GC content of the DNA template made the design of primers with the recommended melting temperature (Tm) impossible.

Primer mutation site	Primer sequence (5’ to 3’)
FemA Histidine 41 to alanine	**Forward primer:** GCTTGCTGAAGGTTATGAAACA**GC**TTTAGTGGGA ATAAAAAA CAATAATAACG **Reverse primer:** CGTTATTATTGTTTTTTATTCCCACTAAAGCTGTTT CATAACCTTCAGCAAGC
FemA Histidine 100 to alanine	**Forward primer:** GAATTATCAAAATATGTTAAAAAA**GC**TCGTTGTC TATACCTACATATCG **Reverse primer:** CGATATGTAGGTATAGACAACGAGCTTTTTTAAC ATATTTTGATAATTC
FemA Histidine 106 to alanine	**Forward primer:** CATCGTTGTCTATACCTA**GC**TATCGATCCATAT TTACCATATC **Reverse primer:** GATATGGTAAATATGGATCGATAGCTAGGTATAG ACAACGATG
FemA Aspartate 396 to alanine	**Forward primer:** GCTGAAATTATTGAATATGTTGGTG**C**CTTTATT AAACCAATTAATAAACC **Reverse primer:** GGTTTATTAATTGGTTTAATAAAGGCACCAACAT ATTCAATAATTTCAGC
159 MurM rational surface mutagenesis cluster 1 oligos	**Forward primer:** CGGAGTTGATGAAAAAAACTGAG**GC**GCGC**GC**A G**C**GATTCATTTAAGAAACGAAGC **Reverse primer:** GCTTCGTTTCTTAAATGAATCGCTGCGCGCGCC TCAGTTTTTTTCATCAACTCCG

Primer mutation site	Primer sequence (5’ to 3’)
159 MurM rational surface mutagenesis cluster 2 oligos	**Forward:** CCATTCAGCCTCGTATTCAGGCGAAAATATAT **GC**AG**C**AAATTTTGAAGAAGATAAACTTTCTAAA TCAACG **Reverse:** CGTTGATTTAGAAAGTTTATCTTCTTCAAAATT TGCTGCATATATTTTCGCCTGAATACGAGGCTG AATGG
Pn16 MurM rational surface mutagenesis cluster 1 oligos	**Forward:** GGCAACATGAGAAGTTTGGTGTTTACAGGG**C**A G**C**A**GC**ATTACTGGCGACAGCTAGTATTTTGATT AG **Reverse:** CTAATCAAAATACTAGCTGTCGCCAGTAATGCT GCTGCCCTGTAAACACCAAACTTCTCATGTTGCC
Pn16 MurM rational surface mutagenesis cluster 2 oligos	**Forward:** GCCTATCTCAAAGTTTAATCAAT**GC**GG**C**A**GC**G ACAGAATTTCCTGAAAATCTGGC **Reverse:** GCCAGATTTTCAGGAAATTCTGTCGCTGCCGCA TTGATTAAACTTTGAGATAGGC
159 MurM Glutamate 229 to alanine	**Forward:** GATAACTTCAAA**GCA**GACTCCTATATCACG **Reverse:** CGTGATATAGGAGTCTGCTTTGAAGTTATC
159 MurM Glutamate 307 to alanine	**Forward:** GCGGCTACTTTGAGTTTG**GCA**TTTGGTAATACCTC TGTC **Reverse:** GACAGAGGTATTACCAAATGCCAAACTCAAAGTA GCCGC

Primer mutation site	Primer sequence (5' to 3')
Pn16 MurM Aspartate 229 to alanine	**Forward:** GTTAGATAATTTTAAG**GCC**AAGGCCTATATCACC **Reverse:** GGTGATATAGGCCTTGGCCTTAAAATTATCTAAC
Pn16 MurM Glutamate 307 to alanine	**Forward:** GCGGCTACTTTGAGTTTG**GCA**TTTGGTACTACCTC TGTC **Reverse:** GACAGAGGTAGTACCAAATGCCAAACTCAAAGT AGCCGC

Table 2.3: Primer sequences used for site-directed mutagenesis of MurM and FemA. All mutations made converted the amino acid of interest to alanine. In each case, both of the primers were designed to incorporate the desired mutation and to anneal to the same sequence of DNA on opposite strands of the plasmid. The Tm and GC content were kept above 78^{o}C and 40% respectively where possible. The region of the sequence highlighted in bold underlined shows the position of the amino acid mutation with respect to the length of the primer.

2.2.10. Isolation of plasmid DNA from *Escherichia coli*

Plasmid DNA was isolated from either 5 mL or 100 mL overnight cultures of *E. coli* using the Qiagen mini-prep kit or the Sigma maxi-prep kit respectively following manufacturer's instructions.

2.2.11. DNA sequencing

All DNA sequencing reactions were performed and analysed by the Molecular Biology Service at the University of Warwick using an ABI-prism DNA sequencer (Applied Biosystems, USA). DNA sequences were annotated using Chromas and sequence alignments were performed using ClustalX and GeneDoc.

2.3. Protein Expression and solubilisation

2.3.1. Bacterial strains and vectors

Chemically-competent *E. coli* Top10 cells were transformed and used as a means of facilitating genetic manipulation of expression vectors pProExHTa (Invitrogen), pET22b and pET28a (Novagen) with PCR products encoding the gene of interest. Maps of the multiple cloning sites for these vectors are shown in Figures 2.1, 2.2 and 2.3 respectively. Chemically competent *E. coli* strains used in this study for optimisation of protein expression include B834 (DE3), BL21 Star (DE3), BL21 Star (DE3).placIRare2 and C41 (DE3).pRIL. Features of all of these strains are shown in Table 2.4.

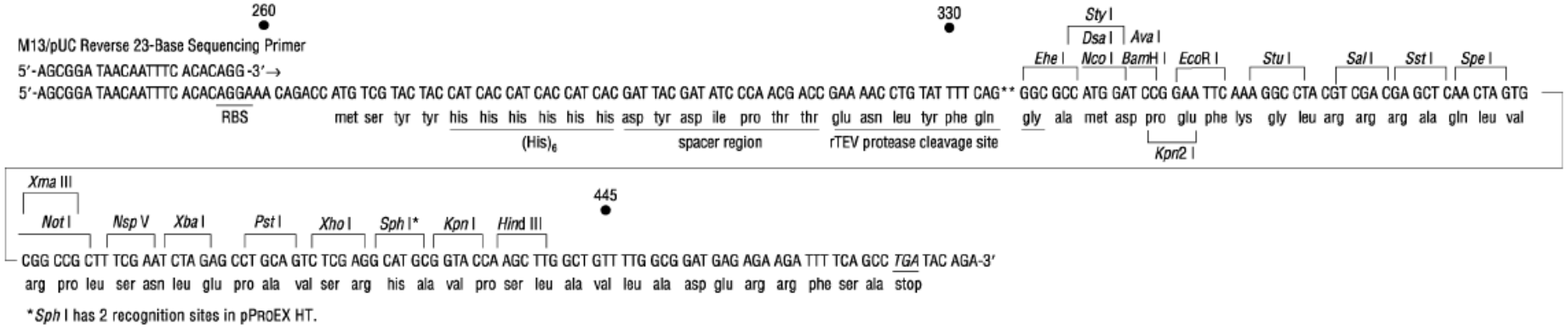

Figure 2.1: Map showing the multiple cloning site of the protein expression vector pProExHTa from Invitrogen.

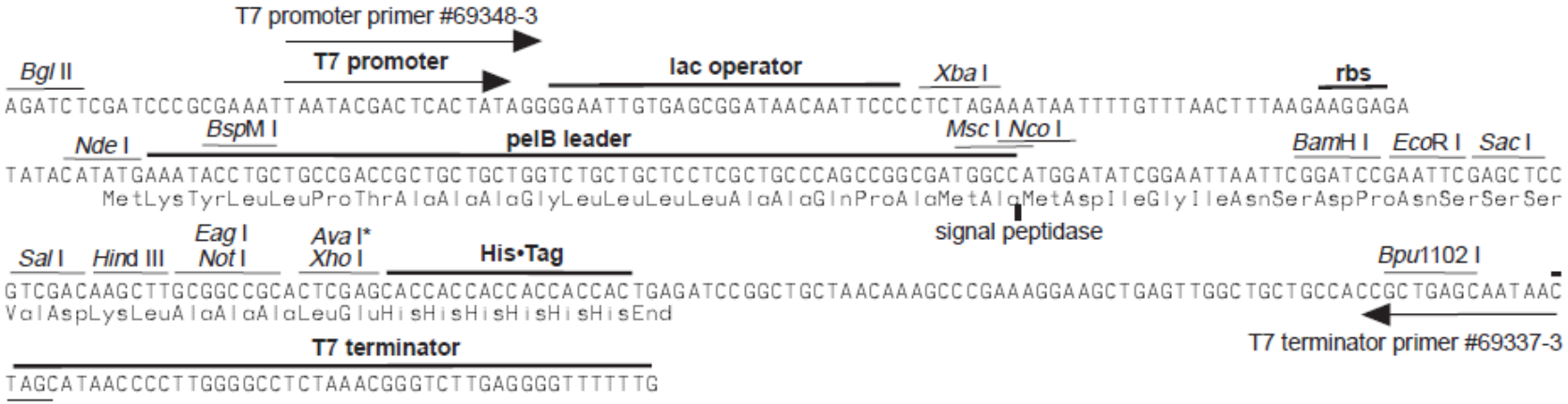

Figure 2.2: Map showing the multiple cloning site of the protein expression vector pET22b (+) (Novagen).

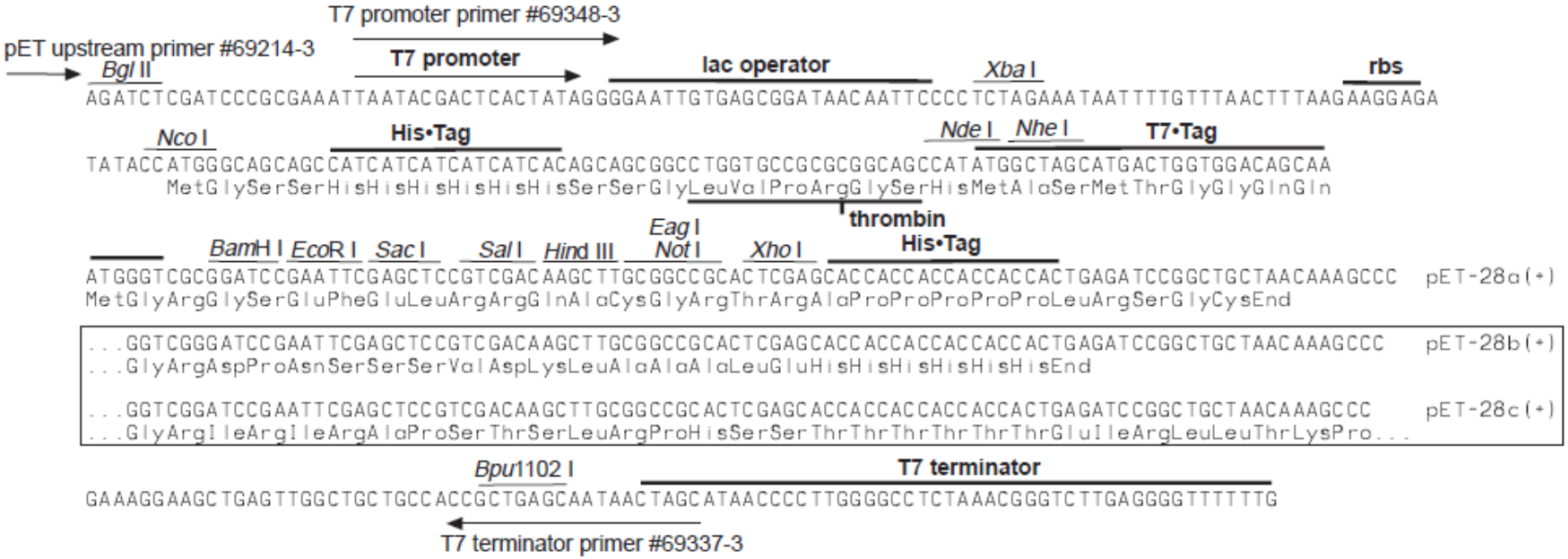

Figure 2.3: Map showing the multiple cloning site of the protein expression vector pET28a-c (+) (Novagen).

***E. coli* strain**	**Parental *E. coli* strain**	**Genotype**	**Description**	**Antibiotic resistance**
B834 (DE3)	*E. coli* B	*F⁻ ompT hsdS$_B$ (r_B^- m_B^-) gal dcm met* (DE3)	*met* auxotroph, general expression host. (Leahy *et al.*, 1992)	None
BL21 Star™ (DE3) (Invitrogen)	B834	*F⁻ ompT hsdS$_B$ (r_B^- m_B^-) gal dcm rne131* (DE3)	High performance expression host. The *rne131* deletion ensures messenger RNAs are not degraded as quickly as they would be in the parent strain. (Lopez *et al.*, 1999)	None
BL21 Star™ (DE3).placIRare2	B834	*F⁻ ompT hsdS$_B$ (r_B^- m_B^-) gal dcm rne131* (DE3) pRARE2[7] (Cam^R)	High performance expression host providing seven rare codon tRNAs.	Chloramphenicol (34 μg ml^{-1})
C41 (DE3).pRIL	BL21 (DE3)	*F⁻ ompT hsdS$_B$ (r_B^- m_B^-) gal dcm* (DE3)	General expression host supportive of the over-expression of membrane associated proteins whose production may be toxic to the parental strain. (Miroux and Walker, 1996)	Chloramphenicol (34 μg ml^{-1})
Top10	MC1061	F⁻, *mrcA*, *endA1*, *rec1*, ϕ80*lacZ*ΔM15, Δ*lacZX74*, *deoR*, *araD139*, *galK*, *rpsL* (Str^R), *nupG*, Δ(*mrr-hsdRMS-mcrBC*)	High efficiency host for cloning and propagation of plasmids. (Grant *et al.*, 1990)	Streptomycin

Table 2.4: Properties of *Escherichia coli* strains used for cloning and protein expression. Strains were acquired from Invitrogen.

2.3.2. Protein expression using auto-induction

For determination of optimal conditions for protein expression, the vector containing the required gene was transformed into a range of *E. coli* expression strains (Table 2.4). A single colony from each transformation was used to inoculate 10 mL of auto-induction medium consisting of 5052 (200 μL), 20 x NPS (500 μL), 1 M $MgSO_4$ (10 μL), LB (up to a final volume of 10 mL) and the appropriate antibiotics. Control expressions were carried out using 10 mL of LB substituted with 50 μL of 40% glucose. These cultures were placed in a shaking incubator at 37^{o}C for 18 h (Studier, 2005). This expression system was scaled up into a 1 L volume where necessary.

2.3.3. Protein expression using Isopropyl-β-D-thio-galactoside (IPTG)

As described for auto-induction, a single colony from each transformation was used to inoculate 5 mL of LB substituted with the appropriate antibiotic. These cultures were placed in a shaking incubator at 37^{o}C until an OD_{600nm} of 0.4 - 0.6 was reached. Protein expression was induced at this stage by the addition of a final concentration of 1 mM IPTG and incubation for 4 h at 28^{o}C unless otherwise stated. This expression system was scaled up into a 1 L volume in the case of all proteins used in this study.

2.3.4. Chaperone co-expression of recombinant proteins

A series of plasmids encoding various chaperones (developed by Takara Bio Inc, Japan) were transformed into chemically-competent *E. coli* B834 (DE3) cells for use in chaperone co-expression experiments. These cells were then made competent (see section 2.2.8) for the uptake of an additional expression vector encoding the protein of interest. The chaperones encoded by these plasmids are shown in Table 2.5.

Number	Plasmid	Chaperone	Promoter	Inducer
1	pG-KJE8	dnaK-dnaJ-grpE groES-groEL	*araB* *pzt1*	L-arabinose tetracycline
2	pGro7	groES-groEL	*araB*	L-arabinose
3	pKJE7	dnaK-dnaJ-grpE	*araB*	L-arabinose
4	pG-Tf2	groES-groEL-tig	*pzt1*	tetracycline
5	pTf16	Tig	*araB*	L-arabinose

Table 2.5: Properties of the Takara chaperone plasmid set. Note that expression of the chaperones from these plasmids is induced by L-arabinose, tetracycline or a combination of both. All five chaperone plasmids contain a chloramphenicol resistance marker.

Unless otherwise stated in the text, chaperone expression was induced following manufacturer's instructions at the start of cell growth to allow for their accumulation prior to over-expression of the protein of interest.

2.3.5. Preparation of crude extracts from *Escherichia coli*

After either auto-induction or IPTG-induction, *E. coli* expression cultures (1 L) were harvested by centrifugation at 6,000 x *g* for 15 min. The pellet obtained was resuspended in 20 mL of 50 mM HEPES pH 7.0, 1 mM $MgCl_2$ unless otherwise stated. The cell resuspension was disrupted on ice using a Bandelin Sonopuls sonicator with three 30 sec bursts at 70% power. A crude extract containing soluble proteins was obtained from the supernatant after centrifugation at 25,000 x *g* for 30 min. Insoluble protein, including MurM, was left in the cell pellet at this stage and was solubilised using salt extraction (see section 2.3.7).

For small-scale 10 mL expression trials, cells were harvested at 15,000 x *g* for 5 min. The cell pellet was resuspended in 300 µL of 50 mM HEPES pH 7.0, 1 mM $MgCl_2$

and sonicated on ice at 15% power for 10 sec. A crude extract was then obtained by additional centrifugation at 15,000 x *g* for 5 min.

2.3.6. Solubilisation of MurM using N-Lauroylsarcosine (Sarcosyl)

After IPTG-induction, *E. coli* expression cultures (1 L) were harvested as described in section 2.3.5. The cell pellet was resuspended in 20 mL of buffer containing 50 mM HEPES pH 7.0, 1 mM $MgCl_2$ and 0.5% (w/v) N-lauroylsarcosine. A crude extract containing soluble proteins was obtained from the supernatant after sonication (see section 2.3.5) and centrifugation at 30,000 x *g* for 30 min.

2.3.7. Solubilisation of MurM using 1 Molar sodium chloride

MurM was solubilised using an adapted form of the methodology described by Lloyd *et al*. (2008). Cell pellets obtained after the preparation of a crude extract were resuspended in 30 mL of 50 mM sodium phosphate pH 7.0, 1 M NaCl and stored at -80^{o}C for 16 h. The cell resuspension was then thawed out at room temperature and allowed to mix at 4^{o}C for 30 min. Soluble protein was found in the supernatant after centrifugation at 50,000 x *g* for 20 min (salt extract 1). Additional insoluble protein remaining in the cell pellet was solubilised by resuspension in 20 mL of 50 mM sodium phosphate pH 7.0, 1 M NaCl and centrifugation at 50,000 x *g* for 20 min (salt extract 2). This methodology was also used for solubilisation of FemX, FemA and FemB.

2.4. Protein purification

2.4.1. Immobilised metal ion affinity chromatography (IMAC)

For affinity purification of proteins on cobalt, 5 mL of Talon-resin (BD Biosciences) was allowed to settle in a 10 mL syringe barrel. Unless otherwise stated, the resin was equilibrated in 50 mL of buffer comprised of 50 mM sodium phosphate pH 7.0, 500 mM NaCl, 10 mM imidazole and 20% glycerol. After gravity flow of a crude extract through the column, three wash steps were carried out in the following order: 50 mL of equilibration buffer, 30 mL of equilibration buffer supplemented with 50 mM imidazole and 30 mL of equilibration buffer supplemented with 200 mM imidazole. For IMAC purification on nickel resin (GE Healthcare), all buffer components were kept the same. However, the imidazole concentration in the final wash buffer was increased to 500 mM.

2.4.2. Ammonium sulphate precipitation of MurM

For purification of MurM, a 25% cut was carried out by adding 13.6 g of ammonium sulphate slowly to every 100 mL of a solubilised protein extract. The extract was left to stir continuously at 4^{o}C for 20 min and then centrifuged at 30,000 x *g* for 20 min. The supernatant was subject to a 50% cut by the addition of 14.8 g of ammonium sulphate to every 100 mL (Lloyd *et al.* 2008). The extract was left to stir at 4^{o}C and centrifuged as previously described prior to resuspension of the pellet in 5 mL of 50 mM sodium phosphate pH 7.0, 500 mM NaCl. This technique was used prior to gel filtration and hydrophobic interaction chromatography.

2.4.3. Size exclusion chromatography (gel filtration)

Gel filtration was carried out on a Superdex-75 column (GE healthcare) using the ÄKTA prime system (GE Healthcare). The column was equilibrated in buffer containing 50 mM sodium phosphate pH 7.0, 500 mM NaCl and protein was loaded onto the column in a total volume of buffer not exceeding 5 mL.

2.4.4. Hydrophobic interaction chromatography (HIC)

HIC was carried out using the ÄKTA prime system and a HiTrap Octyl- or phenyl-sepharose fast flow 1 mL column from GE Healthcare. Prior to purification by HIC, protein was exchanged into buffer A which consisted of 50 mM HEPES pH 7.5, 20% glycerol and 25% ammonium sulphate. Buffer B, comprised of 50 mM HEPES pH 7.5 and 20% glycerol, was used to establish a high to low ammonium sulphate gradient for purification.

2.4.5. Buffer exchange by dialysis

Prior to use, dialysis tubing was boiled for 10 min in buffer comprised of 2% (w/v) sodium bicarbonate and 1 mM EDTA pH 8.0. Tubing was stored at 4^{o}C and rinsed with sterile distilled water immediately before use.

For storage purposes, 20 mL of protein was dialysed for 16 h at 4^{o}C against 2 L of buffer comprised of 50 mM HEPES pH 7.0, 500 mM NaCl, 50% glycerol, 0.2 mM phenylmethylsulphonyl fluoride (PMSF), 1 µM leupeptin and 1 µM pepstatin. A final concentration of 10 mM EDTA was added to this storage buffer for removal of metal ions from proteins. For crystallography, dialysis buffer was comprised either

of 50 mM HEPES pH 7.0, 100 mM NaCl and 20% glycerol or 50 mM ethanolamine pH 10.0, 100 mM NaCl and 20% glycerol

2.4.6. Buffer exchange using a PD10 column

Protein was concentrated to a final volume of 2.5 mL prior to loading onto a PD10 bench-top de-salting column (GE Healthcare) pre-equilibrated in 20 mM HEPES pH 7.0 or 50 mM Tris-HCl pH 8.0, 200 mM NaCl and 20% glycerol. Protein was eluted from the column as per manufacturer's instructions.

2.4.7. Histidine tag removal using TEV protease

In order to remove the histidine tag from the C-terminus of MurM, FemX, FemA and FemB each protein was buffer exchanged using a PD10 column (see section 2.4.6) into 50 mM Tris-HCl pH 8.0, 200 mM NaCl and 20% glycerol (TEV digest buffer). Removal of the histidine tag was achieved by incubation of 1 µg of TEV with every 3 µg of protein for 16 h at 4^{o}C. Protein released from its histidine tag was then re-purified away from hexa-histidine tagged TEV protease using IMAC on cobalt resin pre-equilibrated in the TEV digest buffer.

2.4.8. Protein concentration

Protein solutions were concentrated into a reduced volume of buffer using Sartorius-Stedim Biotech vivaspin columns with a molecular weight cut-off of 10,000 Da. Samples were centrifuged at 4,000 x *g* in an Eppendorf 5810R bench-top centrifuge chilled to 4^{o}C until the desired concentration was obtained.

2.4.9. Protein quantification

The total protein content in samples was determined using Bio-Rad reagent as per manufacturer's instructions. Bovine serum albumin (BSA) at concentrations of 0 to 100 μg was used as a standard for protein quantification. All samples were measured in duplicate. Accurate determination of protein concentration was confirmed by measuring absorbance at 280 nm.

2.4.10. Assessment of protein expression and purity by sodium dodecyl sulphate polyacrylamide gel electrophoresis (SDS PAGE)

Proteins were separated based on their molecular weight by SDS PAGE using the Hoefer mini-gel system. In all cases, a 12.5% (w/v) resolving gel and a 4% (w/v) stacking gel were used and consisted of the components shown in Table 2.6.

12.5% Resolving gel	
1.5 M Tris-HCl pH 8.8	1.41 mL
30% acrylamide	2.28 mL
Sterile distilled water	1.89 mL
10% SDS	60 µL
10% ammonium persulphate (APS)	60 µL
Tetramethylethylenediamine (TEMED)	5 µL
4% Stacking gel	
0.5 M Tris-HCl pH 6.8	835 µL
30% acrylamide	334 µL
Sterile distilled water	2.17 mL
10% SDS	33 µL
10% APS	50 µL
TEMED	10 µL
SDS loading dye	
0.5 M Tris-HCl pH 6.8	100 µL
Sterile distilled water	400 µL
10% SDS	160 µL
Glycerol	160 µL
β-mercaptoethanol	40 µL
Bromophenol blue	A few grains
10 x SDS running buffer	
Glycine	144 g
Tris base	30 g
SDS	10 g
Distilled water	Added to 1 L

Table 2.6: Components required for SDS PAGE analysis of proteins. Resolving gel components shown are enough for one mini-gel whilst stacking gel components are enough for two mini-gels.

Protein samples were mixed with 5 µL of loading dye and heated at 95^{o}C for 10 min prior to separation on a 12.5% SDS PAGE gel. All protein gels were run at 180 V for 1 h using 1 x SDS running buffer. Gels were most commonly stained with Colloidal Coomassie as described in section 2.4.11. Molecular weight was determined by comparison to the Amersham low molecular weight calibration markers for SDS PAGE.

2.4.11. Staining of SDS PAGE gels using Colloidal Coomassie or Pro-Q sapphire histidine tag stain

For visualisation of all proteins, SDS PAGE gels were rinsed in water for 20 min and then left in Colloidal Coomassie for 16 h on an orbital shaker. Colloidal Coomassie stain was comprised of 1.6% phosphoric acid, 8% ammonium sulphate, 0.08% Coomassie Brilliant Blue G-250 and 20% ethanol. Gels were de-stained for 1 h in sterile distilled water (Neuhoff *et al.*, 1988). Staining for visualisation of histidine-tagged proteins required leaving the gel in 25 mL of Pro-Q sapphire 532 oligohistidine gel stain from Molecular Probes for 16 h after following the recommended manufacturer's instructions.

2.5. Preparation of substrates and enzyme assays

2.5.1. Isolation of *Micrococcus flavus* membranes

In order to prepare *M. flavus* membranes, 6 L of cells were grown to an OD_{600nm} of 4.0 and then harvested by centrifugation at 6,000 x *g* for 15 min. The resulting cell pellet was resuspended in 100 mL of buffer containing 20 mM Tris-HCl pH 7.5, 1 mM $MgCl_2$, 2 mM β-mercaptoethanol and 2.5 mg mL^{-1} lysozyme and disrupted using a French Press at 30,000 psi. After centrifugation at 10,000 x *g* for 30 min, the supernatant was centrifuged at 50,000 x *g* for 30 min and the membrane-containing pellet resuspended in the above buffer for use in Lipid II synthesis.

2.5.2. Synthesis and purification of Lipid II

Lipid II was synthesised by the incubation of 1.62 mM undecaprenyl-phosphate (11P), 2 mM UDP-MurNAc lysine pentapeptide and 35 mM GlcNAc with *M. flavus* membranes (final concentration 3.5 mg mL^{-1}) in a final volume of 3.5 mL. All these

components were assembled in buffer consisting of 0.1 M Tris pH 8.0, 1% Triton X-100 and 5 mM magnesium chloride. The reaction was incubated at 37^{o}C for 3.5 h when it was stopped by the addition of an equal volume of 6 M pyridinium acetate (consisting of 4.85 mL 6 M pyridine, 3.44 mL acetic acid and 1.71 mL water). After addition of an equal volume of N-butanol, the reaction was centrifuged at 3,000 x *g* for 10 min at 4^{o}C. An equal volume of sterile distilled water was added to the top phase which was re-centrifuged as above. The top phase, containing Lipid II, was dried down using a rota-vap prior to purification on a 3 mL DEAE sephacel column.

Prior to use, the DEAE sephacel column was washed with 40 mL of 1 M ammonium acetate and 60 mL of water. Equilibration of the resin was achieved using 40 mL of buffer containing chloroform, methanol and water in a 2:3:1 ratio (Solvent A). Lipid II was resuspended in 6 mL of solvent A and loaded onto the gravity flow DEAE sephacel column collecting the flow-through. The column was washed with 12 mL of solvent A. Additional wash steps carried out to elute and purify Lipid II consisted of a series of buffers containing chloroform, methanol and ammonium bicarbonate in a 2:3:1 ratio. The concentration of ammonium bicarbonate was increased across eight 12 mL wash steps (50 mM, 100 mM, 150 mM, 200 mM, 250 mM, 300 mM, 500 mM and 1 M) with 0.5 mL of each fraction being dried down for analysis by thin layer chromatography (TLC). Results of a typical TLC stained using iodine vapour and showing elution of Lipid II in the last three fractions is shown in Figure 2.4.

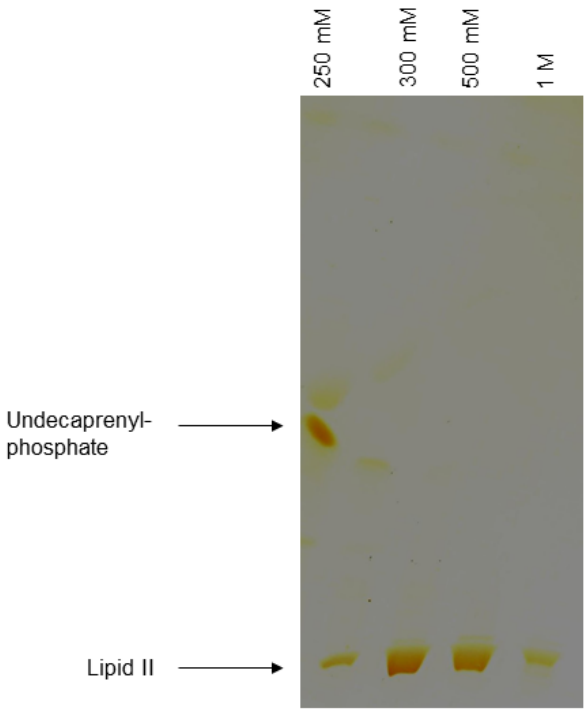

Figure 2.4: TLC showing purification of Lipid II away from undecaprenyl-phosphate and the other components used in the synthesis reaction. The Silica gel TLC plate was developed in chloroform/methanol/water/0.88 ammonia (88 mL: 48 mL: 10 mL: 1 mL) and stained using iodine vapour.

Fractions containing Lipid II were pooled and freeze-dried to remove ammonium bicarbonate. The overall yield was assessed by boiling a sample in hydrochloric acid for 30 min in order to release two phosphates per molecule of Lipid II. 1 M sodium hydroxide was added to the sample to adjust the pH to 7.6. Phosphate release was assessed by measuring the change in A_{360nm} between a boiled and an un-boiled sample of Lipid II in a methylthioguanisine (MESG) based assay. The identity of Lipid II was confirmed by electrospray mass spectrometry.

2.5.3. Production of a single species of *Streptococcus pneumoniae* tRNA^{Ala} and tRNA^{Ser} by *in vitro* transcription

The tRNA^{Ala} gene from *S. pneumoniae* strain R6 with the sequence 5' GGGGCCTTAGCTCAGCTGGGAGAGCGCCTGCTTTGCACGCAGGAGGTCA GCGGTTCGATCCCGCTAGGCTCCACCA 3' (anticodon UGC) was synthesised commercially and cloned into pIDTSMART-Kan by Integrated DNA Technologies (IDT) such that a T7 promoter sequence proceeded the gene and a *Bst*NI site allowed incorporation of the CCA terminus for run-off transcription. In addition to this, the tRNA^{Ser} gene from *S. pneumoniae* strain R6 which had the sequence 5'GGAGGATTACCCAAGTCCGGCTGAAGGGAACGGTCTTGAAAACCGTCA GGCGTGTAAAAGCGTGCGTGGGTTCGAATCCCACATCCTCCTCCA 3' (anticodon UGA) was also cloned into pIDTSMART-Kan in the same way. The sequences submitted to IDT are shown in Figure 2.5.

tRNA^{Ala} (Isoacceptor UGC)

GGATCCCTGCAG*TAATACGACTCACTATA*GGGGCCTTAGCTCAGCTGGGAGAGCGCCTGCTTTGCA
CGCAGGAGGTCAGCGGTTCGATCCCGCTAGGCTCCA**CCAG**GAATTC

tRNA^{Ser} (Isoacceptor UGA)

GGATCCCTGCAG*TAATACGACTCACTATA*GGAGGATTACCCAAGTCCGGCTGAAGGGAACGGTCTT
GAAAACCGTCAGGCGTGTAAAAGCGTGCGTGGGTTCGAATCCCACATCCTCCT**CCAG**GAATTC

Figure 2.5: Sequences for production of a single species of *S. pneumoniae* tRNA^{Ala} and tRNA^{Ser} by *in vitro* transcription submitted to IDT for cloning into their standard vector pIDTSMART-Kan. At the 5' end of the sequence there is a *Bam*HI site (shown in blue) and at the 3' end of the sequence there is an *Eco*RI site (shown in red) used for cloning of the entire sequence into the vector. The T7 promoter region, shown in green, immediately precedes the tRNA gene, shown in purple. The crucial CCA end of the tRNA is added using the *Bst*N1 restriction site shown in bold black font.

Each tRNA gene was amplified from the appropriate vector with Accuprime *Taq* DNA polymerase (see Table 2.1) and primers whose sequences are shown in Table 2.7.

Primer name	Primer sequence (5' to 3')
$tRNA^{Ala/Ser}$ Forward	GGATCCCTGCAGTAATACGACTCACTATAGG
$tRNA^{Ala}$ Reverse	TGGTGGAGCCTAGCGGGATCG
$tRNA^{Ser}$ Reverse	TGGAGGAGGATGTGGGATTCG

Table 2.7: Primer sequences used for the generation of a template suitable for high yield *in vitro* transcription of *S. pneumoniae* $tRNA^{Ala}$ and $tRNA^{Ser}$. Note that the reverse primer is designed to ensure the template has the desired CCA 3' end to allow generation of large quantities of tRNA by run-off transcription.

After PCR, products of the correct mass for $tRNA^{Ala}$ and $tRNA^{Ser}$ were purified with the Qiagen PCR clean-up kit and used in *in vitro* transcription reactions using the Fermentas Transcript-Aid High Yield T7 kit according to manufacturer's instructions. Success of the transcription reactions was assessed according to manufacturer's instructions using a 2% agarose gel after treatment with DNase to remove the template material. Reactions containing RNA of the correct size were subjected to further purification by phenol/chloroform extraction and ethanol precipitation. To avoid dimer formation, the precipitated tRNA was resuspended in 4 mM magnesium chloride, heated to 80^{o}C and allowed to cool to room temperature slowly. Final purity of the tRNA was checked on a 5% or a 10% denaturing 8 M urea acrylamide gel, components for which are shown in Table 2.8.

5% denaturing acrylamide gel	Component	10% denaturing acrylamide gel
7.2 g	Urea	7.2 g
3 mL	5 x TBE	3 mL
2.5 mL	30% acrylamide	5 mL
To 15 mL	Sterile distilled water	To 15 mL

Table 2.8: Composition of 5% and 10% denaturing 8 M urea acrylamide gels for assessment of the purity of RNA produced by *in vitro* transcription. TBE stands for Tris-borate-EDTA buffer.

Prior to the addition of 75 μL 10% ammonium persulphate (APS) and 15 μL TEMED, the gel components were stirred at room temperature until the urea had completely dissolved. In each case, 1 x TBE was used as running buffer and gels were run at 200 V for 40 min prior to staining with ethidium bromide.

2.5.4. Aminoacylation of $tRNA^{Ala}$ and $tRNA^{Ser}$ by *S. pneumoniae* alanyl- and seryl-tRNA synthetase enzymes

For aminoacylation of tRNA species with alanine, 75 μg of *S. pneumoniae* $tRNA^{Ala}$ was incubated at 37^{o}C in a final volume of 0.2 mL consisting of 30 mM HEPES, 15 mM $MgCl_2$, 10 mM dithiothreitol (DTT), 2 mM ATP, pH 7.6, 2 μmol min^{-1} ml^{-1} inorganic pyrophosphatase, 5 μM alanyl-tRNA synthetase from *S. pneumoniae* strain 159 and 37.5 μM (18.53 μCi ml^{-1}) [^{3}H]-L-alanine (adapted from Lloyd *et al.* 2008). For aminoacylation of tRNA species with serine, 75 μg of *S. pneumoniae* $tRNA^{Ser}$ or $tRNA^{Ala}$ (in the case of mis-aminoacylation experiments) was incubated at 37^{o}C as before replacing full-length alanyl-tRNA synthetase with 13 μM *S. pneumoniae* strain Pn16 seryl-tRNA synthetase or 5 μM alanyl-tRNA synthetase catalytic domain (residues 1-460) respectively. In this scenario, L-alanine was replaced by 37.5 μM (24.2 μCi ml^{-1}) [^{3}H]-L-serine. Regardless of the amino acid being used, [^{3}H]-acylated

tRNA species were purified as described by Lloyd *et al.* (1993) after incubation at 37^{o}C for 30 min (Lloyd *et al.*, 1993).

The amount of aminoacylated, radiolabelled [^{3}H]-tRNA was determined by precipitation of a 1 µL sample of the purified product onto Whatman 3 mm filter paper which was subsequently dropped into ice cold 10% (w/v) trichloroacetic acid (TCA) for 45 min. The TCA solution was replaced twice within this time period to remove any contaminating free radiolabel. The filter paper was left to air dry and placed into 5 mL of Optiphase scintillation cocktail (Perkin-Elmer) prior to quantification of the radioactivity by liquid scintillation counting.

2.5.5. Purification of aminoacylated tRNA species using *Thermus thermophilus* EF-Tu (used only in the case of the 2'-amino mini-helix analogue of tRNA^{Ala})

T. thermophilus EF-Tu was cloned into the expression vector pET28a and expressed routinely at 37^{o}C in *E. coli* BL21 Star (DE3).placIRare2 cells. Cultures of cells (1 L) harbouring this expression construct were grown to an OD_{600nm} of 0.6 when expression was induced by the addition of IPTG (to a final concentration of 1 mM). Cells were harvested after 5 h and resuspended in 30 ml of 50 mM HEPES pH 7.0, 1 mM $MgCl_2$. Crude extracts were prepared as described in section 2.3.5. Prior to purification, the crude extract was incubated at 60^{o}C for 30 min exploiting the thermal stability of the protein in comparison to contaminating *E. coli* proteins. After centrifugation at 50,000 x *g* for 20 min, 50 µM guanosine diphosphate (GDP) was added to the remaining soluble protein, which was passed by gravity flow through a 5 mL cobalt column pre-equilibrated 50 mM sodium phosphate pH 7.0, 500 mM NaCl, 50 µM GDP, 5 mM imidazole and 20% glycerol. Elution of protein from the

column was achieved using step washes with the above buffer supplemented with 10 mM, 50 mM and 200 mM imidazole. The protein was dialysed against buffer comprised of 50 mM HEPES pH 7.0, 200 mM NaCl, 50 µM GDP and 50% glycerol as described in section 2.4.5 for storage purposes. Nickel-immobilised EF-Tu was used to purify aminoacylated tRNA away from uncharged tRNA species using the method devised by Ribeiro and others with the omission of β-mercaptoethanol from all buffers (Ribeiro *et al.*, 1995).

2.5.6. MurM kinetic activity assays using radiolabelled [^{3}H]-alanyl-tRNA^{Ala}, [^{3}H]-seryl-tRNA^{Ser} and [^{3}H]-seryl-tRNA^{Ala}

In order to follow incorporation of radiolabelled alanine or serine onto Lipid II, assays were carried out in a 30 µL volume consisting of 50 mM MOPS pH 6.8, 30 mM KCl, 10 mM $MgCl_2$, 1 mM DTT, 1 mM alanine or serine, 1.5% (w/v) CHAPS, MurM (exact concentration specified in the text) and, unless otherwise stated, 10 µM Lipid II. Reactions were always started by the addition of radiolabelled tRNA (0.5 µM and typically 100 cpm pmol^{-1} unless otherwise stated). All reactions were incubated at 37^{o}C in a static water bath for times specified in the text with the initial rate of reaction observed within the first two min. Reactions were stopped by the addition of 30 µL 6 M pyridinium acetate pH 4.5 (section 2.5.2) and 60 µL of ice cold N-butanol. Reactions were mixed using a vortex and centrifuged at 13,000 x *g* for 5 min at 4^{o}C. The butanol phase was washed with 60 µL of water, vortexed and re-centrifuged as before. The top phase was pipetted into 5 mL of Optiphase scintillation fluid and counted for tritium using a Tri-Carb 2900TR liquid scintillation analyser (Perkin-Elmer) (Lloyd *et al.*, 2008). All kinetic data were graphically represented using the Hanes-Woolf plot and analysed using GraphPad

Prism 5. Derivation of the Michaelis-Menten equation and its application in the Hanes-Woolf analysis are shown in Table 2.9.

Assumption	Equation
Enzymes (E) and their substrates (S) associate reversibly to form a complex (ES) generating product (P).	$E + S \rightarrow ES$ (constant k_1) $E + S \leftarrow ES$ (constant k_{-1}) $E + S \rightarrow ES \rightarrow E + P$ (Constant k_2)
The overall concentration of ES remains constant in a given enzymatic reaction (steady-state assumption).	Change (d) in concentration of ES over time (t) is equal to zero: $d[ES]/dt = 0$
All velocity measurements are taken immediately after addition of substrate to the reaction.	The total amount of enzyme in a reaction (E_T) is equal to [E] + [ES] Velocity of the forward reaction (V_f) equals: $k_1 ([E_T]-[ES]) [S]$ Velocity of the dissociation reaction (V_d) equals: $(k_{-1} + k_2) [ES]$ At a steady state V_f and V_d are equal. This can be described by the following equation which is the definition of the Michaelis-Menten constant, K_m: $([E_T] – [ES]) [S] / [ES]$ which can be rewritten as $(k_{-1} + k_2) / k_1$ The rate of production formation (v) can be expressed as: $v = k_2 [ES]$ or $v = k_2 [E_T] [S] / K_m + [S]$ where $V_{max} = k_2 [E_T]$
The Michaelis-Menten equation can thus be written: $V = V_{max} [S] / K_m + [S]$	
Rearrangement for linear transformation using the Hanes-Woolf plot: 1. Take the reciprocal of both sides of the Michaelis-Menten equation: $1/V = (K_m/V_{max}) (1/[S]) + 1/V_{max}$ 2. Multiply both sides of the equation by [S] $[S]/V = (1/V_{max}) [S] + K_m/V_{max}$	

Table 2.9: Derivation of the Michaelis-Menten equation. Adapted from Garrett and Grisham (2005).

In the Hanes-Woolf plot [S]/V is plotted against [S]. Key kinetic parameters can then be calculated from the gradient of the line and the intercepts of the x and y axis as shown in Figure 2.6.

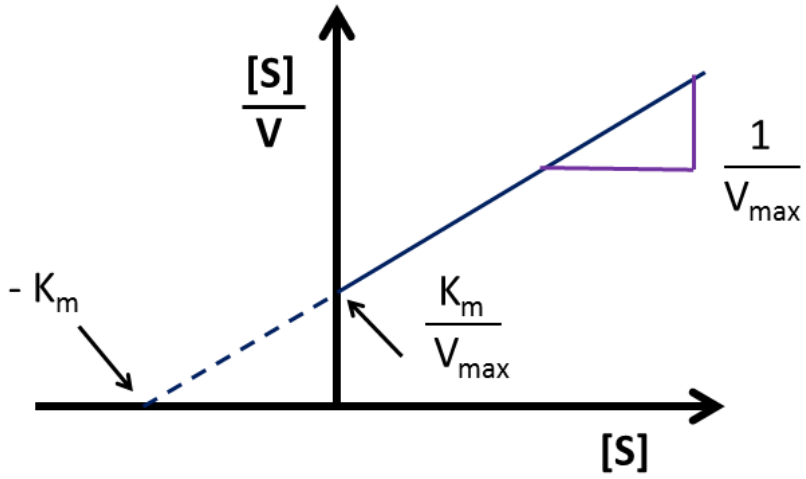

Figure 2.6: Key features of the Hanes-Woolf plot. K_m is the Michaelis-Menten constant, V_{max} is the maximum velocity of the reaction, [S] is the initial substrate concentration and V is the velocity.

From a Hanes-Woolf plot, the x-intercept is $-K_m$, the y-intercept is K_m/V_{max} and the gradient is equivalent to $1/V_{max}$. Analysis of the Hanes-Woolf plot in GraphPad prism allows calculation of error in the slope from which all other parameters are determined.

2.6. Biophysical techniques for protein analysis

2.6.1. Isothermal titration calorimetry (ITC) for characterisation of metal ion binding to proteins

Isothermal titration calorimetry is a biophysical technique used to measure the change in enthalpy that occurs in a liquid sample upon injection of a precise quantity of ligand. In this study, all isothermal titration calorimetry experiments were carried out using a VP-ITC microcalorimeter system (MicroCal, GE Healthcare, USA) at

30°C whereby a known concentration of protein was added to the sample cell and buffer containing a known concentration of a specific metal ion was placed in the syringe (Figure 2.7). Change in enthalpy was then determined by virtue of a feedback system measuring and compensating for differential heat production or absorption by the sample cell with respect a reference cell contained within the same jacket.

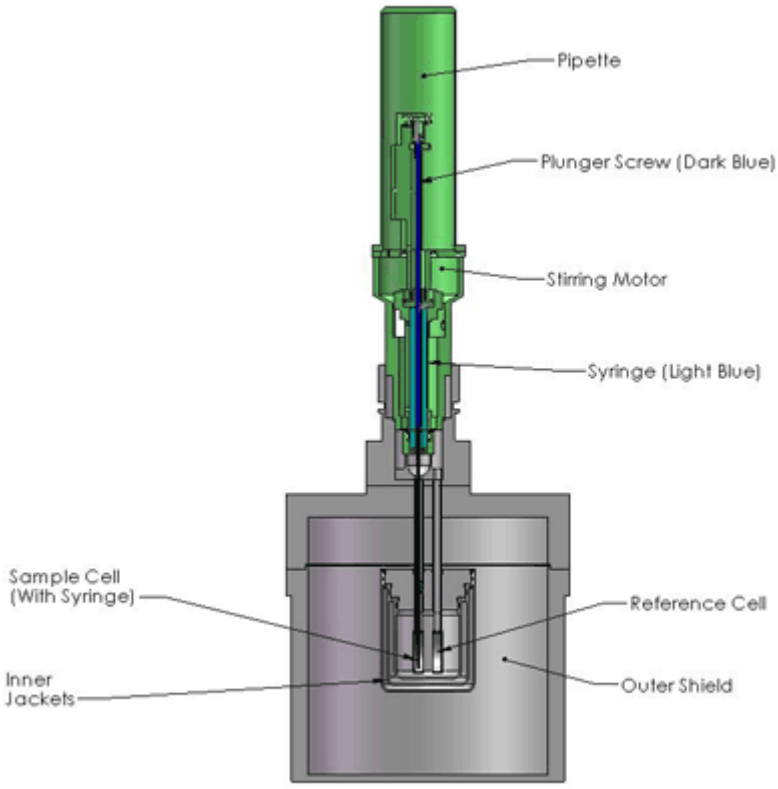

Figure 2.7: Diagram showing the format of the Isothermal Titration Calorimetry sample cell, reference cell and syringe. Constant rotation of the syringe ensures mixing of the ligand with the protein sample during the experiment. Taken from the VP-ITC microcalorimeter instruction manual (GE Healthcare, http://www.microcal.com/technology/itc.asp).

Prior to use, each protein was buffer exchanged into 20 mM HEPES pH 7.0 using a bench-top PD10 column (section 2.4.6). Metal ion solutions were made up in 20 mM HEPES to a final concentration of 1 mM using analytical grade reagents. A total of 27 injections of 10 µL of this buffer containing a given metal ion were made into 2

mL of 20 μM MurM, FemX or FemA unless otherwise stated. Each experiment generated an isotherm with individual peaks representing the heat change upon injection of 10 μL of metal ion into protein. The peaks decreased in size as the protein sample became saturated with the metal ion allowing analysis of the data and determination of a dissociation constant by an iterative process of non-linear regression using Origin data analysis software (MicroCal, GE Healthcare, USA).

2.6.2. Secondary structure determination using circular dichroism (CD)

Circular dichroism (CD) is a biophysical technique that is used to investigate the structure of proteins in solution. The technique itself is based upon plane polarised light which is comprised of two equal components: left and right circularly polarised light. Differential absorption of these two components by a sample gives rise to elliptical polarisation and, hence, a detectable CD signal (Kelly *et al.*, 2005).

Secondary structure information, including the percentage α-helix, β-sheet and turns, can be determined due to the chiral nature of the peptide bond which gives rise to absorption at and below 240 nm (Far UV spectrum). Tertiary structure information can be obtained from the absorption of the side chains of aromatic amino acids in the region between 260 nm and 320 nm (Near UV spectrum). Disulphide bonds can also be detected by a broad absorption peak at approximately 260 nm (Kelly *et al.*, 2005).

Prior to assessment of the Far UV spectrum of MurM and FemA, both proteins were buffer exchanged into 10 mM sodium phosphate pH 7.0 and diluted to a concentration of 0.12 mg mL^{-1}. Each experiment was repeated 20 times and then averaged (Kelly *et al.*, 2005). Controls were carried out using 10 mM sodium

phosphate pH 7.0 in the absence of MurM and FemA. The overall goodness of fit of the generated data was assessed using Dichroweb (Whitmore and Wallace, 2004).

2.6.3. X-ray crystallography

For the purpose of crystallography, all proteins were concentrated to at least 10 mg mL^{-1} as described in sections 2.4.8 and 2.4.9. Unless otherwise stated, all proteins subjected to crystallography in this study were dialysed into 50 mM ethanolamine pH 10.0, 100 mM NaCl and 20% glycerol following their purification and before concentration (section 2.4.5).

2.6.3.1. Preliminary screening in a 96-well format

96-well screens were set up using a HoneyBee robot from Genomic Solutions designed to dispense 70 µL of mother liquor in each well. The protein solution and mother liquor were mixed in a 1:1 ratio with the robot set to dispense 0.2 µL of each into a sitting drop using either an MRC 2-drop or a Greiner 3-drop plate (Molecular Dimensions). Screens used in this set up include JCSG+, PACT, Morpheus, MDL structure and Clear strategy all from Molecular Dimensions. In addition to this, the Emerald Wizard screen from Emerald Biosystems was also used in some circumstances. After set up, all plates were sealed with a ClearVue sheet from Molecular Dimensions and incubated at either $4^{o}C$ or $18^{o}C$ with periodic examination for crystal formation.

2.6.3.2. Expansion of successful hits in a 24-well format

To improve crystal morphology and diffraction, conditions identified as supporting either nucleation or crystal formation in the 96-well screens were further expanded in

a 24-well format. This allowed for changes in crystal formation upon slight adjustments in the pH and concentration of the precipitant to be explored. In this case, 1 mL of mother liquor was dispensed into the well. Typically protein to mother liquor ratios of 1 µL:1 µL and 2 µL:1 µL were set up on the same plastic coverslip which was then placed over the well and sealed with vacuum grease to produce a hanging drop set up. As before, plates were left at either 4^{o}C or 18^{o}C and periodically checked for better crystal formation.

2.6.3.3. Seeding

For seeding experiments, to try and improve crystal growth and/or morphology, a single crystal was extracted from a drop using a cryo-loop and then placed into an Eppendorf containing 50 µL of mother liquor. The solution was vortexed to break up the crystal and diluted 1 in 100 to form a liquid seed stock. Seeding was only attempted in the 24-well system. For liquid seeding, 0.25 µL of the seed stock was added to the protein-mother liquor drops. Alternatively, a horse hair was dipped into the stock and then streaked across each drop resulting in serial dilution of the crystal seed across the plate from left to right.

2.6.3.4. Additive screens

To further refine successful crystallisation conditions, the Hampton Additive and Silver Bullets screens from Hampton Research were exploited. The Additive screen was used for manipulating the interactions between the sample and itself and the sample and the mother-liquor to improve crystal formation primarily by adjusting the solubility of the sample. In contrast, the Silver Bullets screen was used to promote improvements in the formation of a stable crystal lattice structure by influencing

hydrogen bonding, hydrophobic interactions and electrostatic interactions within the protein sample.

In order to set up these screens, 60 μL of mother liquor determined by a successful 96-well screen condition was added to each well of a 2-drop MRC plate. In the case of the Silver Bullets screen, sitting drops, made up of 1 μL of protein sample, 0.5 μL of mother liquor and 0.5 μL of silver bullet, were set up using a Rainin EDP3-plus 1-10 μL multi-channel pipette. In the case of the Hampton Additive screen, for conditions A1 to G8, 7 μL of additive was added to the mother liquor solution in the well and sitting drops comprised of 1 μL of protein sample and 1 μL of the well solution were set up. For conditions, G9 to H12, the set up was as described for the Silver Bullets screen.

2.6.3.5. Visualisation of crystals

For visualisation of initial crystal screens set up in the 96-well format, plates were stored at the appropriate temperature in a crystal pro-HT imager (Molecular Dimensions) which was set up to photograph each drop once a day for two weeks using PC-scope and CrystalLIMS data analysis software. Alternatively, crystals were visualised using a SZ-PT Olympus microscope with an attached JVC colour video camera for imaging.

2.6.3.6. Cryo-protection and freezing of crystals

For conservation of the crystal lattice during freezing, a series of different cryo-protectants were tested in each case including paratone (Molecular Dimensions), silicone oil, Low Viscosity cryo-oil (MiTeGen) and mother liquor enriched with

10%, 20% or 30% glycerol. A single crystal was picked up in a cryo-loop and soaked in 1 µL of cryo-protectant prior to freezing in liquid nitrogen.

2.6.3.7. Data collection

For data collection purposes, frozen crystals were tested for diffraction on either the I03 or I24 (microfocus) X-ray beamlines at the Diamond Light Source Synchrotron, Harwell Science and Innovation Campus, Oxfordshire, UK. A full data set was collected for any crystals diffracting to or further than 3Å. Resulting data were analysed and solved for structural information by Professor Vilmos Fulop (University of Warwick). All protein structure images presented in this thesis have been constructed using PyMol.

Chapter 3

Cloning, overexpression and the development of a purification method for the MurM protein from penicillin-sensitive *Streptococcus pneumoniae* strain R6

3.1. Introduction

In *S. pneumoniae*, it is the *murMN* operon that encodes the enzymes responsible for the synthesis of branched structured muropeptides in the cell wall peptidoglycan (Filipe *et al.*, 2001b). Normally, the pneumococcal peptidoglycan structure is comprised of a combination of linear and branched muropeptides (Filipe *et al.*, 2000). However, mutation in the *murM* gene has been shown to result in the generation of a peptidoglycan structure that is composed only of linear muropeptides. Deletion of the *murM* gene causes a reversion to penicillin sensitivity in strains that were previously resistant (Filipe *et al.*, 2001b; Fiser *et al.*, 2003). As a result of this, the *murM* gene is a potential target for the development of novel antibiotics which, if used in synergy with penicillin, could combat drug-resistant strains of *S. pneumoniae* (Cressina *et al.*, 2007). Despite this, the role of the MurM protein in penicillin resistance is still not very well understood and is complicated by the fact that it is possible for highly resistant strains to carry the same *murM* allele as susceptible strains (Cafini *et al.*, 2006).

S. pneumoniae strain R6 is particularly interesting since it has an unusually high proportion of branched muropeptides in its cell wall compared to other penicillin-sensitive strains (Garcia-Bustos and Tomasz, 1990). The non-encapsulated, non-pathogenic parental strain from which R6 was derived is called R36A. Strain R36A was derived by Avery *et al.* (1944) after 36 serial passages of the encapsulated,

pathogenic strain D39 in type II anti-pneumococcus rabbit serum (Avery *et al.*, 1944; Hoskins *et al.*, 2001). A comparison between levels of linear and branched muropeptides in penicillin-sensitive and penicillin-resistant strains of *S. pneumoniae* is given in Table 3.1.

Strain of *S. pneumoniae*	**Susceptibility to penicillin**	**% peptides**	
		Linear	**Branched**
D39S	Sensitive	73	27
SP96	Sensitive	84	16
SP108	Sensitive	83	17
SA23	Sensitive	82	18
8249	Resistant	20	80
CO7	Resistant	16	84
140	Resistant	27	73
10760	Resistant	14	86
R6	**Sensitive**	**60**	**40**

Table 3.1: Proportion of linear and branched muropeptides within the cell wall peptidoglycan of penicillin-sensitive (MIC < 0.25 µg mL^{-1}) and penicillin-resistant (MIC > 4.00 µg mL^{-1}) strains of *Streptococcus pneumoniae* as determined by HPLC and absorbance at 215 nm. Adapted from Garcia-Bustos and Tomasz (1990).

The work of Garcia-Bustos and Tomasz (1990) showed that penicillin-sensitive strains of *S. pneumoniae,* with an MIC of less than 0.25 µg mL^{-1}, typically have less than 30% of their total peptides branched. In contrast to this, in penicillin-resistant strains of *S. pneumoniae* that have an MIC of greater than 4.00 µg mL^{-1}, more than 70% of the total cell wall peptides are branched. Strain R6 shows a proportion of peptide branching that is at least 10% greater than is normally seen in penicillin-sensitive strains of *S. pneumoniae*. Therefore, studying the MurM protein from this particular strain was considered to be important in terms of resolving the link between penicillin-resistance, levels of cell wall cross-linking and the activity of the MurM protein within this organism.

Studies by Lloyd *et al.* (2008) on the MurM proteins from *S. pneumoniae* strains Pn16 and 159 had indicated that the protein was mostly insoluble upon over-expression. Both of the variants used in this study could be solubilised using 1 M salt and purified in a three step process involving a 25% to 50% ammonium sulphate cut, gel filtration and immobilised metal ion chromatography on cobalt resin. An inability to successfully apply these purification methods to the MurM protein from strain R6 lead to a requirement for the development of a new strategy which is described in this chapter.

3.2. Aims

The main aim of this project was to investigate the relationship between levels and types of amino acids used in indirect cross-linking within pneumococcal peptidoglycan across a range of resistant and susceptible strains. To address this aim, work carried out in this chapter was designed to meet the following objectives:

- Cloning the *murM* gene from penicillin-sensitive *S. pneumoniae* strain R6 into the expression vector pET22b (C-terminal hexa-histidine tag)
- Achieving over-expression of soluble $MurM_{R6}$ protein
- Obtaining $MurM_{R6}$ protein of suitable purity and homogeneity for use in biochemical assays to allow comparison with the work already carried out on the MurM proteins from *S. pneumoniae* strains Pn16 (penicillin-sensitive) and 159 (penicillin-resistant) by Lloyd *et al.* (2008)

However, problems encountered during purification of $MurM_{R6}$ using the published methods for the other two variants of MurM led to a requirement for the following additional objectives to be met:

- Re-cloning of $MurM_{R6}$, $MurM_{Pn16}$ and $MurM_{159}$ into pET22b to encode a C-terminal dodeca-histidine tag
- Development of a single step purification method that could be applied to all three variants of MurM with equal success

3.3. Cloning, expression and purification of MurM

3.3.1. Cloning of *$murM_{R6}$* into pET22b

The *murM* gene from *S. pneumoniae* strain R6 was cloned into the expression vector pET22b such that it would encode a C-terminal hexa-histidine fusion tag for purification purposes. Amplification of the *$murM_{R6}$* gene was achieved by PCR using Accuprime *Taq* DNA polymerase in combination with chromosomal DNA from *S. pneumoniae* strain R6 as a template (provided by Professor Chris Dowson, University of Warwick) and primers 1 and 3 shown in Chapter 2, Table 2.2. $MurM_{Pn16}$ and $MurM_{159}$ hexa-histidine tag expression constructs were obtained from Dr Adrian Lloyd (University of Warwick). Figure 3.1 illustrates successful cloning of *$murM_{R6}$* into pET22b.

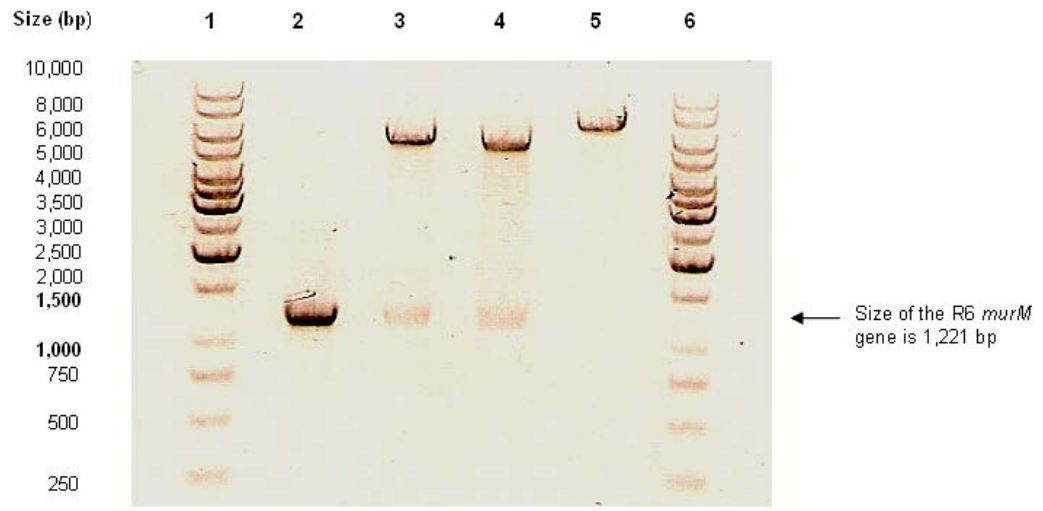

Figure 3.1: Summary agarose gel showing cloning of the *Streptococcus pneumoniae* strain R6 *murM* gene into pET22b. The size of the pET22b vector is 5,493 bp.

Lanes 1 and 6 - 1 kb ladder,
Lane 2 - $murM_{R6}$ PCR product,
Lane 3 - *Bam*HI/*Xho*I restriction digestion of the initial pET22b::$MurM_{R6}$ construct prior to removal of the *Bam*HI site,
Lane 4 - *Nde*I/*Xho*I restriction digestion of the pET22b::$MurM_{R6}$ construct where the *Bam*HI site had been removed by *Nde*I digestion,
Lane 5 - *Bam*HI/*Xho*I restriction digestion of the pET22b::$MurM_{R6}$ construct after removal of the *Bam*HI site by *Nde*I digestion.

Cloning of $murM_{R6}$ into pET22b involved restriction digestion of both the PCR product and the pET vector with *Bam*HI and *Xho*I. Clones whereby *murM* had successfully inserted into pET22b were identified by agarose gel electrophoresis of *Bam*HI/*Xho*I digests and sequencing using the T7 forward and reverse primers (numbers 17 and 18, Chapter 2, Table 2.2). Digestion with *Nde*I was utilised as a means of positioning the 5' end of *murM* close to the ribosome binding site of the vector for expression purposes.

3.3.2. Small-scale MurM expression trials

In order to determine the optimal conditions for expression of $MurM_{R6}$, small-scale trials were carried out using three different *Escherichia coli* expression strains:

B834 (DE3), BL21 Star (DE3) and BL21 Star (DE3).placIRare2. Initially, single colonies from each of these transformations were cultured for 16 h at 37^{o}C in 10 mL of auto-induction medium as described in Chapter 2, section 2.3.2. Crude extracts were obtained from these cultures by sonication at 10% power for 15 sec and centrifugation to obtain both soluble and insoluble fractions. Bradford reagent was used to determine the protein concentration of the crude extracts so that 25 µg of protein could be loaded onto each lane of a 12.5% SDS PAGE gel (Chapter 2, section 2.4.9). The results of this experiment are presented in Figure 3.2.

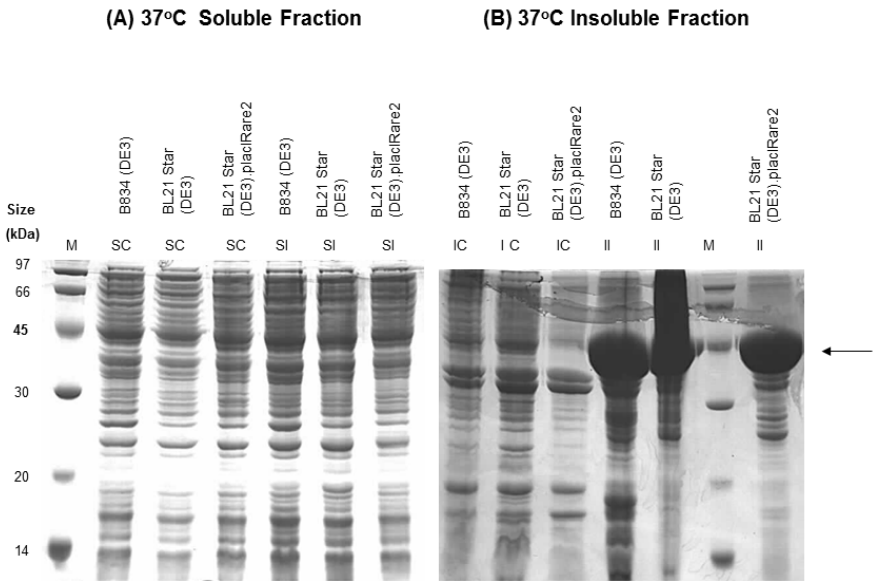

M - molecular weight standards,
SC - soluble proteins expressed by non-induced cells,
SI - soluble proteins expressed by induced cells,
IC - insoluble proteins expressed by non-induced cells,
II - insoluble proteins expressed by induced cells.

Figure 3.2: 12.5% SDS PAGE gels of crude extracts from three expression strains of *Escherichia coli* transformed with pET22b::MurM$_{R6}$ and induced to express protein by auto-induction (AI) at 37^{o}C for 16 h. The molecular weight of MurM$_{R6}$ is 47,310 Da. Controls refer to cells that have been transformed with the MurM construct but prevented from expressing the protein by the replacement of auto-induction medium with glucose.

As shown in Figure 3.2, each strain of *E. coli* appeared to express $MurM_{R6}$ with equal efficiency. To maximise the overall yield of protein obtained, further expression of $MurM_{R6}$ was only carried out using *E. coli* BL21 Star (DE3).placIRare2 cells which provide rare tRNA codons as described in chapter 2. There was no obvious expression product of $MurM_{R6}$ in the soluble fraction of the crude extracts derived from any of the expression strains when cultured at 37^{o}C. However, high levels of over-expression were identified in an insoluble form possibly due to protein precipitation or inclusion body formation as described by Carrio and Villaverde (2001) for other proteins. Expression of MurM in the soluble fraction could not be achieved by induction of protein expression using IPTG or reduction of the growth and expression temperature to 25^{o}C. For this reason, alternative solubilisation strategies utilising detergent, chaperones or high salt concentrations (1 M NaCl) were investigated as described below.

3.3.3. MurM solubilisation trials

3.3.3.1. Solubilisation of MurM using detergent

Initial solubilisation screens were detergent based. For this trial, 1 L of *E. coli* BL21 Star (DE3).placIRare2 cells harbouring the pET22b::$MurM_{R6}$ construct were cultured at 37^{o}C to an OD_{600nm} of 0.4 when $MurM_{R6}$ expression was induced by the addition of IPTG to a final concentration of 1 mM. Addition of IPTG was concurrent with the growth temperature being reduced to 28^{o}C for 4 h (Chapter 2, section 2.3.3).

Harvested cells were resuspended in buffer containing 2.5 mg mL^{-1} lysozyme, subjected to shaking at 4^{o}C for 30 min and then frozen at -80^{o}C. Previous studies (Anne Blewett, PhD thesis University of Warwick) have shown that the MurM protein from various strains of *S. pneumoniae* can be solubilised by supplementing

the sonication buffer with 0.5% (w/v) sarcosyl. Therefore, cells were thawed out, centrifuged and resuspended in HEPES buffer containing sarcosyl prior to sonication (Chapter 2, section 2.3.6). After sonication, the cells were centrifuged to obtain the soluble fraction which was then loaded onto a high-performance his-trap nickel column (GE Healthcare) pre-equilibrated in buffer containing 50 mM sodium phosphate pH 7.5, 200 mM NaCl and 10 mM imidazole. Elution of $MurM_{R6}$ was achieved by running a continuous gradient of imidazole from 10 mM to 500 mM through the column using the ÄKTA prime system (GE Healthcare). Peak fractions obtained from this technique were subjected to SDS PAGE analysis (Figure 3.3) to assess the solubility and purity of $MurM_{R6}$.

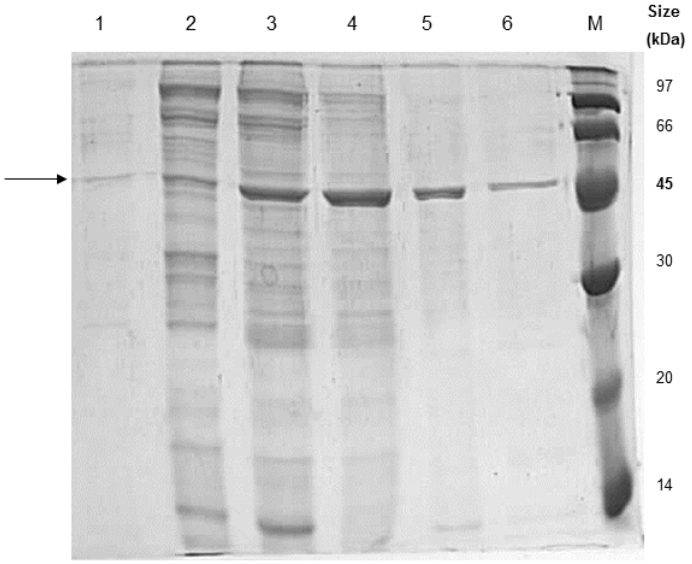

Figure 3.3: His-trap column purification of $MurM_{R6}$ using a continuous gradient of imidazole from 10 mM to 500 mM. Lanes 1 to 6 - samples of protein eluted in the peak fractions as determined by monitoring absorbance at 280 nm. Elution of $MurM_{R6}$ was achieved at approximately 60 mM imidazole. The position of MurM is marked with an arrow. M - molecular weight standards.

Fractions obtained from the His-trap column containing $MurM_{R6}$ were pooled, concentrated to a final volume of 5 mL (Chapter 2, section 2.4.8) and subjected to size exclusion chromatography using a Superdex 75 column (GE Healthcare) pre-equilibrated in buffer containing 50 mM Tris-HCl pH 8.0 and 200 mM NaCl. Peak

fractions obtained using this method were analysed by SDS PAGE, the results of which are shown in Figure 3.4.

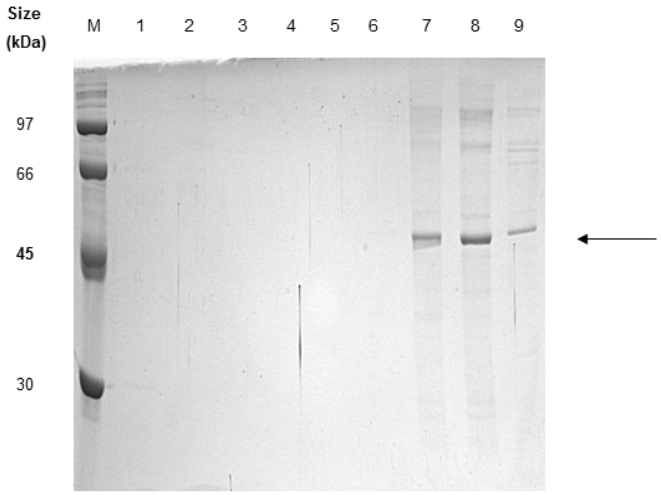

Figure 3.4: Size exclusion chromatography of $MurM_{R6}$. Lanes 1-9 - samples of protein in peak fractions eluting after passage of 100 mL of buffer through the column. M - molecular weight standards. The position of MurM is marked with an arrow.

Given that one of the substrates for MurM is a lipid, it was considered undesirable for any detergent to be present after purification unless it was absolutely necessary for the solubility of the protein. The overall yield and purity of protein obtained by IMAC and size exclusion chromatography after solubilisation with detergent was unsuitable for crystallography. For these reasons, two further methods were investigated in an attempt to improve the overall yield of soluble protein which might then be purified more readily without the need for detergent. The aim of trialling solubilisation of MurM by chaperone co-expression or 1 M NaCl was to address the concern that detergents may have a detrimental effect on both biochemical assays and crystallography.

3.3.3.2. Solubilisation of MurM using chaperone co-expression

Since over-expression of $MurM_{R6}$ rendered the protein insoluble regardless of expression strain and growth temperature, chaperone co-expression was investigated as a means of solubilisation. The aim of this experiment was to determine whether or not the inherent insolubility of $MurM_{R6}$ was attributable to incorrect folding of the protein during over-expression.

Five Takara plasmids encoding various chaperones were transformed into *E. coli* B834 (DE3) cells which were then made chemically-competent for the uptake of the pET22b::$MurM_{R6}$ expression construct. Expression experiments were carried out at 37^{o}C using auto-induction medium and L-arabinose/tetracycline as appropriate to induce chaperone expression (see Chapter 2, section 2.3.4 for details of the chaperones encoded by these plasmids and induction of their expression). The results of this experiment are shown in Figure 3.5.

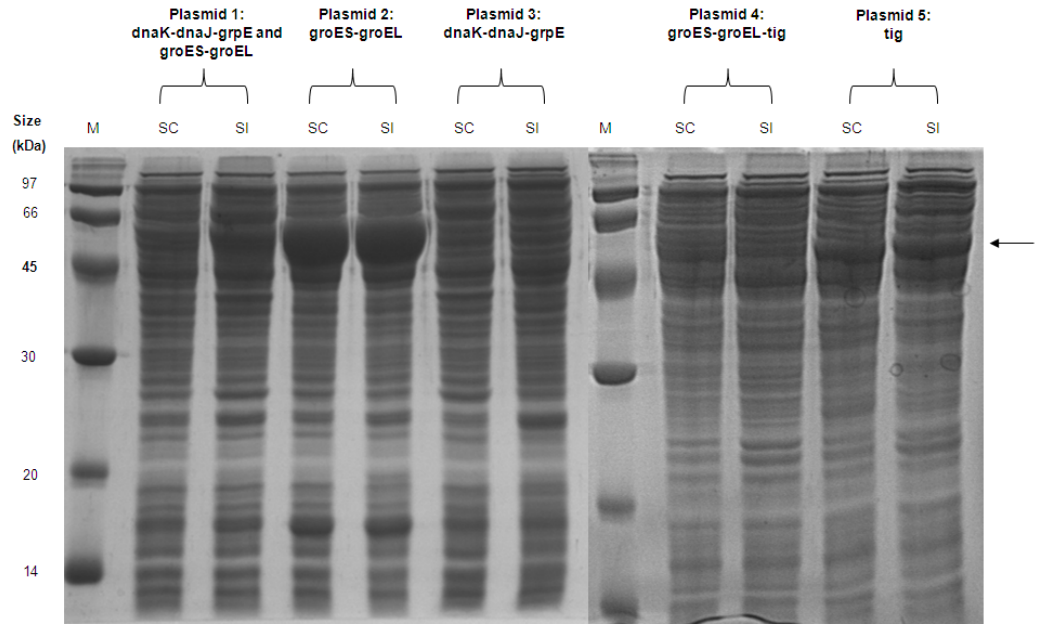

M - standard molecular weight markers,
SC - protein expressed in the soluble fraction of cells induced for chaperone expression but not for $MurM_{R6}$ expression,
SI - protein expressed in the soluble fraction of cells induced both for chaperone and $MurM_{R6}$ expression.

Figure 3.5: 12.5% SDS PAGE gels showing protein in the soluble fraction of *Escherichia coli* B834 (DE3) cells transformed with the Takara plasmid chaperone set and pET22b::$MurM_{R6}$ and induced to express protein by auto-induction (AI) at 37°C. The arrow shows the migratory position of MurM upon expression.

For the chaperone plasmids 1, 3, 4 and 5, there was no obvious expression product for $MurM_{R6}$ in the soluble fraction. For chaperone plasmid 2, a large over-expressed band was seen between 66 and 45 kDa in both the control and the auto-induced sample. Since the band was also present in the control, it was expected to represent an over-expression of the chaperone GroEL rather than MurM. However, these two soluble samples plus all of the insoluble fractions obtained from the chaperone co-expression experiments were subjected to the Pro-Q Sapphire 532 Oligohistidine Gel stain (Molecular probes) to check for expression of histidine-tagged protein. This technique exploits the addition of a poly-histidine tag to the C-terminal end of the

murM gene during cloning into the pET22b expression vector. The chaperones used in this study are not histidine-tagged. Results of this experiment are presented in Figure 3.6.

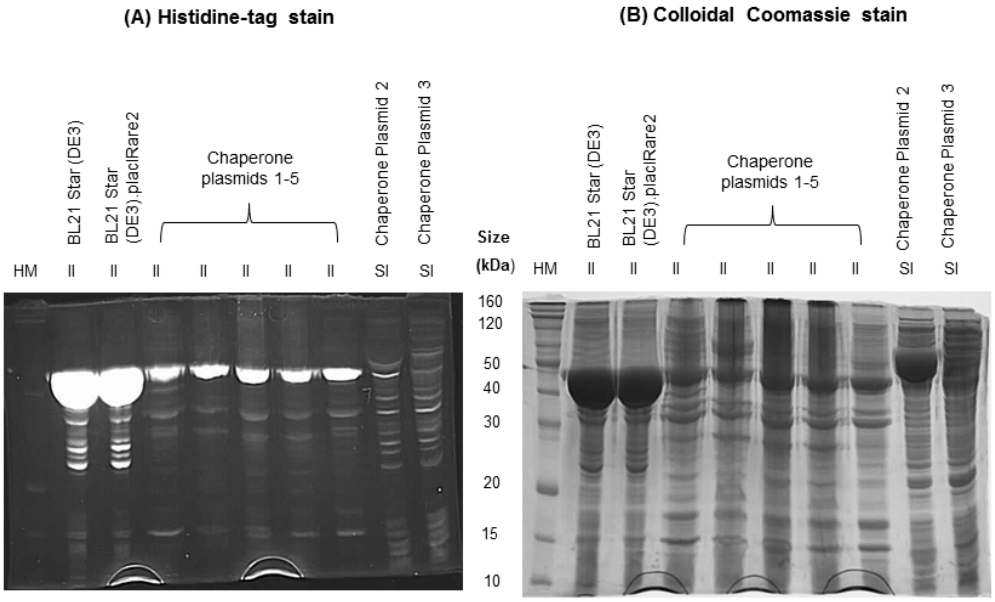

HM - Benchmark Histidine-tagged protein marker (Invitrogen),
II - insoluble proteins produced by induced cells,
SI - soluble proteins produced by induced cells.

Figure 3.6: (A) Histidine-tag stained and (B) Colloidal Coomassie stained 12.5% SDS PAGE gels of the crude extracts obtained during chaperone co-expression of $MurM_{R6}$ in *Escherichia coli* B834 (DE3) cells. In the case of the chaperone co-expression experiment, induced cells have been set up to express both the chaperone and $MurM_{R6}$.

Histidine-tag staining of crude extracts confirmed that $MurM_{R6}$ was being expressed in an insoluble form in *E. coli* BL21 Star (DE3), BL21 Star (DE3).placIRare2, and B834 Takara chaperone co-expression cells. In addition to this, comparison of histidine tag and Colloidal Coomassie staining of the crude extracts from the chaperone co-expression experiment confirmed that the over-expressed protein in the soluble fraction of *E. coli* B834 (DE3) cells harbouring Takara chaperone plasmid 2 was GroEL and not $MurM_{R6}$. Therefore, chaperone co-expression was discarded as a suitable means of generating a high yield of soluble $MurM_{R6}$.

Prior to attempts at solubilising $MurM_{R6}$ using 1 M sodium chloride (see Chapter 2, section 2.3.7), the *murM* genes from *S. pneumoniae* strains R6, Pn16 and 159 were re-cloned into pET22b such that protein expression would result in incorporation of a dodeca-histidine tag at the C-terminus. This was based on the theory that the addition of six extra histidine residues to $MurM_{R6}$ would raise the isoelectric point of the protein such that its solubility would also be increased. A secondary reason for adding the extra histidine residues to the C-terminus of MurM was to allow for the development of a more successful IMAC purification procedure with tighter interaction between the extended histidine tag on MurM and the IMAC resin in case a detergent based environment was ultimately required for solubility of $MurM_{R6}$.

3.3.3.3. Re-cloning of the *murM* genes from *Streptococcus pneumoniae* strains Pn16, R6 and 159 into pET22b to encode a C-terminal dodeca-histidine tag

In order to re-clone the *murM* genes from *S. pneumoniae* strains R6, Pn16 and 159 into pET22b such that they encoded a C-terminal dodeca-histidine tag, the reverse PCR primer was redesigned to include six histidine residues immediately adjacent to the *Xho*I restriction site (Chapter 2, Table 2.2, primer 4). PCR amplification of the genes was carried out as before using Accuprime *Taq* DNA polymerase (Invitrogen) and the hexa-histidine MurM expression constructs as templates for the reaction (Chapter 2, section 2.2.2). A cloning summary for $MurM_{159}$ is shown in Figure 3.7.

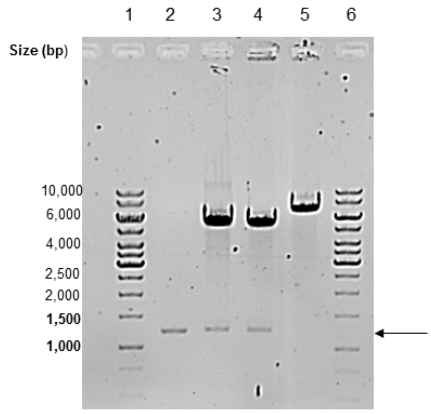

Figure 3.7: Summary agarose gel showing cloning of the *Streptococcus pneumoniae* strain 159 *murM* gene into pET22b to encode a C-terminal dodeca-histidine tag. The size of the pET22b vector is 5,493 bp.

Lanes 1 and 6 - 1 kb ladder,
Lane 2 - *murM*$_{159}$ PCR product,
Lane 3 - *Bam*HI/*Xho*I restriction digestion of the initial pET22b::MurM$_{159}$ construct prior to removal of the *Bam*HI site,
Lane 4 - *Nde*I/*Xho*I restriction digestion of the pET22b::MurM$_{159}$ construct where the *Bam*HI site had been removed by *Nde*I digestion,
Lane 5 - *Bam*HI/*Xho*I restriction digestion of the pET22b::MurM$_{159}$ construct after removal of the *Bam*HI site by *Nde*I digestion.

During re-cloning of the three *murM* genes, extensive sequence analysis was carried out due to a discrepancy between the sequence of MurM$_{Pn16}$ identified in this study compared to that published by Lloyd *et al.* (2008). In the work carried out by Lloyd *et al.* (2008), MurM$_{Pn16}$ and MurM$_{R6}$ were assumed to diverge in sequence at three amino acid residues: 101 (alanine and valine respectively), 134 (methionine and leucine respectively) and 135 (arginine and glutamine respectively). However, chromosomal DNA extraction, PCR amplification and sequencing of the *murM*$_{Pn16}$ gene from all samples of *S. pneumoniae* strain Pn16 in the University of Warwick culture collection indicated that this was not correct. MurM$_{Pn16}$ and MurM$_{R6}$ only diverge in sequence at position 101 with leucine and glutamine conserved at positions 134 and 145 in both proteins respectively. A sequence alignment of MurM$_{159}$ with MurM$_{Pn16}$ and MurM$_{R6}$ generated by this study is shown in Figure 3.8.

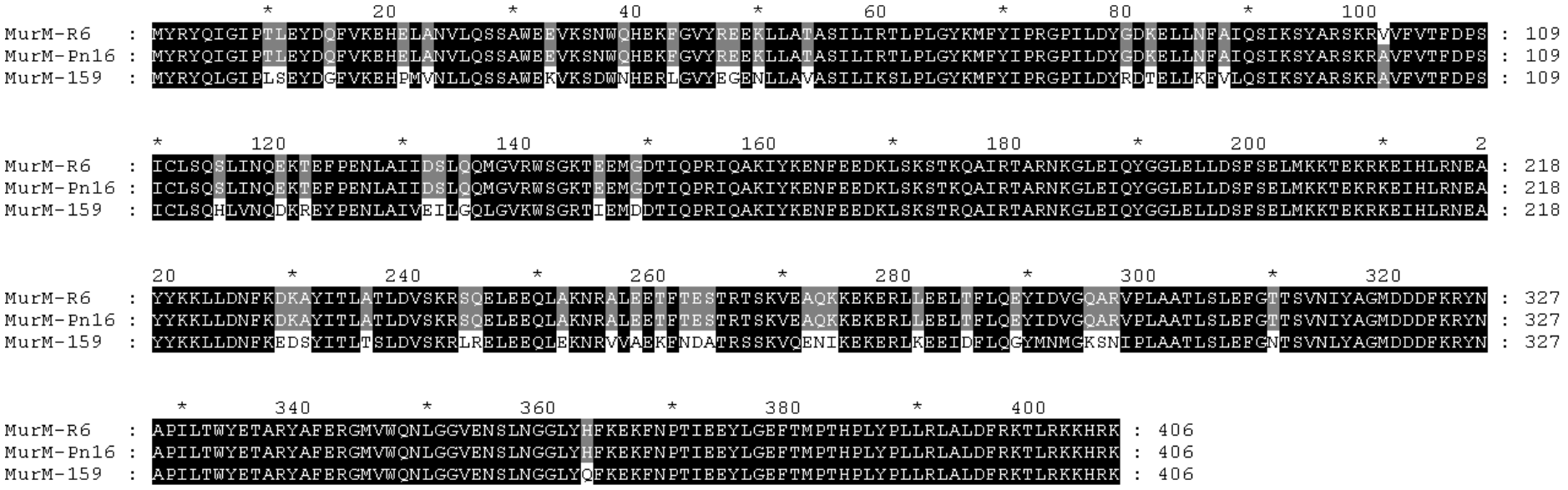

Figure 3.8: Alignment of the amino acid sequences for $MurM_{R6}$, $MurM_{Pn16}$ and $MurM_{159}$ as generated by Clustal X and GeneDoc. Note that $MurM_{R6}$ and $MurM_{Pn16}$ only have one amino acid difference between them and this can be found at position 101. Areas of conservation between the three MurM proteins are highlighted in black.

All three dodeca-histidine tag MurM expression constructs were transformed into *E. coli* BL21 Star (DE3).placIRare2 cells for the purpose of trial auto-induction expressions at 37^{o}C. Crude extracts were made as described in Chapter 2 (sections 2.3.3 and 2.3.5) and analysed by 12.5% SDS PAGE as shown in Figure 3.9.

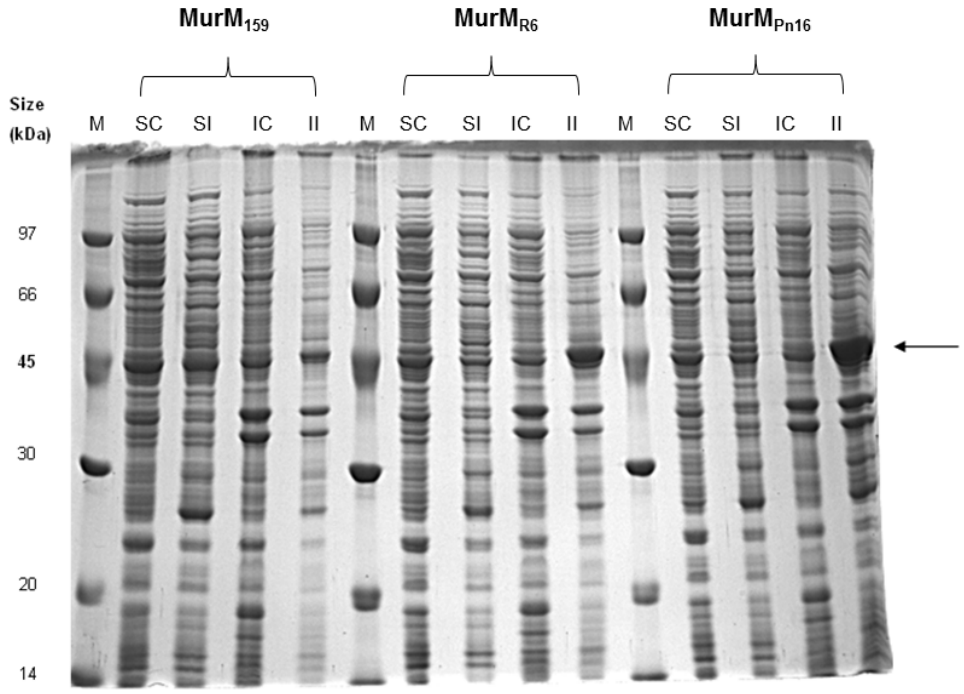

M - molecular weight standards,
SC - soluble proteins expressed by non-induced cells,
SI - soluble proteins expressed by induced cells,
IC - insoluble proteins expressed by non-induced cells,
II - insoluble proteins expressed by induced cells.

Figure 3.9: 12.5% SDS PAGE gel showing crude extracts obtained from *Escherichia coli* BL21 Star (DE3).placIRare2 cells transformed with each pET22b::MurM dodeca-histidine tagged construct and induced to express protein by auto-induction (AI) at 37^{o}C for 16 h. The arrow indicates the migratory position of MurM expression corresponding to the 45 kDa standard in each marker lane.

As shown in Figure 3.9, the presence of an extra six histidine residues on the C-terminus of each variant of MurM did not result in any visual improvement in the solubility of the protein during SDS PAGE analysis. However, both the hexa- and dodeca-histidine tagged versions of each variant of MurM were over-expressed on a

large scale (1 L) in *E. coli* BL21 Star (DE3).placIRare2 cells to enable investigation into solubilising the protein using 1 M sodium chloride (Chapter 2, sections 2.3.3 and 2.3.7).

3.3.3.4. Solubilisation of MurM using 1 M sodium chloride

For each MurM variant, 1 L of *E. coli* BL21 Star (DE3).placIRare2 cells that had been transformed with pET22b::MurM were cultured at 37^{o}C to an OD_{600nm} of 0.4 when MurM expression was induced by the addition of IPTG to a final concentration of 1 mM. Addition of IPTG was concurrent with the growth temperature being reduced to 28^{o}C for 4 h. Solubilisation of MurM by 1 M salt extraction was then trialled on these cells, initially with $MurM_{R6}$, using an adapted form of the methodology developed by Lloyd *et al*. (2008) (Chapter 2, section 2.3.7). Using these methods, four fractions were obtained: a crude supernatant containing protein that was soluble prior to salt extraction, two salt extracted supernatants and a pellet containing proteins that were not solubilised by the salt extraction procedure. All four fractions were analysed by SDS PAGE as shown in Figure 3.10.

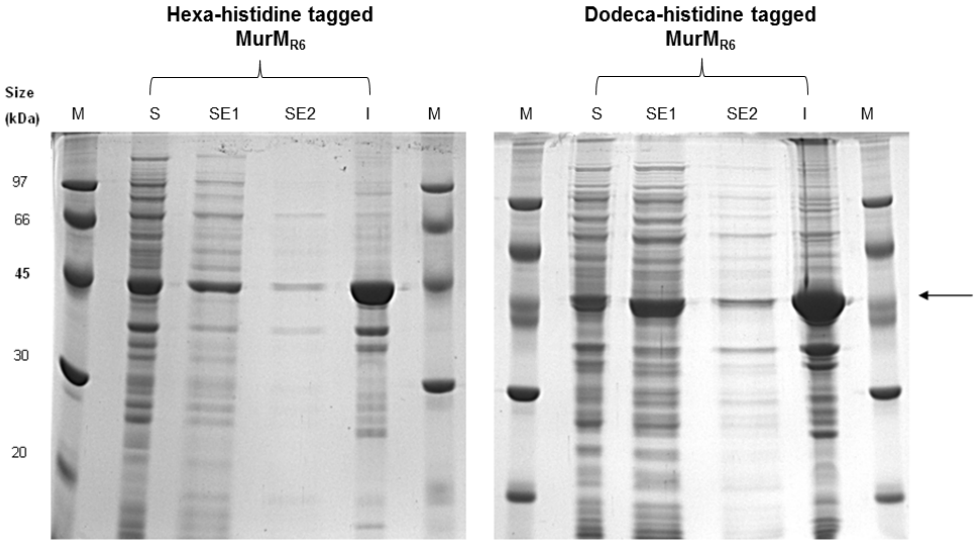

M - standard molecular weight markers,
S - soluble protein prior to salt extraction,
SE1 - soluble protein after the first salt extraction,
SE2 - soluble protein after the second salt extraction,
I - protein that remained insoluble after completion of salt extraction.

Figure 3.10: 12.5% SDS PAGE analysis showing salt-solubilisation of MurM$_{R6}$ from 1 L of *Escherichia coli* BL21 Star (DE3).placIRare2 cells. The position of MurM is marked with an arrow.

Initial solubilisation trials of MurM$_{R6}$ indicated that, whilst a significant proportion of the over-expressed protein remained insoluble after salt extraction, enough protein had been successfully solubilised by this technique. This contrasts with chaperone co-expression and the use of detergent, which resulted in either no or a slight improvement in the solubility of MurM$_{R6}$ respectively. For this reason, the success of salt-solubilisation on strains Pn16 and 159 MurM were investigated and the results of this procedure are given in Figure 3.11.

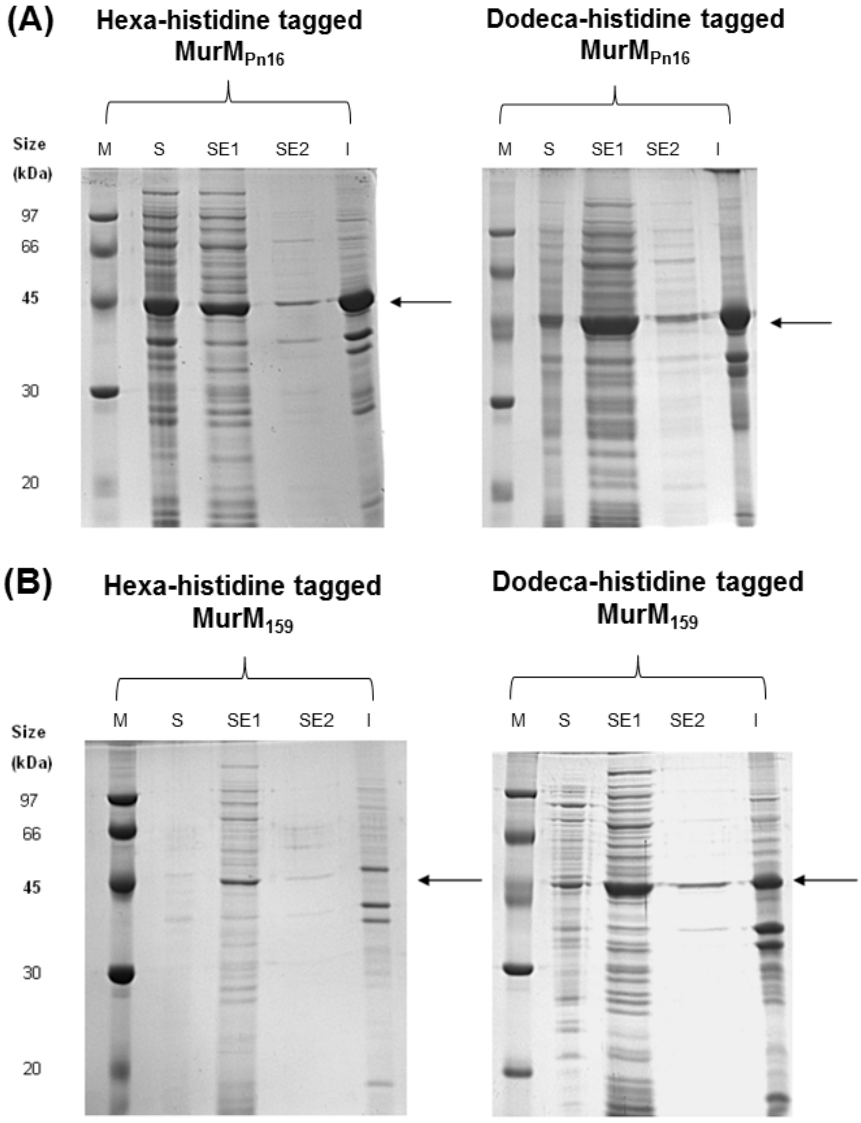

M - standard molecular weight markers,
S - soluble protein prior to salt extraction,
SE1 - soluble protein after the first salt extraction,
SE2 – soluble protein after the second salt extraction,
I - protein that remained insoluble after completion of salt extraction.

Figure 3.11: 12.5% SDS PAGE analysis showing salt-solubilisation of (A) MurM$_{Pn16}$ and, (B) MurM$_{159}$ from 1 L of *Escherichia coli* BL21 Star (DE3).placIRare2 cells. The position of MurM is marked with an arrow.

As shown in Figure 3.11, MurM$_{Pn16}$ and MurM$_{159}$ could also be successfully solubilised using salt extraction methodology. Therefore, further purification

methods were developed based on solubilisation of MurM using 1 M sodium chloride.

3.3.4. Purification of salt-solubilised MurM

Initial purification attempts for salt-solubilised $MurM_{R6}$ reproduced those developed by Lloyd *et al*. (2008) for hexa-histidine tagged $MurM_{Pn16}$ and $MurM_{159}$. However, in the absence of detergent, protein loaded onto high performance nickel and gel filtration columns could not be eluted using the GE ÄKTA Purifier system. One hypothesis for this was that $MurM_{R6}$ undergoes tight hydrophobic interactions with the frits at the ends of the GE Healthcare columns. This was supported by the fact that elution of $MurM_{R6}$ from these columns could only be achieved under strong denaturing conditions (8 M guanidine hydrochloride).

For this reason, high performance nickel resin (GE Healthcare) was used to construct a bench-top purification column plugged with glass wool. Prior to loading of the protein, the column was equilibrated in buffer containing 50 mM sodium phosphate, 500 mM sodium chloride and 20% glycerol at pH 7.0. Elution of protein was achieved by sequential step washing of the column with buffer containing 10 mM, 50 mM, 200 mM and 500 mM imidazole. Results of the purification of dodeca-histidine tagged $MurM_{R6}$ from 1 L of *E. coli* BL21 Star (DE3).placIRare2 cells using this methodology is shown in Figure 3.12.

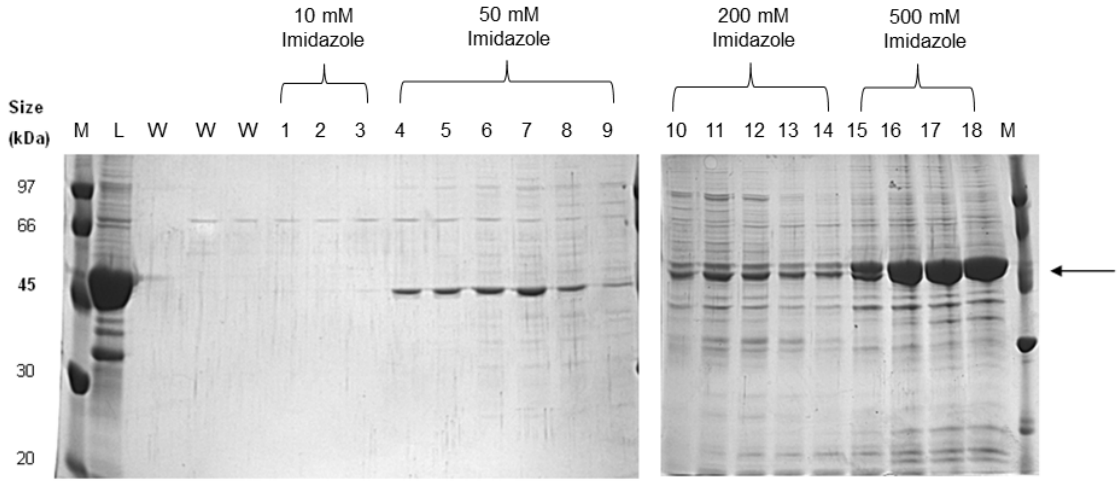

M -molecular weight standards,
L - protein sample prior to loading onto the column,
W - protein collected during wash of the column with equilibration buffer.

Figure 3.12: 12.5% SDS PAGE gel showing purification of salt-solubilised dodeca-histidine tagged $MurM_{R6}$ from 1 L of *Escherichia coli* BL21 Star (DE3).placIRare2 cells on high performance nickel resin (GE Healthcare). Lanes 1 - 18 represent protein eluted from the column during step washes using equilibration buffer supplemented with different concentrations of imidazole (10 mM, 50 mM, 200 mM and 500 mM). The position of large amounts of $MurM_{R6}$ eluted during the 500 mM imidazole wash is marked with an arrow.

As shown in Figure 3.12, purification of dodeca-histidine tagged $MurM_{R6}$ on nickel resin was successful in terms of protein eluting from the column. However, levels of purity were much lower than expected and could not be improved further by hydrophobic interaction chromatography on either phenyl- or octyl-sepharose. For this reason, new purification methodology was developed using BD TALON cobalt metal affinity resin.

Initial purification on cobalt resin was trialled with detergent-solubilised dodeca-histidine tagged $MurM_{R6}$ to determine the most suitable buffer conditions for optimum purity of the enzyme upon elution from the column. Primarily this involved equilibrating BD TALON cobalt resin with pH 7.0 buffer containing 50 mM sodium phosphate and 300 mM sodium chloride as described in the manufacturer's

instructions. Dodeca-histidine tagged $MurM_{R6}$ that had been solubilised with 0.5% (w/v) sarcosyl was then loaded onto the column and eluted with sequential wash steps in equilibration buffer supplemented with no imidazole, 10 mM imidazole and 200 mM imidazole. Overall purity of eluted $MurM_{R6}$ was assessed by SDS PAGE and is shown in Figure 3.13.

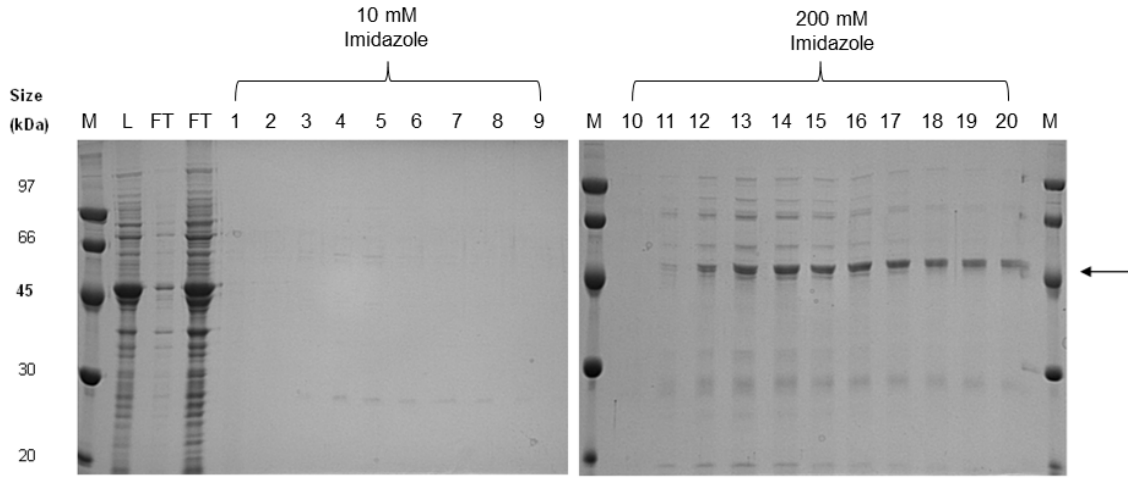

M - molecular weight standards,
L - protein sample prior to loading onto the column,
FT - flow through as protein was loaded onto the column,
W - protein collected during wash of the column with equilibration buffer.

Figure 3.13: 12.5% SDS PAGE gels showing purification of sarcosyl-solubilised dodeca-histidine tagged $MurM_{R6}$ from 1 L of *Escherichia coli* BL21 Star (DE3).placIRare2 cells on BD TALON resin. Lanes 1 - 20 represent protein eluted from the column during step washes using equilibration buffer supplemented with different concentrations of imidazole (10mM and 200 mM). The position of $MurM_{R6}$ eluted during the 200 mM imidazole wash is marked with an arrow.

Improvements to the overall purity of the protein shown in Figure 3.13 were achieved by adding additional wash steps to the protocol. A second round of purification involved sequential washing with equilibration buffer supplemented with 20 mM imidazole, 50 mM imidazole, 100 mM imidazole, 150 mM imidazole and 200 mM imidazole. Protein purity was re-assessed by SDS PAGE as shown in Figure 3.14.

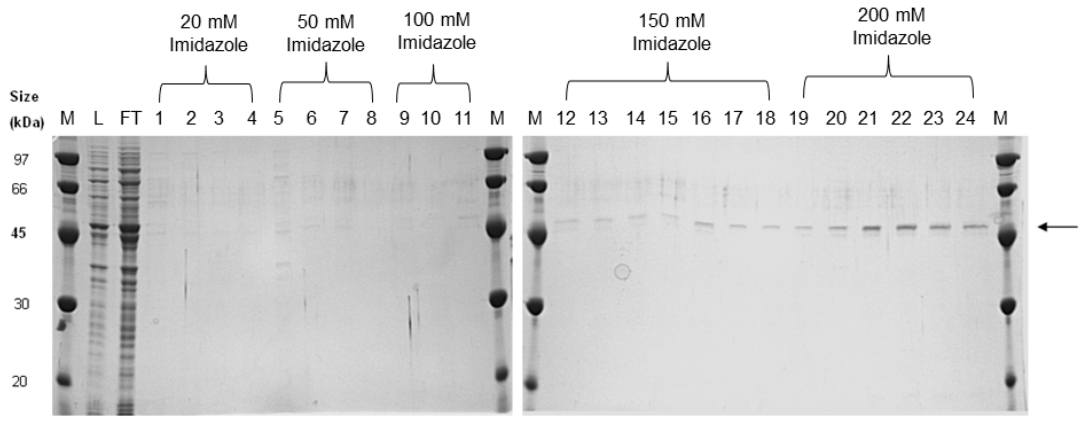

M - molecular weight standards,
L - protein sample prior to loading onto the column,
FT - flow through as protein was loaded onto the column.

Figure 3.14: 12.5% SDS PAGE gel showing purification of sarcosyl-solubilised dodeca-histidine tagged $MurM_{R6}$ from 1 L of *Escherichia coli* BL21 Star (DE3).placIRare2 cells on BD TALON resin. Lanes 1 - 24 represent protein eluted from the column during step washes using equilibration buffer supplemented with different concentrations of imidazole (20 mM, 50 mM, 100 mM, 150 mM and 200 mM). The position of $MurM_{R6}$ is indicated with an arrow.

Problems identified during the first two trials of $MurM_{R6}$ purification on BD TALON resin included the observation that a large proportion of the protein was unable to stick to the column and came off in the flow-through during loading. This was addressed by including 20% glycerol in the elution buffer during the final stages of the development of a purification protocol for MurM on BD TALON resin. The purpose of adding glycerol was to stabilise MurM by preventing protein aggregation at high concentrations.

After these initial trials, purification of salt-solubilised dodeca-histidine tagged $MurM_{R6}$ was tested on cobalt resin pre-equilibrated in buffer containing 50 mM sodium phosphate, 500 mM sodium chloride, 1 μM leupeptin, 1 μM pepstatin and 20% glycerol at pH 7.0. A final concentration of 10 mM imidazole was also added to

the equilibration buffer as initial tests had indicated that the presence of imidazole gave histidine-tagged $MurM_{R6}$ an advantage over contaminants in terms of ability to bind the resin during loading. After loading of the protein onto the column sequential wash steps with equilibration buffer containing 10 mM, 50 mM and 200 mM imidazole were carried out to elute $MurM_{R6}$. Overall purity of $MurM_{R6}$ was assessed by SDS PAGE and is shown in Figure 3.15.

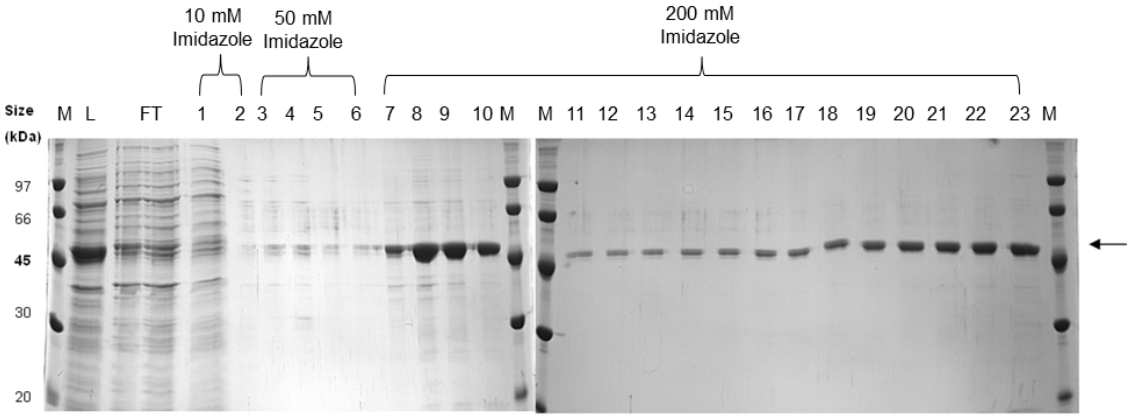

M - molecular weight standards,
L - protein sample prior to loading onto the column,
FT - flow through was protein is loaded onto the column.

Figure 3.15: 12.5% SDS PAGE gel showing purification of salt-solubilised dodeca-histidine tagged $MurM_{R6}$ from 1 L of *Escherichia coli* BL21 Star (DE3).placIRare2 cells on BD TALON cobalt resin. Lanes 1 - 23 represent protein eluted from the column during step washes using equilibration buffer supplemented with different concentrations of imidazole (10 mM, 50 mM and 200 mM). The position of large amounts of $MurM_{R6}$ eluted during the 200 mM imidazole wash is marked with an arrow.

During loading of MurM onto BD TALON cobalt resin, a higher proportion of contaminating proteins were unable to stick to the column and eluted in the flow through when compared to similar trials using nickel resin. Dodeca-histidine tagged $MurM_{R6}$ of high purity was eluted in the 200 mM imidazole wash step. Given the success of this procedure, trials with hexa-histidine tagged $MurM_{R6}$ and cobalt resin

were carried out in the same way and protein purity was assessed by SDS PAGE as shown in Figure 3.16.

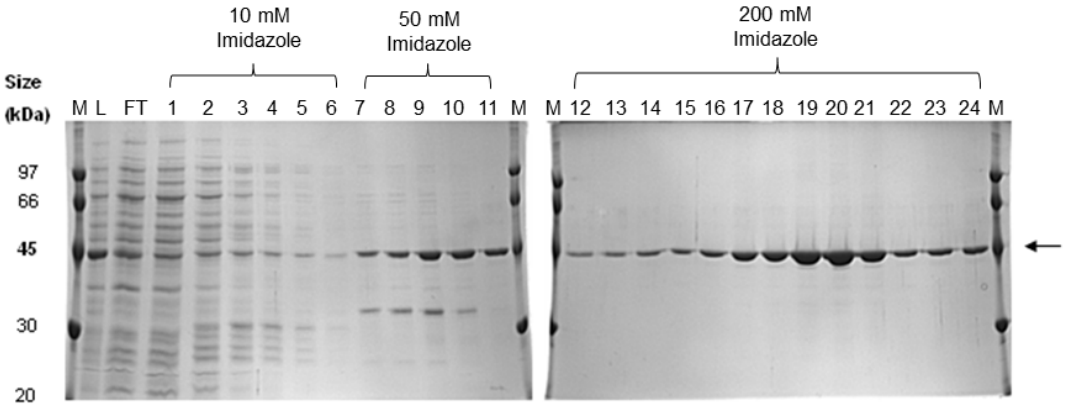

M - molecular weight standards,
L - protein sample prior to loading onto the column,
FT - flow through as protein was loaded onto the column.

Figure 3.16: 12.5% SDS PAGE gel showing purification of salt-solubilised hexa-histidine tagged $MurM_{R6}$ from 1 L of *Escherichia coli* BL21 Star (DE3).placIRare2 cells on BD TALON cobalt resin. Lanes 1 - 24 represent protein eluted from the column during step washes using equilibration buffer supplemented with different concentrations of imidazole (10 mM, 50 mM and 200 mM). The position of large amounts of $MurM_{R6}$ eluted during the 200 mM imidazole wash is marked with an arrow.

Purification of hexa-histidine tagged $MurM_{R6}$ on BD TALON cobalt resin was also successful with the majority of protein eluting in the 200 mM imidazole wash step. In contrast to purification of dodeca-histidine tagged $MurM_{R6}$, protein elution began at 50 mM imidazole rather than 200 mM imidazole. However, this did not affect the overall purity of the eluted protein. Purification of $MurM_{Pn16}$ and $MurM_{159}$ were also attempted using BD TALON resin and SDS PAGE analyses of the overall purity of these enzymes are shown in Figure 3.17 part A and B respectively.

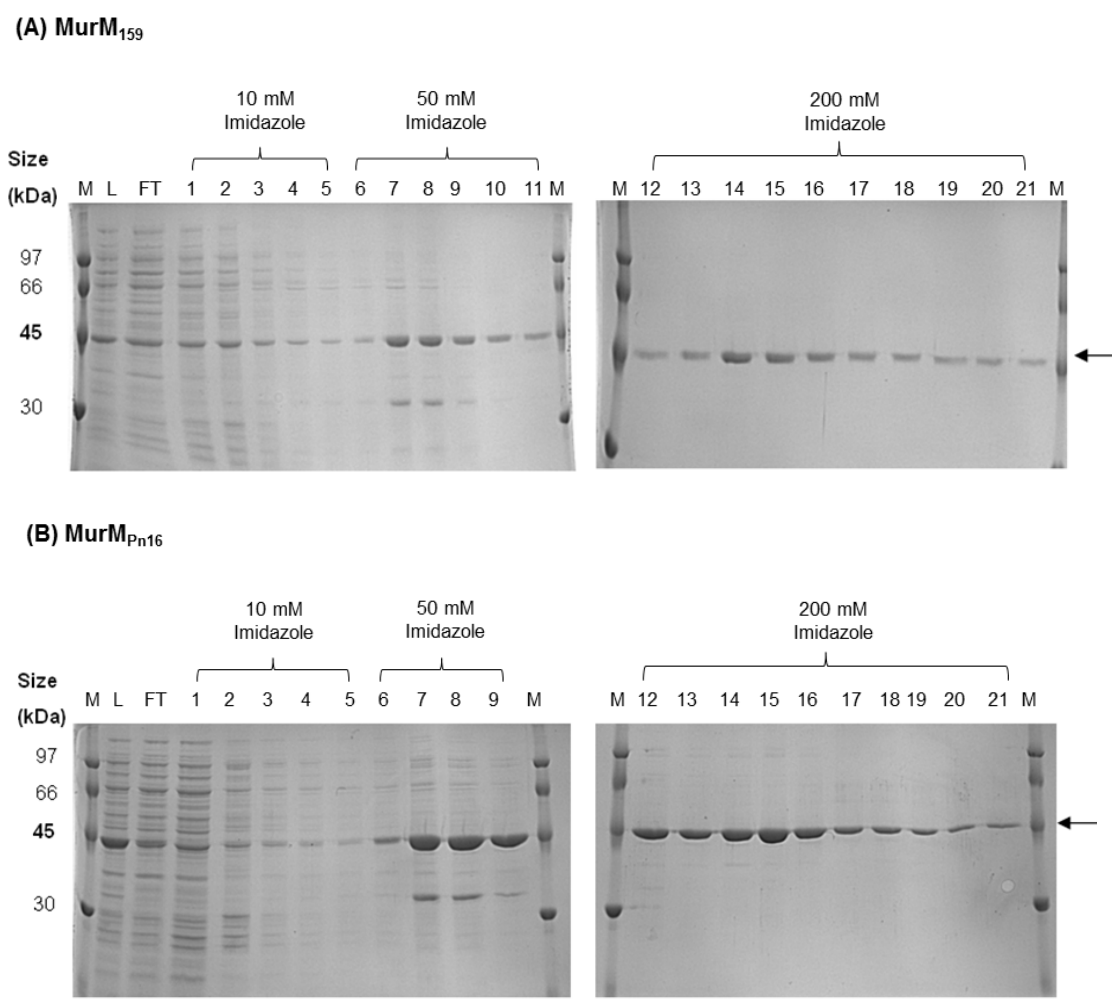

M -molecular weight standards,
L - protein sample prior to loading onto the column,
FT - flow through as protein was loaded onto the column.

Figure 3.17: 12.5% SDS PAGE gels showing purification of salt-solubilised (A) hexa-histidine tagged $MurM_{159}$ and, (B) hexa-histidine tagged $MurM_{Pn16}$ from 1 L of *Escherichia coli* BL21 Star (DE3).placIRare2 cells on BD TALON cobalt resin. Lanes 1 - 21 represent protein eluted from the column during step washes using equilibration buffer supplemented with different concentrations of imidazole (10 mM, 50 mM and 200 mM). The position of large amounts of MurM eluted during the 200 mM imidazole wash is marked with an arrow.

Both the hexa- and dodeca-histidine tagged versions of $MurM_{Pn16}$ and $MurM_{159}$ purified as effectively as $MurM_{R6}$ on BD TALON cobalt resin. This novel single step process consisted of equilibration of a 5 mL cobalt column with 50 mL of buffer containing 50 mM sodium phosphate pH 7.0, 500 mM NaCl, 10 mM imidazole and

20% glycerol. After loading of an extract containing soluble MurM, purification in excess of 95%, as determined by SDS PAGE analysis, was achieved by step washing of the column with 50 mL of equilibration buffer followed by 30 mL of equilibration buffer supplemented with 50 mM imidazole and 30 mL of equilibration buffer supplemented with 200 mM imidazole. This procedure has been used throughout this study to produce pure MurM suitable for biochemical studies and X-ray crystallography.

3.4. Discussion

Due to the unusually high levels of indirect cross-linking in the cell wall of penicillin-sensitive *S. pneumoniae* strain R6, it was considered that studying the properties of the MurM protein from this strain may help decipher the relationship between penicillin-resistance, levels of cell-wall cross-linking and the activity of the MurM protein within *S. pneumoniae*. For this reason, the $murM_{R6}$ gene was cloned into pET22b (Novagen) to encode a C-terminal hexa-histidine tag. The ultimate aim of the work carried out in this chapter was to produce suitable quantities of pure, soluble $MurM_{R6}$ enabling comparisons to be made with the MurM proteins from *S. pneumoniae* strains Pn16 (penicillin-sensitive) and 159 (penicillin-resistant) which were characterised biochemically at Warwick in earlier studies (Lloyd *et al.*, 2008).

Small-scale expressions of $MurM_{R6}$ were carried out in three *E. coli* expression strains: B834 (DE3), BL21 Star (DE3) and BL21 Star (DE3).placIRare2. In each case, $MurM_{R6}$ was expressed at a high level but in the insoluble fraction of the cells. Expression in the soluble fraction could not be achieved by auto-induction or ITPG-induction regardless of the temperature cells were cultured at. In addition to this, no

improvements in solubility were obtained by co-expression of $MurM_{R6}$ with a series of chaperones suggesting that insolubility was not solely attributable to incorrect folding of the protein. This was also found to be the case for $MurM_{Pn16}$ and $MurM_{159}$ in studies undertaken by Lloyd *et al.* (2008). Since one of the substrates for MurM is Lipid II, which is membrane bound, insolubility of MurM was hypothesised to be due to an association of the protein with the cell membrane.

As was the case for $MurM_{Pn16}$ and $MurM_{159}$, it was possible to solubilise $MurM_{R6}$ using 1 M salt thus avoiding the need for detergents which would complicate biochemical assays and crystallography. However, it was not possible to purify salt-solubilised $MurM_{R6}$ using the published methodology of ammonium sulphate precipitation followed by size exclusion and immobilised metal ion affinity chromatography. In the absence of detergent, $MurM_{R6}$ could only be eluted from pre-packed high performance his-trap and gel filtration columns (GE Healthcare) under strong denaturing conditions. This was hypothesised to be due to strong hydrophobic interactions between the protein and the frits found at both ends of the columns made by GE Healthcare. One explanation for this could be the presence of valine at position 101 in $MurM_{R6}$ which is replaced by alanine in $MurM_{Pn16}$ and $MurM_{159}$.

In order to overcome this problem, a novel single step IMAC purification method for MurM was developed using $MurM_{R6}$ as the model protein. In the case of all three variants of MurM, and regardless of the length of the C-terminal histidine tag, at least 10 mg of salt-solubilised purified protein could be obtained per litre culture of *E. coli* BL21 Star (DE3).placIRare2 cells using this methodology. Combined with an overall purity in excess of 95%, as determined by SDS PAGE analysis, this yield

was considered suitable for biochemical analysis and crystallographic studies on the protein. Hence, all of the aims detailed in section 3.2 were successfully met.

Chapter 4

Characterisation of Divalent Metal Ion Binding to the MurM protein from *Streptococcus pneumoniae* using Isothermal Titration Calorimetry (ITC)

4.1. Introduction

Many enzymes that catalyse reactions involving nucleic acids have an essential requirement for divalent metal ion cofactors (Mordasini *et al.*, 2003). In many cases, the functional role of such metal ions remains undetermined. However, it is possible to thermodynamically characterise metal ion binding to proteins using isothermal titration calorimetry (ITC).

Metal ions are crucial for the function of many proteins and have been shown to play a role in the maintenance of catalytic activity and structure. The most common metal ion to associate with proteins is zinc (Parisi and Vallee, 1969). In 1942, carbonic anhydrase II was found to be a zinc metalloenzyme. Since this initial discovery, over 300 other enzymes have been classified as zinc dependent. Amino acid residues commonly involved in zinc binding include cysteine via sulphur, histidine via nitrogen, aspartate via oxygen and glutamate via oxygen (Parisi and Vallee, 1969).

The structure of MurM is as yet unknown but has been modelled on the X-ray crystal structure of the *S. aureus* FemA protein (Benson *et al.*, 2002). With this in mind, MurM is considered to have a structure that is composed of two domains. The first domain is made up of helices that encase two cores of twisted β-sheets. In contrast to this, domain II is a coiled helical arm which is considered to be important for tRNA

recognition (Fiser *et al.*, 2003). Similar structures can be found in tRNA synthetase enzymes, many of which utilise metal ions for substrate recognition.

In *E. coli*, alanyl-tRNA synthetase has been shown to bind zinc with a stoichiometry of one. Loss of zinc from the native enzyme causes a change in conformation and flexibility which can be directly correlated with a loss of activity and structure (Sood *et al.*, 1999). *E. coli* threonyl-tRNA synthetase harbours a zinc atom within its active site that is bound and coordinated by three amino acid residues. Targeted mutation of any one of these three residues has been demonstrated to result in the production of inactive enzyme (Caillet *et al.*, 2007). Many Glutamyl- and Seryl-tRNA synthetases also have structural and catalytic requirements for zinc (Liu *et al.*, 1993; Sankaranarayanan *et al.*, 2000). Despite proposed structural similarities between tRNA synthetases and proteins like MurM and FemXAB, the metal binding requirements of the Fem ligase family is currently under-explored.

4.2. Aims

Other data presented in Chapter 6 regarding structural studies on $MurM_{Pn16}$ identified zinc as a requirement for nucleation and crystal lattice formation. Dialysis of MurM against storage buffer containing 10 mM EDTA resulted in apparent inactivation of the protein when presented with its substrates. Protein activity could be completely restored by the addition of either a molar equivalent or a molar excess of zinc to the assay buffer in the presence of magnesium. Due to the fact that there is no X-ray crystal structure available for MurM, the metal binding properties of one of its homologues, *S. aureus* FemA, was also investigated. A 2.1 Å X-ray crystal structure of FemA has already been published enabling a more intuitive investigation

into the possible residues involved in metal ion binding within these proteins (Benson *et al.*, 2002). Therefore, characterisation of the binding of zinc and other divalent metal ions to MurM encompassed the following aims:

- Cloning of the *femA* gene from *S. aureus* strain Mu50 (encoding the functional homologue of the *S. pneumoniae* MurN protein) into the expression vector pET22b to encode a C-terminal dodeca-histidine tag
- Over-expression and purification of soluble FemA
- Assessment of the metal binding potential of the dodeca-histidine tagged versions of MurM and FemA using ITC
- Re-cloning of the three *murM* genes and the *femA* gene into the expression vector pET22b to incorporate a TEV-cleavable C-terminal hexa-histidine tag
- Cloning of the *femX* gene from *S. aureus* strain Mu50 (encoding the functional homologue of the *S. pneumoniae* MurM protein) into the expression vector pET28a to encode a C-terminal, TEV cleavable hexa-histidine tag
- Achieving over-expression, solubilisation and purification of MurM, FemX and FemA with a TEV cleavable hexa-histidine tag
- Obtaining untagged protein for ITC analysis
- To carry out bioinformatics-informed site directed mutagenesis of FemA and MurM to identify key amino acid residues involved in metal ion binding

4.3. Cloning, expression and purification of FemA

4.3.1. Cloning of *femA* into pET22b to encode a C-terminal dodeca-histidine tag

The *femA* gene from *S. aureus* strain Mu50 was cloned into the expression vector pET22b to encode a C-terminal dodeca-histidine fusion tag for purification purposes. PCR amplification of *femA* from chromosomal DNA was achieved using Accuprime *Taq* DNA polymerase and primers 5 and 7 shown in Chapter 2, Table 2.2. Figure 4.1 summarises successful cloning of the *femA* gene into pET22b.

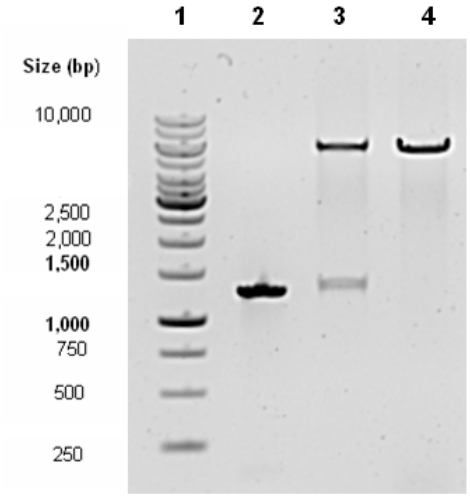

Figure 4.1: Summary agarose gel showing successful cloning of the *Staphylococcus aureus* strain Mu50 *femA* gene into pET22b. Note that *femA* is 1,263 base pairs in length.

Lane 1 - standard 1 kb DNA ladder,
Lane 2 - *femA* PCR product,
Lane 3 - release of the *femA* gene upon digestion of pET22b with *Bam*HI/*Xho*I,
Lane 4 - removal of the *Bam*HI site after digestion of the final construct with *Nde*I to position the start of the gene directly adjacent to the ribosome binding site of the plasmid.

As was the case with *murM*, successful cloning of *femA* into pET22b involved restriction digestion of both the PCR product and the pET vector with *Bam*HI and *Xho*I. Successful clones, whereby *femA* had successfully inserted into pET22b, were identified by agarose gel electrophoresis of *Bam*HI/*Xho*I digests and sequencing.

Digestion with *Nde*I was utilised as a means of positioning the 5' end of *femA* close to the ribosome binding site of the vector for expression purposes.

4.3.2. Small-scale expression trials of the FemA protein

In order to determine optimal conditions for FemA expression, the final construct was transformed into both *E. coli* B834 (DE3) and BL21 Star (DE3).placIRare2 expression strains. Levels of protein expression were investigated after auto-induction at 37^{o}C for 16 h and IPTG-induction at 25^{o}C for 4 h as described in Chapter 2, sections 2.3.2 and 2.3.3, respectively. Crude extracts were obtained from these cultures by sonication at 10% power for 15 sec and centrifugation to obtain both soluble and insoluble fractions. Bradford reagent was used to determine the protein concentration of the crude extracts so that 25 μg of protein were loaded onto each lane of a 12.5% SDS PAGE gel (Chapter 2, section 2.4.9). The overall yield of protein expression was similar in both strains and the results obtained for *E. coli* BL21 Star (DE3).placIRare2 cells are shown in Figure 4.2.

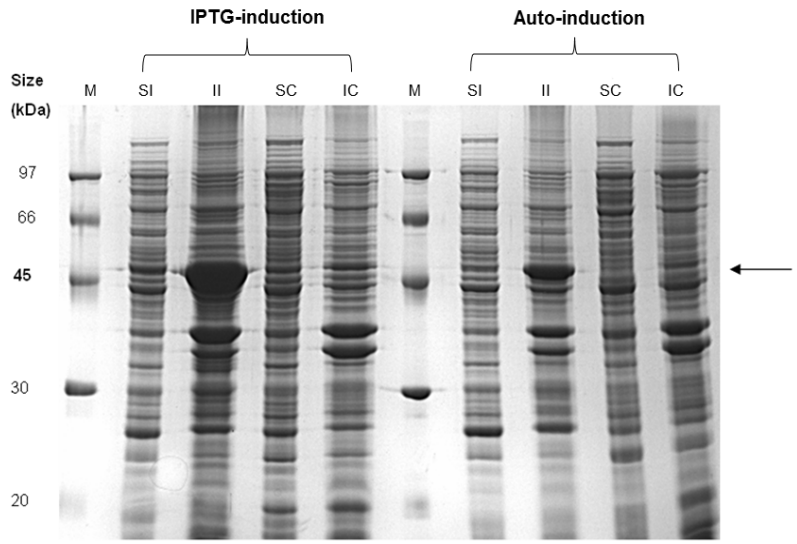

M - molecular weight standards,
SC - soluble proteins expressed by non-induced cells,
SI - soluble proteins expressed by induced cells,
IC - insoluble proteins expressed by non-induced cells,
II - insoluble proteins expressed by induced cells.

Figure 4.2: 12.5% SDS PAGE gel showing the crude extracts obtained from *Escherichia coli* BL21 Star (DE3).placIRare2 cells transformed with pET22b::FemA$_{(12\ his)}$ and induced to express protein either by auto-induction (AI) at 37^{o}C for 16 h or IPTG-induction at 25^{o}C for 4 h. The arrow indicates the migratory position of FemA. The molecular weight of FemA is 49,139 Daltons.

As was the case for MurM, the vast majority of FemA was expressed in an insoluble form regardless of the host *E. coli* strain. It was also noted that the protein could not be solubilised by reducing the temperature of growth or expression to 25^{o}C. As a result of successful solubilisation of MurM with 1 M sodium chloride (Chapter 3), the same method was trialled with FemA.

4.3.3. Solubilisation of FemA with 1 M sodium chloride

E. coli BL21 Star (DE3).placIRare2 cells harbouring pET22b::FemA were cultured at 37^{o}C to an OD_{600nm} of 0.4, when FemA expression was induced by the addition of IPTG to a final concentration of 1 mM. Addition of IPTG was concurrent with reduction in the growth temperature to 25^{o}C for 4 h. Solubilisation with 1 M sodium

chloride was then attempted as described for MurM (Chapter 3) yielding four fractions which were examined by SDS PAGE as shown in Figure 4.3.

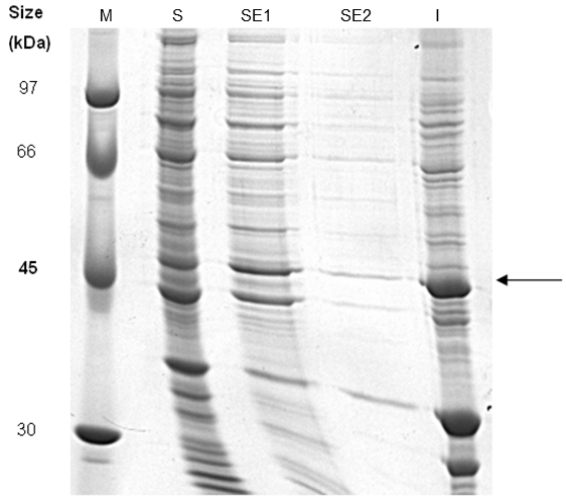

M - standard molecular weight markers,
S - soluble protein prior to salt extraction,
SE1 - soluble protein after the first salt extraction,
SE2 - soluble protein after the second salt extraction,
I - protein that remained insoluble after salt extraction.

Figure 4.3: 12.5% SDS PAGE analysis showing salt solubilisation of FemA from 1 L of *Escherichia coli* BL21 Star (DE3).placIRare2 cells. The position of FemA is marked with an arrow.

As with MurM, FemA was readily soluble upon extraction into buffer containing 1 M sodium chloride without any requirement for maintenance of solubility with detergent. Therefore, solubilisation by salt extraction was carried out prior to purification of FemA.

4.3.4. Purification of FemA

Purification of dodeca-histidine tagged FemA from *E. coli* BL21 Star (DE3).placIRare2 cells was carried out on BD TALON cobalt resin using the methodology developed for MurM (Chapter 3). The overall purity of FemA was assessed by SDS PAGE and is shown in Figure 4.4.

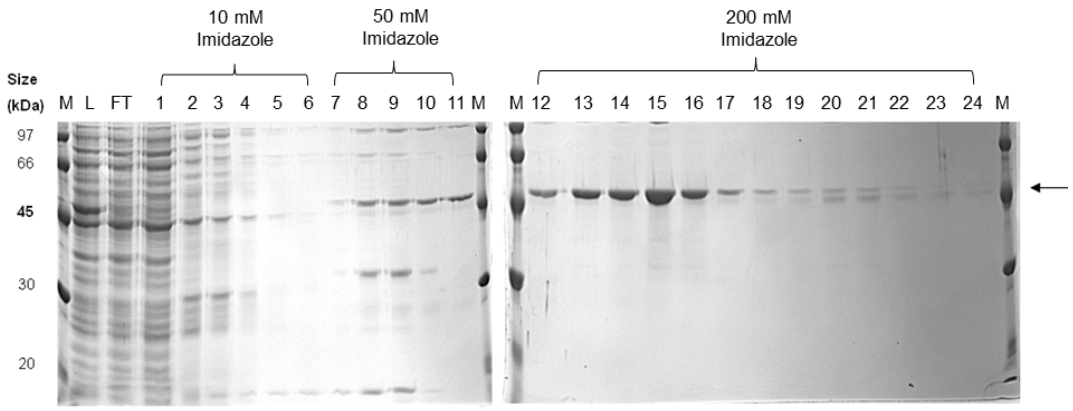

M - molecular weight standards,
L - protein sample prior to loading onto the column,
FT - flow through as protein was loaded onto the column.

Figure 4.4: 12.5% SDS PAGE gels showing purification of salt-solubilised dodeca-histidine tagged FemA from 1 L of *Escherichia coli* BL21 Star (DE3).placIRare2 cells on BD TALON cobalt resin. Lanes 1 - 24 represent protein eluted from the column during step washes using equilibration buffer supplemented with different concentrations of imidazole (10 mM, 50 mM and 200 mM). Elution of FemA during the 200 mM imidazole wash is marked with an arrow.

Solubilisation of FemA with 1 M salt followed by purification on cobalt resin using the methodology developed for MurM was successful. Protein obtained from the 200 mM imidazole wash was dialysed into storage buffer (50 mM HEPES, 500 mM NaCl, 1 μM leupeptin, 1 μM pepstatin and 50% glycerol pH 7.0) and stored at -80^{o}C until required.

4.4. Initial Characterisation of the metal binding requirements of MurM and FemA using histidine-tagged versions of each protein

4.4.1. Removal of metal ions from MurM and FemA using EDTA

In order to successfully remove metal ions bound to FemA and MurM, extensive dialysis was carried out against protein storage buffer supplemented with 10 mM EDTA as described in Chapter 2, section 2.4.5. Removal of EDTA from the protein

was achieved by further dialysis against storage buffer followed by buffer exchange on a PD10 column (GE Healthcare). Unless otherwise stated, the data presented in this chapter are based upon the response of the $MurM_{159}$ protein given that this strain of *S. pneumoniae* is the most clinically relevant. However, all three variants of MurM were found to respond to metal ions in the same way.

As shown in Figure 4.5, attempts to assay the activity of EDTA-treated MurM were unsuccessful indicating that the protein was no longer functional. In addition to this, it was found that enzymatic activity could be partially restored by pre-incubating EDTA-treated MurM with a molar excess of either zinc or cobalt. Full recovery of activity was obtained by pre-incubation of MurM with both zinc and magnesium. However, incubation with magnesium alone was not sufficient to restore full activity.

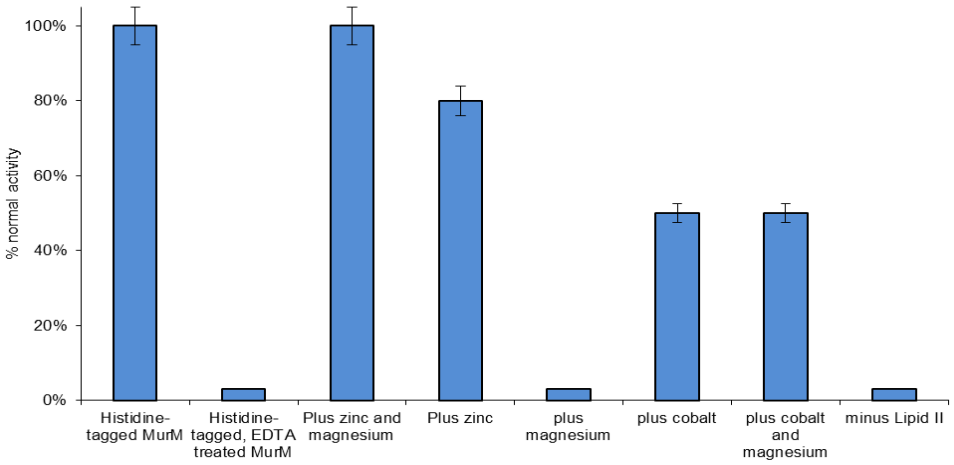

Figure 4.5: Assessment of the activity of EDTA-treated MurM in the presence and absence of selected metal ions. Each activity measurement was based on the percentage of radiolabelled alanine found in the butanol phase after an incubation period of 30 min. 100% activity is defined as normal activity of the enzyme prior to treatment with EDTA. As a control, the percentage of radiolabelled alanine found in the butanol phase was recorded when Lipid II was omitted from the reaction. This accounted for the solubility of the free radiolabel that allows it to be extracted into the butanol phase and is a product of tRNA deacylation. Error bars represent variation in the duplicated raw data.

Additional studies with $MurM_{159}$ that were undertaken prior to EDTA-treatment, also suggested that magnesium might be important for the function of the protein. This hypothesis was based on the observation that incorporated counts over a 30 min assay were three-fold lower when magnesium was omitted from the assay buffer. With these findings in mind and, in the absence of a suitable assay system for FemA, the interactions of FemA and MurM with zinc, cobalt and magnesium were investigated using isothermal titration calorimetry (ITC).

4.4.2. Characterisation of metal binding to FemA and MurM using ITC

For the purpose of ITC, EDTA-treated FemA and MurM were buffer exchanged into 20 mM HEPES pH 7.0. Initially, each protein was loaded into the sample cell at a final concentration of 50 µM. Divalent metal ions of interest were dissolved in 20 mM HEPES pH 7.0 to a final concentration of 1 mM. All samples were de-gassed before use and each ITC experiment was run as described in Chapter 2, section 2.6.1. Control experiments involving injection of the metal ion solution into 20 mM HEPES and injection of 20 mM HEPES into protein were carried out in each case. An example of the calorimetric titration plot obtained for histidine-tagged MurM challenged with zinc chloride is shown in Figure 4.6.

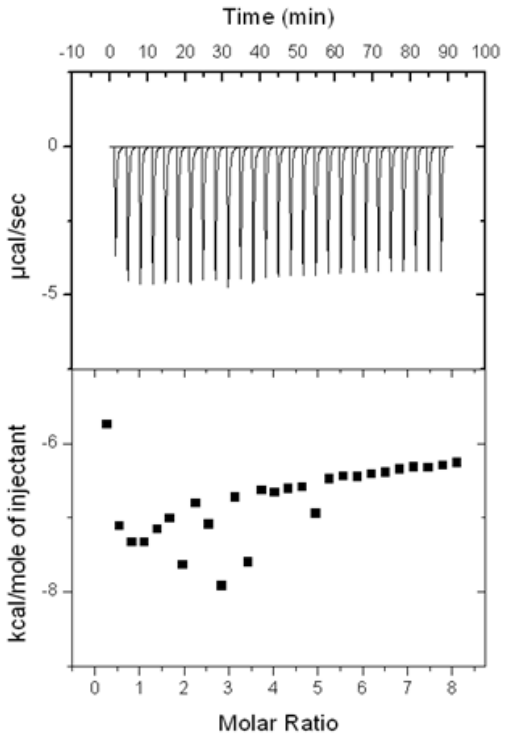

Figure 4.6: ITC profile for injections of 10 µL aliquots of 1 mM zinc chloride into a sample cell containing 50 µM $MurM_{159}$. Both baseline equilibration and metal ion injection were carried out at a temperature of 30^{o}C. Generated data could not be fitted to any analysis models as it was not possible to achieve saturation of the protein with the metal ion.

Despite subtraction of the controls, data generated using histidine-tagged protein could not be analysed and generated poor values for the stoichiometry (n) of metal ion binding. This effect was much more pronounced in the case of divalent metal ions, such as nickel and zinc, in comparison to magnesium due to the high affinity of these particular metal ions for poly-histidine tags. For this reason, it was considered essential for each variant of the MurM protein to be re-cloned into the expression vector pET22b such that the C-terminal histidine tag could be removed by Tobacco Etch Virus (TEV) protease after it had served its purpose in purification. The FemX and FemA proteins from *S. aureus* were subsequently re-cloned in the same way.

4.5. Cloning, expression and purification of MurM, FemX and FemA to encode a C-terminal hexa-histidine tag preceded by a Tobacco Etch Virus (TEV) protease recognition site

4.5.1. Cloning of *murM* and *femA* into pET22b to encode a C-terminal hexa-histidine tag preceded by a TEV protease recognition site

In order to incorporate the TEV protease recognition site (amino acid sequence ENLYFQG) at the C-terminus of each gene, the reverse PCR primer was redesigned in each case. Due to the increase in length of the reverse primer, PAGE purification of each oligonucleotide was requested from Integrated DNA Technologies (IDT) to increase cloning efficiency. PCR and restriction digestions were carried out as described in section 4.3.1. Successful incorporation of the TEV site was determined by sequencing the final construct with the T7 forward and T7 reverse primer. All oligo sequences can be found in Chapter 2, Table 2.2.

4.5.2. Cloning of *femX* into pET28a to encode a C-terminal hexa-histidine tag preceded by a TEV protease recognition site

Due to the presence of an internal *Nde*I site, it was not possible to clone *femX* into pET22b in the same way. For this reason, pET28a was selected as a more suitable vector allowing cloning of the gene between *Nco*I and *Xho*I restriction sites (see Chapter 2, Figures 2.2 and 2.3 for maps of the multiple cloning regions of these vectors). In order to clone *femX* into pET28a so that restriction digestion would allow for ATG to be the first expression codon, the forward primer was designed to add a *Bsa*I site to the 5' end of *femX*. This was necessary given that *femX* also contains an internal *Nco*I site. The reverse primer was designed to incorporate the

TEV protease recognition site and an *Xho*I restriction site at the 3' end of the *femX* gene.

PCR amplification of *femX* was achieved using *S. aureus* Mu50 chromosomal DNA, Accuprime *Taq* DNA polymerase and the above primers (Chapter 2, Table 2.2 primer number 12 and 13) with an annealing temperature of 58^{o}C. Success of the PCR procedure is illustrated in Figure 4.7.

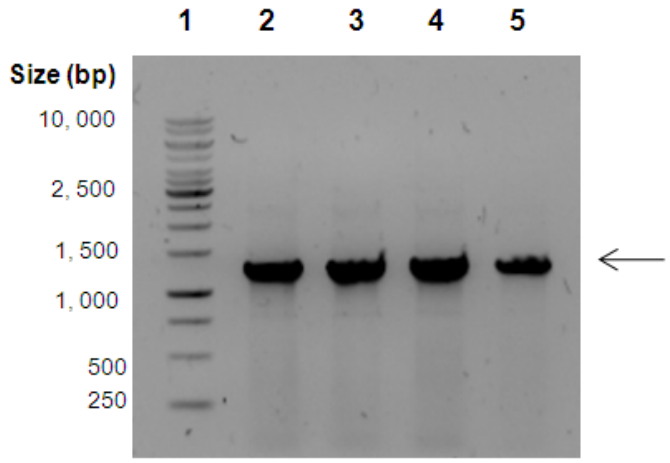

Figure 4.7: Summary 0.8% agarose gel showing successful PCR amplification of the *Staphylococcus aureus* strain Mu50 *femX* gene. Note that *femX* is 1,266 base pairs in length and successful amplifications generating a product of the correct size are indicated by an arrow.

Lane 1 - standard 1 kb DNA ladder,
Lanes 2 to 5 - the PCR product obtained for *femX* using Invitrogen Accuprime *Taq* DNA polymerase and an annealing temperature of 58^{o}C.

The PCR products shown in Figure 4.7 were pooled, purified and quantified as described in Chapter 2, sections 2.2.4 and 2.2.6, prior to restriction digestion with *Xho*I and *Bsa*I as described in section 2.2.5. In order to sub-clone *femX* into pET28a, the vector was digested with *Nco*I and *Xho*I. Given that *Bsa*I is known to produce *Nco*I compatible sticky ends, it was possible to ligate the purified, restricted PCR

fragments into the purified, restricted pET28a vector using T4 DNA ligase as described in Chapter, section 2.2.7. The ligated product was transformed into *E. coli* Top10 cells and the uptake of pET28a was selected for using kanamycin. Plasmid was extracted from a selection of the obtained colonies using the Fermentas mini-prep kit. Successful clones containing the *femX* gene insert were identified by *Xba*I/*Xho*I digestion as shown in Figure 4.8.

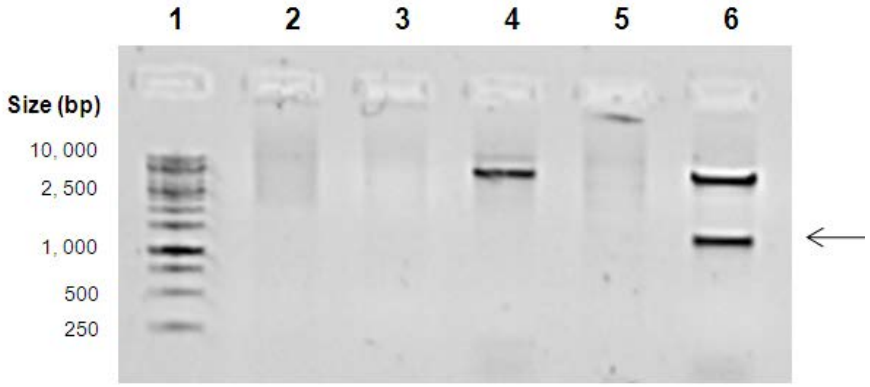

Figure 4.8: 0.8% agarose gel showing *Xba*I/*Xho*I double digests of potential pET28a::FemX clones.

Lane 1 - standard 1 kb DNA ladder,
Lanes 2 to 6 - double digest for the plasmid extracted from five *E. coli* Top10 clones potentially harbouring the expression construct. Only the plasmid DNA in lane 6 (clone 5) appears to contain the *femX* gene which has been released from pET28a by the *Xba*I/*Xho*I double digest.

Clone 5 shown in Figure 4.8, which demonstrated the correct restriction pattern was sequenced with the T7 forward and T7 reverse primer to ensure the inserted *femX* gene was of the correct sequence prior to use in protein expression experiments.

4.5.3. Small-scale expression trials of the MurM, FemA and FemX proteins

Given previous success with MurM and FemA (Chapter 3 and Chapter 4 respectively), the final pET28a::FemX construct was transformed into *E. coli* BL21

Star (DE3).placIRare2 cells for protein expression by IPTG-induction at 25°C for 4 h. Crude extracts were obtained as described previously and overall levels of expression were assessed by SDS PAGE as shown in Figure 4.9.

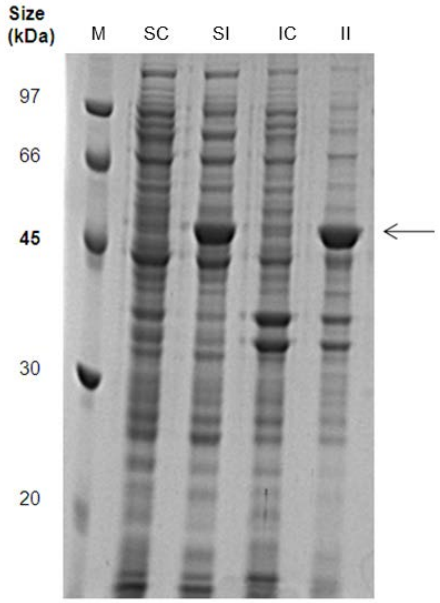

M - molecular weight standards,
SC - soluble proteins expressed by non-induced cells,
SI - soluble proteins expressed by induced cells,
IC - insoluble proteins expressed by non-induced cells,
II - insoluble proteins expressed by induced cells.

Figure 4.9: 12.5% SDS PAGE gel showing crude extracts obtained from *Escherichia coli* BL21 Star (DE3).placIRare2 cells transformed with pET28a::FemX and induced to express protein by IPTG-induction at 25°C for 4 h. The position of FemX is indicated by an arrow.

Small-scale expression trials indicated that FemX was produced in both a soluble and an insoluble form under the conditions described. Small-scale expressions were also carried out for MurM and FemA after addition of the TEV protease recognition site adjacent to the vector-encoded histidine tag with identical findings to those presented in Chapter 3 and Chapter 4, respectively.

4.5.4. Solubilisation of the MurM, FemA and FemX proteins with 1 M salt

Salt-solubilisation of MurM and FemA with the TEV-cleavable hexa-histidine tag was tested as described in Chapter 3 and Chapter 4 respectively, with the same level of success as shown for proteins with non-cleavable histidine tags. In the case of FemX, 1 L of *E. coli* BL21 Star (DE3).placIRare2 cells harbouring pET28a::FemX were cultured at 37^{o}C to an OD_{600nm} of 0.4 when protein expression was induced by the addition of IPTG to a final concentration of 1 mM. Addition of IPTG was concurrent with the growth temperature being reduced to 25^{o}C for 4 h. To obtain the maximum possible yield of protein for the purpose of purification, solubilisation of FemX with 1 M sodium chloride was attempted as described for MurM (Chapter 3) yielding four fractions, which were examined by SDS PAGE. The solubility of FemX after treatment with 1 M salt is shown in Figure 4.10.

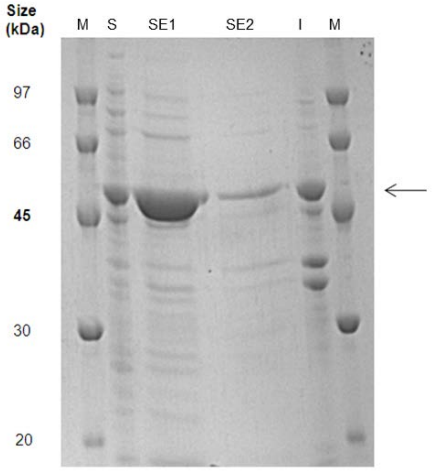

M - standard molecular weight markers,
S - soluble protein prior to salt extraction,
SE1 - soluble protein after the first salt extraction,
SE2 - soluble protein after the second salt extraction,
I - protein that remained insoluble after salt extraction.

Figure 4.10: 12.5% SDS PAGE analysis showing salt solubilisation of FemX from 1 L of *Escherichia coli* BL21 Star (DE3).placIRare2 cells. The position of FemX is marked with an arrow.

The results presented in Figure 4.10 indicated that additional FemX protein expressed in the insoluble fraction could be readily solubilised by salt extraction. Given that a successful purification procedure applicable to both salt-solubilised MurM and FemA had already been developed (Chapter 3), salt-solubilisation of FemX was considered to be a valuable means of obtaining high yields of protein that would potentially purify very readily in a single step IMAC procedure. The validity of this assumption was tested by application of the MurM purification protocol to FemX (section 4.5.5).

4.5.5. Purification of MurM, FemA and FemX before removal of the histidine tag by TEV protease

Purifications of hexa-histidine tagged MurM, FemA and FemX from 1 L of *E. coli* BL21 Star (DE3).placIRare2 cells were carried out on BD TALON cobalt resin using the methodology developed for MurM (Chapter 3). As before, the column was equilibrated in buffer containing 50 mM sodium phosphate, 500 mM sodium chloride, 10 mM imidazole and 20% glycerol at pH 7.0 Elution of protein was achieved by sequential step washing of the column with buffer containing 10 mM, 50 mM and 200 mM imidazole. The overall purity of FemA and MurM was assessed by SDS PAGE and gave results equivalent to those obtained with proteins that had non-cleavable histidine tags. The purity of FemX is shown in Figure 4.11.

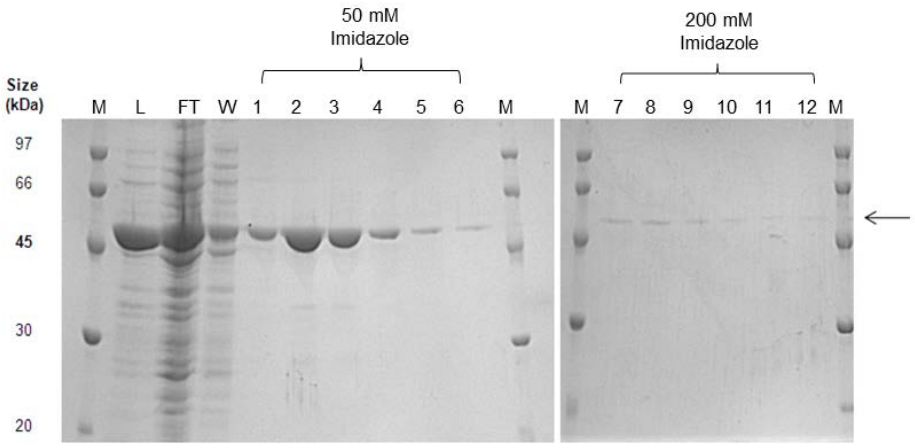

M - molecular weight standards,
L - protein sample prior to loading onto the column,
FT - flow through as protein was loaded onto the column,
W - protein eluted from the column during wash with equilibration buffer.

Figure 4.11: 12.5% SDS PAGE gel showing purification of salt-solubilised TEV-cleavable hexa-histidine tagged FemX from 1 L of *Escherichia coli* BL21 Star (DE3).placIRare2 cells on BD TALON cobalt resin. Lanes 1 - 12 represent protein eluted from the column during step washes using equilibration buffer supplemented with different concentrations of imidazole (50 mM and 200 mM). The position of FemX eluted during the 50 mM imidazole wash is marked with an arrow.

The results in Figure 4.11 show that solubilisation of FemX with 1 M salt and purification on cobalt resin using the methodology developed for MurM was successful. Elution of FemX was achieved when the column was washed with buffer supplemented with 50 mM imidazole, as was the case for MurM tagged on its C-terminus with six histidine residues (see Chapter 3).

4.5.6. Removal of the histidine tag from purified MurM, FemA and FemX using TEV protease

In all of the new expression constructs, the TEV protease recognition site was placed directly adjacent to the vector-encoded hexa-histidine tag without the use of spacer amino acids which are sometimes required for efficient cleavage. For this reason, a small-scale TEV cleavage reaction was carried out with $MurM_{Pn16}$ to determine an

appropriate incubation time, incubation temperature, reaction buffer and protein to TEV ratio. In these trials it was decided that appropriate incubation temperatures were 4^{o}C, to allow for maximum stability of MurM, and 25^{o}C to allow maximum efficiency of the TEV protease.

In each case, 25 μg of $MurM_{Pn16}$ was incubated in a total reaction volume of 150 μL with 4 μL of TEV (3.5 mg mL^{-1}). Samples were taken from each reaction after 1 h, 2 h, 4 h, 6 h and 24 h incubation. At each time point, 30 μL was removed from the reaction, mixed with an equal volume of SDS loading dye and stored at -20^{o}C. A final volume of 40 μL was then loaded onto an SDS PAGE gel for analysis. The results of this experiment are shown in Figure 4.12.

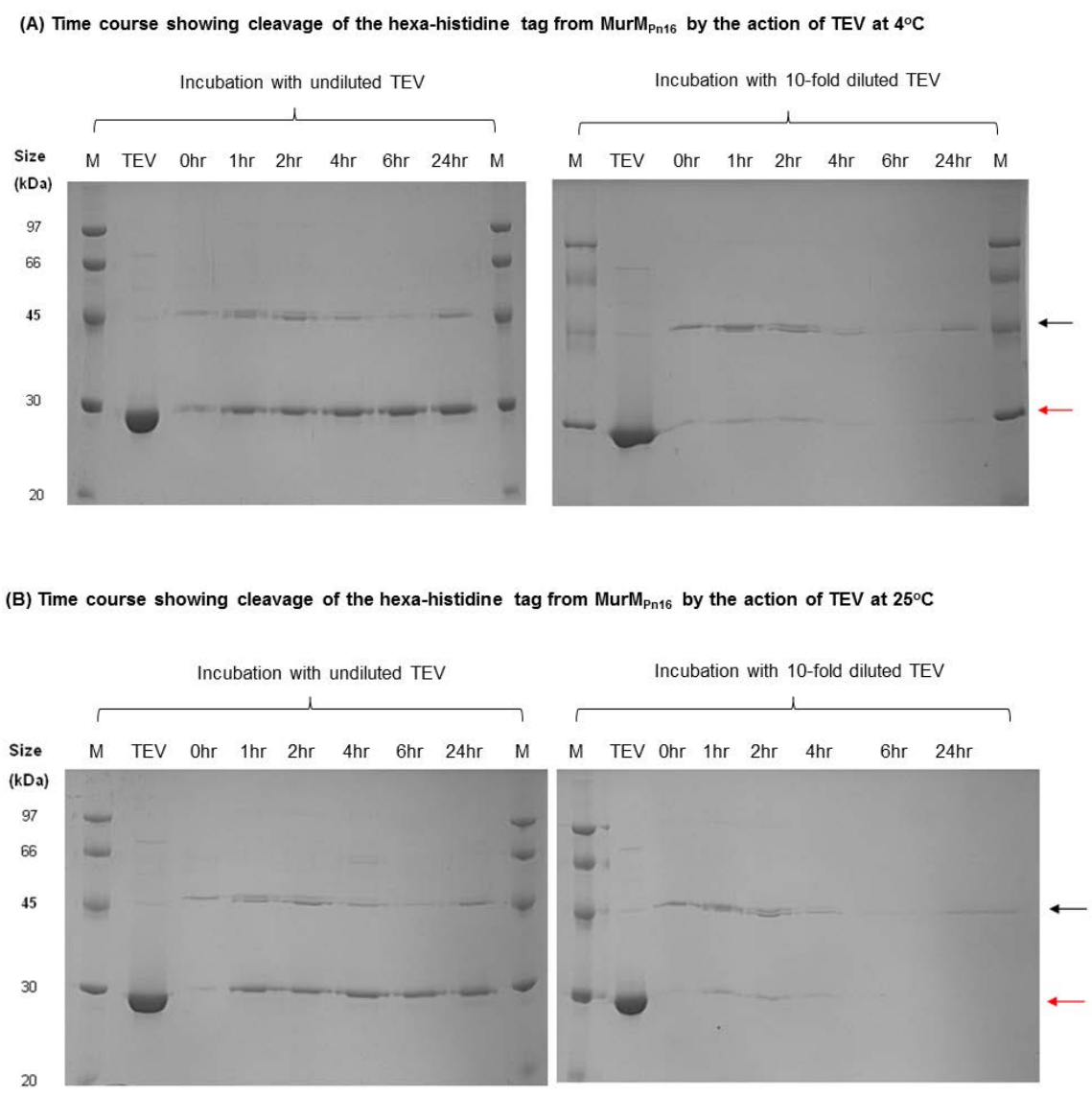

M - standard molecular weight markers,
TEV - a sample of the protease prior to incubation with MurM.

Figure 4.12: 12.5% SDS PAGE gel showing cleavage of the hexa-histidine tag from MurM$_{Pn16}$ by TEV protease at (A) 4°C and (B) 25°C. The remaining lanes are marked with the time, in hours, at which a sample was taken from the incubation reaction between TEV protease and MurM. The position of MurM is marked with a black arrow and the position of TEV, which has a weight of 27,000 Da, is marked with a red arrow.

In the case of the TEV cleavage reaction that was carried out at 25°C with undiluted protease, the double band of MurM, showing tagged and untagged protein, disappeared after approximately 4 h incubation. The equivalent reaction carried out

at 4^{o}C was complete after 24 h incubation. Given the overall instability of MurM and the fact that TEV efficiency was not completely compromised at 4^{o}C, this temperature was chosen as the best option for large-scale removal of the histidine tag from these proteins.

For large-scale removal of the hexa-histidine tag from FemX and FemA, purified protein that eluted from the cobalt column in the 50 mM and 200 mM imidazole wash fractions were pooled and concentrated to a final volume of 2.5 mL. The protein was loaded onto a bench top PD10 de-salting column that had been pre-equilibrated in 25 mL of TEV cleavage buffer (50 mM Tris-HCl pH 8.0, 200 mM NaCl and 20% glycerol). Elution of protein was achieved by collecting the flow through from the column upon the addition of 3.5 mL of TEV cleavage buffer. After collection, 100 µL of TEV protease at 3.5 mg mL^{-1} (obtained from the work carried out by Gianfranco de Pascale, University of Warwick PhD thesis) was added to FemX and FemA which were incubated for 24 h at 4^{o}C.

In the case of MurM, stability issues were counteracted by dialysis of the protein overnight into TEV cleavage buffer. In the absence of imidazole, MurM was concentrated using a vivaspin concentrator to a final volume of approximately 2.5 mL (Chapter 2, section 2.4.8). At this stage, it was possible to add TEV protease as described for FemX and FemA. Incubation of TEV protease and MurM was carried out for 24 h at 4^{o}C. After completion of incubation, the protein sample was loaded onto a 2 mL cobalt column which had been pre-equilibrated in TEV cleavage buffer. The aim of this procedure was to purify untagged protein away from TEV protease

(which has a C-terminal histidine tag) and protein that had not been successfully separated from its histidine tag after incubation with TEV.

Flow-through fractions collected during loading of the protein onto the cobalt column were expected to contain the vast majority of the untagged enzyme of interest. However, the column was also washed with 10 mL of equilibration buffer to account for the void volume prior to the addition of buffer supplemented with 250 mM imidazole to elute TEV protease from the resin. The results of removal of the histidine tag and purification of each protein away from TEV protease are shown in Figure 4.13.

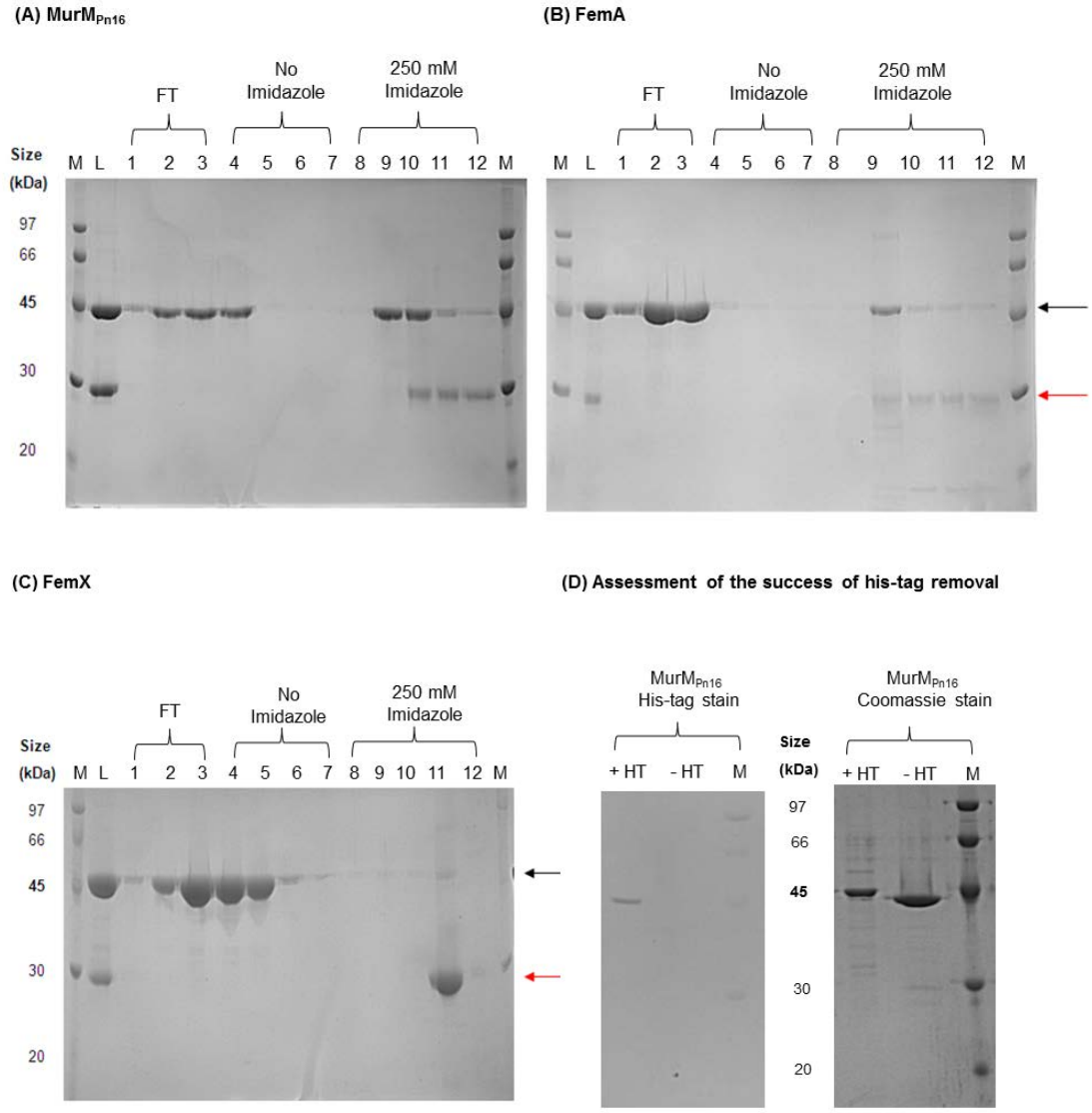

M - standard molecular weight markers,
L - a sample of the TEV digest prior to loading onto the column,
FT - flow-through from the column as the protein was loaded onto it,
+ HT - 10 µg of histidine-tagged protein before incubation with TEV,
- HT - 10 µg of protein that has lost its histidine tag after incubation with TEV.

Figure 4.13: 12.5% SDS PAGE showing purification of (A) MurM$_{Pn16}$, (B) FemA and (C) FemX on BD TALON cobalt resin after incubation with TEV protease to remove the C-terminal hexa-histidine tag. The success of removal of the histidine tag by TEV protease was assessed using Pro-Q Sapphire 532 Oligohistidine Gel staining (Molecular probes) of samples taken before and after the digest. In each case, Elution of MurM, FemA and FemX in the flow-through and the wash with 10 mL equilibration buffer are indicated with a black arrow. Elution of hexa-histidine tagged TEV protease during the wash with buffer containing 250 mM imidazole is indicated with a red arrow.

In every case, fractions containing protein eluted in the flow through and in the wash with equilibration buffer were pooled. Half of the pooled volume was stored at -80^{o}C after dialysis against buffer containing 50 mM HEPES pH 7.0, 500 mM NaCl and 50% glycerol. The remaining volume was dialysed against buffer supplemented with 10 mM EDTA prior to dialysis against storage buffer for the purpose of ITC analysis. Protein that eluted in the 250 mM imidazole wash along with the TEV protease was discarded.

Prior to storage of the protein samples in this manner, the success of removal of the histidine tag by incubation with TEV protease was assessed by running equivalent concentrations of protein before and after the digestion on an SDS PAGE gel stained first with Pro-Q Sapphire 532 Oligohistidine Gel stain (Molecular probes) and then with Colloidal Coomassie. As shown in Figure 4.13 (D), prior to TEV digestion MurM was detectable on an SDS PAGE gel under UV light after incubation with gel stain specific for oligohistidine-tagged proteins. In contract to this, after purification of the TEV digest, pooled protein eluted in both the flow through and wash with buffer containing no imidazole was not visible using this stain indicating successful removal of the histidine tag. Staining of the same gel with Colloidal Coomassie also indicated success of the technique given the change in molecular weight of the protein before and after removal of the histidine tag causing a clear difference in migratory distance on an SDS PAGE gel. Whilst the data presented here are for MurM only, the histidine tag was removed from FemX and FemA with equal success.

4.6. Characterisation of the metal binding requirements of untagged FemA, MurM and FemX

4.6.1. Binding of divalent metal ions to the FemA protein

Given the availability of an X-ray crystal structure for the FemA protein from *S. aureus* (Benson *et al.* 2002; PDB code 1LRZ), which is a functional homologue of the *S. pneumoniae* MurN protein; it was considered important to investigate the metal ion binding properties of this protein by ITC. Initial ITC experiments involved challenging FemA with magnesium and zinc. The results of this experiment are shown in Figure 4.14.

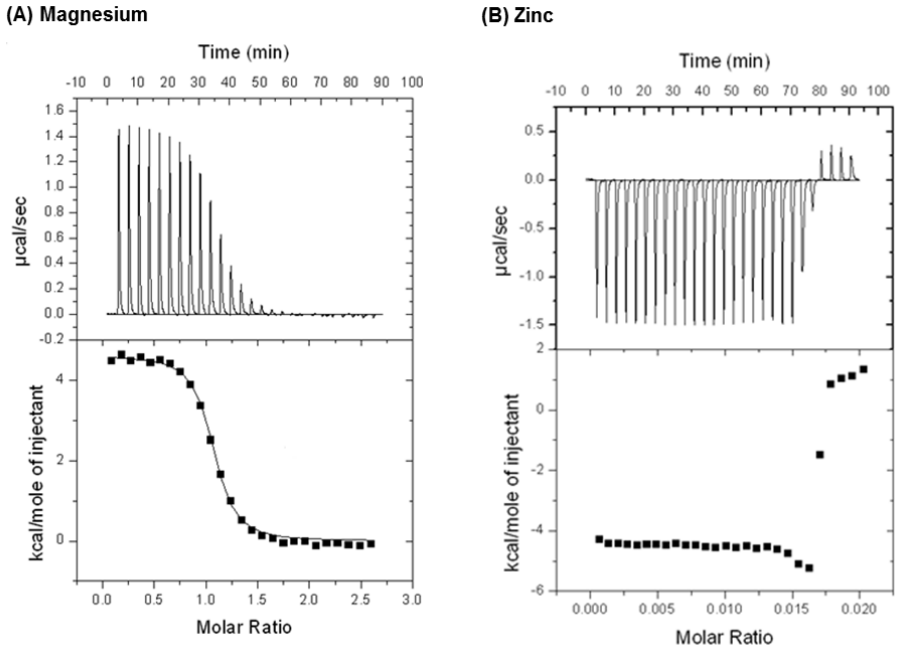

Metal ion	Stoichiometry (n)	K_d	ΔH (cal mole^{-1})	ΔS (cal mole^{-1} degree^{-1})
Magnesium	1.15 ± 0.00	0.78 ± 0.07 µM	4670.00 ± 21.97	43.40

Figure 4.14: Isotherms generated by 10 µL injections of (A) 1 mM magnesium chloride or (B) 1 mM zinc chloride into a sample cell containing 50 µM FemA at pH 7.0. Both baseline equilibration and metal ion injection were carried out at a temperature of 30^{o}C. Data have been corrected for the heat of metal ion dilution and fitted to the one site model. Data for zinc binding could not be fitted to the same model even when the experiment was repeated at 25^{o}C to investigate the effects of protein aggregation on the ITC profile.

The data comprising the isotherm generated for binding of zinc to FemA were complicated and could not be fitted to the one site model during analysis. One hypothesis for this was that FemA has two metal ion binding sites: one with a high affinity for zinc and the other with a high affinity for magnesium, but a low affinity for zinc at the same time. In order to test this hypothesis, FemA was saturated with magnesium prior to challenge with other divalent metal ions. Results of this experiment are shown in Figure 4.15.

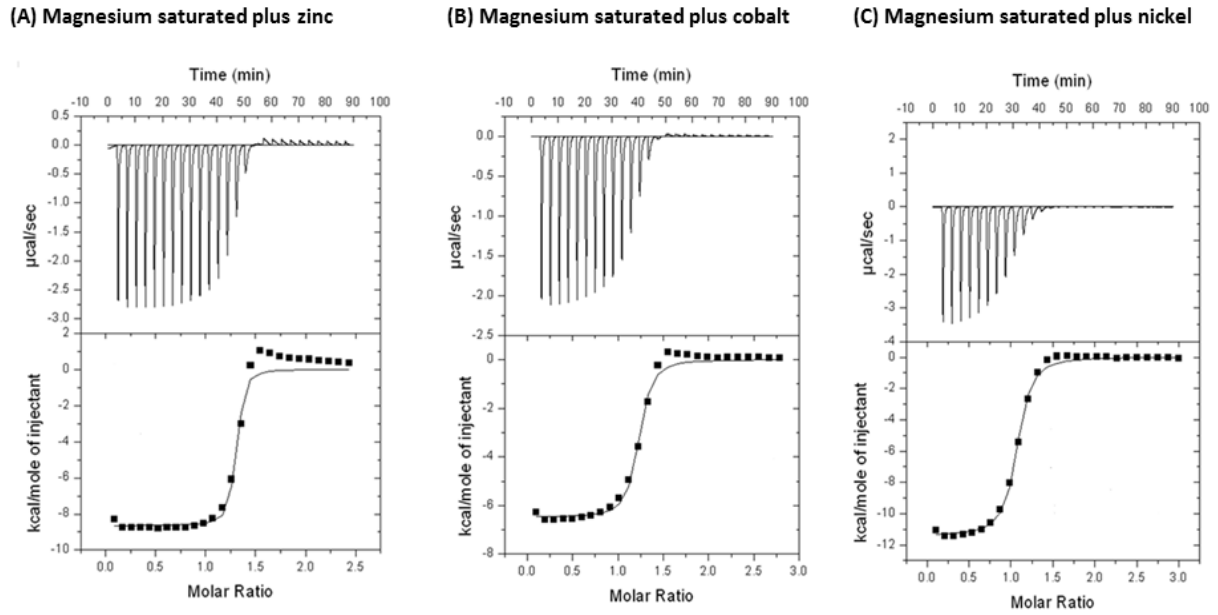

Metal ion	Stoichiometry (n)	K_d	ΔH (cal $mole^{-1}$)	ΔS (cal $mole^{-1}$ $degree^{-1}$)
Zinc	1.27 ± 0.01	0.08 ± 0.06 µM	-8652.00 ± 163.30	3.79
Cobalt	1.19 ± 0.01	0.28 ± 0.05 µM	-6489.00 ± 85.91	8.58
Nickel	1.03 ± 0.01	0.44 ± 0.09 µM	-11400.00 ± 92.52	-8.71

Figure 4.15: Isotherms generated by injections of 10 µL aliquots of (A) 1 mM zinc chloride, (B) 1 mM cobalt chloride or (C) 1 mM nickel sulphate into a sample cell containing 50 µM of magnesium-saturated FemA at pH 7.0. Both baseline equilibration and metal ion injection were carried out at a temperature of 30°C. Data have been corrected for the heat of metal ion dilution and fitted to the one site model where possible. When the two site model was applied, zinc binding to magnesium-saturated FemA gave a stoichiometry (n) of 1.11 ± 0.05, K_d = 0.05 ± 0.01 nM, ΔH = -8804.00 ± 224.00 cal $mole^{-1}$, ΔS = 18.00 cal $mole^{-1}$ $degree^{-1}$. The stoichiometry for the binding of zinc to the site already occupied with magnesium was 0.22 ± 0.03 indicating poor affinity.

The ITC data presented for FemA in Figure 4.15 were indicative of the enzyme having two metal binding sites, as had been predicted for MurM based upon assay of the protein before and after treatment with EDTA. The generated ITC profiles for FemA seemed to indicate that one of the metal ion binding sites had a high affinity for magnesium and that both sites had affinity for zinc. Further investigation with FemA led to titration of both copper and manganese into magnesium-saturated enzyme (Figure 4.16).

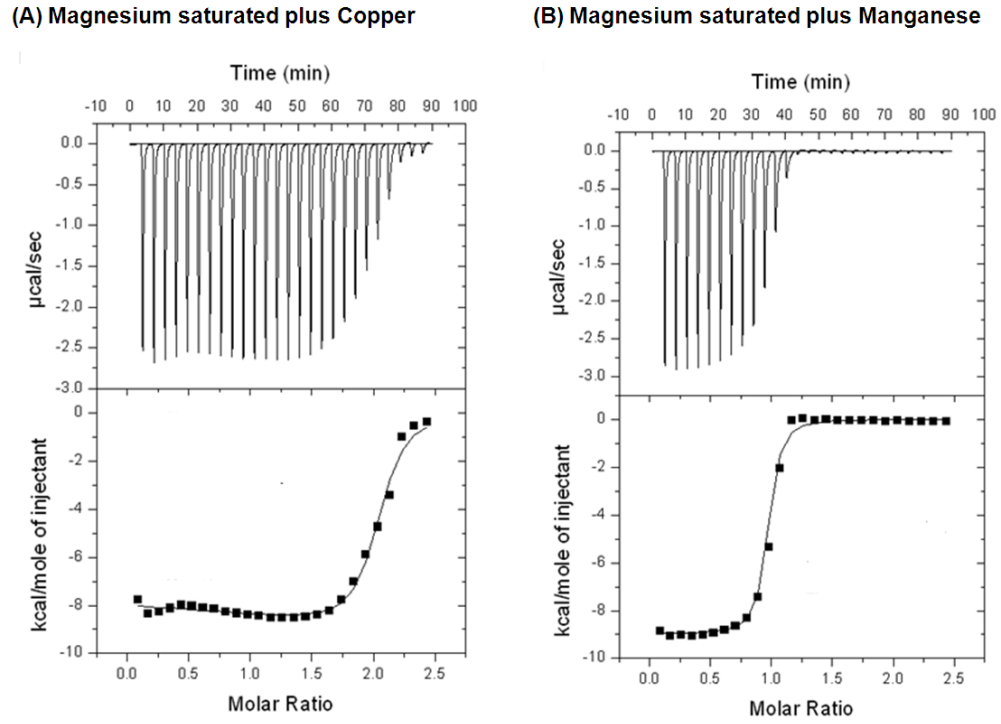

Metal ion	Stoichiometry (n)	K_d	ΔH (cal mole^{-1})	ΔS (cal mole^{-1} degree^{-1})
Copper	n_1: 0.80 ± 0.69 n_2: 1.19 ± 0.68	K_{d1}: 0.75 ± 0.54 µM K_{d2}: 0.26 ± 0.12 µM	ΔH_1: -9810.00 ± 4650.00 ΔH_2: -7633.00 ± 2290.00	ΔS_1: -4.34 ΔS_2: 1.23
Manganese	0.96 ± 0.00	0.22 ± 0.03 µM	-8965.00 ± 66.37	1.23

Figure 4.16: Isotherms generated by injection of 10 µL aliquots of (A) 1 mM copper sulphate or, (B) 1 mM manganese chloride into a sample cell containing 50 µM of magnesium-saturated FemA at pH 7.0. Both baseline equilibration and metal ion injection were carried out at a temperature of 30^{o}C. Data have been corrected for the heat of metal ion dilution and fitted to the one site model where possible. Copper ion binding to FemA fitted the two site model.

ITC data presented in Figure 4.16 indicated that copper ions could occupy both of the proposed divalent metal ion binding sites within FemA by displacing magnesium. Copper ions are often able to replace other divalent metal ions in numerous metalloproteins. However, this is prevented *in vivo* by chaperones that chelate free copper and thus enable such proteins to be saturated with their true metal ions (Mellor and Maley, 1948; Waldron and Robinson, 2009; Waldron *et al.*, 2009).

In the case of FemA, the dissociation constant (K_d) for copper (0.75 ± 0.54 μM) was similar to that of magnesium (0.78 ± 0.07 μM) but approximately 10 times higher than that for zinc (0.08 ± 0.06 μM) taking into account the error in the dataset. This was indicative of FemA having a lower overall binding affinity for this metal ion. Manganese was also able to occupy the proposed zinc binding site but with a higher dissociation constant of 0.22 ± 0.03 μM. In order to further investigate the metal binding properties of FemA, it was possible to load the X-ray crystal structure of the protein (PDB code 1LRZ) onto the CHED server for prediction of transition metal ion binding sites. The results of this bioinformatics analysis are presented in section 4.6.2.

4.6.2. Bioinformatics analysis of metal binding sites in FemA based on the X-ray crystal structure of the protein solved by Benson *et al.* (2002)

In order to search for potential transition metal ion binding sites, the PDB structure of *S. aureus* FemA (PDB code 1LRZ) was loaded onto the CHED server (Babor *et al.*, 2008). The name CHED is derived from the fact that most transition metal ions bind to proteins using either three or four amino acid residues that are present in catalytic, co-catalytic or structural sites. The amino acid residues responsible for

such metal ion binding are almost invariably cysteine (C), histidine (H), glutamate (E) and aspartate (D). When the PDB file for FemA was loaded onto this server, two potential metal ion binding sites were detected and are shown in relation to the structure of the protein in Figure 4.17.

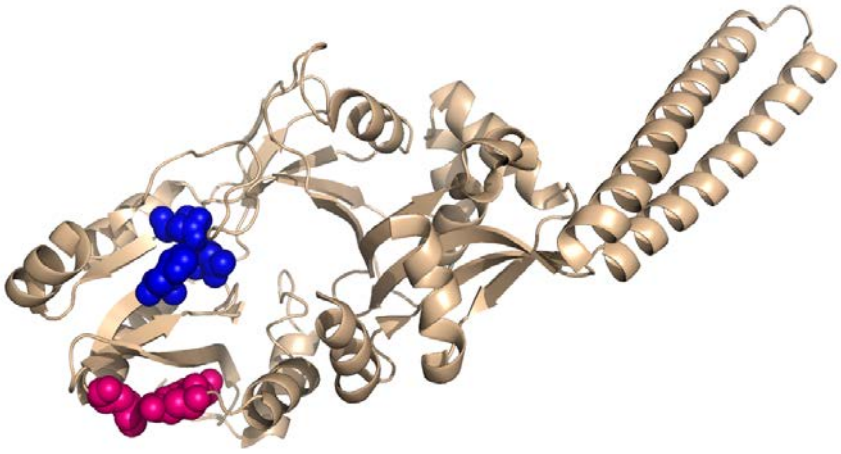

Figure 4.17: CHED server predicted metal ion binding sites within the structure of apo-FemA. One predicted metal ion binding site is comprised of E39, H41 and H100 (pink). The other site is comprised of H106, D108 and D396 (blue). PDB file 1LRZ.

Information gained from the CHED server indicated that FemA has two potential metal ion binding amino acid clusters within its structure, each consisting of three residues. One of these sites comprises two aspartate residues and a histidine residue. It has already been established in the literature that aspartate residues often play a key role in magnesium ion binding to proteins (Huang and Cowan, 1994). The other site comprises two histidine residues and a glutamate residue giving it the potential to serve as a high affinity zinc site.

The validity of this bioinformatics-based prediction was tested by making a series of site-directed mutants of FemA whereby the amino acid of interest was changed to

alanine. Alanine was chosen as the replacement amino acid since it does not possess a side chain within its structure that could participate in metal ion binding. Residue D108 was excluded from the mutagenesis studies given that this has been shown to be a key catalytic site residue in *W. viridescens* FemX (Hegde and Shrader, 2001; Hegde and Blanchard, 2003). It is, therefore, assumed to have a similar role within the other members of the Fem ligase family although this has yet to be formerly proven. Residue E39 was also excluded from these studies due to difficulties in primer design which ultimately resulted in poor mutagenesis efficiency and an inability to produce a clone harbouring the correct mutation. Generation and characterisation of these mutants is described in section 4.6.3.

4.6.3. Site-directed mutagenesis of predicted metal ion binding residues in FemA

In order to determine the involvement of the predicted CHED server identified amino acid residues in divalent metal ion binding, four mutants of FemA (H41A, H100A, H106A and D396A) were made using guidelines given in the Stratagene QuikChange site directed mutagenesis kit instruction manual. Wild-type pET22b::FemA was used as a template in each PCR with Pfu Ultra *Taq* DNA polymerase and primers designed to incorporate the desired mutation (see Chapter 2, Table 2.3 for oligo sequences).

Success of the mutagenesis procedure was confirmed by sequencing of the plasmid DNA from potential clones using the T7 forward and T7 reverse oligos (Chapter 2, Table 2.2). Mutant FemA proteins were expressed and purified as described in Chapter 3 for MurM. The histidine tag was removed from the purified FemA

mutants, as described in section 4.5.6, using TEV protease. Mutant proteins were dialysed against storage buffer containing 10 mM EDTA and prepared for ITC by buffer exchange into 20 mM HEPES pH 7.0, as described in section 4.4.3. Initially, each of the mutant FemA proteins were challenged with magnesium alongside the wild-type enzyme and the results of these experiments are shown in Figure 4.18.

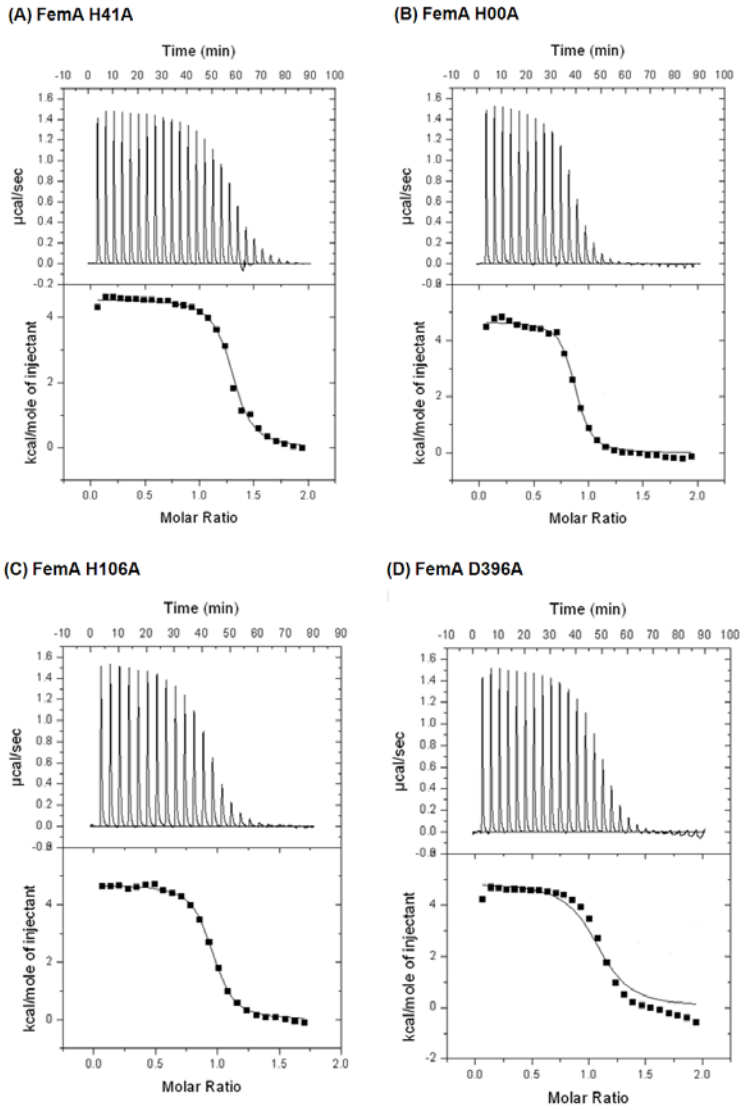

FemA Mutant	Stoichiometry (n)	K_d	ΔH (cal $mole^{-1}$)	ΔS (cal $mole^{-1}$ $degree^{-1}$)
H41A	1.28 ± 0.01	0.63 ± 0.08 µM	4550.00 ± 36.74	43.40
H100A	0.85 ± 0.01	0.55 ± 0.09 µM	4670.00 ± 52.65	44.00
H106A	0.93 ± 0.00	0.70 ± 0.06 µM	4709.00 ± 29.65	43.70
D396A	1.08 ± 0.01	0.49 ± 0.13 µM	4583.00 ± 73.06	44.00

Figure 4.18: Isotherms generated for injections of 10 µL aliquots of 1 mM magnesium chloride into a sample cell containing 50 µM of (A) FemA H41A, (B) FemA H100A, (C) FemA H106A and, (D) FemA D396A at pH 7.0. Both baseline equilibration and metal ion injection were carried out at a temperature of 30°C. Data have been corrected for the heat of metal ion dilution and fitted to the one site model where possible.

In the case of each of the four mutant FemA proteins, saturation with magnesium was still achieved suggesting that mutation at the level of a single amino acid was not sufficient to cause a significant reduction in the ability of the protein to bind this metal ion. Changes in stoichiometry and K_d for each mutant protein in comparison to wild-type FemA are summarised in Table 4.1.

	FemA wild-type	**FemA H41A**	**FemA H100A**	**FemA H106A**	**FemA D396A**
N	1.15 ± 0.00	1.28 ± 0.01	0.85 ± 0.01	0.93 ± 0.00	1.08 ± 0.01
K_d (µM)	0.78 ± 0.07	0.63 ± 0.08	0.55 ± 0.09	0.70 ± 0.06	0.49 ± 0.13

Table 4.1: Comparison of the stoichiometry (n) and dissociation constant (K_d) for magnesium ion binding to wild-type and mutant FemA. Data have been fitted to the one site model.

In all four mutants and wild-type FemA, the stoichiometry (n) of magnesium ion binding stayed consistent at one. There was also no significant change in the dissociation constant for magnesium ion binding when comparisons were made between the wild-type and mutant forms of the enzyme. Given that metal ion binding sites within proteins are usually made up of three to five amino acid residues in total, it is possible that other amino acids within the structure of FemA can compensate for mutation of these residues. One other explanation is that the CHED server prediction of metal ion binding sites is incorrect in the case of FemA. To investigate these two hypotheses further, two double mutants of FemA were constructed (H106A:D396A and H41A:H100A). Prior to assessment of the metal binding properties of these double mutants by ITC, all four single mutants were tested in terms of their ability to bind zinc ions after saturation with magnesium. The results of this experiment are shown in Figure 4.19.

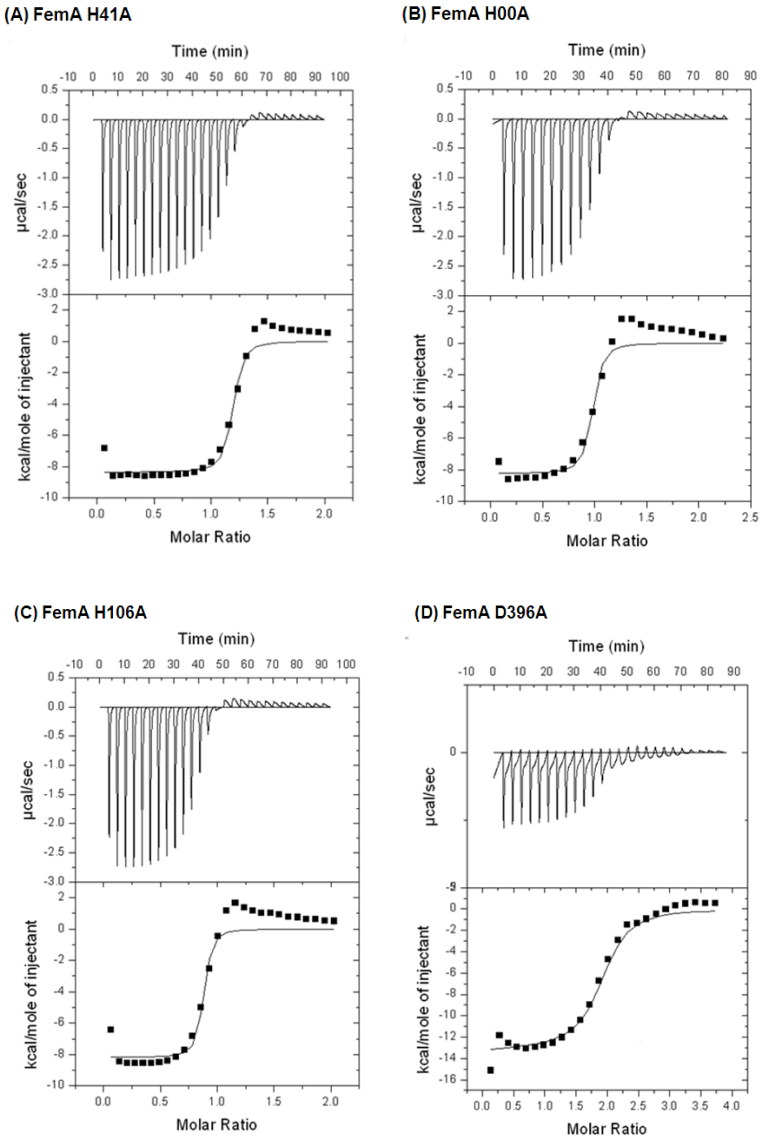

FemA Mutant	Stoichiometry (n)	K_d	ΔH (cal mole^{-1})	ΔS (cal mole^{-1} degree^{-1})
H41A	1.16 ± 0.01	0.14 ± 0.01 µM	-8355.00 ± 195.20	3.81
H100A	0.94 ± 0.02	0.17 ± 0.01 µM	-8220.00 ± 303.20	3.84
H106A	1.06 ± 0.02	0.13 ± 0.01 µM	-8177.00 ± 303.40	4.55
D396A	1.83 ± 0.03	1.11 ± 0.26 µM	-13300.00 ± 266.50	-16.60

Figure 4.19: Isotherms generated by injections of 10 µL aliquots of 1 mM zinc chloride into a sample cell containing 50 µM of magnesium-saturated FemA (A) H41A, (B) H100A, (C) H106A and, (D) D396A at pH 7.0. Both baseline equilibration and metal ion injection were carried out at a temperature of 30^{o}C. Data have been corrected for the heat of metal ion dilution and fitted to the one site model where possible.

The data presented in Figure 4.19 show that it was still possible to saturate all of the single mutant FemA proteins with zinc after saturation with magnesium. Table 4.2 presents the key values of stoichiometry and K_d for each mutant protein in comparison to wild-type FemA.

	FemA wild-type	**FemA H41A**	**FemA H100A**	**FemA H106A**	**FemA D396A**
n	1.27 ± 0.01	1.16 ± 0.01	0.94 ± 0.02	1.06 ± 0.02	1.83 ± 0.03
K_d	0.08 ± 0.06 µM	0.14 ± 0.01 µM	0.17 ± 0.01 µM	0.13 ± 0.01 µM	1.11 ± 0.26 µM

Table 4.2: Comparison of the stoichiometry (n) and dissociation constant (K_d) for zinc ion binding to magnesium-saturated wild-type and single mutant FemA proteins. Data have been fitted to both the one site model.

In the case of zinc ion binding to magnesium-saturated FemA, all of the single amino acid mutations were found to result in an increase in the dissociation constant for zinc ion binding indicating a weakening in binding affinity between the protein and the metal ion. The most significant mutation was D396. D396 has been hypothesised to be involved in magnesium ion binding. The data presented in Figure 4.19 and Table 4.2 suggested that magnesium could be displaced by zinc in the case of FemA that is mutated at this position, consequently increasing the stoichiometry of zinc ion binding. This could indicate that D396 is a key determinant for metal ion binding within FemA controlling the preference for magnesium at a site which also appears to have a low affinity for zinc. In a magnesium-saturated state, wild-type FemA was found to have a dissociation constant for zinc that was at least 14 times lower than that of FemA D396A. This could indicate that magnesium ion binding at

the first site is required to coordinate zinc ion binding in the second site, possibly by inducing structural changes within the protein.

The effects on metal ion binding seen in single site mutants of FemA were further investigated by constructing two double mutants: H41A:H100A and H106A: D396A. The data obtained for these mutants upon titration of magnesium are shown in Figure 4.20.

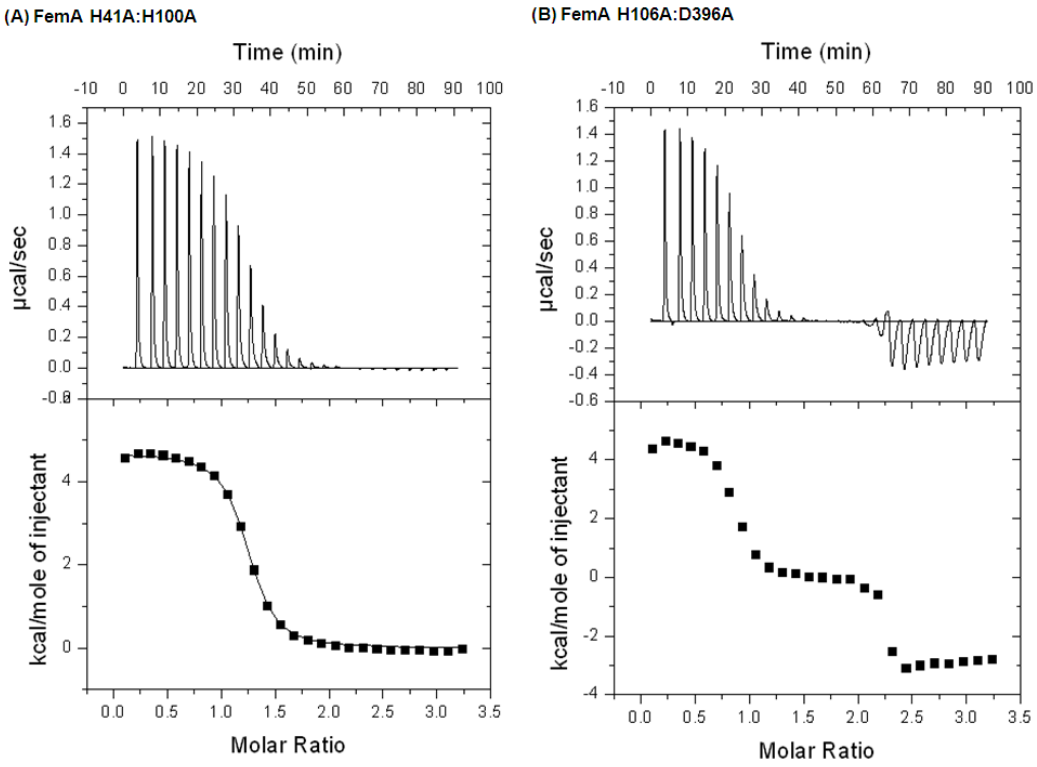

FemA Mutant	Stoichiometry (n)	K_d	ΔH (cal mole^{-1})	ΔS (cal mole^{-1} degree^{-1})
H41A:H100A	1.21 ± 0.01	0.73 ± 0.05 µM	4690.00 ± 26.23	43.60

Figure 4.20: Isotherms generated by injection of 10 µL aliquots of 1 mM magnesium chloride into a sample cell containing 50 µM FemA H41A:H100A (A) and FemA H106A:D396A (B) at pH 7.0. Both baseline equilibration and metal ion injection were carried out at a temperature of 30°C. Data have been corrected for the heat of metal ion dilution and fitted to the one site model where possible. Magnesium ion binding to FemA H106A:D396A could not be fitted to data analysis models indicating disruption of the site.

Magnesium ion binding to FemA H41A:H100A was found to occur with a K_d (0.73 ± 0.05 μM) equivalent to that of the wild-type enzyme (0.78 ± 0.07 μM). This supports the hypothesis that these residues are more likely to be implicated in zinc ion binding within FemA.

However, the ITC profile generated by magnesium ion binding to FemA H106A: D396A showed significant differences when compared to the profile obtained from the wild-type enzyme. It was not possible to fit the data generated by this mutant to any of the analysis models indicating disruption of the site. In order to determine whether magnesium ion binding is crucial for coordination of zinc ion binding by the other site, zinc ions were titrated into these double mutants of FemA after saturation with magnesium. Data obtained in these experiments are shown in Figure 4.21.

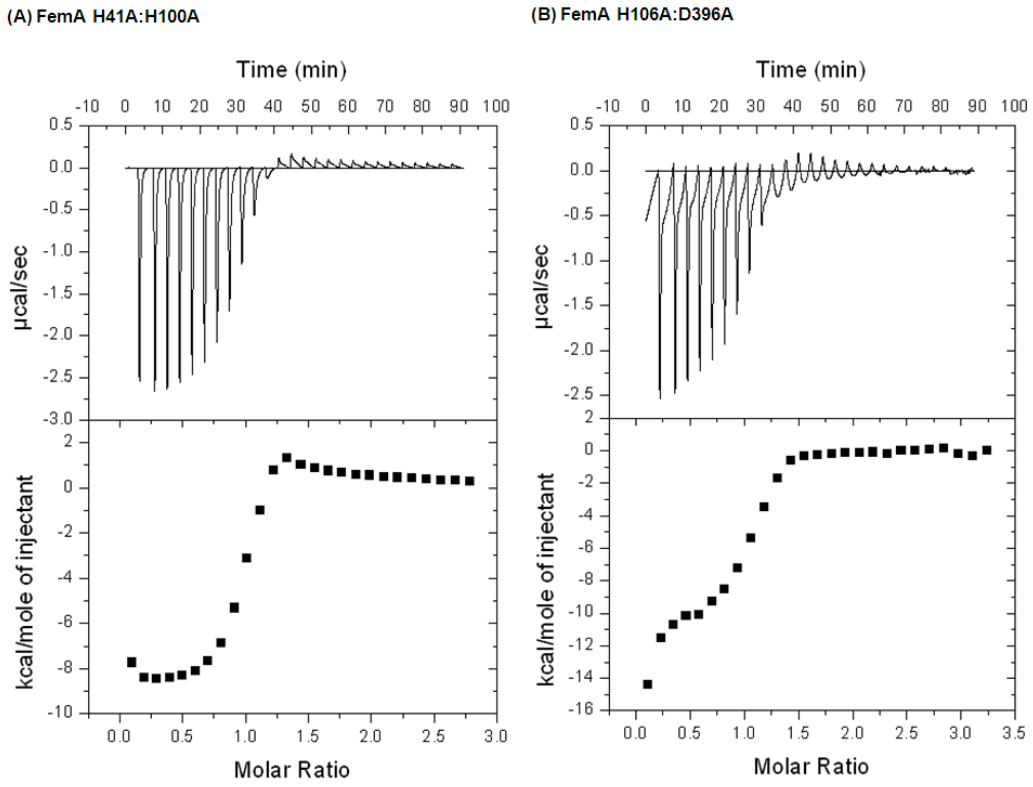

FemA Mutant	Stoichiometry (n)	K_d	ΔH (cal mole^{-1})	ΔS (cal mole^{-1} degree^{-1})
H41A:H100A	0.92 ± 0.02	0.23 ± 0.04 µM	-8169.00 ± 271.50	-3.43

Figure 4.21: ITC profile for injections of 10 µL aliquots of 1 mM zinc chloride into a sample cell containing 50 µM of magnesium-saturated FemA mutants (A) H41A:H100A and, (B) H106A:D396A at pH 7.0. Both baseline equilibration and metal ion injection were carried out at a temperature of 30°C. Data have been corrected for the heat of metal ion dilution and fitted to the one site model where possible. Zinc ion binding to FemA H106A:D396A could not be fitted to data analysis models indicating disruption of the site.

In the case of both FemA H41A:H100A and FemA H106A:D396A, there was a significant increase in the dissociation constant measured for zinc ion binding in comparison to the wild-type enzyme. The K_d of zinc ion binding for FemA H41A:H100A had increased from the wild-type value of 0.08 ± 0.06 µM to 0.23 ± 0.04 µM, implicating both of these amino acid residues in the coordination of this metal ion. Compared to single mutation of H41 and H100 to alanine, the K_d obtained for the double mutant was 1.6 and 1.4 times higher respectively, suggesting a

weakening in the binding interaction between the protein and zinc. However, zinc ion binding had not been completely abolished in the case of the double mutant. This could be explained if surrounding amino acid residues within FemA also play a role in zinc ion binding or if E39, which could not be mutated in this study, is crucial to this process.

In the case of FemA H106A:D396A, zinc ion binding could not be fitted to any of the data analysis models. This may indicate that disruption of the magnesium ion binding site by mutation of these two residues caused a critical loss of coordination in the zinc ion binding site. In combination with each other, the ITC results determined for the single and double mutants of FemA seem to suggest that the CHED server predictions of amino acid residues involved in the metal ion binding requirements of this protein are likely to be correct. However, other amino acid residues not picked up by this analysis software may also be critical to the process, which would explain why complete abolishment of the ITC signal was not observed. Bearing this in mind, similar studies were carried out on MurM and the results are described below in section 4.6.4.

4.6.4. Binding of divalent metal ions to the MurM protein

All three variants of the MurM protein were subjected to metal ion binding analysis by ITC with no significant differences between them. Data presented in this section were obtained using the MurM protein from *S. pneumoniae* strain 159 and are intended to be representative of all three protein variants. All experiments were set up and duplicated as described in Chapter 2, section 2.6.1. Initial metal ion binding studies were carried out using magnesium and zinc. The results of these experiments are presented in Figure 4.22.

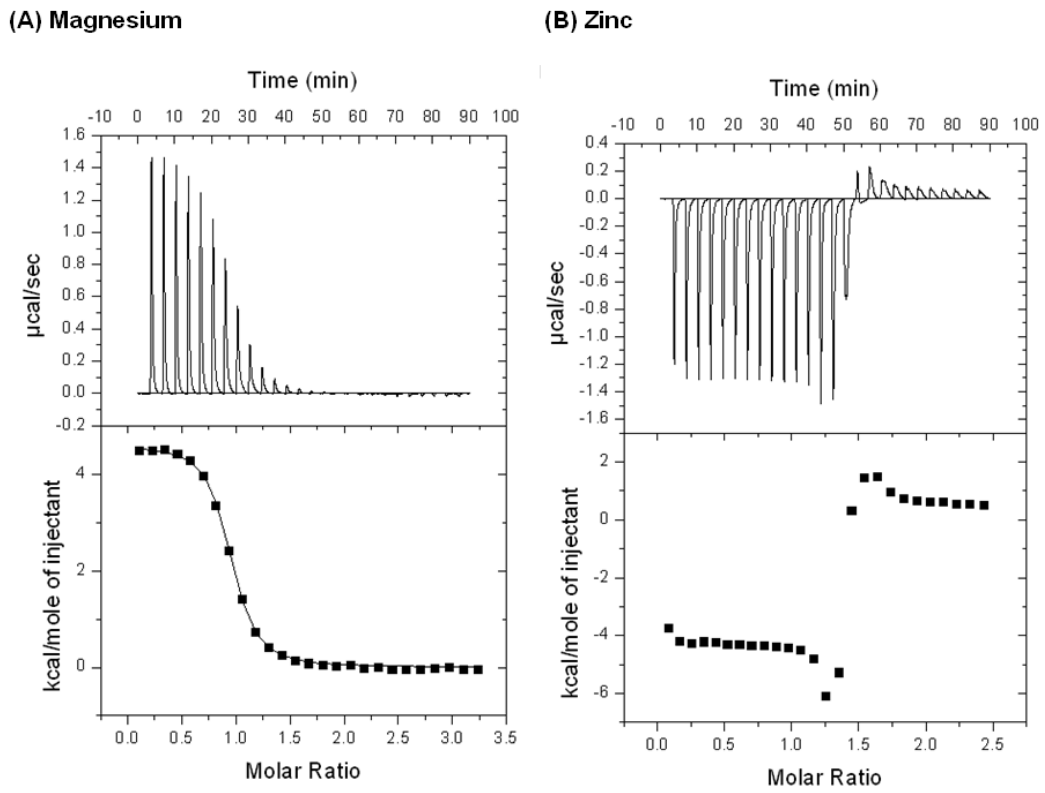

Metal ion	Stoichiometry (n)	K_d	ΔH (cal mole^{-1})	ΔS (cal mole^{-1} degree^{-1})
Magnesium	0.91 ± 0.00	0.89 ± 0.06 µM	4605.00 ± 28.00	42.90

Figure 4.22: Isotherms generated by 10 µL injections of (A) 1 mM magnesium chloride or (B) 1 mM zinc chloride into a sample cell containing 50 µM $MurM_{159}$ at pH 7.0. Both baseline equilibration and metal ion injection were carried out at a temperature of 30^{o}C. Data have been corrected for the heat of metal ion dilution and fitted to the one site model. Data for zinc binding could not be fitted to the same model even when the experiment was repeated at 25^{o}C to investigate the effects of protein aggregation on the ITC profile.

The data presented in Figure 4.22 suggested that MurM has a single binding site for magnesium with a dissociation constant (K_d) of 0.89 ± 0.06 µM. As was the case with FemA, the binding of magnesium to MurM at pH 7.0 resulted in an endothermic reaction represented by positive peaks. In contrast to this, the interaction between MurM and zinc ions was exothermic and much more complex. It was not possible to fit the data obtained for zinc binding to the one site analysis model. One hypothesis for this was that, like FemA, MurM has two divalent metal ion binding sites, one with a high affinity for magnesium and a low affinity for zinc and the other with a high affinity for zinc. In order to test this hypothesis, MurM was saturated with magnesium and then presented with zinc (Figure 4.23).

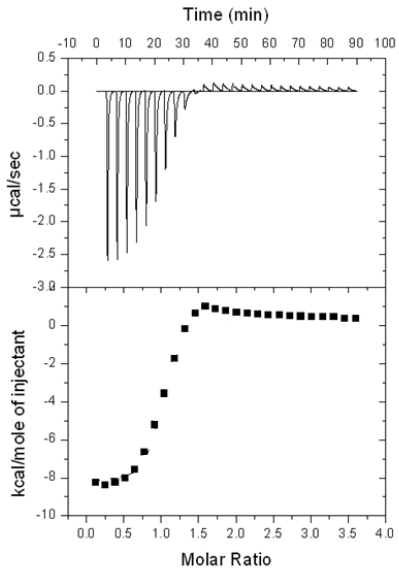

Metal ion	Stoichiometry (n)	K_d	ΔH (cal mole^{-1})	ΔS (cal mole^{-1} degree^{-1})
Zinc	0.90 ± 0.12	0.50 ± 0.04 µM	-8723.00 ± 1160.00	12.40

Figure 4.23: Isotherm generated by injections of 10 µL aliquots of 1 mM zinc chloride into a sample cell containing 50 µM magnesium-saturated $MurM_{159}$ at pH 7.0. Both baseline equilibration and metal ion injection were carried out at a temperature of 30°C. Data have been corrected for the heat of metal ion dilution. When the two site model was applied, the stoichiometry for the binding of zinc to the site already occupied with magnesium was 0.31 ± 0.10 which was indicative of a poor binding affinity between zinc and this site as was the case with FemA. Zinc ion binding to the high affinity site was found to take place with a K_d of 1 nM when the data were analysed with the two site model.

The data presented in Figure 4.23 show that zinc ion binding to MurM could be fitted to both the one site and the two site analysis models after saturation with magnesium. Combined with the results of the ITC data obtained for FemA, this led to the hypothesis that zinc is able to bind to two different affinity sites within MurM, one of which has a preference for magnesium. In order to investigate the promiscuity of MurM in terms of its metal binding potential, various other metal ions were titrated into protein that had already been saturated with magnesium. The results of these experiments are shown in Figure 4.24.

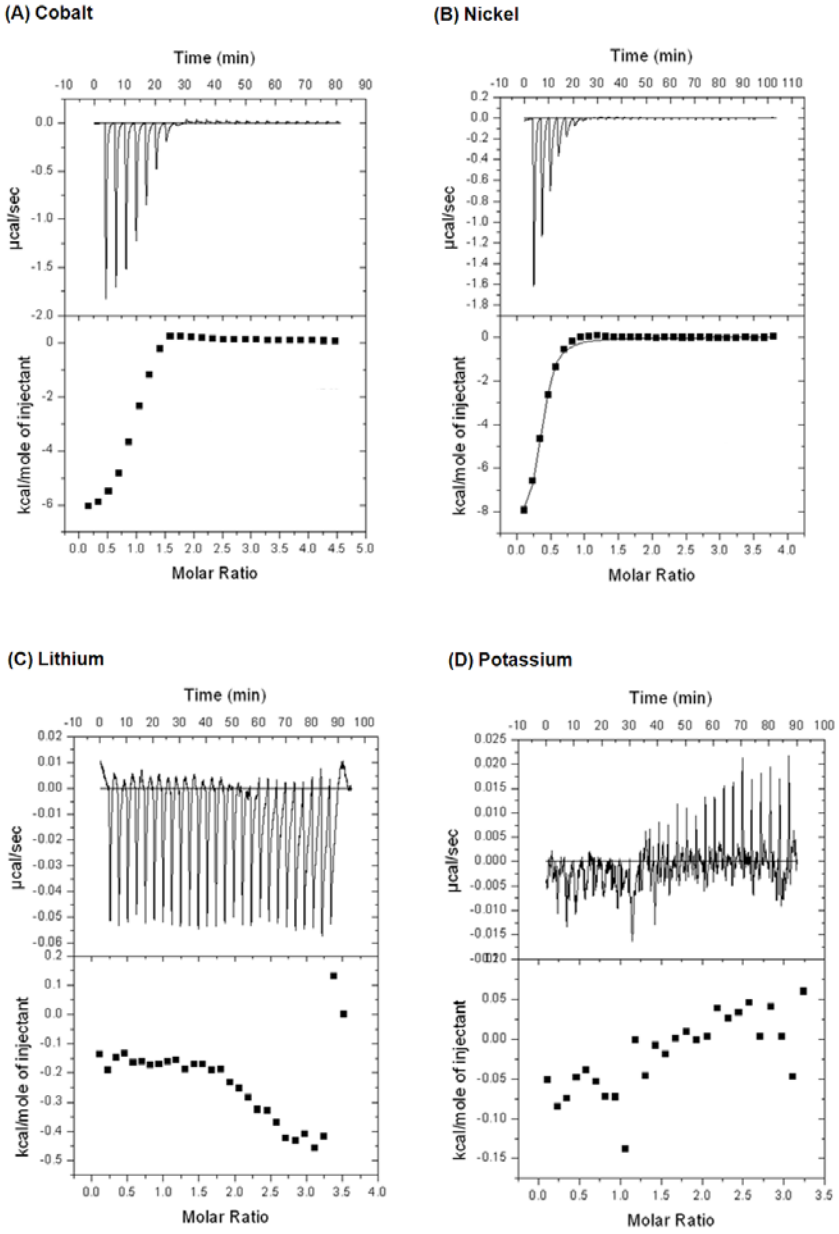

Metal ion	Stoichiometry (n)	K_d	ΔH (cal mole^{-1})	ΔS (cal mole^{-1} degree^{-1})
Cobalt	0.89 ± 0.02	0.88 ± 0.23 µM	-6053.00 ± 175.30	7.75
Nickel	0.34 ± 0.01	1.87 ± 0.22 µM	-8826.00 ± 210.00	-2.90

Figure 4.24: Isotherms generated by injections of 10 µL aliquots of (A) 1 mM cobalt chloride, (B) 1 mM nickel sulphate, (C) 1 mM lithium chloride or, (D) 1 mM potassium chloride into a sample cell containing 50 µM of magnesium-saturated $MurM_{159}$ at pH 7.0. Both baseline equilibration and metal ion injection were carried out at a temperature of 30°C. Data have been corrected for the heat of metal ion dilution and fitted to the one site model where possible. Lithium and potassium did not show significant binding to MurM as indicated by very small heat changes upon injection.

The data presented in Figure 4.24 support the finding that zinc can be replaced by cobalt in activity assays. It is likely that cobalt is unable to restore full activity of EDTA-treated MurM because the dissociation constant for this metal ion is 2 times higher than that for zinc, indicating a lower overall binding affinity towards the protein. Challenging magnesium-saturated protein with nickel gave a very low value for the stoichiometry of binding (0.34 ± 0.01) suggesting that nickel is not the preferred metal ion. This result is concurrent with assay data whereby the activity of EDTA-treated MurM could only be fully restored by the addition of saturating concentrations of zinc in the presence of magnesium (Section 4.4.2). One other reason that would explain why nickel cannot restore the activity of EDTA-treated MurM is that only a sub-population of the enzyme present in the sample cell was capable of binding this metal ion when compared to zinc and cobalt. The lack of interaction between MurM and either lithium or potassium suggests that only divalent metal ions are bound by the enzyme in a specific manner.

4.6.5. CHED server prediction of metal ion binding sites within MurM

A three-dimensional model of MurM was constructed by Dr Adrian Lloyd at the University of Warwick using the X-ray crystal structure of *S. aureus* FemA and the amino acid sequence of $MurM_{159}$. Making the assumption that MurM adopts the same fold as FemA, it was possible to load the model onto the CHED server for bioinformatics-based prediction of transition metal ion binding sites within proteins (Babor *et al.*, 2008). When the MurM model was loaded onto this server, only one metal ion binding site was predicted and this is highlighted in Figure 4.25.

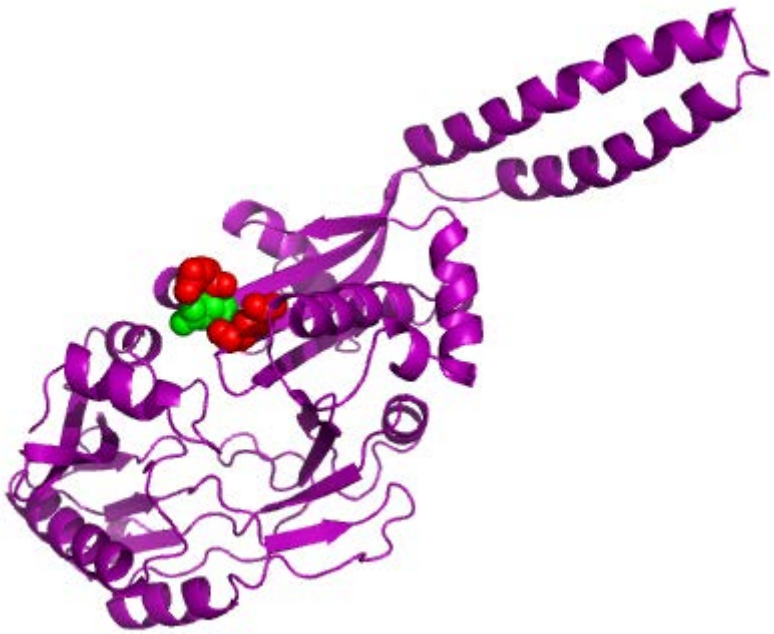

Figure 4.25: Model of $MurM_{159}$ based on the X-ray crystal structure of *S. aureus* FemA (PDB code 1LRZ). CHED server predicted metal binding site residues are highlighted in red (E229 is functionally conserved as an aspartate or a glutamate and E307 is conserved as glutamate across all currently sequenced variants of MurM) and green (D230) which is not conserved between MurM variants.

The CHED server predicted only one metal ion binding site within $MurM_{159}$ comprised of residues E229, D230 and E307. The apparent absence of a second site is likely to be due to the poor sequence homology between FemA and MurM which are only 26% identical at the amino acid level. It was not possible to readily identify the position of the second binding site by a simple alignment of the amino acid sequences of FemA and any of the MurM variants. This is illustrated using $MurM_{Pn16}$ in Figure 4.26.

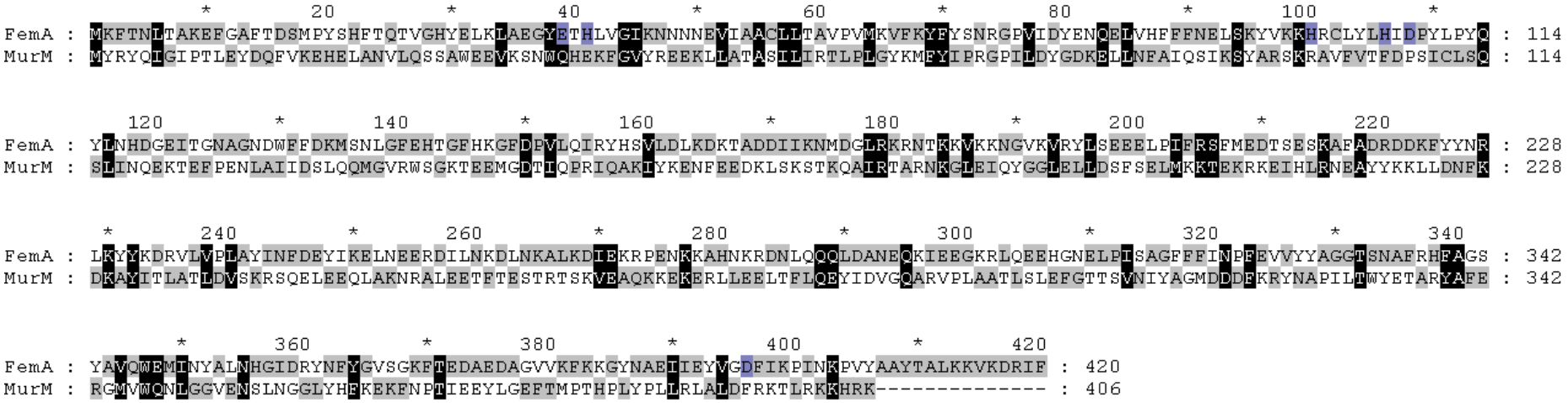

Figure 4.26: Sequence alignment of *Streptococcus pneumoniae* strain Pn16 MurM and *Staphylococcus aureus* FemA. Residues highlighted in purple are the putative metal binding residues identified in FemA. Note that the proteins are only 26% identical at the amino acid level.

In addition to this, it was noted that D230 was not conserved across all variants of MurM. However, as shown in Figure 4.27, there are other conserved aspartate and glutamate residues surrounding this position within MurM which may be involved in metal ion binding.

```
MurM-B6          TARNKGVEIQFGGTELLESFSFLMKKTEKRKEIHLRNEAYYKKLLDNFKEDSYITLTSLD
MurM-HU15        TARNKGLEIQYGGLELLDSFSELMKKTEKRKEIHLRNEAYYKKLLDNFKEDSYITLTSLD
MurM-4790        TARNKGLEIQYGGLELLDSFSELMKKTEKRKEIHLRNEAYYKKLLDNFKDKAYITLATLD
MurM-5084        TARNKGLEIQYGGLELLDSFSELMKKTEKRKEIHLRNEAYYKKLLDNFKDKAYITLATLD
MurM-5259        TARNKGLEIQYGGLELLDSFSELMKKTEKRKEIHLRNEAYYKKLLDNFKDKAYITLATLD
MurM-R6          TARNKGLEIQYGGLELLDSFSELMKKTEKRKEIHLRNEAYYKKLLDNFKDKAYITLATLD
MurM-Pn16        TARNKGLEIQYGGLELLDSFSELMKKTEKRKEIHLRNEAYYKKLLDNFKDKAYITLATLD
MurM-4883        TARNKGVEIQFGGTELLESFSFLMKKTEKRKEIHLRNETYYKKLLDNFKDKAYITLATLD
MurM-UO8         TARNKGVEIQFGGTELLESFSFLMKKTEKRKEIHLRNEAYYKKLLDNFKEDSYITLTSLD
MurM-10712       SARNKGVEIQIGRDELLESFSFLMKKTEKRKDIHLRNEAYYKKLLDNFKDKAYITLATLD
MurM-HU9         TARNKGLEIQYGGLELLDSFSELMKKTDKRKEIHLRNEAYYKKLLDNFKEDSYITLASLD
MurM-159         TARNKGLEIQYGGLELLDSFSELMKKTEKRKEIHLRNEAYYKKLLDNFKEDSYITLTSLD
MurM-8249        TARNKGLEIQYGGLELLDSFSELMKKTEKRKEIHLRNEAYYRKLLDNFKEDSYITLTNLD
MurM-5245        TARNKGLEVQYGGLELLDSFSELMKKTEKRKEIHLRNEAYYKKLLDNFKDKAYITLATLD
                 :*****:*:* *  ***:*** *****:***:******:**:*******:.:****:.**
```

Figure 4.27: Sequence alignment of the MurM protein from various strains of *Streptococcus pneumoniae* focussed on position 230 (highlighted in purple) which is not conserved. However there is a conserved aspartate residue found at position 225 which may substitute as a metal binding residue due to a slight difference in protein fold between FemA and MurM.

In order to determine the involvement of E229 and E307 in metal ion binding, these residues were mutated to alanine in $MurM_{159}$ both individually and in combination with each other (see Chapter 2 for experimental details). These mutants were then subjected to ITC as described previously. The isotherms generated upon presentation of magnesium to these mutant versions of $MurM_{159}$ are shown in Figure 4.28.

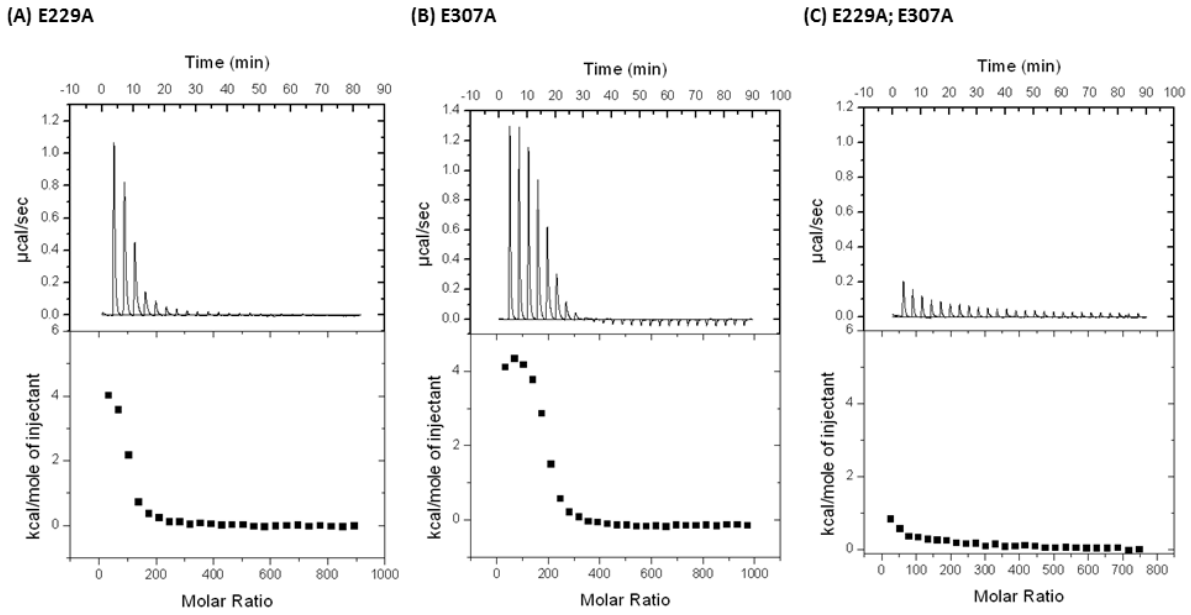

MurM Mutant	Stoichiometry (n)	K_d	ΔH (cal $mole^{-1}$)	ΔS (cal $mole^{-1}$ $degree^{-1}$)
E229A	1.00 ± 0.01	7.87 ± 0.63 µM	349800.00 ± 60830.00	1180.00
E307A	1.00 ± 0.02	22.83 ± 0.33 µM	7129.00 ± 1114.00	256.00

Figure 4.28: Isotherms generated by 10 µL injections of 1 mM magnesium chloride into a sample cell containing 50 µM of EDTA-treated $MurM_{159}$ predicted metal binding site mutants at 30°C in 20 mM HEPES pH 7.0. Responses of the mutants are as follows (A) E229A mutant (B) E307A mutant (C) E229A:E307A double mutant. Metal binding was fitted to the one site model in each case. The signal given by MurM E229A:E307A was equivalent to the background signal obtained upon injection of 1 mM $MgCl_2$ into 20 mM HEPES pH 7.0 and is indicative of a loss of metal ion binding by the protein.

As shown in Figure 4.28, individual mutation of E229 and E307 to alanine caused a 10 or a 25-fold increase in the dissociation constant of MurM for magnesium respectively in comparison to the wild-type enzyme. The ability of the protein to bind zinc was also affected as shown in Table 4.3.

(A) Magnesium			
	wild-type	**E229A**	**E307A**
N	0.91 ± 0.00	1.00 ± 0.01	1.00 ± 0.02
K_d (µM)	0.89 ± 0.06	7.87 ± 0.63	22.83 ± 0.33
(B) Zinc			
	wild-type	**E229A**	**E307A**
n	0.90 ± 0.12	1.00 ± 0.05	1.00 ± 0.07
K_d	0.50 ± 0.04 µM	10.00 ± 0.12 µM	10.26 ± 0.09 µM

Table 4.3: Comparison of the stoichiometry (n) and dissociation constant (K_d) for magnesium ion binding and zinc ion binding to magnesium-saturated wild-type and mutant $MurM_{159}$.

Mutation of E307 to alanine had the most significant effect on the dissociation constant of both magnesium and zinc ion binding to MurM. Data acquired for zinc ion binding to $MurM_{159}$ E307A fitted the two site model and this was hypothesised to be due to the 25-fold increase in the dissociation constant for magnesium ion binding in comparison to the wild-type enzyme. Such a significant increase in K_d was indicative of a reduced binding affinity for magnesium which could have subsequently enabled out-competition of this metal ion by zinc in this site. This

suggests that E307 is important for metal ion selectivity and maintenance of the overall preference for magnesium within this site.

In addition to this, when both mutations were present in combination with each other, magnesium ion binding was significantly reduced with only a background signal equivalent to that obtained for injection of magnesium into HEPES recorded. Despite an inability to bind magnesium tightly, $MurM_{159}$ E229A:E307A was still catalytically active with its substrates (see Chapter 5) confirming an earlier observation that the activity of EDTA-treated MurM was recoverable by the addition of zinc alone (Figure 4.5). A more detailed investigation into the kinetic properties of this enzyme in comparison to the wild-type is given in Chapter 5.

4.6.6. Binding of divalent metal ions to the FemX protein

For the purpose of comparison to the data obtained for MurM and to investigate further the metal ion requirements of cell wall branching enzymes, *S. aureus* FemX was subjected to analysis by ITC in the same way. All experiments were conducted as described in section 4.4.3.

Initially the protein was challenged separately with magnesium and zinc. In this scenario, it was found that zinc binding was complicated and could not be fitted to the one site model as was the case with MurM and FemA. For this reason, the protein was saturated with magnesium prior to challenge with other divalent metal ions (Figure 4.29).

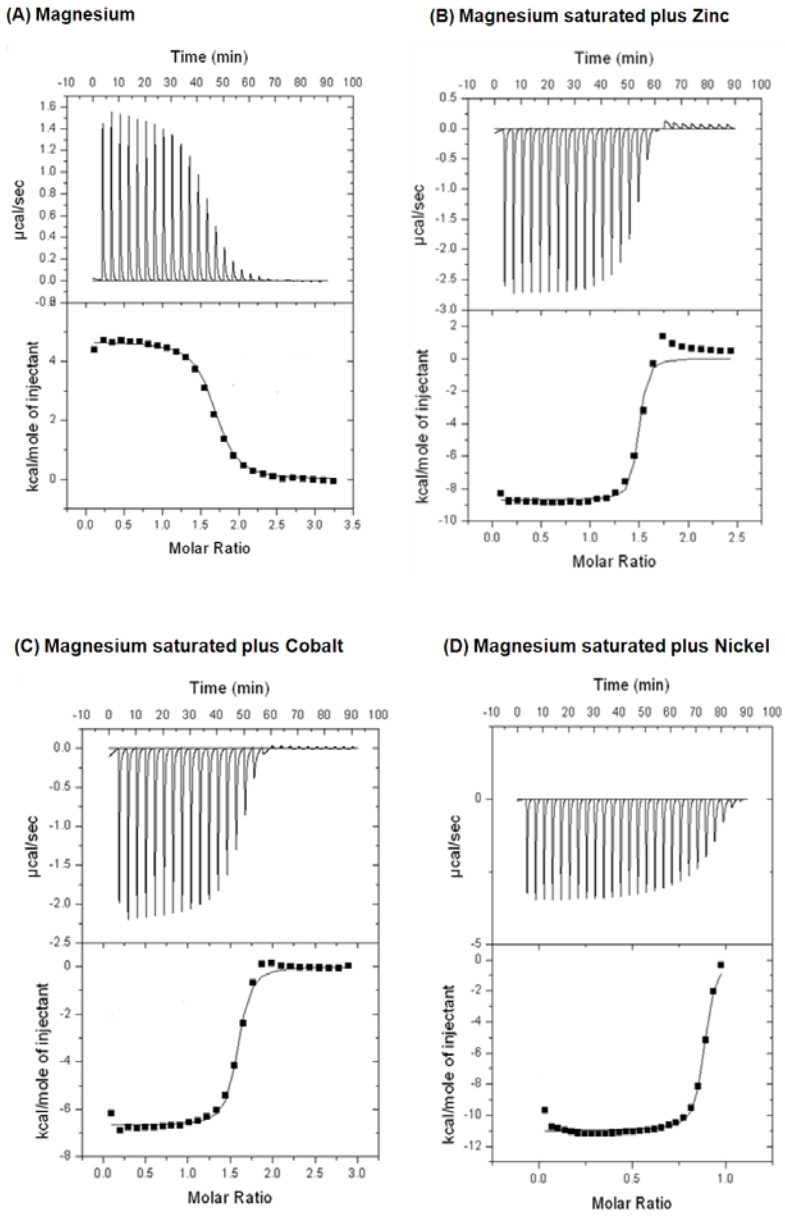

Metal ion	Stoichiometry (n)	K_d	ΔH (cal $mole^{-1}$)	ΔS (cal $mole^{-1}$ $degree^{-1}$)
Magnesium	1.50 ± 0.01	0.81 ± 0.07 µM	4704.00 ± 29.30	43.40
Zinc	1.45 ± 0.01	0.08 ± 0.04 µM	-8683.00 ± 159.60	3.94
Cobalt	1.54 ± 0.01	0.24 ± 0.05 µM	-6680.00 ± 62.55	8.29
Nickel	0.87 ± 0.00	0.69 ± 0.15 µM	-11000.00 ± 79.44	-5.02

Figure 4.29: Isotherms generated by injections of 10 µL aliquots of (A) 1 mM magnesium chloride, (B) 1 mM zinc chloride, (C) 1 mM cobalt chloride or, (D) 1 mM nickel sulphate, into a sample cell containing 50 µM of FemX at pH 7.0. In the case of B, C and D titrations were made into magnesium-saturated FemX. Both baseline equilibration and metal ion injection were carried out at a temperature of 30°C. Data have been corrected for the heat of metal ion dilution and fitted to the one site model where possible.

The ITC data presented in Figure 4.29 suggested that FemX has either two or three divalent metal ion binding sites. The dissociation constant for magnesium ion binding to one site was equivalent to that calculated for MurM. The dissociation constant for zinc ion binding to FemX was in the micromolar range as was the case for MurM and FemA when the one site data analysis model was applied. In the absence of any structural data for MurM and FemX, the isotherms generated by ITC suggest that both of these enzymes have a requirement for divalent metal ions. In order to investigate whether divalent metal ions are required for maintenance of the structure of MurM and FemA, these proteins were subjected to circular dichroism before and after treatment with EDTA. The results of this experiment are described in section 4.6.7.

4.6.7. Assessment of the structural effects of metal ion removal by EDTA on wild-type MurM and FemA using circular dichroism (CD)

Circular dichroism (CD) can be used as a direct technique for the assessment of the secondary structure of proteins. Peptide bonds located in the polypeptide backbone of proteins have electronic transitions that change with conformation and produce different absorption spectra upon exposure to circularly polarised light.

In order to investigate whether treatment with EDTA had any obvious structural effect on MurM and FemA, both proteins were buffer exchanged into 10 mM sodium phosphate to a final concentration of 0.12 mg mL^{-1} for study by circular dichroism. Other studies have indicated that sodium phosphate is a suitable buffer for this technique as it gives very little background signal in the ultraviolet region

(Kelly *et al.*, 2005). This was confirmed by correcting spectra obtained for MurM and FemA with a blank run containing only 10 mM sodium phosphate.

The far ultraviolet spectra obtained for $MurM_{Pn16}$ and FemA before and after treatment with EDTA were analysed using Dichroweb in order to determine differences in secondary structure between the samples (Whitmore and Wallace, 2004; Lees *et al.*, 2006b). Results of this analysis using the CDSSTR method and the SP175 database are presented in Figure 4.30, Figure 4.31 and Table 4.4.

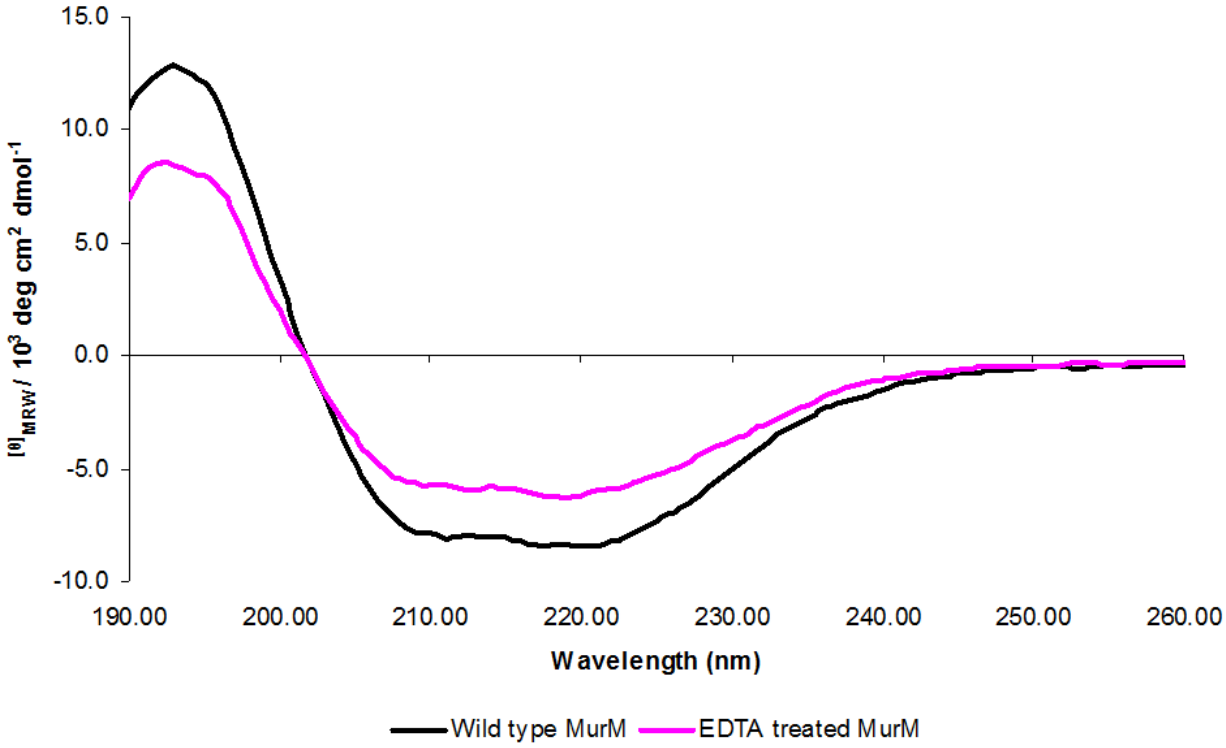

Figure 4.30: Far Ultraviolet spectra showing changes in secondary structure of wild-type $MurM_{Pn16}$ after treatment with EDTA to remove bound metal ions. Protein was concentrated to 0.12 mg mL^{-1} in 10 mM sodium phosphate pH 7.0 prior to analysis by circular dichroism. The traces shown have been generated from 16 repeats on the same sample.

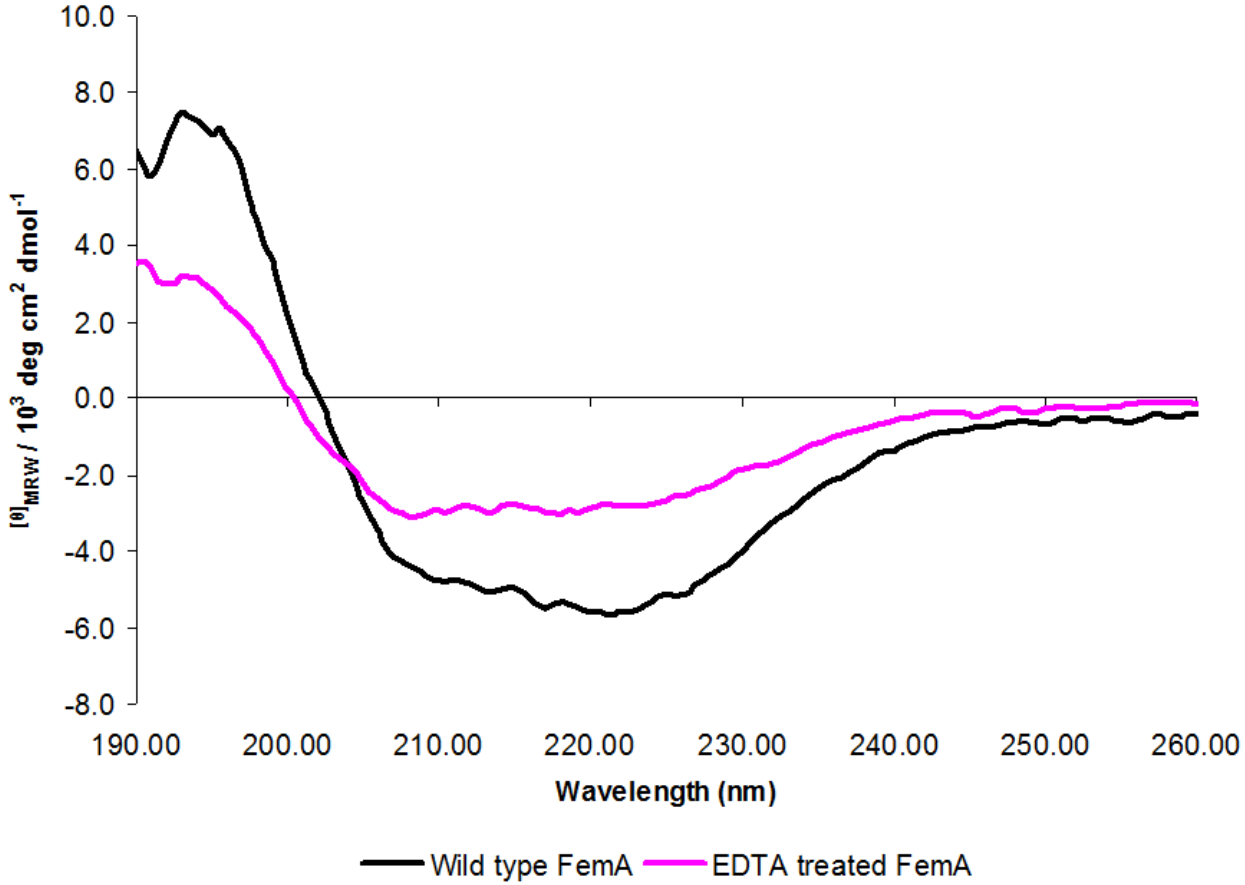

Figure 4.31: Far Ultraviolet spectra showing changes in secondary structure of wild-type FemA after treatment with EDTA to remove bound metal ions. Protein was concentrated to 0.12 mg mL^{-1} in 10 mM sodium phosphate pH 7.0 prior to analysis by circular dichroism. The traces shown have been generated from 16 repeats on the same sample.

Analysis of the data with Dichroweb indicated that MurM showed a significant reduction in secondary structure after treatment with EDTA and that this effect was much less pronounced in the case of FemA. Results of this analysis using the CDSSTR method and the SP175 database are presented in Table 4.4 (Lees *et al.*, 2006a; Lees *et al.*, 2006b).

	MurM	**EDTA-treated MurM**	**FemA**	**EDTA-treated FemA**
NRMSD	0.02	0.03	0.05	0.05
Total α helix	20%	10%	9%	8%
Total strand	31%	38%	39%	34%
Total turns	12%	12%	13%	17%
Total unordered	37%	40%	39%	41%

Table 4.4: Analysis of CD data obtained for MurM and FemA before and after treatment with EDTA using Dichroweb. NRMSD stands for normalised root mean square derivation where values of above 0.10 imply that the correspondence between the calculated secondary structure and the actual secondary structure are likely to be incorrect.

In the case of MurM, removal of metal ions by treatment with EDTA resulted in a 50% loss in alpha helical structure. In addition to this, total strand content was increased by 7% indicating denaturation of the protein. With both FemA and MurM, the total amount of unordered structure increased by 3% upon removal of metal ions by EDTA. When taken together, the data presented in Table 4.4 and the activity data obtained for MurM suggest that metal ions are likely to be involved in maintaining both the structure and the catalytic activity of these proteins.

4.7. Discussion

Comparative modelling of MurM on the X-ray crystal structure of *S. aureus* FemA (PDB code 1LRZ) has indicated that these proteins are likely to have a similar overall fold (Fiser *et al.*, 2003). This means that FemA is an acceptable homology model for the prediction of the structure of MurM. Within the predicted structure of MurM, domain I consists of a twisted β-sheet core surrounded by α-helices and domain II consists of a coiled helical arm. Fiser *et al.* (2003) have used distance matrix alignment and combinatorial extension to compare the predicted structure of MurM domain II to the structure of other proteins within the protein data bank. This process identified structural similarities between MurM and several tRNA synthetase enzymes. In addition to this, structural similarities between the coiled helical arm of FemA and seryl-tRNA synthetase were identified when the X-ray crystal structure of the former was solved by Benson *et al*. (2002). These similarities are not surprising given that members of the Fem ligase family and all tRNA synthetase enzymes have the requirement for a tRNA substrate in common with each other.

Many tRNA synthetase enzymes have been shown to require divalent metal ions either for catalysis, maintenance of structure or both. For example, *E. coli* alanyl-tRNA synthetase (AlaRS) requires zinc with a stoichiometry of one for the recognition of its cognate tRNA species. In addition to this, removal of zinc from the enzyme caused a loss in the secondary structure measured by circular dichroism (Sood *et al.*, 1999). In threonyl-tRNA synthetase (ThrRS), zinc has been shown to be important for the recognition of threonine. Whilst the requirement for bound zinc in ThrRS cannot be described as either strictly catalytic or structural, the function of this metal ion is to ensure that activation only takes places with amino acids that

have a hydroxyl-group attached at the β-position (Sankaranarayanan *et al.*, 2000). An essential catalytic zinc ion has also been found in the active site of the seryl-tRNA synthetase enzyme of methanogenic archaea (Bilokapic *et al.*, 2006). Despite this, the metal ion requirements of members of the Fem ligase family have remained unexplored in the literature until now. In addition to this, the current X-ray crystal structure of *S. aureus* FemA (PDB code 1LRZ) has no information regarding bound metal ions which is likely to be a direct result of purification the protein using an inhibitor cocktail containing EDTA (Benson *et al.*, 2002).

In order to investigate the metal ion binding requirements of some members of the Fem ligase family in this study, it was considered necessary to re-clone FemA and MurM such that the vector-encoded C-terminal hexa-histidine tag could be removed from the proteins after purification. Histidine tags engineered onto either terminus of a protein during cloning are known to bind to divalent metal ions and this property is exploited in immobilised metal ion affinity chromatography (IMAC). This accounted for the fact that ITC data gathered for histidine-tagged versions of these proteins could not be readily interpreted. Incubation of histidine-tagged protein with TEV protease followed by further purification on cobalt resin and SDS PAGE analysis indicated that it was possible to obtain sufficient quantities of untagged protein within the region of 8 to 10 mg L^{-1} for determination of the metal ion binding properties of MurM, FemX and FemA by ITC.

Determination of which metal ions to present to these enzymes by ITC was based on key observations made with MurM. Structural data presented in Chapter 6 indicated that MurM could only nucleate under crystallisation conditions where the mother

liquor solution contained zinc. In order to remove bound metal ions, each protein was dialysed against buffer containing the strong chelating reagent, EDTA (Nyborg and Peersen, 2004). Activity assays carried out on MurM before and after this process indicated that EDTA-treated protein was no longer catalytically active. Total activity could only be restored by pre-incubation of EDTA-treated MurM with a molar excess of zinc in the presence of magnesium. Approximately 80% activity could be restored by zinc alone and 45% activity could be restored by cobalt.

Titration of zinc into MurM, FemA and FemX resulted in the acquisition of complicated isotherms which could not be fitted to any of the ITC data analysis models available in VP-Viewer and Origin software. Given an earlier observation that full recovery of the activity of EDTA-treated MurM required pre-incubation with a molar excess of both zinc and magnesium, this was hypothesised to be due to the presence of two metal ion binding sites within these proteins: one with a high affinity for zinc and the other with a preference for magnesium but a low zinc affinity at the same time. This hypothesis was tested by saturating each protein with magnesium prior to the presentation of zinc. Saturation of both FemA and MurM with magnesium suggested that both of these proteins have one binding site for this metal ion with a K_d of 0.78 ± 0.07 µM and 0.89 ± 0.06 µM, respectively. In addition to this, when zinc was presented to magnesium-saturated FemX, FemA and MurM, the generated data points could be fitted to the one site data analysis model within Origin, thus supporting the two metal binding site hypothesis.

Within all three magnesium-saturated proteins, it was possible to replace the zinc with cobalt and still obtain a stoichiometry of one. However the K_d for cobalt was

higher than that of zinc indicating tighter binding in the latter case. Investigations with magnesium-saturated FemA also showed that zinc could be replaced by nickel and that copper could replace both magnesium and zinc. Substitutions of zinc by metals including cobalt, cadmium, copper, nickel and iron is common and has been reported for zinc finger proteins (Sarkar, 1995).

In addition to this, the Irving-Williams series, which describes the natural order of stability of divalent metal ions, states that copper and zinc form the tightest complexes followed by ferrous iron and manganese. The series ends with calcium and magnesium which form the weakest complexes (Mellor and Maley, 1948). As a result of this, exclusion of the wrong metal ions from proteins *in vivo* is thought to be a complex problem given that some proteins have a requirement for those which form the weakest complexes (Waldron *et al.*, 2009). Acquisition of the correct metal ion *in vivo* is considered to involve a series of metal-sensing proteins, metallo-chaperones and also the metal ion availability in the cellular location of protein folding (Waldron and Robinson, 2009; Waldron *et al.*, 2009). Taken together with the fact that the concentration of free Mg^{2+} in a bacterial cell is within the millimolar range, and the total concentration of free Zn^{2+} is tightly regulated within the sub-micromolar range, it is reasonable to assume that *in vivo* the two metal binding sites detected in this study are occupied by their high affinity metal ligands as described (Blencowe and Morby, 2003; Finney and O'Halloran, 2003; Feng *et al.*, 2008).

Using the X-ray crystal structure of FemA determined by Benson *et al*. (2002), it was possible to use a bioinformatics-based approach for prediction of possible transition metal ion binding sites within this protein. Analysis of the FemA crystal

structure (PDB code 1LRZ) using the CHED server resulted in the prediction of two metal ion binding sites (Babor *et al.*, 2008). One of the predicted sites was comprised of E39, H41 and H100. The other was comprised of H106, D108 and D396. After single mutation of H41, H100, H106 and D396 to alanine, no significant increases in the K_d for magnesium ion binding were observed. However, all four mutations resulted in an increase in the K_d of zinc ion binding from 0.08 ± 0.06 μM in the wild-type enzyme to within the range of 0.14 to 1.11 μM in the single site alanine mutants.

Double mutation of H41 and H100 to alanine resulted in no significant change in the K_d for magnesium ion binding but an increase in the K_d of zinc ion binding to 0.23 ± 0.04 μM. This suggested that both of these residues are important in zinc ion binding. The fact that zinc ion binding was not completely abolished in this double mutant indicated either that E39 is a key residue in this process or that other surrounding residues not picked up by the CHED server are also involved in the binding of zinc at this site. To determine which of these scenarios is correct, further mutagenesis studies or an X-ray crystal structure of FemA containing the bound zinc atom are required. Double mutation of H106 and D396 to alanine resulted in a significant disturbance to the binding of magnesium which resulted in an inability to fit the data to analysis models within Origin.

When the FemA-based homology model of $MurM_{159}$ was loaded onto the CHED server, only one metal ion binding site was predicted. The position of this predicted site is located near to the region of the protein that is thought to interface with the membrane. FemA and MurM are only 26% identical at the amino acid level so slight

differences in the fold of the two proteins may explain why only one site was identified despite biochemical and biophysical evidence supporting the hypothesis that the enzyme has two metal binding sites. Individual mutation of the two functionally conserved residues, E229 and E307, to alanine caused a 9 and a 25-fold increase in the K_d of magnesium ion binding respectively in comparison to the wild-type enzyme. Complete abolition of the ITC signal for magnesium ion binding was achieved by mutation of both of these residues to alanine at the same time indicating the importance of these residues in this process.

It was also noted that EDTA-treatment of MurM resulted in a significant change to the secondary structure of the protein as determined by CD. Combined with the ITC data, this suggests that magnesium and zinc are important for both the structure and the catalytic activity of MurM. Given the proposed structural similarities between members of the Fem ligase family and tRNA synthetase enzymes, one hypothesis is that zinc is required for recognition of tRNA by MurM.

In addition it is interesting to speculate upon the role of the magnesium site. Following protein over-expression, MurM remains in the insoluble fraction until 1 M sodium chloride is used in a solubilisation buffer (see Chapter 3). This suggests that MurM has significant hydrophobic character, consistent with it being a membrane-associated protein. Association of MurM with the membrane has not been formerly proven, however it is likely to be the case given that it utilises Lipid II as opposed to soluble UDP-MurNAc-pentapeptide as a substrate (Lloyd *et al.*, 2008). Given the location of the proposed magnesium site is on the outer edge of the predicted structure of MurM, it is possible that this metal ion is responsible for localising the

protein to the cytoplasmic side of the cell membrane. Once in this position, co-ordination of MurM with phospholipid head groups in the membrane could be achieved using magnesium as a bridge. This would locate the enzyme in the correct orientation over the substrate at the correct cellular location for subsequent utilisation of the reaction product by MurN. A similar role for Mg^{2+} has been described for methanol dehydrogenase where it facilitates the association of the enzyme with the membrane-bound, terminal respiratory chain (Carver *et al.*, 1984). Investigations into the effects of these mutations on the overall activity of MurM and its interaction with cardiolipin, an abundant phospholipid in the membrane of *S. pneumoniae*, are detailed in Chapter 5.

In conclusion, the Zn^{2+} dependent activity of MurM and other Fem ligases has not been documented previously and has significance for both enzyme mechanism and the design of potential inhibitory compounds. All of the aims laid out in section 4.2 were achieved. However, further work should include identification of other amino acid residues within MurM that are involved in zinc ion binding. All currently sequenced variants of MurM contain a single cysteine residue that is an obvious target for zinc ion binding. Unfortunately, mutation of this residue to alanine in this study resulted in production of protein that could not be solubilised for biophysical and biochemical characterisation. As a result of this, obtaining a high resolution X-ray crystal structure of this protein is of great importance. In addition, development of a means for producing a high yield of Lipid II-Gly will enable kinetic analysis to be carried out on all of the FemA mutants constructed in this study which may shed more light on the role of the CHED server predicted amino acid residues in metal ion binding.

Chapter 5

Kinetic Characterisation of MurM from penicillin-resistant (159) and penicillin-sensitive (R6 and Pn16) strains of *Streptococcus pneumoniae*

5.1. Introduction

Within pneumococcal peptidoglycan, the MurM protein is responsible for the addition of either L-alanine or L-serine as the first amino acid of an indirect dipeptide branch that is appended to the stem peptide lysine of the pentapeptide side chain. Deletion of the *murM* gene has been shown to cause a reversion to penicillin sensitivity in strains that were previously resistant. However, the protein itself does not appear to be essential for cell viability (Filipe and Tomasz, 2000). This is unusual since, whilst the *murM* gene has become mosaic in nature across penicillin-resistant variants of *S. pneumoniae,* its functionality is conserved across all strains suggesting it may have a specialised role within the organism that has not yet been determined.

In order to further understand the link between MurM activity, levels of cell wall cross-linking and penicillin resistance in pneumococci, Lloyd *et al.* (2008) cloned the *murM* gene from a penicillin-sensitive (Pn16) and a penicillin-resistant (159) strain of the organism into an expression vector thus enabling over-expression of histidine tagged MurM for *in vitro* studies. These studies demonstrated for the first time that MurM is an aminoacyl-tRNA-dependent ligase and that the proportion of branched structured muropeptides in the pneumococcal cell wall is directly related to the activity of this enzyme. $MurM_{159}$ was found to be more catalytically active than

$MurM_{Pn16}$ and had a preference for the addition of alanine to Lipid II as opposed to serine. This preference was consistent with the enzyme having a lysine residue at position 260, which is thought to be the key residue within the region of the protein identified by Filipe *et al.* (2001a) as having a role in the determination of substrate specificity. In the work carried out by Lloyd *et al.* (2008), $MurM_{Pn16}$ was found to have a preference for the addition of serine to Lipid II which was consistent with the enzyme having threonine at position 260.

In this study, determination of kinetic parameters for the MurM protein from *S. pneumoniae* strain R6, which has threonine at position 260, was considered to be a valuable addition to the work carried out by Lloyd *et al.* (2008). Strain R6 is penicillin-sensitive but has an unusually high proportion of branched muropeptides within its peptidoglycan structure (Garcia-Bustos and Tomasz, 1990). For the first time, $MurM_{R6}$ has been kinetically characterised with both its tRNA and its lipid substrate allowing comparisons to be made with $MurM_{Pn16}$ and $MurM_{159}$. In addition, given the findings made in Chapter 4, untagged $MurM_{R6}$, $MurM_{Pn16}$ and $MurM_{159}$ were kinetically characterised in the presence of saturating concentrations of zinc and magnesium. The development of methodology for the production of a single species of pure *S. pneumoniae* $tRNA^{Ala}$ and $tRNA^{Ser}$ by *in vitro* transcription has also enabled the first investigations into the substrate specificity of MurM to be undertaken.

5.2. Aims

The main aim of the work carried out in this chapter was to characterise the kinetic activity of $MurM_{R6}$ and compare it to previous studies that had characterised

$MurM_{Pn16}$ and $MurM_{159}$ in the same way (Lloyd *et al.*, 2008). Detailed kinetic characterisation of the three MurM variants encompassed the following objectives:

- Purification of the appropriate *S. pneumoniae* tRNA synthetase enzymes (AlaRS and SerRS) for the production of aminoacylated Ser-$tRNA^{Ser}$ and Ala-$tRNA^{Ala}$
- Generation of an *in vitro* transcription-based method for the production of large amounts of a single species of *S. pneumoniae* $tRNA^{Ala}$ and $tRNA^{Ser}$ that could be used as substrates for MurM
- Assessment of key kinetic parameters for all three variants of MurM, for the first time in the absence of a histidine tag and the presence of 0.5 μM zinc, when the concentration of Lipid II was varied using Ala-$tRNA^{Ala}$ and subsequently, Ser-$tRNA^{Ser}$ as a co-substrate
- Assessment, for the first time, of key kinetic parameters for all three variants of MurM when the concentration of Ala-$tRNA^{Ala}$ and subsequently, Ser-$tRNA^{Ser}$, was varied in the presence of the co-substrate Lipid II
- Assessment of the effects of a significant reduction in the affinity of magnesium binding on key kinetic parameters obtained for $MurM_{159}$ E229A:E307A in comparison to the wild-type enzyme
- The major phospholipids present in the cell membrane of pneumococcus are cardiolipin and phosphatidylglycerol (Trombe *et al.*, 1979). Given that MurM has a Lipid substrate it is likely to interface with the membrane. Hence, the effects of the presence of cardiolipin on the kinetic parameters obtained for all three variants of MurM and $MurM_{159}$ E229A:E307A were investigated. This was intended to expand unpublished work already carried out by Dr Adrian Lloyd (University of Warwick)

In order to investigate the substrate specificity of MurM, these objectives were expanded further as follows:

- In order to determine the degree to which MurM recognises the aminoacyl and tRNA sections of its acyl-tRNA substrate, it was necessary to over-express and purify *S. pneumoniae* AlaRS catalytic domain. This was to enable generation of high yields of mis-aminoacylated Ser-tRNA^{Ala} to use as a substrate for MurM
- Further analysis of aminoacyl and tRNA recognition by MurM was carried out using a 2'-amino mini-helix tRNA^{Ala} analogue with the aim of determining whether MurM is specific for removal of the amino acid from the 2' or the 3' hydroxyl of the terminal adenine of its substrate tRNA

5.3. Expression and purification of *Streptococcus pneumoniae* Alanyl-tRNA synthetase (AlaRS) and Seryl-tRNA synthetase (SerRS)

5.3.1. Small-scale expression trials of AlaRS and SerRS

Expression constructs containing the *S. pneumoniae* strain 159 *AlaRS* gene and the *S. pneumoniae* strain Pn16 *SerRS* gene were obtained from Dr Adrian Lloyd (University of Warwick). Trial expressions were carried out for each synthetase using *E. coli* BL21 Star (DE3).placIRare2 cells and either IPTG-induction at 25^{o}C for 3 h or auto-induction for 16 h at 37^{o}C (Figure 5.1).

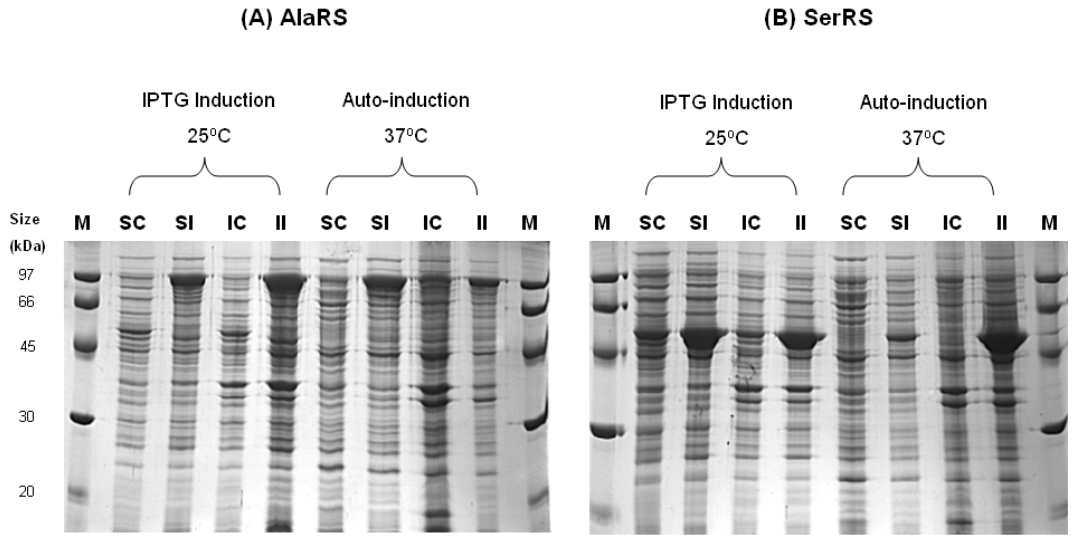

M - molecular weight standards,
SC - soluble proteins expressed by non-induced cells,
SI - soluble protein expressed by induced cells,
IC - insoluble protein expressed by non-induced cells,
II - insoluble proteins expressed by induced cells.

Figure 5.1: 12.5% SDS PAGE gels showing crude extracts obtained from *Escherichia coli* BL21 Star (DE3).placIRare2 cells transformed with expression constructs harbouring either (A) *AlaRS* or, (B*) SerRS* and induced to express protein by IPTG-induction at 25°C for 3 h or auto-induction at 37°C for 16 h. The molecular weight of *S. pneumoniae* SerRS is approximately 50,000 Da. The molecular weight of *S. pneumoniae* AlaRS is 96,525 Da.

After auto-induction at 37°C, AlaRS was visible in a soluble form but SerRS was mostly insoluble. However, both AlaRS and SerRS were produced in a soluble form during IPTG-induction at 25°C. Hence, this expression condition was used for large-scale production of both enzymes.

5.3.2. Large-scale expression and purification of AlaRS and SerRS

For large-scale protein production, *E. coli* BL21 Star (DE3).placIRare2 cells that had been transformed with a vector containing either AlaRS or SerRS were cultured at 37°C to an OD_{600nm} of 0.5 when protein expression was induced by the addition of IPTG. Addition of IPTG to a final concentration of 1 mM was concurrent with the

growth temperature being reduced to 25^{o}C for 3 h. Cells were harvested and a crude extract containing soluble protein was obtained as described in Chapter 2, section 2.3.5 The crude extract was loaded onto a 5 mL cobalt column pre-equilibrated in 50 mM sodium phosphate pH 7.0, 500 mM NaCl and 10 mM imidazole for purification of soluble protein using a modified version of the procedure developed by Lloyd *et al.* (2008). Protein was eluted from the column using wash steps containing 10 mM, 20 mM, 50 mM, 100 mM and 200 mM imidazole. Overall purity of the protein was assessed using SDS PAGE (Figure 5.2).

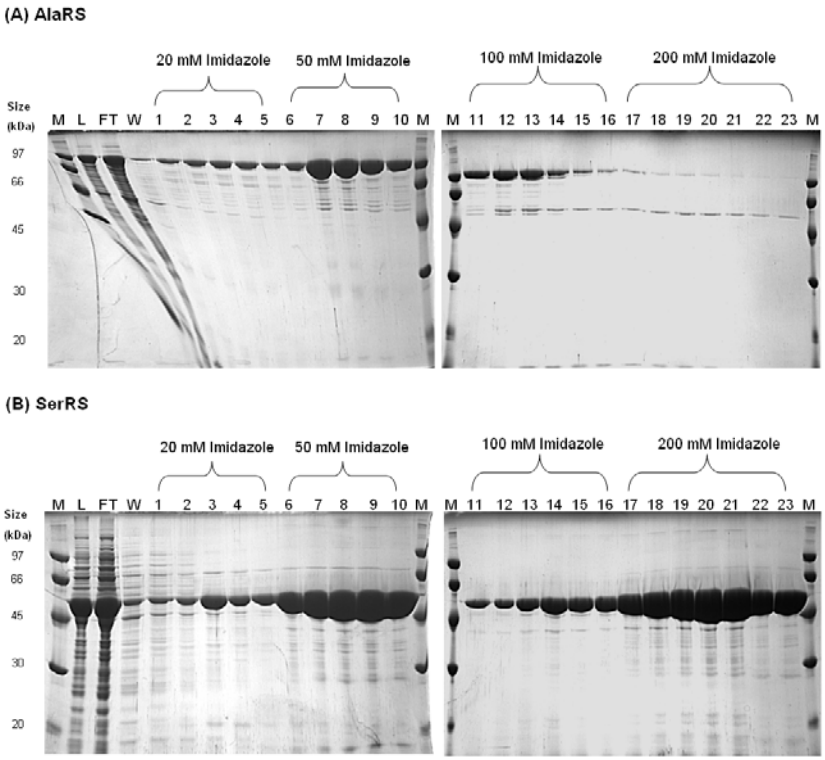

M - molecular weight standards,
L - protein sample prior to loading onto the column,
FT - flow through from the column during protein loading,
W - protein collected during wash of the column with equilibration buffer.

Figure 5.2: 12.5% SDS PAGE gels showing purification of hexa-histidine tagged *S. pneumoniae* AlaRS (A) and SerRS (B) from 1 L of *Escherichia coli* BL21 Star (DE3).placIRare2 cells on BD TALON cobalt resin. Lanes 1 - 23 represent protein eluted from the column using equilibration buffer substituted with different concentrations of imidazole. The molecular weight of *S. pneumoniae* SerRS is approximately 50,000 Da. The molecular weight of *S. pneumoniae* AlaRS is 96,525 Da.

In the case of both AlaRS and SerRS, most protein eluted from the column during wash with buffers containing 50 mM, 100 mM and 200 mM imidazole. Protein present in these fractions was dialysed against storage buffer containing 50 mM HEPES pH 7.0, 100 mM NaCl, 1 mM $MgCl_2$, 1 mM DTT and 50% glycerol prior to freezing at -80^{o}C. In order to check whether or not the enzymes were active, a small-scale aminoacylation experiment was carried out using a pool of *Micrococcus flavus* tRNA isolated *in vivo* in combination with radiolabelled alanine and serine (Lloyd *et al*., 2008; von Ehrenstein, 1967; Zubay, 1962)

5.4. Production of a single species of *Streptococcus pneumoniae* $tRNA^{Ala}$ and $tRNA^{Ser}$ by *in vitro* transcription

5.4.1. Identification of $tRNA^{Ala}$ and $tRNA^{Ser}$ gene sequences from the genome of *Streptococcus pneumoniae* strain R6

A search of the TIGR database identified four gene sequences within *S. pneumoniae* strain R6 encoding $tRNA^{Ala}$ (all UGC anticodon) and a further four gene sequences encoding $tRNA^{Ser}$ (anticodons GGA, GCU and two with anticodon UGA). All four $tRNA^{Ala}$ genes were of identical sequence. Only one sequence was selected for production of $tRNA^{Ser}$ (UGA anticodon).

The sequence of the pneumococcal $tRNA^{Ala}$ gene (anticodon UGC) 5’ GGGGCCTTAGCTCAGCTGGGAGAGCGCCTGCTTTGCACGCAGGAGGTCA GCGGTTCGATCCCGCTAGGCTCCACCA 3’ was synthesised commercially and cloned into pIDTSMART-Kan by Integrated DNA Technologies (IDT) such that a T7 promoter sequence proceeded the gene and a 3’ *Bst*NI site allowed incorporation

of the essential CCA terminus whilst ensuring suitability of the template for run-off transcription.

The pneumococcal $tRNA^{Ser}$ gene (anticodon UGA) with the sequence 5'GGAGGATTACCCAAGTCCGGCTGAAGGGAACGGTCTTGAAAACCGTCA GGCGTGTAAAAGCGTGCGTGGGTTCGAATCCCACATCCTCCTCCA 3' was cloned into pIDTSMART-Kan in the same way.

5.4.2. Production of $tRNA^{Ala}$ and $tRNA^{Ser}$ by run-off *in vitro* transcription using *Bst*NI digested vector as template

In order to obtain sufficient quantities of pIDTSMART-Kan-$tRNA^{Ala}$ and pIDTSMART-Kan-$tRNA^{Ser}$ for run-off transcription, each vector was transformed into *E. coli* Top10 cells. A single colony from each transformation was used to inoculate 250 mL of LB. After growth for 12 h at 37^{o}C, sufficient quantities of each vector were extracted from these cells using the Sigma maxi-prep kit. Each vector was digested with *Bam*HI to determine overall DNA quality and *Bst*NI in a separate reaction to check suitability for use as a template in run-off *in vitro* transcription (Figure 5.3).

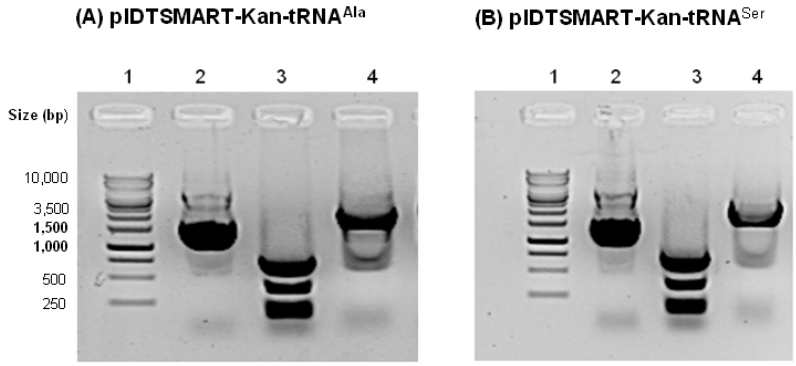

Figure 5.3: 0.8% agarose gel showing suitability of (A) pIDTSMART-Kan-tRNA^{Ala} and (B) pIDTSMART-Kan-tRNA^{Ser} as templates for *in vitro* transcription before and after restriction digestion.

Lane 1 - standard 1 kb ladder,
Lane 2 - uncut vector,
Lane 3 - *Bst*NI restricted vector,
Lane 4 - *Bam*HI restricted vector.

Given that, in each case, *Bst*NI digestion successfully released the fragment encoding the tRNA gene, each digest reaction was scaled-up to obtain enough DNA to use as template for *in vitro* transcription. For large-scale template preparation, 1.5 µg of each vector was digested with *Bst*NI for 1 h at 65^{o}C. The restriction digest was stopped and processed by the addition of 0.5 M EDTA pH 8.0 (1/20th of the total volume), 3 M sodium acetate pH 4.5 (1/10th of the total volume) and ethanol (2 volumes). Each reaction was vortexed and left at -20^{o}C overnight to precipitate the DNA fragments. The DNA was pelleted and dried prior to resuspension in water.

At this stage, the DNA was trialled as a template for *in vitro* transcription using the Ambion MEGAscript kit alongside the provided pTri-Xef control template as per manufacturer's instructions. After DNase treatment to remove the template and phenol/chloroform extraction to remove free nucleotides, the yield of RNA produced

was assessed using both 25% and 15% denaturing acrylamide 8 M urea gels set up as described in Chapter 2, section 2.5.3 (Figure 5.4).

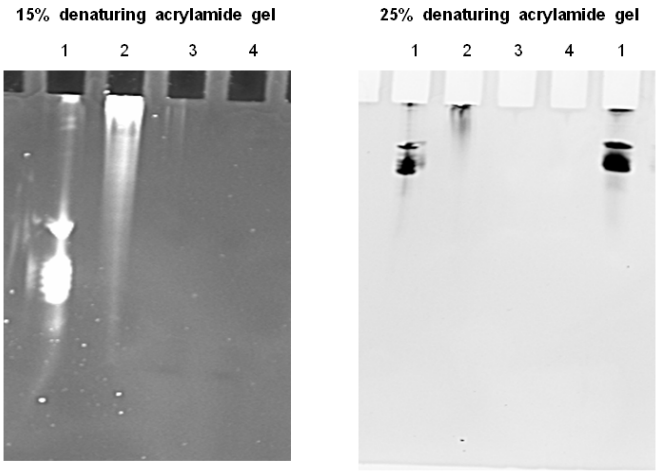

Figure 5.4: Assessment of the yield of tRNA^{Ala} and tRNA^{Ser} produced by *in vitro* transcription from *Bst*NI digested template vector. Gels were stained with ethidium bromide.

Lane 1 – sample of a control pool of *Micrococcus flavus* tRNA made *in vivo*,
Lane 2 – RNA obtained from the 1.89 kb control template,
Lane 3 – RNA obtained from *Bst*NI digested pIDTSMART-Kan-tRNA^{Ala},
Lane 4 – RNA obtained from *Bst*NI digested pIDTSMART-Kan-tRNA^{Ser}.

As shown above, *in vitro* transcription from the *Bst*NI digested templates was unsuccessful in the case of both tRNA^{Ala} and tRNA^{Ser}. One hypothesis for this was that there was not enough T7 RNA polymerase in the reaction to generate a high yield of product from such a small template fragment. In order to rectify this, the T7 RNA polymerase gene was cloned from *E. coli* BL21 Star (DE3).placIRare2 chromosomal DNA into two expression vectors: pProExHTa (providing an N-terminal hexa-histidine tag) and pET28a (providing a C-terminal hexa-histidine tag). PCR amplification of the T7 RNA polymerase gene was carried out using *pfx* polymerase from Invitrogen as shown in Figure 5.5 (Chapter 2, section 2.2.2).

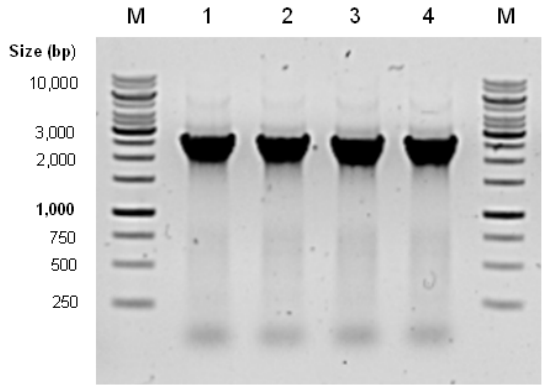

Figure 5.5: 0.8% agarose gel showing PCR amplification of the T7 RNA polymerase gene from the chromosomal DNA of *Escherichia coli* BL21 Star (DE3).placIRare2. Primers were designed to allow ligation into each vector by restriction of the PCR product with either *Bsa*I or *Bam*HI in combination with *Xho*I (see materials and methods for primer sequences).

M - standard 1 kb ladder,
Lanes 1 - 4 - T7 RNA polymerase PCR product.

After successful amplification, the PCR product was restricted with *Bsa*I and *Xho*I for ligation into *Nco*I/*Xho*I restricted pET28a. For ligation into pProExHTa, both the PCR product and the vector were digested with *Bam*HI and *Xho*I. Successful clones were identified by sequencing.

One clone with the correct sequence for each vector was used for protein expression experiments. In addition to this, a construct containing a mutant form of the polymerase (P266L) was obtained from Professor Dreyfus (Centre National de la Recherché Scientifique, France). The mutation P266L within T7 RNA polymerase is known to cause stabilisation of the transcription complex between nucleotides five and eight which results in significant reduction in abortive cycling during the transcription process in comparison to the wild-type enzyme (Guillerez *et al*. 2005). Both wild-type and P266L T7 RNA polymerase were subjected to small-scale protein expression trials to determine optimal conditions (Figure 5.6).

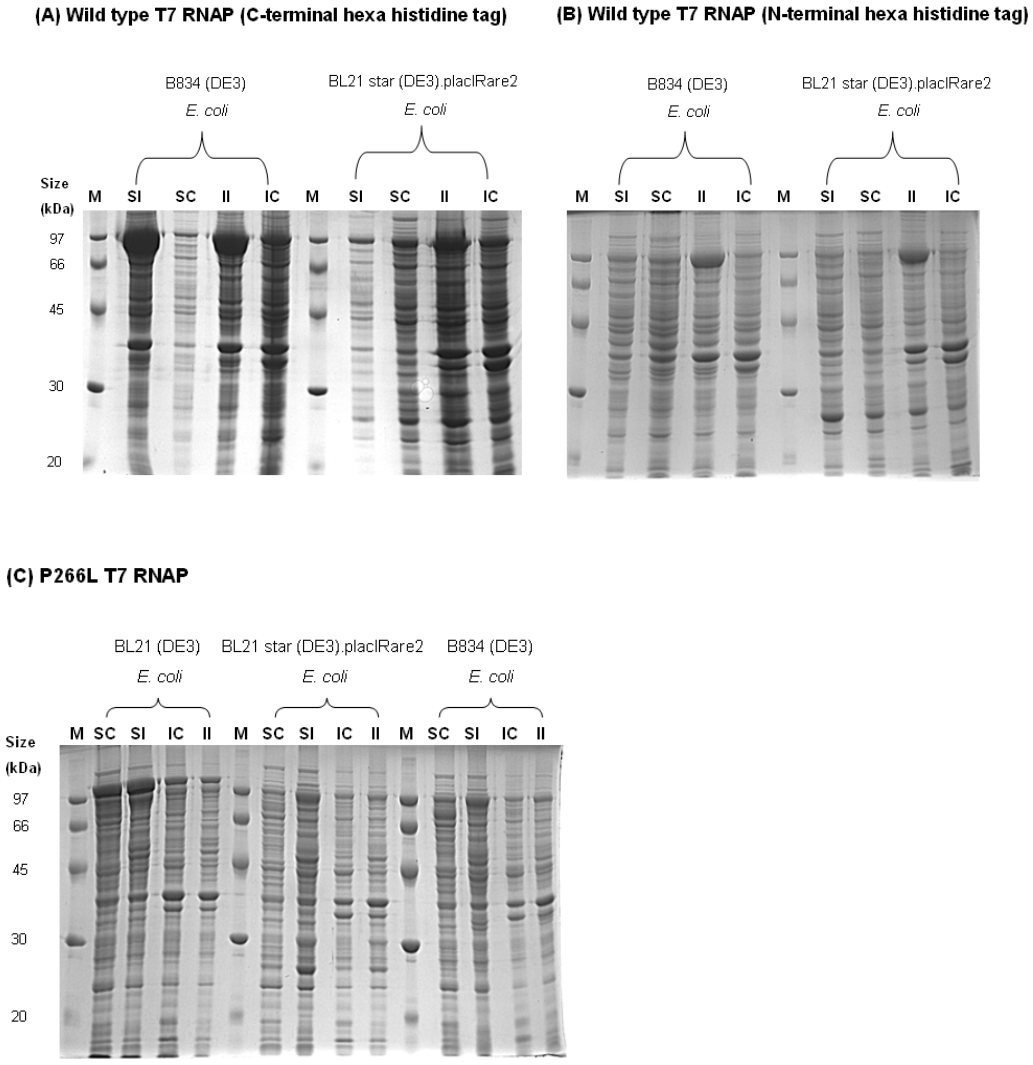

M - molecular weight standards,
SC - soluble proteins expressed by non-induced cells,
SI - soluble protein expressed by induced cells,
IC - insoluble protein expressed by non-induced cells,
II - insoluble proteins expressed by induced cells.

Figure 5.6: 12.5% SDS PAGE gels of crude extracts from three expression strains of *Escherichia coli* transformed with either wild-type (A and B) or P266L (C) T7 RNA polymerase and induced to express protein by IPTG-induction at 25°C for 4 h. The molecular weight of T7 RNAP is 98,855 Da.

In the case of wild-type T7 RNA polymerase, expression in the soluble fraction was only visible for protein tagged on the C-terminus. *E. coli* B834 (DE3) cells were found to give the best overall yield of protein for both wild-type and P266L RNA

polymerase and were thus deemed the most appropriate host for large-scale expression.

For large-scale expression, *E. coli* B834 (DE3) cells that had been transformed with a vector containing either the wild-type or P266L *RNAP* gene were cultured at 37^{o}C to an OD_{600nm} of 0.6 when protein expression was induced by the addition of 1 mM IPTG. Addition of IPTG was concurrent with the growth temperature being reduced to 25^{o}C for 4 h. Cells were harvested and a crude extract of soluble protein was obtained as described in Chapter 2, section 2.3.5. The crude extract was loaded onto a 5 mL cobalt column pre-equilibrated in 50 mM sodium phosphate pH 7.0, 500 mM NaCl, 10 mM imidazole and 5% glycerol for purification of soluble protein. Protein was eluted from the column using wash steps containing 10 mM, 20 mM, 50 mM and 200 mM imidazole. Overall purity of the protein was assessed using SDS PAGE (Figure 5.7).

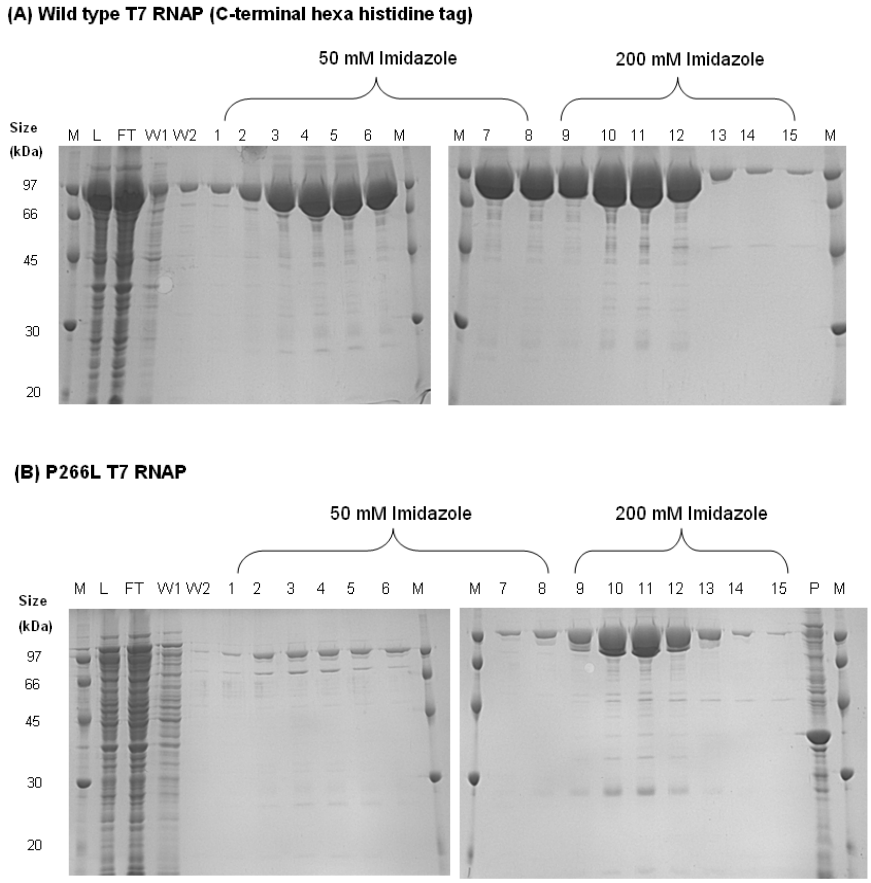

M - molecular weight standards,
L - protein sample prior to loading onto the column,
FT - flow through from the column during protein loading,
W1 - protein collected during wash of the column with equilibration buffer,
W2 - protein collected during wash with buffer containing 20 mM imidazole,
P - insoluble protein remaining in the cell pellet.

Figure 5.7: 12.5% SDS PAGE gels showing purification of hexa-histidine tagged wild-type (A) and P266L (B) T7 RNA polymerase from 1 L of *Escherichia coli* B834 (DE3) cells on BD TALON cobalt resin. Lanes 1 - 15 represent protein eluted from the column using equilibration buffer substituted with different concentrations of imidazole. The molecular weight of T7 RNAP is 98,855 Da.

In the case of both wild-type and P266L T7 RNAP, most of the polymerase eluted in the fractions collected when the column was washed with buffers containing 50 mM and 200 mM imidazole. These fractions were pooled and concentrated using vivaspin columns before dialysis against storage buffer containing 50 mM HEPES pH 7.0, 200 mM NaCl, 1 mM DTT and 50% glycerol (Chapter 2, sections 2.4.8 and

2.4.5). Each protein was at a final concentration of approximately 30 mg mL^{-1} prior to storage at -80^{o}C.

Both wild-type and P266L T7 RNAP were used to replace the RNA polymerase provided in the Ambion MEGAscript kit with the aim of producing large quantities of $tRNA^{Ala}$ and $tRNA^{Ser}$. After repeat of the run-off transcription reaction described above, the overall yield of RNA produced using these enzymes was assessed by denaturing 8M urea acrylamide gel electrophoresis (Figure 5.8).

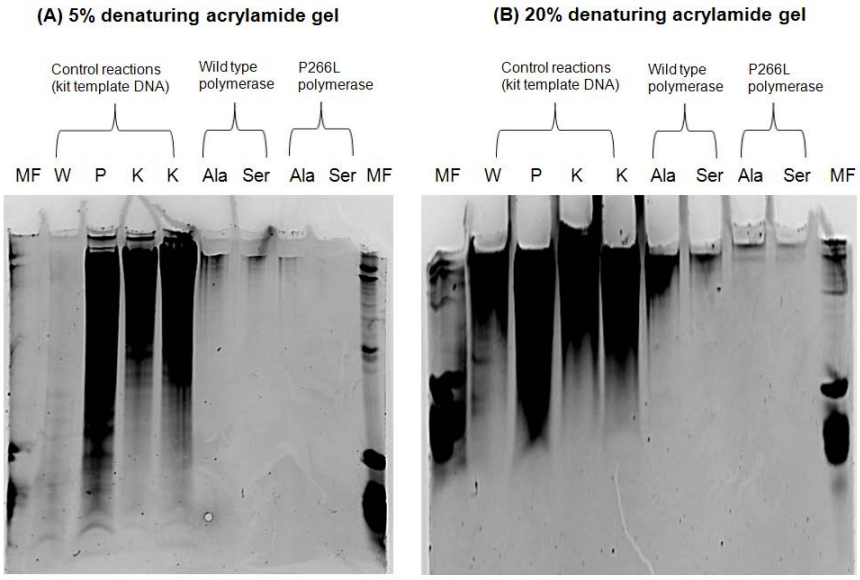

W - wild-type polymerase,
P - P266L polymerase,
K - polymerase provided with the Ambion MEGAscript kit,
MF - control pool of *Micrococcus flavus* tRNA made *in vivo*.

Figure 5.8: Assessment of the yield of $tRNA^{Ala}$ and $tRNA^{Ser}$ produced by *in vitro* transcription from *Bst*NI digested template vector using wild-type and P266L RNAP. Control reactions were carried out using the 1.89 kb template provided in the Ambion MEGAscript kit. Ala and Ser refer to reactions whereby *Bst*NI restricted pIDTSMART-Kan-$tRNA^{Ala}$ and pIDTSMART-Kan-$tRNA^{Ser}$ were used as templates respectively with the indicated polymerase. Half of the total *in vitro* transcription reaction was loaded in each case. Gels were stained with ethidium bromide.

When run on denaturing urea acrylamide gels, the *in vitro* transcription products formed using wild-type and P266L polymerase resulted in a combination of smearing and distinct bands. In addition to this, the generated RNA products were not recognised as substrates by the appropriate tRNA synthetase enzymes and could not be aminoacylated. This could have been due to abortive cycling of the enzymes resulting in transcripts that did not contain the correct CCA end or, alternatively, RNase degradation. *Bst*NI digestion of the template DNA could have resulted in insufficient quantities of the fragment of interest being precipitated after the digest. This would have resulted in insufficient amounts of template being added to the transcription reactions and would thus explain the low yield of tRNA produced. In order to address this, primers were designed to amplify the tRNA gene from the vectors with the aim of producing a high yield template for *in vitro* transcription.

5.4.3. Production of $tRNA^{Ala}$ and $tRNA^{Ser}$ by run-off *in vitro* transcription using PCR products of the tRNA genes as template

In order to amplify both tRNA genes by PCR, primers were designed to ensure that the amplified products would have a 5' T7 promoter region and a 3' CCA end which is important for the function of tRNA (see Chapter 2, Table 2.7 for primer sequences). Amplification of the tRNA genes was only obtained using Accuprime *Taq* polymerase and an annealing temperature of 55^{o}C (Figure 5.9).

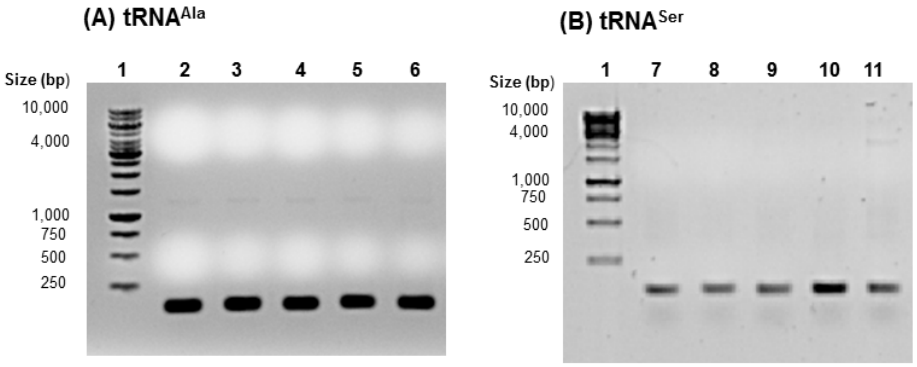

Figure 5.9: 2% agarose gel showing amplification of (A) tRNA^{Ala} from pIDTSMART-Kan-tRNA^{Ala} and (B) tRNA^{Ser} from pIDTSMART-Kan-tRNA^{Ser} using Accuprime *Taq* DNA polymerase. The tRNA^{Ala} and tRNA^{Ser} PCR products were 94 and 111 base pairs in length, respectively, including the T7 promoter region.

Lane 1 - Standard 1 kb ladder,
Lanes 2 – 6 - tRNA^{Ala} PCR product,
Lanes 7 – 11 - tRNA^{Ser} PCR product.

After amplification, the PCR products for each gene were pooled and purified using the Qiagen PCR clean-up kit. Purified DNA was quantified using the nanodrop with typical yields from five pooled PCR reactions estimated at between 150 and 200 ng. Typically, 2 μL of this template DNA was used per 20 μL *in vitro* transcription reaction with either the Ambion MEGAscript or the Fermentas T7 high yield kit.

Initial yields of tRNA obtained using PCR product as template were assessed on a 2% agarose gel (Figure 5.10). Prior to loading, the tRNA was diluted 1 in 20. Subsequently, 1 μL of this diluted RNA was added to an equal volume of loading dye (provided with the Fermentas kit) and heat denatured at 80^{o}C for 10 min. After purification of the RNA by phenol/chloroform extraction and ethanol precipitation, the pellet was resuspended in 4 mM $MgCl_2$. To ensure correct folding of the tRNA, the final product was heated to 80^{o}C for 10 min and then left to cool slowly to room

temperature. The purity of the final product was assessed by denaturing urea acrylamide electrophoresis (Figure 5.10).

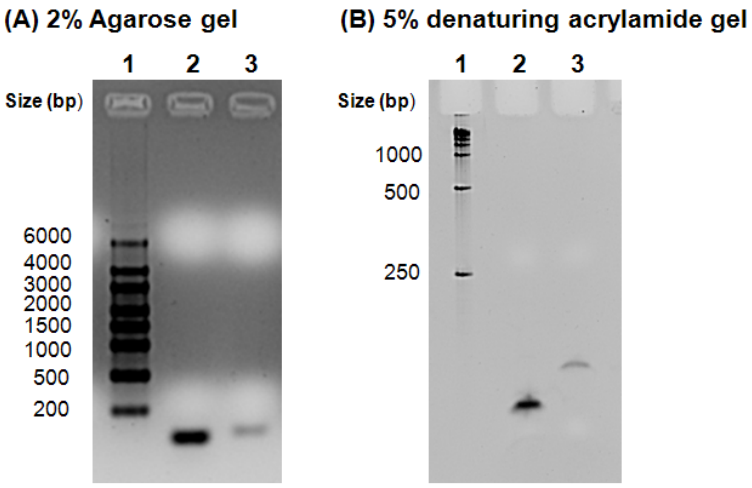

Figure 5.10: Assessment of the yield of tRNA^{Ala} and tRNA^{Ser} produced by *in vitro* transcription using PCR product as a template. (A) Samples were diluted 1 in 20 and run on a 2% agarose gel before purification. (B) After purification and re-folding, overall purity of the tRNA was assessed by running 2 µL of the final 50 µL volume on a 5% denaturing 8M urea acrylamide gel. The tRNA^{Ala} transcript was 72 bases in length and the tRNA^{Ser} transcript was 87 bases in length. Gels were stained with ethidium bromide.

Lane 1 - Fermentas High Range Riboruler RNA ladder,
Lane 2 - tRNA^{Ala},
Lane 3 - tRNA^{Ser}.

For both tRNA^{Ala} and tRNA^{Ser}, the product produced by *in vitro* transcription ran as a single band on both agarose and denaturing acrylamide gels. This suggested that only full-length tRNA was being produced as opposed to numerous different species of different lengths. To test the suitability of this RNA as a substrate for MurM, the ability of the appropriate tRNA synthetase enzyme to aminoacylate each species with the cognate amino acid was tested according to Lloyd *et al.* (2008).

Each small-scale charging experiment contained 20 µg of tRNA and 40 µg of the appropriate tRNA synthetase enzyme. The aminoacylation reaction was followed

over time by spotting 10 μL onto filter paper and then carrying out TCA precipitation of the RNA to remove un-incorporated radiolabel. The attachment of radiolabelled amino acid to tRNA was monitored by scintillation counting as described in Chapter 2, section 2.5.3 (Figure 5.11).

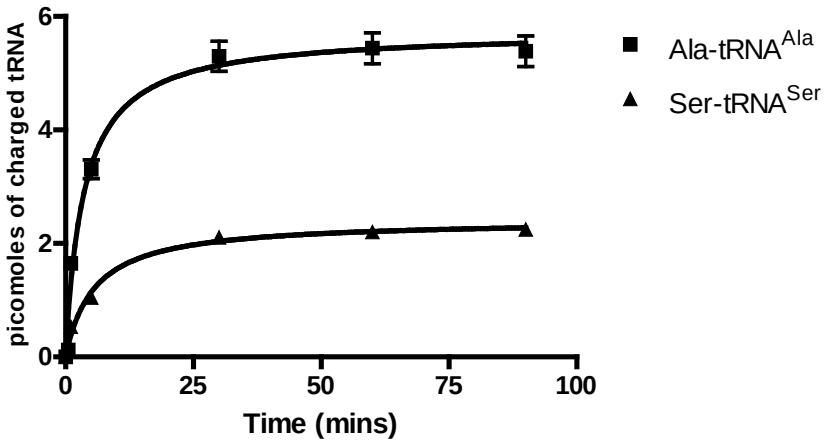

Figure 5.11: Charging of $tRNA^{Ala}$ and $tRNA^{Ser}$ with alanine and serine by pneumococcal AlaRS and SerRS respectively at 37°C. Control data values carried out in the absence of any tRNA have been subtracted from each dataset. The specific activity of the alanine label was calculated to be 220 counts per minute (cpm) per picomole. The specific activity of the serine label was calculated to be 379 cpm per picomole. Error bars represent variation in the duplicated raw data and, where not visible, are less than the size of the symbol that marks individual data points.

The data presented in Figure 5.11 indicated that the tRNA produced by *in vitro* transcription was readily utilised as a substrate by the appropriate tRNA synthetase enzyme. This clearly demonstrated that any secondary modifications made to the tRNA within an *in vivo* situation have no appreciable impact on the ability of the tRNA to act as substrate for either the synthetase enzymes or MurM.

For both $tRNA^{Ala}$ and $tRNA^{Ser}$, the aminoacylation reaction was complete after 40 min incubation at 37°C. Therefore, this length of incubation was used for large-scale aminoacylation to generate substrate for MurM. Incubation of this aminoacylated

tRNA with MurM and Lipid II resulted in the production of radiolabelled Lipid II indicating that the tRNA made by *in vitro* transcription was both recognised and utilised by MurM as substrate.

5.5. Kinetic characterisation of MurM using pure *in vitro* transcribed *Streptococcus pneumoniae* Ala-tRNA^{Ala} and Ser-tRNA^{Ser} as substrate

In order to determine the kinetic properties of each MurM enzyme, the concentration of Lipid II and aminoacylated tRNA were varied in separate experiments. Time courses were carried out at the highest and lowest concentration of the substrate whose concentration was being varied in the assay. This allowed for selection of a single time point in the linear region of MurM activity and also provided a means of determining appropriate concentrations of MurM to add to each assay. Typically, the linear region for MurM activity occurred within the first 2 min of the reaction as was also found to be the case by Lloyd *et al.* (2008).

Measurement of MurM activity within the first 10 min of the reaction was considered to be essential for avoidance of interference to the measurement of kinetic parameters caused by depletion of the aminoacylated tRNA substrate. This follows the finding made by Lloyd *et al.* (2008) indicating that the half-life of Ala-tRNA^{Ala} is 46 min upon incubation in the pH 6.8 MurM assay buffer used in this study. With this in mind, the overall activity of MurM was assessed by following the incorporation of radiolabelled [H^3]-alanine or [H^3]-serine onto Lipid II within the first 2 min of the reaction. Lipid II was separated away from other assay components using butanol extraction as described in Chapter 2, section 2.5.5.

When the concentration of $tRNA^{Ala}$ or $tRNA^{Ser}$ was varied between 0.1 and 1.8 μM, a typical 30 μL assay consisted of 50 mM MOPS pH 6.8, 30 mM KCl, 10 mM $MgCl_2$, 1.5% (w/v) CHAPS, 1 mM DTT, 1 mM L-alanine or L-serine, 10 μM Lipid II and MurM. When the concentration of Lipid II was varied between 5 and 200 μM, a typical 30 μL assay consisted of 50 mM MOPS pH 6.8, 30 mM KCl, 10 mM $MgCl_2$, 1.5% (w/v) CHAPS, 1 mM DTT, 1 mM L-alanine or L-serine, 5 μM [H^3]-Alanyl-$tRNA^{Ala}$ or [H^3]-Seryl-$tRNA^{Ser}$ (with a specific activity of between 50-100 cpm per picomole) and MurM. In each case, the reaction was always initiated by the addition of the radiolabelled tRNA substrate. Assays were stopped and processed as described by Lloyd *et al.* (2008).

5.5.1. Kinetic characterisation of *Streptococcus pneumoniae* strain R6 MurM

In the case of $MurM_{R6}$, 126 nM of enzyme was found to be sufficient to determine the linear region of activity when [H^3]-Ala-$tRNA^{Ala}$ was used as substrate. During time course experiments, the 1 min time sample was found to be within the linear region of activity when both [H^3]-Ala-$tRNA^{Ala}$ and Lipid II concentration were varied. For this reason, 1 min was chosen as the ideal time for incubation for collection of kinetic data in both cases (Figure 5.12, A and C).

When the same concentration of enzyme was used with [H^3]-Ser-$tRNA^{Ser}$, reactions proceeded very quickly and were over within the first 30 sec. Repetition of time courses at different concentrations of $MurM_{R6}$ indicated that 11 nM of protein was most suitable for visualisation of the linear region of activity. In this case, the 1 min time sample was within the linear region when both Lipid II and [H^3]-Ser-$tRNA^{Ser}$ concentrations were varied (Figure 5.12, B and D). Hence, this time point was used

for the collection of kinetic data. All data collected were in counts per minute (cpm) and, for the purpose of the Hanes-Woolf plot, this was converted to μM of radiolabelled Lipid II formed per min using the specific activity of the label. An example of the calculations used for determination of the key kinetic parameters of MurM from the Hanes-Woolf plot is shown in Table 5.1, page 228. Time course data for $MurM_{R6}$ are presented in Figure 5.12.

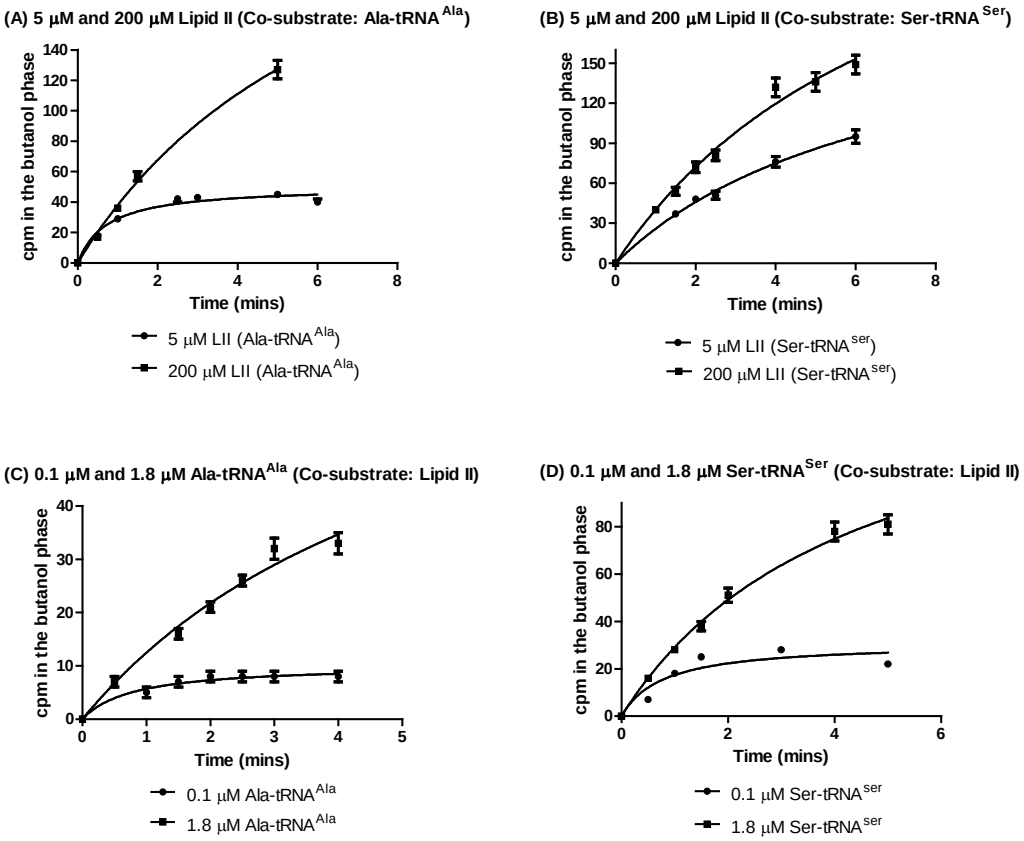

Figure 5.12: Time course data obtained for $MurM_{R6}$ with (A) 126 nM of enzyme in the presence of 5 μM and 200 μM Lipid II (LII) with $[H^3]$-Ala-$tRNA^{Ala}$ as a co-substrate; (B) 11 nM of enzyme in the presence of 5 μM and 200 μM LII with $[H^3]$-Ser-$tRNA^{Ser}$ as a co-substrate; (C) 126 nM of enzyme in the presence of 0.1 μM and 1.8 μM $[H^3]$-Ala-$tRNA^{Ala}$ with LII as a co-substrate; (D) 11 nM of enzyme in the presence of 0.1 μM and 1.8 μM $[H^3]$-Ser-$tRNA^{Ser}$ with LII as a co-substrate. Control data, obtained by omission of LII from the reaction, have been subtracted from the raw counts to give cpm in the butanol phase presented on the y-axis. Note that cpm is a direct measure of the formation of radiolabelled LII. Error bars represent variation in the duplicated raw data and, where not visible, are less than the size of the symbol that marks individual data points.

Given the nature of the assays, the Hanes-Woolf plot was considered to be the best way to represent the data. The Hanes-Woolf plot represents the data graphically with the ratio of initial substrate concentration, [S], to reaction velocity, (V), being plotted against initial substrate concentration, [S]. This relationship produces a straight line plot where the gradient is equal to $1/V_{max}$, the y intercept equals K_m/V_{max} and the x intercept is equivalent to $-K_m$.

In the Lineweaver-Burk plot (1/V against 1/[S]); data points are not distributed homogeneously across the linear transformation resulting in a gross misrepresentation of the error in the values. In addition to this, the presence of the error containing variable (V) on both axes of the Eadie-Hofstee plot (V against V/[S]) causes angular distortion of the error in the data set. Therefore, in contrast to other kinetic plots, the Hanes-Woolf plot does not over-emphasise data that are acquired at a low substrate concentration (Sangeetha *et al.*, 2008). The kinetic data collected for $MurM_{R6}$ are presented graphically using the Hanes-Woolf plot in Figure 5.13.

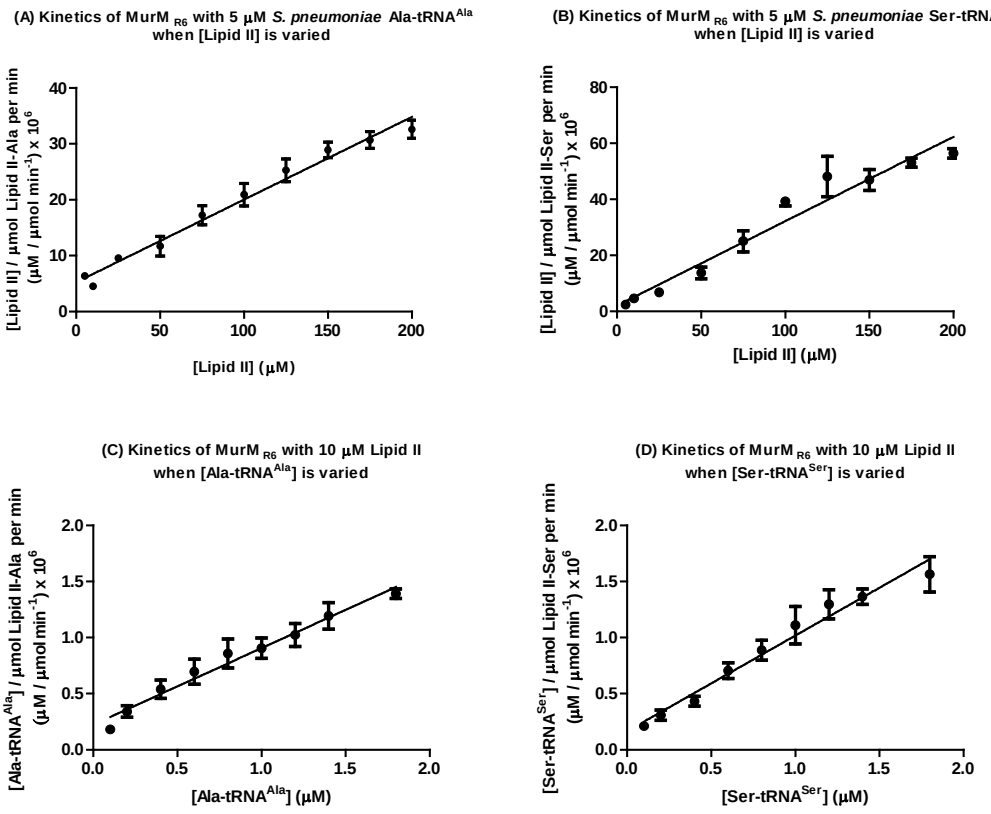

Figure 5.13: Hanes-Woolf plots of kinetic data obtained for $MurM_{R6}$ when (A) the concentration of LII was varied in the presence of 5 µM [H^3]-Ala-$tRNA^{Ala}$, (B) the concentration of LII was varied in the presence of 5 µM [H^3]-Ser-$tRNA^{Ser}$, (C) the concentration of [H^3]-Ala-$tRNA^{Ala}$ was varied in the presence of 10 µM LII, (D) the concentration of [H^3]-Ser-$tRNA^{Ser}$ was varied in the presence of 10 µM LII. The r^2 values for these data are 0.98, 0.96, 0.98 and 0.97 respectively. Error bars represent variation in the duplicated raw data and, where not visible, are less than the size of the symbol that marks individual data points.

From the Hanes-Woolf plots shown in Figure 5.13, it was possible to use GraphPad Prism 5 to determine the x-intercept and 1/slope for each of the four conditions described. This enabled calculation of the key kinetic parameters for $MurM_{R6}$ which are presented in Table 5.1 alongside an example calculation.

Substrate	Apparent K_m (μM)	Apparent V_{max} (moles sec^{-1} mg^{-1})	Apparent k_{cat} (min^{-1})	k_{cat}/K_m (min^{-1}. μM^{-1})	r^2 value
Lipid II (Ala-$tRNA^{Ala}$)	35.49 ± 1.70	6.26×10^{-10} ± 0.30	1.78 ± 0.09	0.05	0.98
Lipid II (Ser-$tRNA^{Ser}$)	6.77 ± 0.51	3.69×10^{-9} ± 0.28	10.50 ± 0.79	1.55	0.96
Ala-$tRNA^{Ala}$	0.33 ± 0.02	1.36×10^{-10} ± 0.08	0.39 ± 0.02	1.18	0.98
Ser-$tRNA^{Ser}$	0.19 ± 0.01	1.30×10^{-9} ± 0.08	3.71 ± 0.22	19.53	0.97

Example calculation of kinetic parameters when [Lipid II] was varied in the presence of Ala-$tRNA^{Ala}$ for $MurM_{R6}$:

The stock of $MurM_{R6}$ was at 0.45 mg ml^{-1}. This was diluted 2 in 3 and then 1 in 5 prior to use in assays.
The molecular weight of $MurM_{R6}$ is 47441.20 Da.
3 μl was used in each reaction = 0.00018 mg of protein

The X intercept ($-K_m$) = -35.49, therefore K_m = 35.49 μM
Gradient = 1 / V_{max}, so V_{max} = 1/slope = 0.000006764
V_{max} = 0.000006764 μM min^{-1} 0.00018 mg $MurM^{-1}$
V_{max} = 0.037578 μM min^{-1} mg^{-1}
$V_{max} = 0.037578 \times 10^{-6}$ M min^{-1} mg^{-1}
$V_{max} = 6.26296 \times 10^{-10}$ M sec^{-1} mg^{-1}
$V_{max} = 3.77 \times 10^{14}$ molecules sec^{-1} mg^{-1}
How many molecules does 1 mg of $MurM_{R6}$ contain?
$(1 \times 10^{-3}$ g/47441.2) x $(6.02 \times 10^{23}) = 1.27 \times 10^{16}$ molecules
Therefore turnover number = $(3.77 \times 10^{14})/ (1.27 \times 10^{16})$
= 0.03 sec^{-1} = 1.78 min^{-1}

Table 5.1: Summary of key kinetics parameters for $MurM_{R6}$ as calculated from the Hanes-Woolf plots shown in Figure 5.13. The column entitled substrate refers to the substrate whose concentration was being varied in the assay. The enzyme used in each assay had no histidine tag and the tRNA was a single species in each case.

In the case of $MurM_{R6}$, the apparent K_m for Lipid II was 5-fold lower in the presence of Ser-$tRNA^{Ser}$ in comparison to Ala-$tRNA^{Ala}$. This was also partly reflected in the lower apparent K_m for Ser-$tRNA^{Ser}$ when compared to Ala-$tRNA^{Ala}$ at a constant concentration of Lipid II. As was the shown to be the case for $MurM_{Pn16}$ in the work undertaken by Lloyd *et al.* (2008), $MurM_{R6}$ appeared to have an overall preference for the addition of serine over alanine to Lipid II.

In order to determine the differences between the catalytic efficiencies of $MurM_{R6}$ when provided with Ser-$tRNA^{Ser}$ compared to Ala-$tRNA^{Ala}$, an additional constant referred to as apparent k_{cat}/K_m was calculated. This constant is able to provide a measure of the catalytic efficiency of an enzyme as it functions at substrate concentrations that are below saturating. This is because apparent K_m is inversely proportional to the affinity of an enzyme for its substrate and apparent k_{cat} is directly proportional to the turnover efficiency of the enzyme. Using this constant and the data shown in Table 5.1, the catalytic efficiency of $MurM_{R6}$ with Lipid II was found to be 31-fold greater when Ser-$tRNA^{Ser}$ as opposed to Ala-$tRNA^{Ala}$ was provided as the co-substrate. In the presence of a constant concentration of Lipid II, the catalytic efficiency of $MurM_{R6}$ was found to be 17-fold greater when Ser-$tRNA^{Ser}$ was provided as the substrate.

5.5.2. Kinetic characterisation of *Streptococcus pneumoniae* strain Pn16 MurM

In the case of $MurM_{Pn16}$, 91 nM of enzyme was found to be sufficient to determine the linear region of activity when [H^3]-Ala-$tRNA^{Ala}$ was used as substrate. During time course experiments, the 1 min time sample was found to be within the linear region of activity when both [H^3]-Ala-$tRNA^{Ala}$ and Lipid II concentration were

varied. Therefore, this time point was used for collection of kinetic data in both cases (Figure 5.14, A and C).

However, when [H^3]-Ser-$tRNA^{Ser}$ was used as substrate the reaction proceeded too quickly and the linear region could not be detected when 91 nM of enzyme was used in the assay. As a result of this, the enzyme was diluted further and time courses were repeated. The most appropriate amount of enzyme to use in the presence of [H^3]-Ser-$tRNA^{Ser}$ was found to be 18 nM (Figure 5.14, B and D). Determination of the linear region in this case resulted in the 1 min time sample being suitable. Time course data acquired for $MurM_{Pn16}$ at the chosen enzyme concentrations are shown in Figure 5.14.

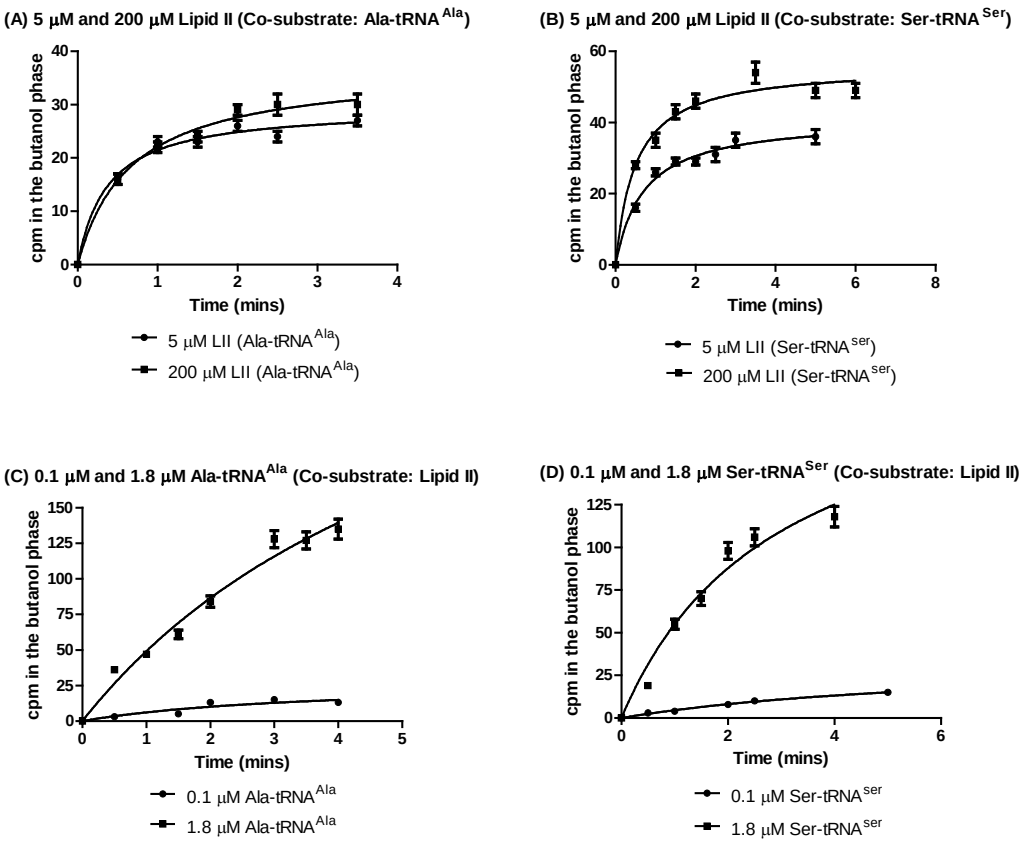

Figure 5.14: Time course data obtained for $MurM_{Pn16}$ with (A) 91 nM of enzyme in the presence of 5 μM and 200 μM Lipid II (LII) with [H^3]-Ala-$tRNA^{Ala}$ as a co-substrate; (B) 18 nM of enzyme in the presence of 5 μM and 200 μM LII with [H^3]-Ser-$tRNA^{Ser}$ as a co-substrate; (C) 91 nM of enzyme in the presence of 0.1 μM and 1.8 μM [H^3]-Ala-$tRNA^{Ala}$ with LII as a co-substrate; (D) 18 nM of enzyme in the presence of 0.1 μM and 1.8 μM [H^3]-Ser-$tRNA^{Ser}$ with LII as a co-substrate. Control data, obtained by omission of LII from the reaction, have been subtracted from the raw counts to give cpm in the butanol phase presented on the y-axis. Note that cpm is a direct measure of the formation of radiolabelled LII. Error bars represent variation in the duplicated raw data and, where not visible, are less than the size of the symbol that marks individual data points.

Using the 1 min time point in each case, a series of kinetic data comparable to that obtained for $MurM_{R6}$ were collected for $MurM_{Pn16}$. Hanes-Woolf plots obtained for $MurM_{Pn16}$ are shown in Figure 5.15.

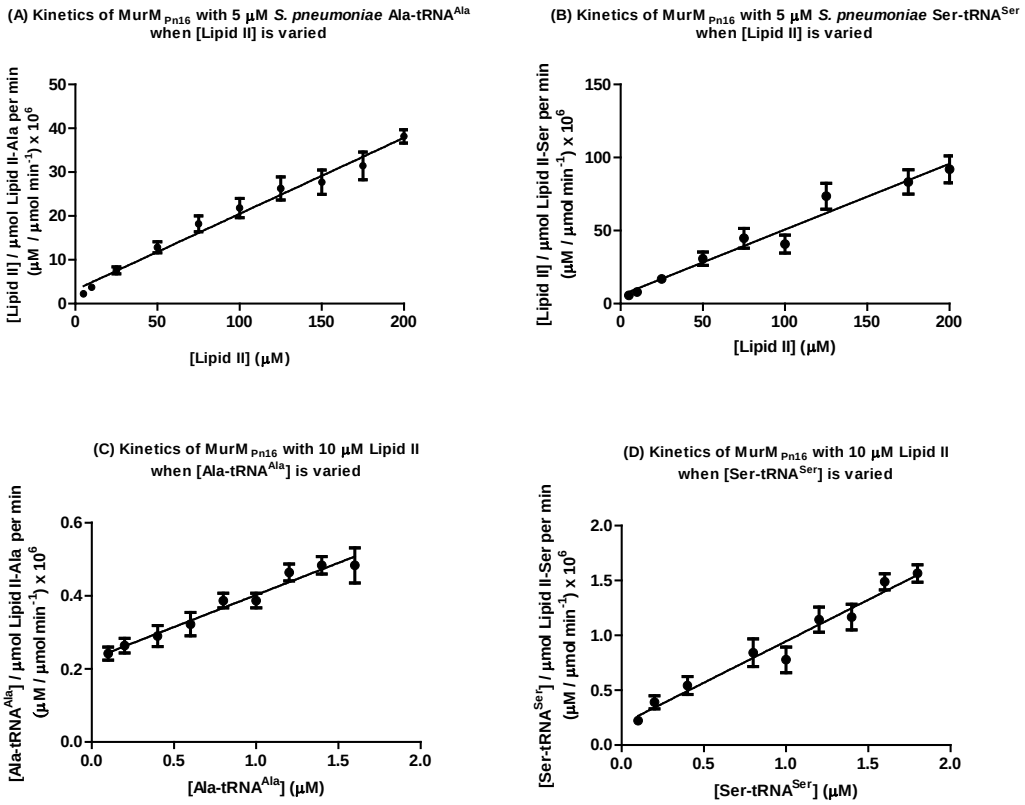

Figure 5.15: Hanes-Woolf plots of kinetic data obtained for $MurM_{Pn16}$ when (A) the concentration of LII was varied in the presence of 5 µM [H^3]-Ala-$tRNA^{Ala}$, (B) the concentration of LII was varied in the presence of 5 µM [H^3]-Ser-$tRNA^{Ser}$, (C) the concentration of [H^3]-Ala-$tRNA^{Ala}$ was varied in the presence of 10 µM LII, (D) the concentration of [H^3]-Ser-$tRNA^{Ser}$ was varied in the presence of 10 µM LII. The r^2 values for these data are 0.99, 0.97, 0.97 and 0.96 respectively. Error bars represent variation in the duplicated raw data and, where not visible, are less than the size of the symbol that marks individual data points.

From the Hanes-Woolf plots shown in Figure 5.15, it was possible to use GraphPad Prism 5 to determine the x-intercept and 1/slope for each of the four conditions described. This enabled calculation of the key kinetic parameters for $MurM_{Pn16}$ which are presented in Table 5.2.

Substrate	Apparent K_m (μM)	Apparent V_{max} (moles sec^{-1} mg^{-1})	Apparent k_{cat} (min^{-1})	k_{cat}/K_m (min^{-1}. μM^{-1})	r^2 value
Lipid II (Ala-$tRNA^{Ala}$)	17.98 ± 0.79	7.39×10^{-10} ± 0.33	2.10 ± 0.09	0.12	0.99
Lipid II (Ser-$tRNA^{Ser}$)	12.82 ± 0.92	1.43×10^{-9} ± 0.10	4.06 ± 0.29	0.32	0.97
Ala-$tRNA^{Ala}$	1.29 ± 0.09	7.30×10^{-10} ± 0.49	2.08 ± 0.14	1.61	0.97
Ser-$tRNA^{Ser}$	0.25 ± 0.02	8.47×10^{-10} ± 0.57	2.41 ± 0.16	9.64	0.96

Table 5.2: Summary of key kinetics parameters for $MurM_{Pn16}$ as calculated from the Hanes-Woolf plots shown in Figure 5.15. The column entitled substrate refers to the substrate whose concentration was being varied in the assay. The enzyme used in each assay had no histidine tag and the tRNA was a single species in each case.

In the case of $MurM_{Pn16}$, the apparent K_m of the enzyme for Lipid II was 1.4-fold lower in the presence of Ser-$tRNA^{Ser}$ as opposed to Ala-$tRNA^{Ala}$ indicating a possible preference for this co-substrate. In addition to this, a 5-fold lower value in apparent K_m for Ser-$tRNA^{Ser}$ was determined in comparison to Ala-$tRNA^{Ala}$ when the concentration of Lipid II was kept constant.

The catalytic efficiency of $MurM_{Pn16}$ with Lipid II was found to be 3-fold greater when Ser-$tRNA^{Ser}$ was the co-substrate. This was exacerbated further at constant Lipid II concentration, when the catalytic efficiency of the enzyme was found to be 6-fold greater when Ser-$tRNA^{Ser}$ was provided as the tRNA substrate. Therefore, $MurM_{Pn16}$ was found to have a preference for Ser-$tRNA^{Ser}$ over Ala-$tRNA^{Ala}$ in this

study. This preference has also been confirmed in the work carried out by Lloyd *et al.* (2008). However, the serine specificity of $MurM_{Pn16}$ was found to be much less pronounced when compared to that of $MurM_{R6}$.

5.5.3. Kinetic characterisation of *Streptococcus pneumoniae* strain 159 MurM

In the case of $MurM_{159}$, 13 nM of enzyme was found to be sufficient to determine the linear region of activity when [H^3]-Ala-$tRNA^{Ala}$ was used as substrate. During time course experiments, the 1 min time sample was within the linear region of activity when both [H^3]-Ala-$tRNA^{Ala}$ and Lipid II concentration were varied and hence was used for collection of kinetic data in both cases (Figure 5.16, A and C).

When [H^3]-Ser-$tRNA^{Ser}$ was used as a substrate, 6 nM of $MurM_{159}$ was found to be suitable for determining the linear region of activity at both the highest and lowest concentrations of tRNA and Lipid II. Time course data with $MurM_{159}$ at this concentration showed that the 1 min sample was within the linear region in each case and this was therefore a suitable time point for the collection of kinetic data (Figure 5.16, B and D).

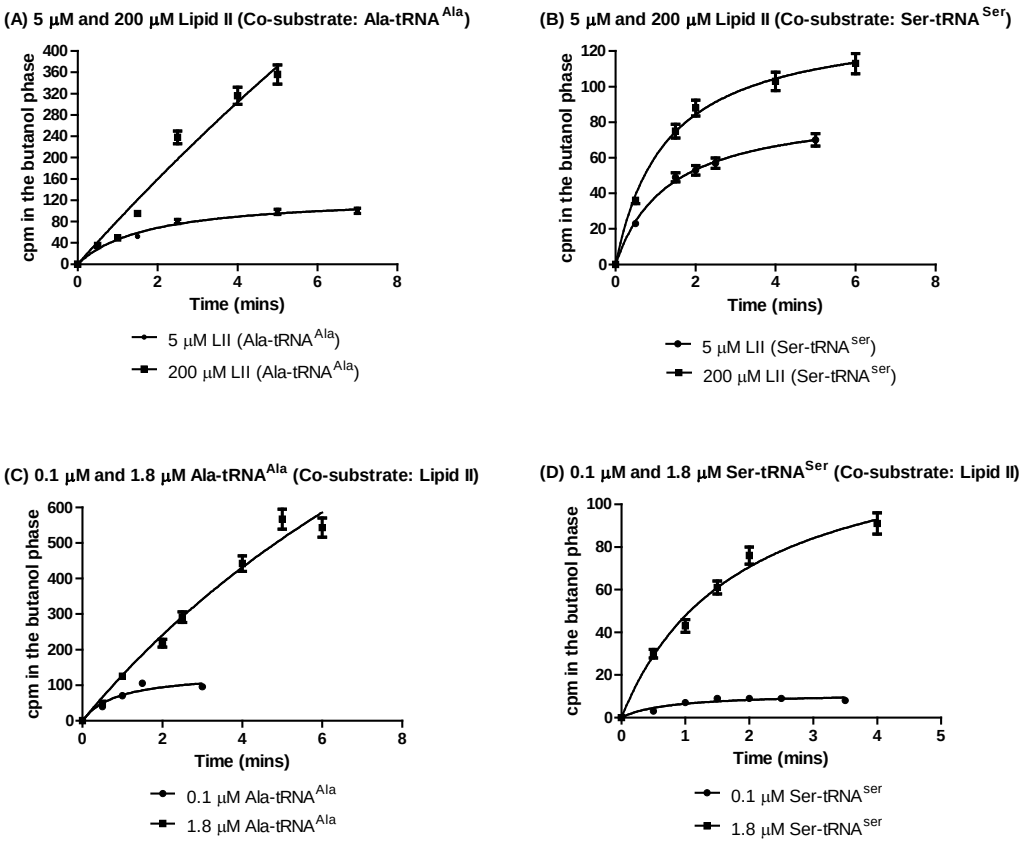

Figure 5.16: Time course data obtained for $MurM_{159}$ with (A) 13 nM of enzyme in the presence of 5 μM and 200 μM Lipid II (LII) with $[H^3]$-Ala-$tRNA^{Ala}$ as a co-substrate; (B) 6 nM of enzyme in the presence of 5 μM and 200 μM LII with $[H^3]$-Ser-$tRNA^{Ser}$ as a co-substrate; (C) 13 nM of enzyme in the presence of 0.1 μM and 1.8 μM $[H^3]$-Ala-$tRNA^{Ala}$ with LII as a co-substrate; (D) 6 nM of enzyme in the presence of 0.1 μM and 1.8 μM $[H^3]$-Ser-$tRNA^{Ser}$ with LII as a co-substrate. Control data, obtained by omission of LII from the reaction, have been subtracted from the raw counts to give cpm in the butanol phase presented on the y-axis. Note that cpm is a direct measure of the formation of radiolabelled LII. Error bars represent variation in the duplicated raw data and, where not visible, are less than the size of the symbol that marks individual data points.

A series of kinetic data equivalent to that obtained for both $MurM_{R6}$ and $MurM_{Pn16}$ were collected for $MurM_{159}$ using the 1 min time sample as a representative of the linear region of activity. The kinetic data collected for $MurM_{159}$ are presented graphically in Figure 5.17.

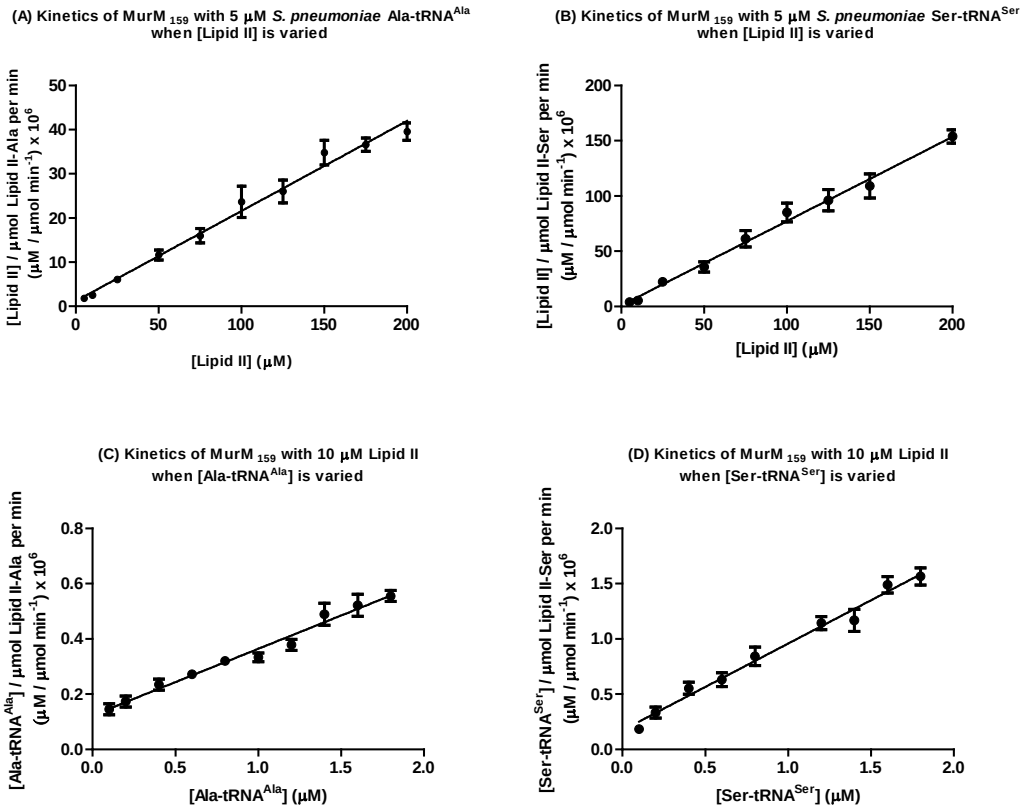

Figure 5.17: Hanes-Woolf plots of kinetic data obtained for $MurM_{159}$ when (A) the concentration of LII was varied in the presence of 5 µM [H^3]-Ala-$tRNA^{Ala}$, (B) the concentration of LII was varied in the presence of 5 µM [H^3]-Ser-$tRNA^{Ser}$, (C) the concentration of [H^3]-Ala-$tRNA^{Ala}$ was varied in the presence of 10 µM LII, (D) the concentration of [H^3]-Ser-$tRNA^{Ser}$ was varied in the presence of 10 µM LII. The r^2 values for these data are 0.99, 0.99, 0.98 and 0.99 respectively. Error bars represent variation in the duplicated raw data and, where not visible, are less than the size of the symbol that marks individual data points.

From the Hanes-Woolf plots shown in Figure 5.17, it was possible to use GraphPad Prism 5 to determine the x-intercept and 1/slope for each of the four conditions described. This enabled calculation of the key kinetic parameters for $MurM_{159}$ which are presented in Table 5.3.

Substrate	Apparent K_m (μM)	Apparent V_{max} (moles sec^{-1} mg^{-1})	Apparent k_{cat} (min^{-1})	k_{cat}/K_m (min^{-1}. μM^{-1})	r^2 value
Lipid II (Ala-$tRNA^{Ala}$)	5.96 ± 0.23	4.54×10^{-9} ± 0.17	13.00 ± 0.49	2.18	0.99
Lipid II (Ser-$tRNA^{Ser}$)	1.11 ± 0.03	2.43×10^{-9} ± 0.07	6.92 ± 0.21	6.23	0.99
Ala-$tRNA^{Ala}$	0.51 ± 0.02	3.84×10^{-9} ± 0.18	11.00 ± 0.53	21.57	0.98
Ser-$tRNA^{Ser}$	0.22 ± 0.01	2.36×10^{-9} ± 0.11	6.73 ± 0.30	30.59	0.99

Table 5.3: Summary of key kinetics parameters for $MurM_{159}$ as calculated from the Hanes-Woolf plots shown in Figure 5.17. The column entitled substrate refers to the substrate whose concentration was being varied in the assay. The enzyme used in each assay had no histidine tag and the tRNA was a single species in each case.

In the case of $MurM_{159}$, the apparent K_m of the enzyme for Lipid II was 5-fold lower, thus potentially indicating tighter binding, when Ser-$tRNA^{Ser}$ was provided as the co-substrate. Despite this, the apparent turnover of Lipid II was 2-fold higher when Ala-$tRNA^{Ala}$ was provided as the co-substrate. This was also found to be the case when the concentration of Lipid II was kept constant in the presence of Ser-$tRNA^{Ser}$ and Ala-$tRNA^{Ala}$. Overall, the catalytic efficiency of $MurM_{159}$ with Lipid II was found to be 3-fold greater when Ser-$tRNA^{Ser}$ was the co-substrate and this effect was attributable to a reduction in apparent K_m. In addition to this, the catalytic efficiency of the enzyme was 2-fold higher when Ser-$tRNA^{Ser}$ was the substrate at a constant concentration of Lipid II.

Whilst the turnover number of $MurM_{159}$ was greater in the presence of Ala-$tRNA^{Ala}$, matching previous observations made by Lloyd *et al.* (2008), for the first time data in this study have indicated that, regardless of the allelic variant, MurM is more catalytically efficient when provided with Ser-$tRNA^{Ser}$ as the co-substrate. In the case of the three variants of MurM used in this study, this effect has been shown to be independent of the penicillin sensitivity of the strain of *S. pneumoniae* from which the enzyme was derived.

5.5.4. Partial kinetic characterisation of *Streptococcus pneumoniae* strain 159 MurM E229A:E307A in comparison to the wild-type enzyme

As part of the metal binding work carried out in Chapter 4, a double mutant of $MurM_{159}$ was made converting two functionally conserved glutamate residues, at positions 229 and 307, to alanine. Characterisation of this mutant protein by ITC indicated that its ability to bind magnesium was significantly reduced compared to the wild-type enzyme. Therefore, it was considered essential to determine the effect of the absence of bound magnesium on the catalytic mechanism of this mutant form of $MurM_{159}$ in comparison to the wild-type enzyme. This was achieved by determination of the key kinetic parameters for the enzyme when the concentration of Lipid II was varied in the presence of the co-substrate [H^3]-Ala-$tRNA^{Ala}$.

Under these conditions, 11 nM of the mutant form of $MurM_{159}$ was found to be sufficient to determine the linear region of activity for the enzyme. During time course experiments, the 30 sec time sample was found to be within the linear region of activity as shown in Figure 5.18 (A). Therefore, this time point was used for the

collection of a complete set of kinetic data for this enzyme which have been presented as a Hanes-Woolf plot in Figure 5.18 (B).

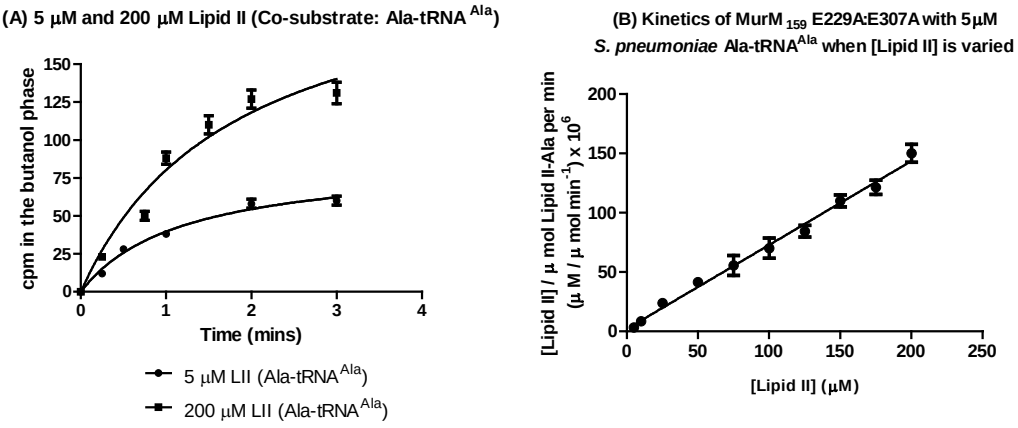

Figure 5.18: (A) Time course data collected for 11 nM of $MurM_{159}$ E229A: E307A in the presence of 5 µM and 200 µM LII with [H^3]-Ala-$tRNA^{Ala}$ as the co-substrate. Control data, obtained by omission of Lipid II from the reaction, have been subtracted from the raw counts to give cpm in the butanol phase presented on the y-axis. Note that cpm is a direct measure of the formation of radiolabelled LII. Error bars represent variation in the duplicated raw data and, where not visible, are less than the size of the symbol that marks individual data points. (B) Hanes-Woolf plot showing kinetic data obtained for 11 nM $MurM_{159}$ E229A:E307A when the concentration of LII was varied in the presence of 5 µM [H^3]-Ala-$tRNA^{Ala}$. The r^2 value obtained for these data was 0.99.

For the purpose of comparison to the data obtained for wild-type $MurM_{159}$, the key kinetic parameters obtained for this enzyme and $MurM_{159}$ E229A:E307A are summarised below in Table 5.4. The kinetic parameters for $MurM_{159}$ E229A: E307A were only assessed by varying the concentration of Lipid II in the presence of [H^3]-Ala-$tRNA^{Ala}$.

Form of $MurM_{159}$	Apparent K_m (μM)	Apparent V_{max} (moles sec^{-1} mg^{-1})	Apparent k_{cat} (min^{-1})	k_{cat}/K_m (min^{-1}. μM^{-1})	r^2 value
Wild-type	5.96 ± 0.23	4.54×10^{-9} ± 0.17	13.00 ± 0.49	2.18	0.99
E229A: E307A	2.93 ± 0.08	2.00×10^{-9} ± 0.06	5.70 ± 0.17	1.95	0.99

Table 5.4: Comparison of the key kinetics parameters obtained for wild-type $MurM_{159}$ and $MurM_{159}$ E229A:E307A as calculated from the Hanes-Woolf plots shown in Figures 5.17 (A) and 5.18 (B), respectively. The enzyme used in each assay had no histidine tag and the concentration of Lipid II was varied between 5 μM and 200 μM in the presence of [H^3]-Ala-$tRNA^{Ala}$.

Kinetic analysis of $MurM_{159}$ E229A:E307A indicated that, whilst the enzyme appeared to have a 2-fold lower apparent K_m for Lipid II than the wild-type enzyme when utilising Ala-$tRNA^{Ala}$ as a co-substrate, the overall catalytic efficiencies of both mutant and wild-type $MurM_{159}$ were very similar. This was caused by a 2-fold decrease in the apparent turnover number of the mutant enzyme which compensated for the overall reduction in apparent K_m. This supports the data generated in Chapter 4, which suggests that magnesium is not required for the catalytic activity of MurM.

Thus, the hypothesis stated in Chapter 4 that magnesium may be responsible for co-ordination of MurM with phospholipid head groups in the membrane was tested. This required assessment of the effects of cardiolipin, one of the major phospholipids within the pneumococcal cell membrane, on the apparent kinetic parameters obtained for all three variants of MurM in addition to $MurM_{159}$ E229A:E307A

(Trombe *et al.*, 1979). The results of these experiments are described in section 5.5.5 below.

5.5.5. Assessment of the effect of cardiolipin on the kinetic activities of $MurM_{R6}$, $MurM_{Pn16}$, $MurM_{159}$ and $MurM_{159}$ E229A:E307A

According to Trombe *et al.* (1979), the membrane of *S. pneumoniae* is comprised of two glycolipids (monoglucosyldiacylglycerol and galactosylglucosyldiacylglycerol), two acidic phospholipids (phosphatidylglycerol and cardiolipin) and one neutral lipid (diacylglycerol). Given that MurM has a lipid substrate, it is hypothesised to interact with the membrane during catalysis. Therefore, prior to this study, Dr Adrian Lloyd (University of Warwick) assessed the impact of both cardiolipin and phosphatidylglycerol on histidine-tagged versions of $MurM_{Pn16}$ and $MurM_{159}$. In the presence of cardiolipin, the catalytic efficiencies of $MurM_{159}$ and $MurM_{Pn16}$ with respect to Lipid II were found to be increased by 2-fold and 10-fold, respectively. In contrast to this, response to phosphatidylglycerol was found to be strain dependent causing an inhibitory and a mild stimulatory effect on $MurM_{159}$ and $MurM_{Pn16}$, respectively (unpublished data).

Given that the stimulatory effect of cardiolipin was conserved across both variants of MurM, the ability of $MurM_{159}$ E229A:E307A to respond to this phospholipid was tested alongside untagged forms of $MurM_{159}$, $MurM_{Pn16}$ and $MurM_{R6}$. Kinetic parameters were determined for each enzyme when the concentration of Lipid II was varied between 5 µM and 200 µM in the presence of $[H^3]$-Ala-$tRNA^{Ala}$ and a final concentration of 2 mg mL^{-1} cardiolipin (dispensed in methanol and dried down under nitrogen prior to resuspension in the other assay components listed in Chapter 2,

section 2.5.5). This experiment was ultimately designed to test the hypothesis that magnesium is required by MurM for coordination with phospholipid head groups in the membrane.

As described in sections 5.5.1 to 5.5.4, time course experiments were carried out in each case to allow determination of an appropriate enzyme concentration and for assessment of a suitable time point within the linear region of activity to use for further kinetic analysis. In each case the 30 sec time point was found to fall within the linear region when enzyme concentrations of 16 nM ($MurM_{R6}$), 12 nM ($MurM_{Pn16}$), 6 nM ($MurM_{159}$) and 11 nM ($MurM_{159}$ E229A:E307A) were used (Figure 5.19).

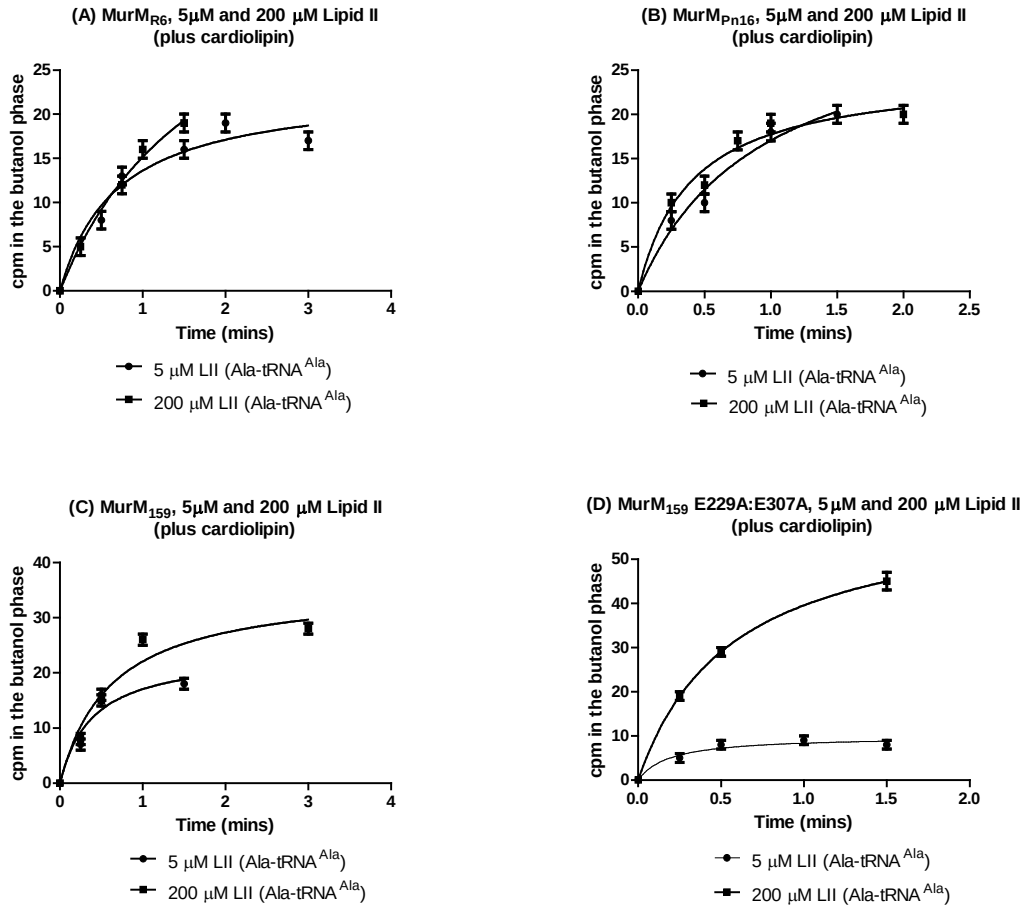

Figure 5.19: Time course data obtained with 5 μM and 200 μM LII in the presence of 5 μM [H^3]-Ala-tRNA^{Ala} and a final concentration of 2 mg mL^{-1} cardiolipin for (A) 16 nM MurM$_{R6}$, (B) 12 nM MurM$_{Pn16}$, (C) 6 nM MurM$_{159}$ and, (D) 11 nM MurM$_{159}$ E229A:E307A. Control data, obtained by omission of LII from the reaction, has been subtracted from the raw counts to give cpm in the butanol phase presented on the y-axis. Note that cpm is a direct measure of the formation of radiolabelled LII. Error bars represent variation in the duplicated raw data and, where not visible, are less than the size of the symbol that marks individual data points.

A series of kinetic data, whereby the concentration of Lipid II was varied in the presence of constant concentrations of both [H^3]-Ala-tRNA^{Ala} and cardiolipin, were collected for each form of MurM using the 30 sec time sample as a representative of the linear region of activity. These data sets are presented in the form of Hanes-Woolf plots in Figure 5.20.

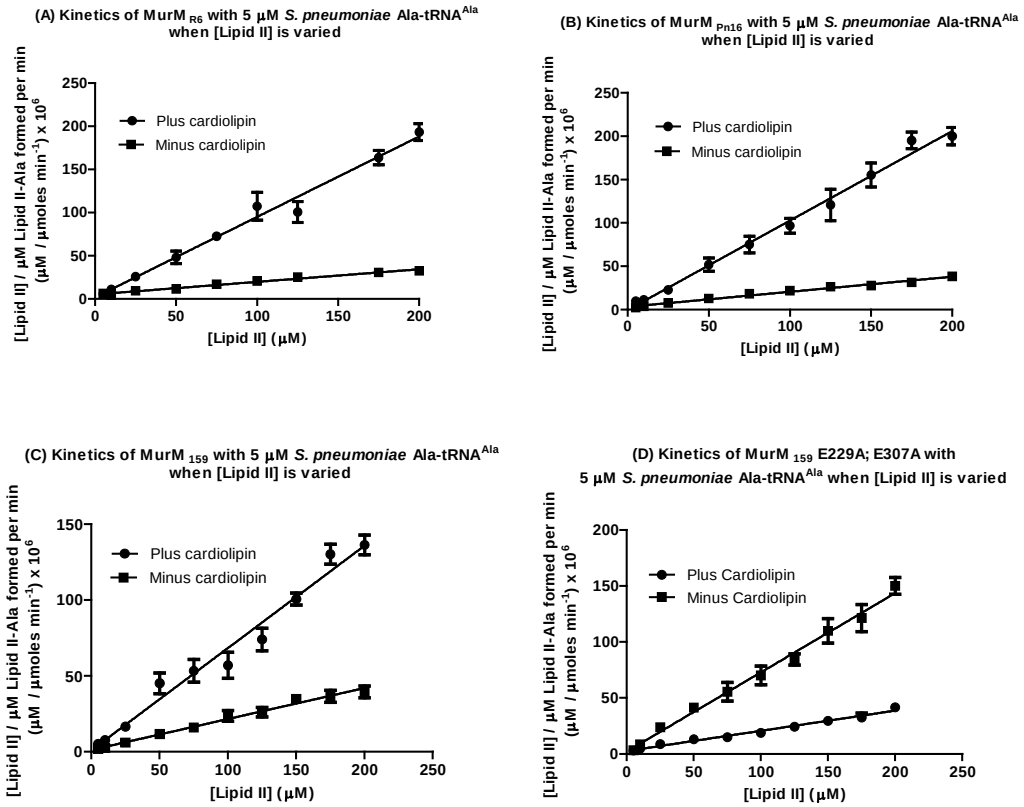

Figure 5.20: Hanes-Woolf plots showing kinetic data obtained when the concentration of LII was varied between 5 µM and 200 µM with 5 µM [H^3]-Ala-$tRNA^{Ala}$ as a co-substrate in the presence and absence of cardiolipin for (A) $MurM_{R6}$, (B) $MurM_{Pn16}$, (C) $MurM_{159}$ and (D) $MurM_{159}$ E229A:E307A. The r^2 values obtained for the plus cardiolipin datasets were 0.99, 0.99, 0.98 and 0.99, respectively. Error bars represent variation in the duplicated raw data and, where not visible, are less than the size of the symbol that marks individual data points.

Differences between key kinetic parameters determined for each enzyme in the presence and absences of cardiolipin are shown in Table 5.5. The effect of cardiolipin on each form of MurM was only investigated by varying the concentration of Lipid II in the presence of [H^3]-Ala-$tRNA^{Ala}$.

MurM variant	Apparent K_m (μM)	Apparent V_{max} (moles sec^{-1} mg^{-1})	Apparent k_{cat} (min^{-1})	k_{cat}/K_m (min^{-1}. μM^{-1})	r^2 value
R6 (- cardiolipin)	35.49 ± 1.70	6.26×10^{-10} ± 0.30	1.78 ± 0.09	0.05	0.98
R6 (+ cardiolipin)	2.05 ± 0.09	8.06×10^{-10} ± 0.36	2.30 ± 0.10	1.12	0.99
Pn16 (- cardiolipin)	17.98 ± 0.79	7.39×10^{-10} ± 0.33	2.10 ± 0.09	0.12	0.99
Pn16 (+ cardiolipin)	0.60 ± 0.02	9.32×10^{-10} ± 0.31	2.65 ± 0.09	4.42	0.99
159 (- cardiolipin)	5.96 ± 0.23	4.54×10^{-9} ± 0.17	13.00 ± 0.49	2.18	0.99
159 (+ cardiolipin)	1.38 ± 0.12	3.00×10^{-9} ± 0.23	7.80 ± 0.61	5.70	0.98
159 E229A:E307A (- cardiolipin)	2.93 ± 0.08	2.00×10^{-9} ± 0.06	5.70 ± 0.17	1.95	0.99
159 E229A:E307A (+ cardiolipin)	14.39 ± 0.66	6.00×10^{-9} ± 0.28	17.50 ± 0.81	1.20	0.99

Table 5.5: Summary of the kinetic parameters obtained for $MurM_{R6}$, $MurM_{Pn16}$, $MurM_{159}$ and $MurM_{159}$ E229A:E307A in the presence and absence of cardiolipin. The enzymes used in each assay had no histidine tag and the concentration of Lipid II was varied between 5 μM and 200 μM in the presence of [H^3]-Ala-$tRNA^{Ala}$.

As shown in Table 5.5, wild-type $MurM_{R6}$, $MurM_{Pn16}$ and $MurM_{159}$ were all stimulated by cardiolipin. The catalytic efficiency of $MurM_{R6}$ with respect to Lipid II when Ala-$tRNA^{Ala}$ was the co-substrate was increased by 20-fold in the presence of cardiolipin. This effect was largely attributable to a 17-fold reduction in the apparent

K_m of Lipid II binding in the presence of this phospholipid. $MurM_{Pn16}$ was found to be stimulated to a greater degree than $MurM_{R6}$. The presence of cardiolipin increased the catalytic efficiency of $MurM_{Pn16}$ with Lipid II by 35-fold when Ala-$tRNA^{Ala}$ was provided as the co-substrate. Again, this effect was attributable to a significant reduction (30-fold) in the apparent K_m of Lipid II binding.

In the case of $MurM_{159}$, the stimulatory effect was much milder than that demonstrated for the MurM proteins from penicillin-sensitive strains R6 and Pn16. The overall catalytic efficiency of $MurM_{159}$ was increased 2-fold in the presence of cardiolipin supporting unpublished findings made by Dr Adrian Lloyd (University of Warwick). Interesting, the apparent K_m of Lipid II binding and the turnover number of $MurM_{159}$ E229A:E307A were both increased, by 5-fold and 3-fold respectively, in the presence of cardiolipin. However, this caused no appreciable increase in the catalytic efficiency of the enzyme. These results support the hypothesis that the magnesium-deficient mutant of $MurM_{159}$, E229A:E307A cannot respond to stimulation by cardiolipin in the same way as the wild-type enzyme. For the first time, these results implicate magnesium in the interaction of MurM with the phospholipid bilayer and confirm a regulatory role for cardiolipin in the activity of this enzyme.

Unfortunately, $MurM_{Pn16}$ mutated at positions 229 and 307 was inactive with its substrates. Therefore, it can only be assumed that mutation of these residues in this variant of MurM would also prevent stimulation by cardiolipin. In addition, this has prevented investigation into the role of these residues in the strain-dependent regulation of MurM by phosphatidylglycerol. Further work is required to determine

whether the MurM proteins found in penicillin-sensitive strains of *S. pneumoniae* are more sensitive to stimulation by cardiolipin and, hence, to mutation at these residues than mosaic MurM variants found in penicillin-resistant strains. In addition, assessment of changes in the pneumococcal membrane phospholipid composition during antibiotic stress may provide more insight into the relationship between the activity of the MurM protein, levels of cell wall cross-linking and penicillin-resistance.

5.6. Investigation into the substrate specificity of MurM: The use of mis-aminoacylated Ser-tRNA^{Ala} as a substrate

In all living organisms, the first stage in the maintenance of the fidelity of protein synthesis is achieved by tRNA synthetase enzymes. These enzymes are essential to the cell and responsible for the transfer of matching amino acids to the 3' end of their cognate tRNA species. Initially, this process involves activation of the carboxyl-group of an amino acid by ATP to form aminoacyl-adenylate. The amino acid can then be transferred from adenylate to the tRNA molecule. This process is highly selective and controlled by differences in binding energies between amino acids and the synthetase and also by editing functions of the enzyme (Fersht, 1977). Therefore, mis-activation of both glycine and serine by alanyl-tRNA synthetase (AlaRS) is of particular interest.

Within AlaRS, two mechanisms exist for correction of mis-acylation of tRNA^{Ala} with either glycine or serine. One mechanism involves the editing domain of AlaRS and the other is concerned with free-standing homologues of the AlaRS editing

domain, called AlaXps proteins, which are encoded in the genomes of many organisms across all three kingdoms of life (Chong *et al.*, 2008; Guo *et al.*, 2009).

The fact that AlaRS is the only tRNA synthetase known to have such a widely distributed homologue of its editing domain encoded separately within the genome suggests that mis-aminoacylation of $tRNA^{Ala}$ with either glycine or serine has been a difficult problem for evolution to contend with. In addition, the toxic effects of this mis-aminoacylation are more pronounced with serine than glycine in both the mouse and the bacterial model system. This finding alone explains why, whilst the editing domain of AlaRS can hydrolyse Gly-$tRNA^{Ala}$ and Ser-$tRNA^{Ala}$, many of the free-standing AlaXps proteins can only hydrolyse the latter (Sokabe *et al.*, 2005). This implies that mis-aminoacylation with serine is particularly problematic for AlaRS and that AlaXps proteins may have evolved to contend specifically with this problem.

Mis-aminoacylation of $tRNA^{Ala}$ with serine by AlaRS has been exploited in this study to enable characterisation of the substrate specificity of MurM, which utilises both Ala-$tRNA^{Ala}$ and Ser-$tRNA^{Ser}$. Characterisation of the kinetics of MurM with Ser-$tRNA^{Ala}$ was thus expected to allow for determination of whether recognition of the tRNA or the amino acid moiety of the substrate is more important for catalysis. Given that MurM is conserved across all strains of *S. pneumoniae* but has so far not been found to be essential, characterisation of the enzyme with Ser-$tRNA^{Ala}$ was also thought to be important when combined with the knowledge that no homologues of AlaXps proteins have been identified within the genome of this organism. This suggested that either the editing domain of *S. pneumoniae* AlaRS is very efficient at

hydrolysing Ser-tRNA^{Ala} or that this organism has a different mechanism for ensuring that the fidelity of protein synthesis is not disrupted by the production of Ser-tRNA^{Ala}. These two possibilities were investigated in this study by examination of the ability of full-length *S. pneumoniae* AlaRS to produce Ser-tRNA^{Ala} and presentation of this mis-aminoacylated tRNA species to MurM.

5.6.1. Investigation into the ability of full-length *Streptococcus pneumoniae* Alanyl-tRNA synthetase (AlaRS) to mis-aminoacylate tRNA^{Ala} with serine

In order to investigate the ability of full-length *S. pneumoniae* AlaRS to mis-aminoacylate tRNA^{Ala} with serine, small-scale aminoacylation experiments were carried out as described in section 5.4.3. The synthetase enzyme was incubated with tRNA^{Ala} in combination with radiolabelled serine and the mis-aminoacylation reaction was followed by TCA precipitation and scintillation counting. A comparison of the results obtained for acylation of tRNA^{Ala} with alanine and serine by AlaRS is shown in Figure 5.21.

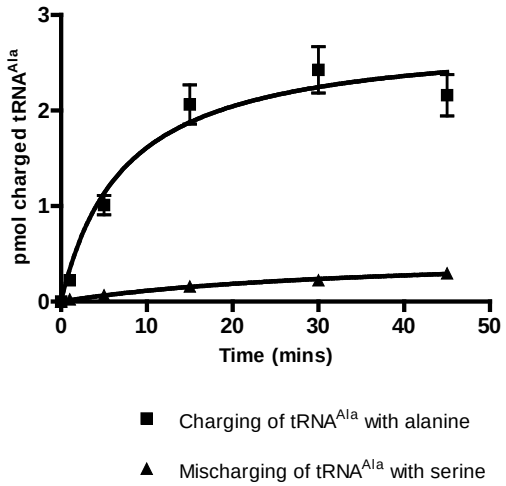

Figure 5.21: Time course data showing acylation of tRNA^{Ala} with alanine and serine by full-length *Streptococcus pneumoniae* AlaRS. Error bars represent variation in the duplicated raw data and, where not visible, are less than the size of the symbol that marks individual data points.

From the data presented in Figure 5.21, it was determined that 0.003 pmol of AlaRS were able to generate 2.500 pmol of aminoacylated Ala-tRNA^{Ala} using the conditions described in Chapter 2, section 2.5.3. The overall efficiency of this reaction according to the specific activity of the [H^3]-labelled alanine was determined to be 80%. In addition to this, 0.003 pmol of AlaRS were able to generate 0.300 pmol of mis-aminoacylated Ser-tRNA^{Ala}. The overall efficiency of the mis-aminoacylation reaction was 10%. However, given that the concentration of Ser-tRNA^{Ala} produced was 100-fold in excess of the concentration of AlaRS in the reaction, it can be assumed that mis-aminoacylated Ser-tRNA^{Ala} is produced by and released from pneumococcal AlaRS as a viable threat to protein synthesis.

The inability of AlaRS to prevent the production of Seryl-tRNA^{Ala} potentially compromises the fidelity of protein synthesis. Therefore, the ability of MurM to correct this inaccuracy by utilisation of the mis-aminoacylated Ser-tRNA^{Ala} product was investigated. The structure of AlaRS can be subdivided into four independent domains based on their function: aminoacylation, tRNA recognition, editing and oligomerisation (Jasin *et al.*, 1983; Naganuma *et al.*, 2009). Given that low amounts of Ser-tRNA^{Ala} were generated by full-length *S. pneumoniae* AlaRS, the ability of the catalytic domain (residues 1 - 460) to carry out this mis-aminoacylation was investigated as a means of generating large amounts of tRNA substrate that could be used in kinetics experiments with MurM.

5.6.2. Expression and purification of the catalytic domain of *Streptococcus pneumoniae* AlaRS

An expression construct containing a histidine-tagged version of the catalytic domain of *S. pneumoniae* AlaRS was obtained from Dr Adrian Lloyd (University of Warwick). Small-scale IPTG-induction expression trials were carried out using *E. coli* B834 (DE3) and BL21 Star (DE3).placIRare2 cells (Figure 5.22).

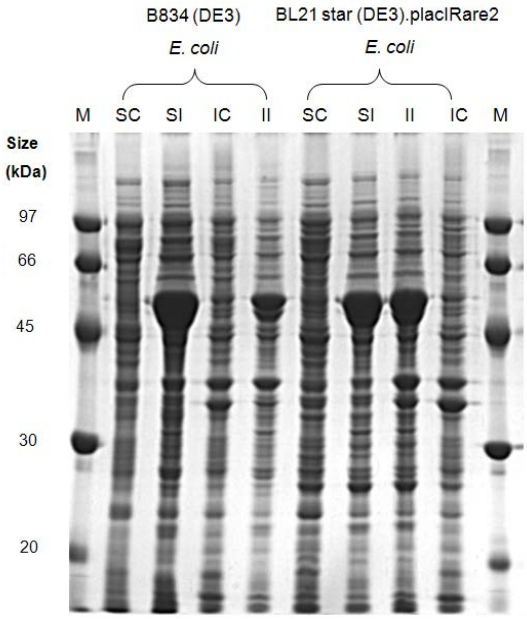

M - molecular weight standards,
SC - soluble proteins expressed by non-induced cells
SI - soluble proteins expressed by induced cells,
IC - insoluble proteins expressed by non-induced cells,
II - insoluble proteins expressed by induced cells.

Figure 5.22: 12.5% SDS PAGE gel showing the crude extracts from two expression strains of *Escherichia coli* transformed with the catalytic domain of *S. pneumoniae* AlaRS and induced to express protein by 1mM IPTG-induction at 28^{o}C for 4 h.

Small-scale expression trials indicated that both *E. coli* B834 (DE3) and BL21 Star (DE3).placIRare2 cells were able to express the catalytic domain of *S. pneumoniae* AlaRS in a soluble form under the described condition. For large-scale expression,

E. coli BL21 Star (DE3).placIRare2 cells harbouring the catalytic domain expression construct were cultured at 37^{o}C to an OD_{600nm} of 0.5 when expression was induced by the addition of IPTG to a final concentration of 1 mM. Upon the addition of IPTG, the growth temperature was reduced to 28^{o}C for 3 h. After induction, cells were harvested and sonicated to obtain a crude extract as described for full-length AlaRS. The crude extract was loaded onto a 5 mL cobalt column pre-equilibrated in buffer containing 50 mM sodium phosphate pH 7.0, 500 mM NaCl and 20% glycerol. Protein was eluted from the column by step washing with buffer containing 0 mM, 10 mM, 50 mM and 200 mM imidazole (Figure 5.23).

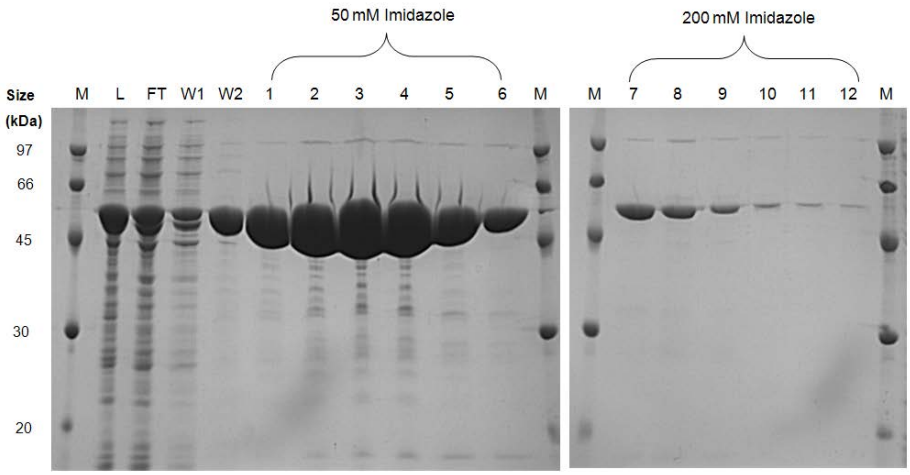

M - molecular weight standards,
L - a sample of the soluble protein loaded onto the column,
FT - a sample of the flow through from the column during protein loading,
W1 - protein eluted during wash with column equilibration buffer,
W2 - protein eluted during wash with buffer containing 10 mM imidazole.

Figure 5.23: 12.5% SDS PAGE gels showing purification of the catalytic domain of *Streptococcus pneumoniae* AlaRS on BD Talon cobalt resin. Lanes 1 – 12 show samples of protein eluted from the column during two wash steps with buffer supplemented with 50 mM and 200 mM imidazole, respectively.

Most protein eluted from the column during wash with buffer containing 50 mM imidazole. These fractions were pooled and dialysed against storage buffer as described previously in section 5.3.2 before freezing at -80^{o}C.

5.6.3. Mis-aminoacylation of $tRNA^{Ala}$ with serine by the catalytic domain of *Streptococcus pneumoniae* AlaRS

Activity of the catalytic domain of *S. pneumoniae* AlaRS was tested in small-scale aminoacylation experiments with $tRNA^{Ala}$ using both alanine and serine as substrate. Results of these time courses are shown in Figure 5.24.

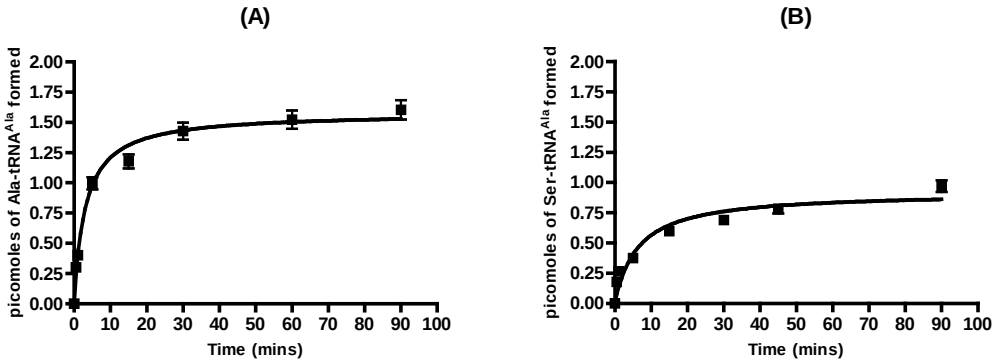

Figure 5.24: Time course data showing (A) aminoacylation of $tRNA^{Ala}$ with alanine and (B) mis-aminoacylation of $tRNA^{Ala}$ with serine by the catalytic domain of *Streptococcus pneumoniae* AlaRS. Error bars represent variation in the duplicated raw data and, where not visible, are less than the size of the symbol that marks individual data points.

The data presented in Figure 5.24 indicated that the catalytic domain of *S. pneumoniae* AlaRS was able to generate mis-aminoacylated Ser-$tRNA^{Ala}$ with the same efficiency as was demonstrated for the production of Ala-$tRNA^{Ala}$. Consequently, this enzyme was used for large-scale preparation of mis-aminoacylated Ser-$tRNA^{Ala}$ for use in MurM kinetic activity assays.

5.6.4. Kinetic characterisation of $MurM_{R6}$, $MurM_{Pn16}$ and $MurM_{159}$ with mis-aminoacylated Ser-$tRNA^{Ala}$ as a substrate

The kinetic properties of $MurM_{R6}$, $MurM_{Pn16}$ and $MurM_{159}$ with mis-aminoacylated [H^3]-Ser-$tRNA^{Ala}$ as a substrate were investigated by keeping the concentration of Lipid II constant (10 μM) and varying the concentration of tRNA between 0.1 and

1.8 μM as described previously in section 5.5. In each case, time courses were used to ensure that the linear region of activity could be identified and a suitable time point for collection of kinetic data selected.

Initial time courses were carried out using the concentrations of each enzyme that were found to be most suitable during previous assays with Ala-tRNA^{Ala} and Ser-tRNA^{Ser}. In every case, the reaction proceeded very quickly and was over in the first 30 sec when these enzyme concentrations were applied. A further 10-fold dilution of each MurM was required in order to visualise the linear region of activity with the 30 sec time sample falling within this region. The final concentrations of MurM used in the assay were as follows: 0.63 nM ($MurM_{159}$), 1.00 nM ($MurM_{R6}$) and 2.00 nM ($MurM_{Pn16}$). Time course data collected at these enzyme concentrations are presented in Figure 5.25.

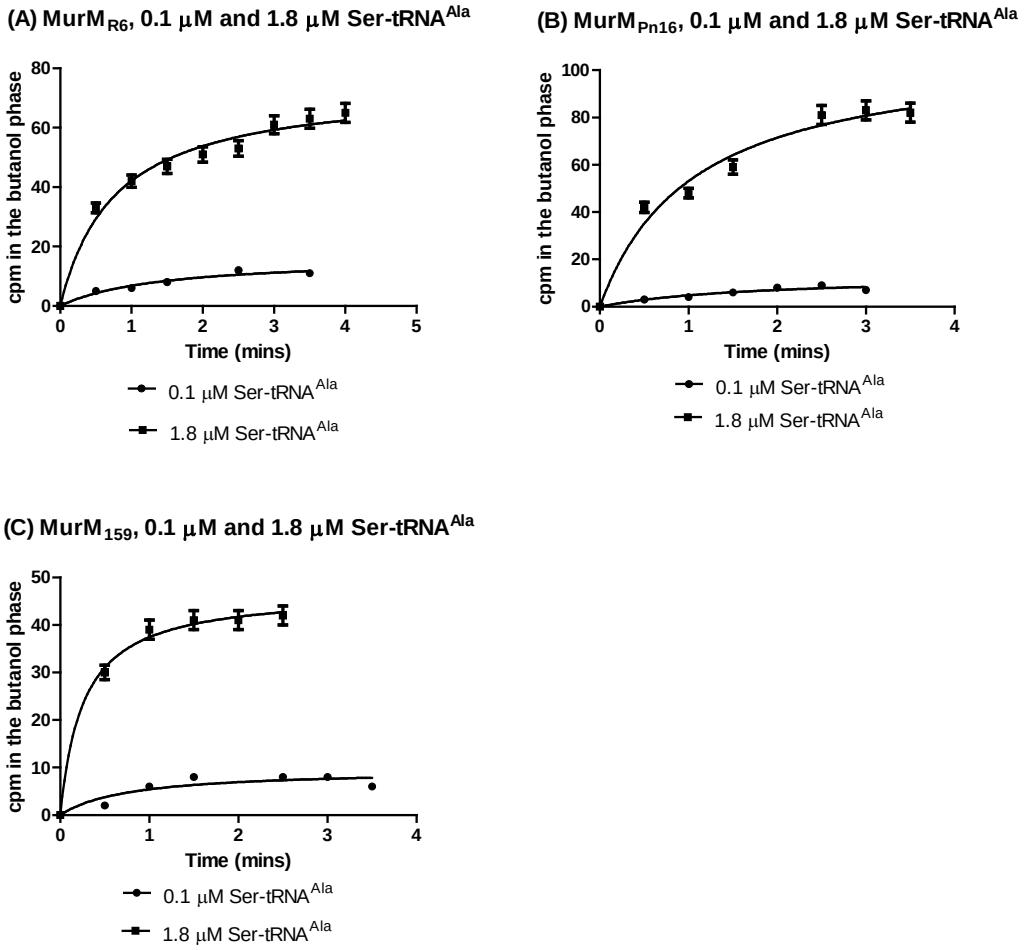

Figure 5.25: Time course data obtained using 0.1 μM and 1.8 μM [H^3]-Ser-tRNA^{Ala} in the presence of 10 μM LII for (A) 1.00 nM MurM$_{R6}$, (B) 2.00 nM MurM$_{Pn16}$ and, (C) 0.63 nM MurM$_{159}$. Control data, obtained by omission of LII from the reaction, have been subtracted from the raw counts to give cpm in the butanol phase presented on the y-axis. Note that cpm is a direct measure of the formation of radiolabelled LII. Error bars represent variation in the duplicated raw data and, where not visible, are less than the size of the symbol that marks individual data points.

A series of kinetic data, whereby the concentration of [H^3]-Ser-tRNA^{Ala} was varied in the presence of a constant concentration of Lipid II, were collected for each form of MurM using the 30 sec time sample as a representative of the linear region of activity. These data sets have been presented as Hanes-Woolf plots in Figure 5.26.

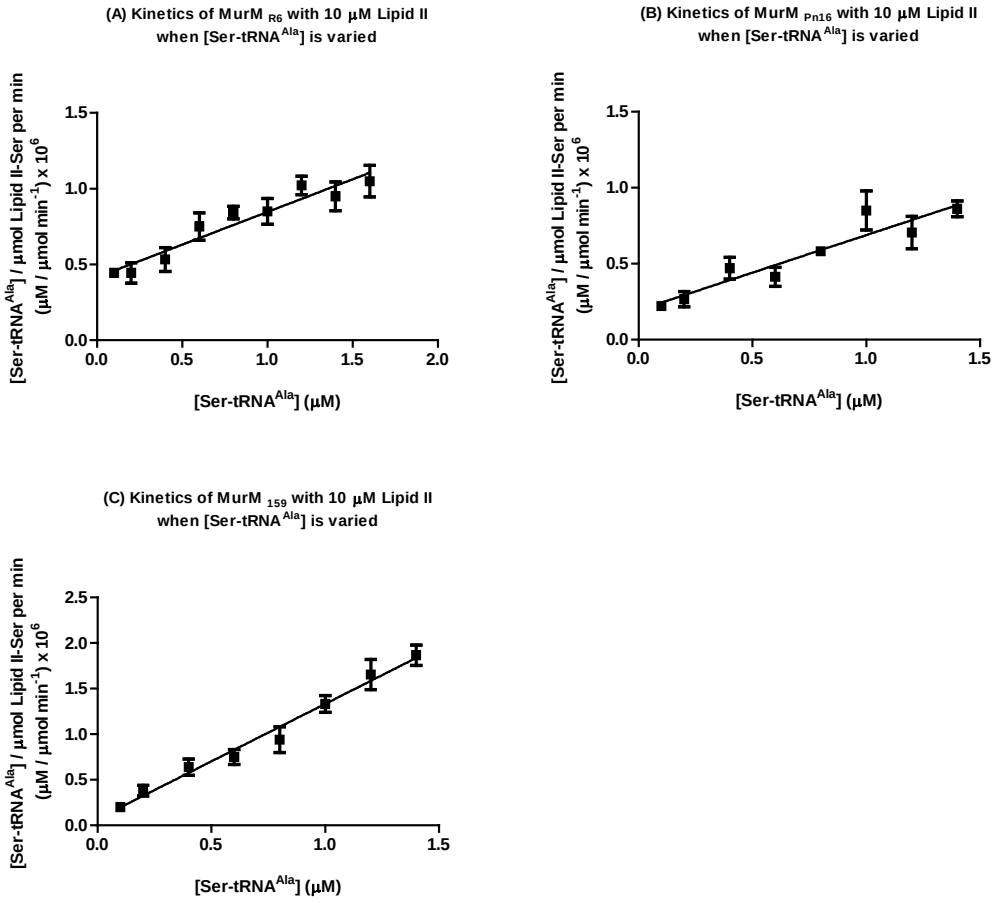

Figure 5.26: Hanes-Woolf plots of kinetic data obtained for (A) $MurM_{R6}$, (B) $MurM_{Pn16}$ and (C) $MurM_{159}$ when mis-aminoacylated Ser-$tRNA^{Ala}$ was used as substrate. Kinetic data were collected by varying the concentration of Ser-$tRNA^{Ala}$ between 0.1 and 1.8 µM in the presence of 10 µM Lipid II. The r^2 values for these data sets are 0.92, 0.89 and 0.98 respectively. Error bars represent variation in the duplicated raw data and, where not visible, are less than the size of the symbol that marks individual data points.

For the purpose of comparison to the data sets obtained when Ala-$tRNA^{Ala}$ and Ser-$tRNA^{Ser}$ were provided as substrates in the presence of a constant concentration of Lipid II, the key kinetic parameters obtained from the Hanes-Woolf plots shown in Figure 5.26 have been summarised in Table 5.6.

tRNA substrate	Apparent K_m (μM)	Apparent V_{max} (moles sec^{-1} mg^{-1})	Apparent k_{cat} (min^{-1})	k_{cat}/K_m (min^{-1}. μM^{-1})	r^2 value
$MurM_{R6}$					
Ala-$tRNA^{Ala}$	0.33 ± 0.02	1.36 x 10^{-10} ± 0.08	0.39 ± 0.02	1.18	0.98
Ser-$tRNA^{Ser}$	0.19 ± 0.01	1.30 x 10^{-9} ± 0.08	3.71 ± 0.22	19.53	0.97
Ser-$tRNA^{Ala}$	**0.96 ± 0.09**	**2.60 x 10^{-8} ± 0.26**	**73.40 ± 7.34**	**76.46**	**0.92**
$MurM_{Pn16}$					
Ala-$tRNA^{Ala}$	1.29 ± 0.09	7.30 x 10^{-10} ± 0.49	2.08 ± 0.14	1.61	0.97
Ser-$tRNA^{Ser}$	0.25 ± 0.02	8.47 x 10^{-10} ± 0.57	2.41 ± 0.16	9.46	0.96
Ser-$tRNA^{Ala}$	**0.39 ± 0.05**	**1.30 x 10^{-8} ± 0.18**	**36.90 ± 5.17**	**94.62**	**0.89**
$MurM_{159}$					
Ala-$tRNA^{Ala}$	0.51 ± 0.02	3.84 x 10^{-9} ± 0.18	11.00 ± 0.53	21.57	0.98
Ser-$tRNA^{Ser}$	0.22 ± 0.01	2.36 x 10^{-9} ± 0.11	6.73 ± 0.30	30.59	0.99
Ser-$tRNA^{Ala}$	**0.06 ± 0.01**	**1.5 x 10^{-8} ± 0.08**	**41.90 ± 2.10**	**698.33**	**0.98**

Table 5.6: Summary of key kinetic parameters for $MurM_{R6}$, $MurM_{Pn16}$ and $MurM_{159}$ when mis-aminoacylated Ser-$tRNA^{Ala}$ was provided as substrate. Values were calculated from the Hanes-Woolf plots shown in Figure 5.26. The enzyme used in each assay had no histidine tag and the tRNA was a single species in each case.

When mis-aminoacylated Ser-$tRNA^{Ala}$ was provided as a substrate in the presence of a constant concentration of Lipid II, the catalytic efficiency of MurM was increased dramatically regardless of the strain from which the protein was derived. The catalytic efficiency of $MurM_{R6}$ was increased by 65-fold in comparison to Ala-$tRNA^{Ala}$ and 4-fold in comparison to Ser-$tRNA^{Ser}$. This effect was attributable to a 190-fold and a 20-fold improvement in apparent k_{cat}, respectively. This is indicative

of MurM recognising both the tRNA and the aminoacyl-moieties of its tRNA substrate.

The catalytic efficiency of $MurM_{Pn16}$ was increased 58-fold in comparison to Ala-$tRNA^{Ala}$ and 10-fold in comparison to Ser-$tRNA^{Ser}$. As was the case with $MurM_{R6}$, this effect was mostly due to an 18-fold and a 15-fold improvement in apparent k_{cat}, respectively. The improvement in the catalytic efficiency of $MurM_{159}$ was also significant with a 30-fold increase in comparison to Ala-$tRNA^{Ala}$ and a 20-fold increase in comparison to Ser-$tRNA^{Ser}$. This effect was attributable to an 8-fold and a 3-fold reduction in apparent K_m, respectively, as well as an increase in apparent k_{cat}.

The overall improvement in the catalytic efficiency of MurM when mis-aminoacylated Ser-$tRNA^{Ala}$ was provided as a substrate suggests that MurM may substitute for AlaXps proteins in *S. pneumoniae*, protecting the fidelity of protein synthesis by correcting mistakes made by AlaRS. This is a novel finding linking peptidoglycan biosynthesis and the fidelity of protein synthesis together. Further investigations into the interaction of MurM with its tRNA substrate and the specificity of this reaction were made using a 2'-amino mini-helix analogue of $tRNA^{Ala}$ (section 5.7).

5.7. Investigation into the substrate specificity of MurM: Characterisation of the acceptance of the amino acid moiety from the tRNA substrate using a 2'-amino mini-helix analogue of Ala-tRNA^{Ala}

During aminoacylation of a tRNA species, the appropriate tRNA synthetase enzyme is responsible for transferring amino acid residues from an adenylate species to either the 2' or the 3' hydroxyl of the terminal adenine nucleotide (A^{76}) of a molecule of tRNA. Upon completion of this process, spontaneous trans-esterification occurs resulting in flipping of the amino acid residue between these two positions. AlaRS belongs to the class II tRNA synthetase family and, therefore, always aminoacylates A^{76} at the 3' hydroxyl (Arnez and Moras, 1997). This process is illustrated in Figure 5.27.

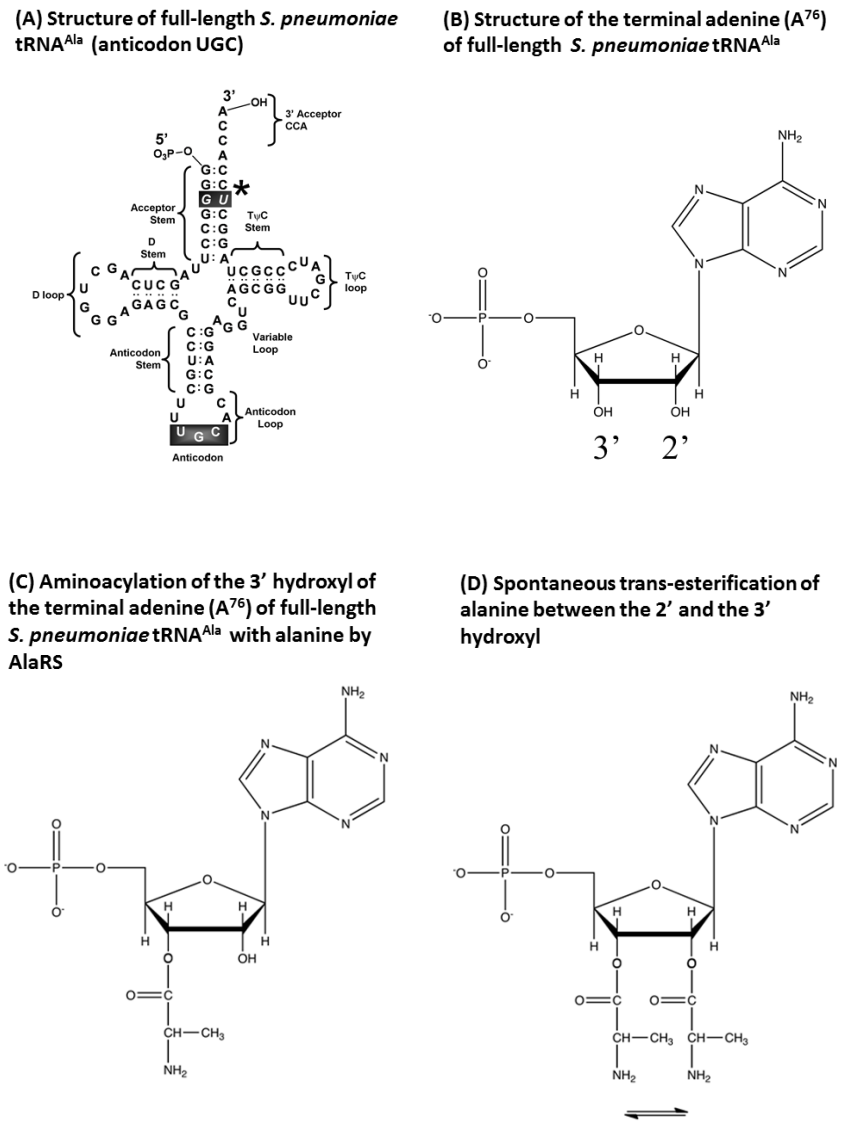

Figure 5.27: Illustration of alanylation at the 3' hydroxyl of the terminal adenine (A^{76}) of *S. pneumoniae* $tRNA^{Ala}$ by AlaRS. Usually, the availability of two hydroxyl groups on A^{76} means that, after alanylation by AlaRS, alanine remains associated with the tRNA in equilibrium between the 2' and the 3' state (D).

Prior to the work undertaken in this study, Dr Adrian Lloyd (University of Warwick) used both a substrate and a 2'-deoxy substrate mini-helix $tRNA^{Ala}$ derivative to determine if the non-esterified hydroxyl present on the 3' terminal adenosine of Ala-$tRNA^{Ala}$ is involved in MurM catalysis (unpublished data).

The structure of the 2'- deoxy mini-helix $tRNA^{Ala}$ is shown in Figure 5.28. The terminal adenine of the substrate mini-helix $tRNA^{Ala}$ was as shown in Figure 5.27 (B).

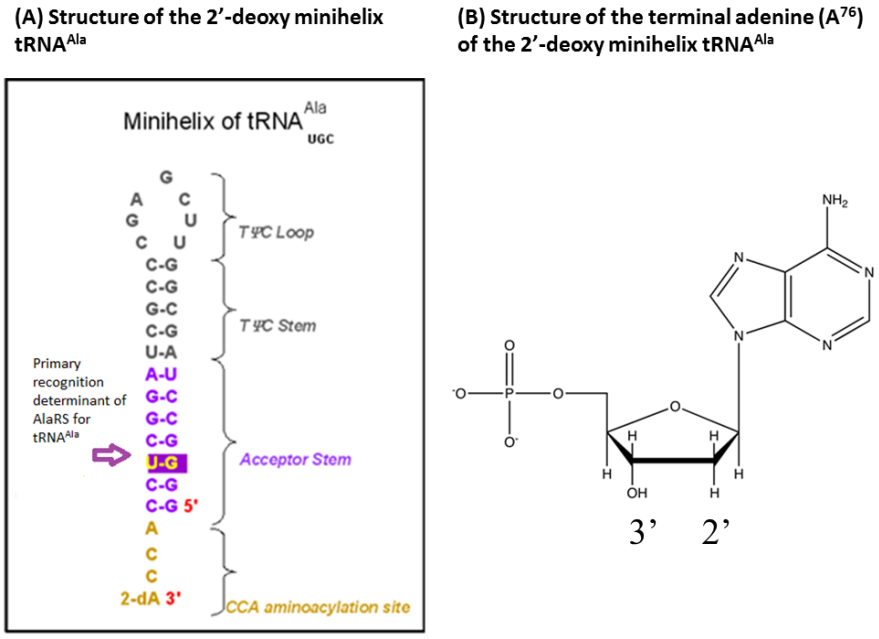

Figure 5.28: Structure of the 2'-deoxy mini-helix substrate of $tRNA^{Ala}$ used in studies undertaken by Dr Adrian Lloyd (University of Warwick). Note the replacement of the 2'- OH on A^{76} with H. The structure of the mini-helix shown in (A) was adapted from Beuning and Musier-Forsyth (2000).

Both the substrate mini-helix $tRNA^{Ala}$ and the 2'-deoxy mini-helix $tRNA^{Ala}$ could be aminoacylated on the 3' hydroxyl of A^{76} by full-length *S. pneumoniae* AlaRS. However, whilst the alanine moiety was able to undergo spontaneous trans-esterification between the 2' and the 3' hydroxyl in the substrate mini-helix, it remained associated with the 3' hydroxyl of A^{76} in the 2'-deoxy mini-helix. Upon presentation to MurM, the substrate mini-helix Ala-$tRNA^{Ala}$, with a 3' and a 2' hydroxyl on A^{76}, was utilised by the enzyme with the production of Lipid II-Ala in the same way as full-length Ala-$tRNA^{Ala}$. However, the 2'-deoxy mini-helix Ala-$tRNA^{Ala}$ was neither a substrate nor an inhibitor of MurM (Dr Adrian Lloyd,

unpublished data). This implied that MurM will only accept alanine from the 2' hydroxyl of Ala-tRNA^{Ala}.

Further confirmation of the acceptance of the amino acid by MurM from the 2' hydroxyl of A^{76} was achieved in this study using an additional 2'- amino mini-helix analogue of tRNA^{Ala}. In this mini-helix analogue of tRNA^{Ala}, the adenine of the CCA end (A^{76}) is comprised of a 2' amine group in place of the hydroxyl group as shown in Figure 5.29.

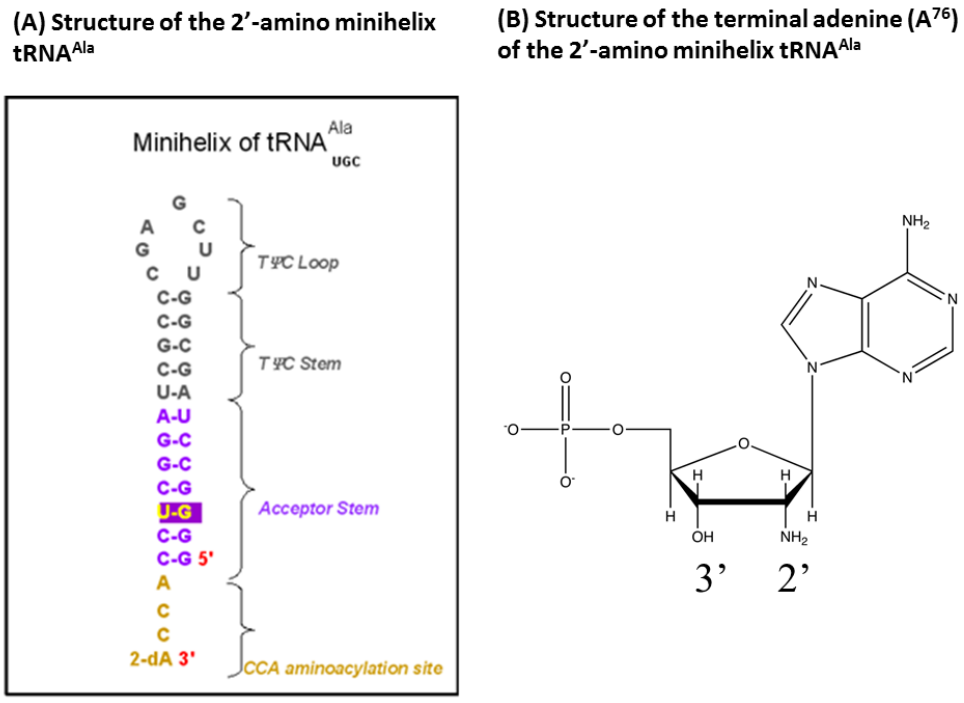

Figure 5.29: Structure of the 2'-amino mini-helix substrate of tRNA^{Ala} used in this study and synthesised by Thermo Scientific, USA. Note the replacement of the 2'- OH on A^{76} with NH_2. The structure of the mini-helix shown in (A) was adapted from Beuning and Musier-Forsyth (2000).

The design of the 2'-amino mini-helix analogue of tRNA^{Ala} was based on the work of Fraser and Rich (1973), who demonstrated that aminoacylation of 2'-amino tRNA^{Ala} on the 3' hydroxyl of A^{76} resulted in irreversible trans-esterification of

alanine to the 2' amino group and subsequent tethering of the amino acid at this position by the formation of a stable peptide bond. Given the inherent stability of this peptide bond, it was hypothesised that the 2'-amino mini-helix Ala-tRNA^{Ala} would only inhibit the MurM catalysed reaction if the protein accepts the amino acid from the 2' position of A^{76} subsequently supporting the unpublished findings made by Dr Adrian Lloyd with the 2'-deoxy mini-helix of Ala-tRNA^{Ala}.

5.7.1. Recognition of the 2'-amino mini-helix analogue of tRNA^{Ala} by AlaRS

In this study, the 2'-amino mini-helix tRNA^{Ala} analogue was exploited for the purpose of characterisation of the recognition of the aminoacyl moiety of tRNA by MurM. In order to achieve this, it was necessary to ensure that AlaRS recognised the species as a substrate for the generation [H^3]-Ala-tRNA^{Ala}. A small-scale aminoacylation experiment was carried out as described previously (section 5.4.3) to determine acceptance of the 2'-amino mini-helix tRNA^{Ala} as a substrate (Figure 5.30).

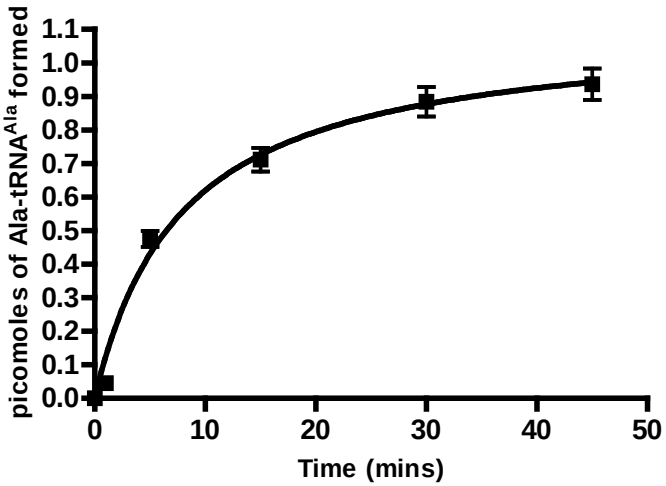

Figure 5.30: Time course data showing acylation of the 2'-amino mini-helix analogue of tRNA^{Ala} with [H^3]-alanine by full-length *Streptococcus pneumoniae* AlaRS. Using the specific activity of the label, the overall efficiency of the acylation reaction with alanine was found to be the 53%. Error bars represent variation in the duplicated raw data and, where not visible, are less than the size of the symbol that marks individual data points.

Given that the 2'-amino mini-helix analogue of $tRNA^{Ala}$ was recognised and aminoacylated by full-length AlaRS, it was possible scale-up the reaction presented in Figure 5.30 to generate enough analogue to present to MurM. Modification of the mini-helix to replace the 2' hydroxyl group with an amino group should have resulted in the formation of a stable peptide bond between the RNA and the amino acid as opposed to the normal ester bond upon aminoacylation by AlaRS.

In order to ensure this had occurred, the stability of the 2' amino bond was tested by following the deacylation rate of the 2'-amino mini-helix analogue of $[H^3]$-Ala-$tRNA^{Ala}$ in the assay buffer used for determining the kinetics of MurM (see Chapter 2, section 2.5.5). As a control, the deacylation rate of full-length $[H^3]$-Ala-$tRNA^{Ala}$ was also monitored (Figure 5.31). At each time point, a 10 μL sample was taken from the reaction and spotted onto filter paper. This was dropped into 10% TCA (w/v) to separate the charged tRNA from free radiolabel. Deacylation was monitored by a reduction in signal over time as detected by scintillation counting.

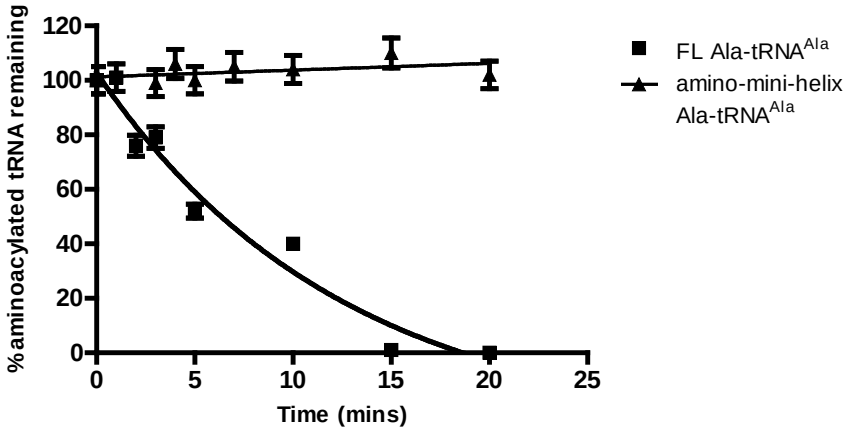

Figure 5.31: Time courses showing deacylation of the 2'-amino mini-helix $[H^3]$-Ala-$tRNA^{Ala}$ analogue and full-length $[H^3]$-Ala-$tRNA^{Ala}$ over time in MurM assay buffer. Counts per minute have been plotted as a percentage of the zero time point reading. Error bars represent variation in the duplicated raw data and, where not visible, are less than the size of the symbol that marks individual data points.

As predicted, the bond between the amino acid and the tRNA in the aminoacylated 2'-amino mini-helix [H^3]-Ala-$tRNA^{Ala}$ analogue was stable with no drop in signal over the 20 min incubation period. In contrast to this, full-length [H^3]-Ala-$tRNA^{Ala}$ showed complete deacylation after just 20 min incubation in MurM assay buffer. The half-life for full-length [H^3]-Ala-$tRNA^{Ala}$ was calculated to be 8.7 min from the data shown in Figure 5.31.

5.7.2. Presentation of the 2'-amino mini-helix analogue of [H^3]-Ala-$tRNA^{Ala}$ to *Streptococcus pneumoniae* strains R6 and 159 MurM

In order to investigate whether MurM could utilise the aminoacylated 2'-amino mini-helix analogue as substrate, time courses were carried out in the presence of a constant concentration of Lipid II (10 μM) and [H^3]-Ala-$tRNA^{Ala}$ 2'-amino mini-helix analogue (0.5 μM) as described in sections 5.5.1 and 5.5.3. These time courses were carried out with 126 nM and 13 nM MurM proteins from a highly penicillin-resistant strain of S. *pneumoniae* (159) and a penicillin-sensitive strain of *S. pneumoniae* (R6), respectively (Figure 5.32).

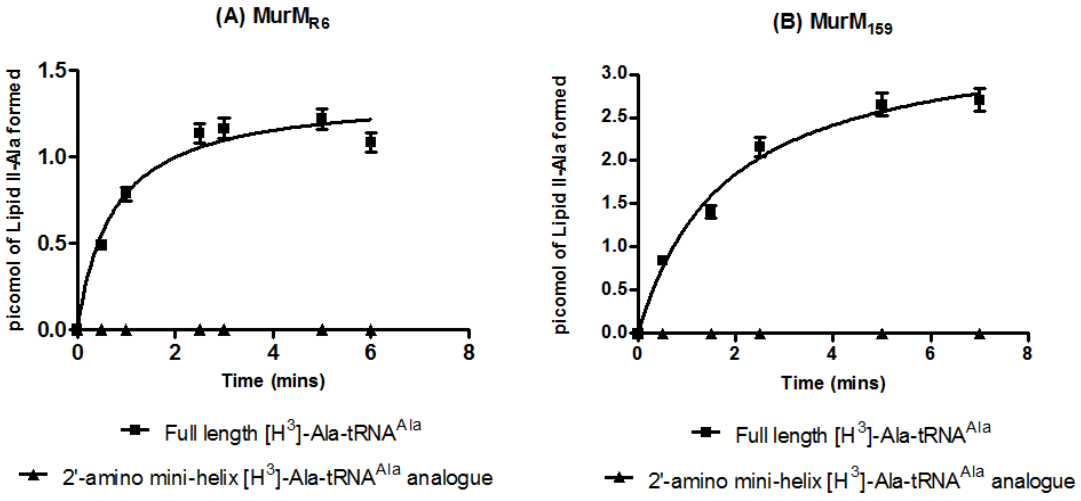

Figure 5.32: Time courses comparing the activity of (A) MurM$_{R6}$ and (B) MurM$_{159}$ with the aminoacylated 2'-amino mini-helix [H^3]-Ala-tRNA^{Ala} analogue and full-length [H^3]-Ala-tRNA^{Ala}. Control data was obtained in the same way when Lipid II was omitted from the reaction. Control data have been subtracted from the data shown in these plots. Error bars represent variation in the duplicated raw data and, where not visible, are less than the size of the symbol that marks individual data points.

The results shown in Figure 5.32 suggested that the 2'-amino mini-helix [H^3]-Ala-tRNA^{Ala} analogue was not a substrate for MurM as assessed by the attachment of radiolabelled alanine to Lipid II. In order to determine whether the 2'-amino mini-helix Ala-tRNA^{Ala} analogue was an inhibitor of MurM, it was necessary to aminoacylate this tRNA species with non-radiolabelled alanine. Following aminoacylation by AlaRS, it was essential to purify any remaining non-aminoacylated analogue away from aminoacylated analogue. This was achieved using nickel-immobilised *Thermus thermophilus* EF-Tu as described in Chapter 2, section 2.5.4 (Ribeiro *et al*., 1995).

To assess the inhibitory potential of the 2'-amino mini-helix Ala-tRNA^{Ala} analogue, a series of 30 min single time-point assays were carried out using MurM$_{Pn16}$. MurM$_{Pn16}$ was chosen as the most appropriate enzyme to use in inhibition studies

because it was found to have the highest apparent K_m for Ala-tRNA^{Ala} in the kinetics studies presented in sections 5.5.1 to 5.5.3.

In each of these experiments, total cpm in the butanol phase was assessed after incubation of 91 nM MurM$_{Pn16}$ with 10 µM Lipid II and 0.6 µM full-length [H^3]-Ala-tRNA^{Ala} under the conditions described in Chapter 2, section 2.5.5. Two additional reactions were set-up as above after supplementation with either 2 µM aminoacylated 2'-amino mini-helix analogue or 2 µM non-aminoacylated 2'-amino mini-helix analogue. The results of these experiments are shown in Table 5.7.

MurM assay condition	cpm in the butanol phase after 30 min
Minus Lipid II control reaction	25 ± 2
Minus 2'-amino mini-helix analogue	101 ± 8
Plus 2 µM aminoacylated 2'-amino mini-helix analogue	52 ± 5
Plus 2 µM non-aminoacylated 2'-amino mini-helix analogue	111 ± 8

Table 5.7: Results of four 30 min single time-point assays carried out with MurM$_{Pn16}$ to assess whether the 2'-amino mini-helix analogue of tRNA^{Ala} was an inhibitor of MurM in either the non-aminoacylated or the aminoacylated form.

The results shown in Table 5.7, suggested that the non-aminoacylated form of the 2'-amino mini-helix analogue of tRNA^{Ala} was not an inhibitor of MurM as the cpm in the butanol phase was equivalent to that obtained in the absence of this tRNA species. In contrast to this, a reduction in cpm was seen when 2 µM aminoacylated 2'-amino mini-helix analogue was included in the reaction. This result established that an IC_{50} determination for the aminoacylated 2'-amino mini-helix analogue was required.

IC_{50} determination was carried out using 91 nM $MurM_{Pn16}$ in the presence of 10 µM Lipid II and full-length [H^3]-Ala-$tRNA^{Ala}$ at half apparent K_m (0.6 µM). Given that 2 µM aminoacylated 2'-amino mini-helix analogue appeared to cause a 50% inhibition of MurM activity under these conditions, the concentration of this tRNA species was varied between 0.25 µM and 6 µM for the purpose of generating an IC_{50} curve. All assays were incubated at 37°C for 1 min prior to being stopped and processed as described in Chapter 2, section 2.5.5. The IC_{50} plot generated from these data, using 0% inhibition as the cpm in the butanol phase in the absence of any aminoacylated 2'-amino mini-helix analogue, is shown in Figure 5.33.

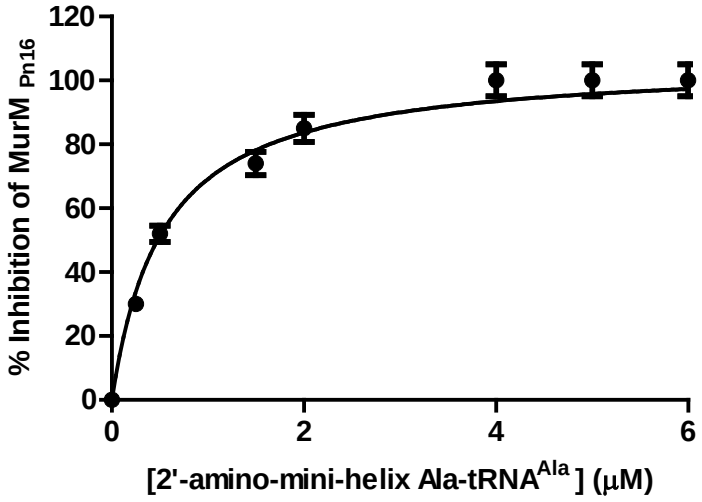

Figure 5.33: IC_{50} curve showing % inhibition of $MurM_{Pn16}$ by 2'-amino mini-helix Ala-$tRNA^{Ala}$ in the presence of 10 µM Lipid II and 0.6 µM full-length [H^3]-Ala-$tRNA^{Ala}$. Control data obtained by omission of Lipid II from the reaction have been subtracted in each case. Error bars represent variation in the duplicated raw data and, where not visible, are less than the size of the symbol that marks individual data points.

The data presented in Figure 5.33 indicated that the 2'-amino mini-helix Ala-$tRNA^{Ala}$ analogue was a potent inhibitor of $MurM_{Pn16}$ with an IC_{50} of 0.5 µM. Unpublished data generated by Dr Adrian Lloyd (University of Warwick) using an aminoacylated 2'-deoxy mini-helix analogue of $tRNA^{Ala}$ showed that, when alanine

was attached to the 3' hydroxyl of the terminal adenine of $tRNA^{Ala}$, it was not recognised as a substrate by MurM. Together, these results provide the first confirmatory evidence for MurM catalysis proceeding by selective transfer of the aminoacyl moiety from the 2' hydroxyl of the terminal adenine of the tRNA substrate to Lipid II.

5.8. Discussion

High-level penicillin resistance in *S. pneumoniae* requires the acquisition of low-affinity penicillin-binding proteins in combination with the activity of the MurM protein (Filipe *et al.*, 2002). As a result of this, determination of the factors that influence the activity of MurM is essential for the development of successful inhibitors towards the enzyme. In this study, kinetic characterisation was carried out for the MurM protein from *S. pneumoniae* strain R6. This strain is unusual in that it has a high proportion of branched muropeptides within its cell wall despite being classed as penicillin-sensitive (Garcia-Bustos and Tomasz, 1990). Characterisation of this particular MurM enzyme was thus considered to be important for investigation into the links between levels of cell wall cross-linking, activity of the MurM protein and penicillin resistance.

The sequence of $MurM_{R6}$ differs from $MurM_{Pn16}$ only at position 101 where valine substitutes for alanine, respectively (Chapter 3). When compared to available sequence data for other variants of MurM (acquired from the National Center for Biotechnology Information, http://www.ncbi.nlm.nih.gov/protein), the substitution of valine for alanine at this position can only be found in one other strain of *S. pneumoniae*: D39 (Lanie *et al.*, 2007).

According to Garcia-Bustos and Tomasz (1990), the proportions of linear and branched muropeptides in strain D39 are 73% and 27%, respectively. In contrast to this, the proportions of linear and branched muropeptides in strain R6 are 60% and 40%, respectively. Whilst no approximations of error are given for these values, the MurM proteins from these two strains are 100% identical in amino acid sequence. This suggests that the difference in the proportion of branched muropeptides between the two strains cannot be solely attributable to differences in the kinetic activities of MurM and that other factors, such as overall level of MurM expression and the availability of Lipid II and tRNA *in vivo* must also be involved.

With this in mind, it is difficult to justify that the differences in the kinetic parameters measured for $MurM_{R6}$ and $MurM_{Pn16}$ can be explained by the single amino acid change between the two proteins. However, it may, in part, explain why $MurM_{R6}$ is much more serine-specific than $MurM_{Pn16}$ and $MurM_{159}$, especially if the *in vivo* tRNA pool of strain R6 is richer in $tRNA^{Ser}$ than $tRNA^{Ala}$. Out of the three MurM variants characterised in this study, $MurM_{R6}$ was found to have the lowest catalytic efficiency with respect to Lipid II when Ala-$tRNA^{Ala}$ was the co-substrate and with Ala-$tRNA^{Ala}$ itself. Yet, the catalytic efficiency of the enzyme with Ser-$tRNA^{Ser}$ exceeded that of $MurM_{Pn16}$ by 2-fold and was only 2-fold lower than that of $MurM_{159}$. The work of Lloyd *et al.* (2008) has demonstrated that differences in the composition of the tRNA pool only made a small contribution to the overall proportion of branched muropeptides in the cells walls of *S. pneumoniae* strains Pn16 and 159 in comparison to the catalytic activity of MurM. However, this has yet to be investigated in the case of strain R6. In combination with an analysis of the *in vivo* levels of MurM expression within these three strains of *S. pneumoniae*, data

provided by such an investigation might offer some explanation for the apparent differences in measured kinetic parameters between $MurM_{R6}$, $MurM_{Pn16}$ and $MurM_{159}$.

The success of production of a single species of pure *S. pneumoniae* $tRNA^{Ala}$ and $tRNA^{Ser}$ in this study has enabled the first detailed kinetic analysis of MurM with respect to its tRNA substrate to be carried out. As has been shown to be the case for yeast $tRNA^{Phe}$, *in vivo* modifications were non-essential for recognition of $tRNA^{Ala}$ and $tRNA^{Ser}$ by the appropriate synthetase enzyme and MurM (Sampson and Uhlenbeck, 1988). In the presence of a constant concentration of Lipid II, the catalytic efficiencies of all three MurM proteins were shown to be greater when Ser-$tRNA^{Ser}$ was provided as substrate in comparison to Ala-$tRNA^{Ala}$.

In the case of $MurM_{159}$, this contradicts preliminary findings made by Lloyd *et al.* (2008) which demonstrated that the ability of this variant of MurM to use Ser-$tRNA^{Ser}$ was poor in comparison to Ala-$tRNA^{Ala}$. This could suggest that the presence of zinc in the assay buffer was required to observe maximal activity of MurM. Another explanation could be that the other non-aminoacylated tRNA species in the crude extract used by Lloyd *et al.* (2008) masked the kinetic properties of the enzyme with Ser-$tRNA^{Ser}$, thus highlighting the value of re-determining the kinetic parameters of $MurM_{159}$ in the presence of a single species of pure *S. pneumoniae* Ser-$tRNA^{Ser}$.

The catalytic efficiencies of all three MurM enzymes were found to be significantly greater with mis-aminoacylated Ser-$tRNA^{Ala}$ when compared to Ala-$tRNA^{Ala}$ and

Ser-tRNA^{Ser}. MurM$_{R6}$ and MurM$_{Pn16}$ were at least 60-fold more efficient with this mis-aminoacylated substrate in comparison to Ala-tRNA^{Ala} and MurM$_{159}$ was found to be 32-fold more efficient under the same conditions. This suggests that MurM recognises both the amino acid and the tRNA moiety of its substrate. When combined with the finding that *S. pneumoniae* AlaRS routinely generates and releases Ser-tRNA^{Ala} in the apparent absence of any free standing AlaXps proteins, these data are suggestive of MurM having a role in the maintenance of the fidelity of protein synthesis. This would explain why MurM is found in all strains of *S. pneumoniae.*

S. pneumoniae is known to produce hydrogen peroxide during aerobic carbohydrate metabolism by virtue of pyruvate oxidase (Pesakhov *et al.*, 2007). In *E. coli*, exposure to hydrogen peroxide has been shown to result in a reduction in the fidelity of translation. This effect can be directly attributed to the oxidation of cysteine-182 within threonyl-tRNA synthetase which subsequently impairs the editing ability of the enzyme and results in the production of mis-aminoacylated Ser-tRNA^{Thr} (Ling and Söll, 2010). Thus it is possible that, in *S. pneumoniae,* hydrogen peroxide generation encourages the production of Ser-tRNA^{Ala} by AlaRS and Ser-tRNA^{Thr} by ThrRS which, in the absence of MurM, would severely damage the fidelity of protein synthesis. To test this hypothesis, future work should include investigation into the effects of hydrogen peroxide on the rate of mis-aminoacylation by *S. pneumoniae* AlaRS and ThrRS. In addition, the validity of this hypothesis could be confirmed if Ser-tRNA^{Thr} but not Thr-tRNA^{Thr} was a substrate for MurM. It is also likely that *in vivo, S. pneumoniae* MurM knockouts grown in the presence of an excess of serine would show reduced viability. However, this remains to be tested.

Additional evidence in support of the role of MurM in the maintenance of the fidelity of protein synthesis comes from an analysis of the phospholipid composition of the *S. pneumoniae* cell membrane in the presence and absence of hydrogen peroxide. In this study, cardiolipin was shown to increase the catalytic efficiency of $MurM_{159}$, $MurM_{R6}$ and $MurM_{Pn16}$ with Lipid II by 3-fold, 22-fold and 37-fold, respectively. Cardiolipin is one of the major phospholipids in the pneumococcal cell membrane and Pesakhov *et al.* (2007) have shown that its expression is regulated by hydrogen peroxide. Following a switch between aerobic and anaerobic growth conditions, the amount of cardiolipin in the pneumococcal membrane was found to decrease from 15.3 ± 0.9% to 8.2 ± 1.6% (Pesakhov *et al.*, 2007).

These findings have led to the hypothesis that, when *S. pneumoniae* is growing aerobically, the increase in hydrogen peroxide concentration would result in an up-regulation in the expression of cardiolipin in the pneumococcal membrane. This would subsequently stimulate the activity of MurM at a time when the pool of mis-aminoacylated Ser-$tRNA^{Ala}$ and Ser-$tRNA^{Thr}$ in the cell would presumably be at its highest. In order to fully test this hypothesis, future work should involve investigation into the effect of cardiolipin on the catalytic efficiency of MurM with Ser-$tRNA^{Ala}$ and also Ser-$tRNA^{Thr}$ if this is shown to be a substrate for the enzyme. $MurM_{159}$ E229A:E307A, which shows a markedly reduced affinity for magnesium, would presumably show a more pronounced difference in catalytic efficiency compared to the wild-type enzyme in this scenario.

In addition to this, the difference in response of $MurM_{159}$ and $MurM_{Pn16}$ to phosphatidylglycerol discovered by Dr Adrian Lloyd (University of Warwick)

suggests that the activity of MurM *in vivo* could be controlled by the ratio of cardiolipin to phosphatidylglycerol in the cell membrane. Thus, the ratio of these phospholipids in the cell membrane may influence the level of penicillin resistance expressed by a specific strain of *S. pneumoniae*. Future work to investigate this would involve an extensive analysis of the levels of phospholipids expressed in various penicillin-sensitive and penicillin-resistant strains of the organism. Several studies have already indicated that a 15-fold increase in lipid secretion occurs upon exposure of Streptococci to penicillin and that half of the material secreted is phosphatidylglycerol and cardiolipin (Horne *et al.*, 1977; Cabacungan and Pieringer, 1980; Brissette *et al.*, 1982; Brissette and Pieringer, 1985). Therefore, up and down regulation of phospholipids upon exposure of pneumococcus to various antibiotics should be fully investigated.

Investigation into the regio-specificity of MurM using a 2'-deoxy mini-helix analogue of $tRNA^{Ala}$ (Dr Adrian Lloyd, unpublished data) and a 2'-amino mini-helix analogue of $tRNA^{Ala}$ has indicated that MurM specifically accepts the amino acid from the 2' hydroxyl group of A^{76} on its aminoacylated tRNA substrate. This specificity is shared by the *W. viridescens* FemX enzyme which is also a member of the Fem ligase family (Fonvielle *et al.*, 2010). However, it contrasts with the specificity of the ribosome which utilises tRNA species that are aminoacylated on the 3' hydroxyl group of A^{76} (Weinger *et al.*, 2004). According to the work of Reese and Trentham (1965), spontaneous trans-esterification of the amino acid between the 3' and the 2' hydroxyl group ensures that these species exist in a 2:1 ratio at equilibrium. In addition, it has been estimated that spontaneous trans-esterification between the two hydroxyls occurs at a rate of 5 sec^{-1} (Taiji *et al.*, 1983). Given that

the values of apparent k_{cat} calculated for all three forms of MurM with Ala-tRNA^{Ala} and Ser-tRNA^{Ser} have been shown to be significantly less than 5 sec^{-1}, it is likely that spontaneous trans-esterification is able to support the activity of this enzyme. Thus the requirement for MurM to catalyse transfer of amino acids from the 3' to the 2' hydroxyl of A^{76} before it can catalyse transfer from the 2' hydroxyl to Lipid II is avoided.

In conclusion, the fact that MurM specifically accepts tRNA substrate that has been aminoacylated on the 2' hydroxyl of A^{76} and the ribosome accepts tRNA substrate that has been aminoacylated on the 3' hydroxyl of A^{76} may be exploited in the design of potent, specific inhibitors which have no detrimental effects on protein synthesis. Future work should include full characterisation of the inhibitory mechanism exerted by the 2'-amino mini-helix Ala-tRNA^{Ala} analogue on MurM. Investigation into the substrate specificity of MurM using mis-aminoacylated Ser-tRNA^{Ala} has also identified a possible role for MurM in the maintenance of the fidelity of protein synthesis. This has not been documented previously and would provide an explanation for the conservation of MurM functionality across all strains of *S. pneumoniae*.

Chapter 6

Towards an X-ray crystal structure of the MurM protein from *Streptococcus pneumoniae*

6.1. Introduction

Crystallography can be broadly defined as the process of determining the way in which atoms are arranged and bonded together within a crystalline solid. X-ray crystallography is the most widely used mechanism for determining the macromolecular structure of proteins with approximately 90% of all models placed in the protein data bank (PDB) determined using this technique. The remaining 10% of structures within the PDB have been solved by nuclear magnetic resonance (NMR) spectroscopy in solution (Rupp, 2010).

X-ray crystallography allows the fine details of molecular interactions to be determined at the atomic level and is important for structure-based drug design and clarification of enzymatic reaction mechanisms by relation of structure to function. The first visualisation of protein crystallisation was made with haemoglobin in 1840 after Hünefeld pressed earthworm blood between two glass microscopy slides and allowed it to dry.

Regardless of the method used, the process of crystallisation can be split into two separate phases: nucleation and growth. In the nucleation phase, a mass of aggregated material of a critical size forms a pre-requisite for crystal growth. The initiation of both of these processes requires phase-transition of the aqueous protein

solution into the supersaturation zone as illustrated in Figure 6.1 (Chayen *et al.*, 2010).

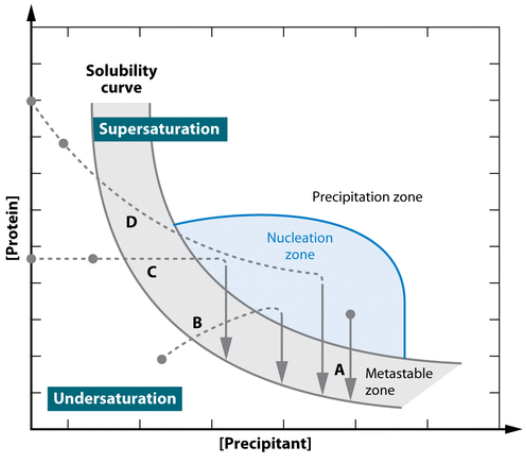

Figure 6.1: Protein crystallisation phase diagram based on variation of the concentration of the protein and the precipitant. The four major crystallisation methods illustrated on this diagram are (A) Batch crystallisation, (B) Vapour diffusion, (C) Dialysis and, (D) free-interface diffusion. Regardless of the method, crystal growth requires transition into the nucleation zone. This is followed by transition into the metastable zone and, finally, arrival at the solubility curve. Note that the grey circles represent the starting points of the protein solution. Taken from Chayen (1998) and Li and Ismagilov (2010).

As shown in Figure 6.1, the supersaturation zone can be further subdivided into the nucleation, precipitation and metastable zones. In the nucleation zone, the concentration of the protein is sufficient to enable spontaneous formation of nucleation points from which crystals can grow. However, if the protein concentration is too high, transition into the precipitation zone will occur resulting in rapid nucleation and crystal growth. This can lead to the formation of crystals with disordered structures as well as the formation of precipitates and aggregated material. In the metastable zone, the protein concentration is too low to support the generation of new nucleation points. However, continuous growth of pre-existing crystals is still supported. Transition between these different zones is influenced by many factors including temperature, pH, precipitant concentration, protein concentration and the addition of additives. Therefore, understanding the phase

transition process can provide a basis for the design of successful crystallisation experiments (Chayen *et al.*, 2010; Li and Ismagilov, 2010).

So far the structures of only two members of the Fem ligase family have been successfully solved by X-ray crystallography. They are the FemX protein from *W. viridescens* (Biarrotte-Sorin *et al*. 2004) and the FemA protein from *S. aureus* (Benson *et al*. 2002). The structures of these enzymes have been presented and discussed in Chapter 1 sections 1.7 and 1.4.2, respectively.

In summary, the 2.1 Å X-ray crystal structure of FemA demonstrated that the protein is comprised of two domains. Domain I adopts a globular structure, whilst domain II adopts a helical structure. Further analysis of domain I by Benson *et al*. (2002) indicated that it could be further divided into sub-domains 1A and 1B, the latter of which was found to correspond to a deep channel suitable for the binding of Lipid II-Gly. In addition, acquisition of the structure of FemA has indicated that the tRNA substrate is likely to be bound by the enzyme in the region located at the junction between domains I and II. It has been proposed that the coiled helical arm within domain II is responsible for tethering the aminoacylated-tRNA molecule in the correct position for catalytic transfer of the amino acid to Lipid II. However, more structural information is required to formally prove this.

In contrast to FemA, the FemX protein from *W. viridescens* accepts the soluble UDP-MurNAc pentapeptide as its substrate. When the structure of this protein was solved by Biarrotte-Sorin *et al*. (2004) it became clear that FemX is comprised of two equivalent domains which are joined together by the UDP-MurNAc binding

cleft. Interestingly, unlike FemA, these studies have shown that FemX does not have a coiled helical arm. This subsequently led to the decision to further sub-divide the Fem ligase family into two groups based upon the presence or absence of this structural feature. Currently it is known that *S. aureus* FemA, which does have a coiled helical arm in its structure, belongs to subgroup I. Subgroup I is predicted to comprise a large proportion of the 50 described FemXAB-related sequences including those found within the genera *Streptococcus* and *Enterococcus* (Rohrer and Berger-Bächi, 2003b). In contrast to this, FemX belongs to subgroup II, which is also predicted to contain the Fem-like proteins identified in *Streptomyces coelicolor*. However, further structural information is required to validate this classification system and to elucidate the general catalytic mechanism of Fem ligases.

As a result of this, obtaining high resolution crystal structures of other important members of the Fem ligase family, including the FemX protein from *S. aureus* and the MurM protein from *S. pneumoniae*, is of great importance. The acquisition of such information would enable a greater understanding of the links between the structure and function of these enzymes to be derived which, in turn, would be beneficial to the design of novel inhibitory compounds.

6.2. Aims

Given that there is no X-ray crystal structure available for MurM, or indeed *S. aureus* FemX and FemB, one of the goals of this project was to attempt to achieve this. This work encompassed the following aims:

- Development of a protocol to enable successful concentration of MurM to 10 mg mL^{-1} so that crystallisation screens could be carried out. Previous work

carried out on the protein at University of Warwick had suggested that it became unstable and precipitated at concentrations of above 3 mg mL^{-1}

- Cloning, expression and purification of *S. aureus* FemB
- Identification of suitable conditions for MurM, FemX and FemB crystal nucleation and growth using 96-well screens
- Expansion of initial hits identified from 96-well screens to produce single, diffraction quality crystals of MurM, FemX and FemB

In order to meet these aims a scheme was developed for crystallisation of these proteins. In each case, the procedures outlined in Figure 6.2 were followed in the order given.

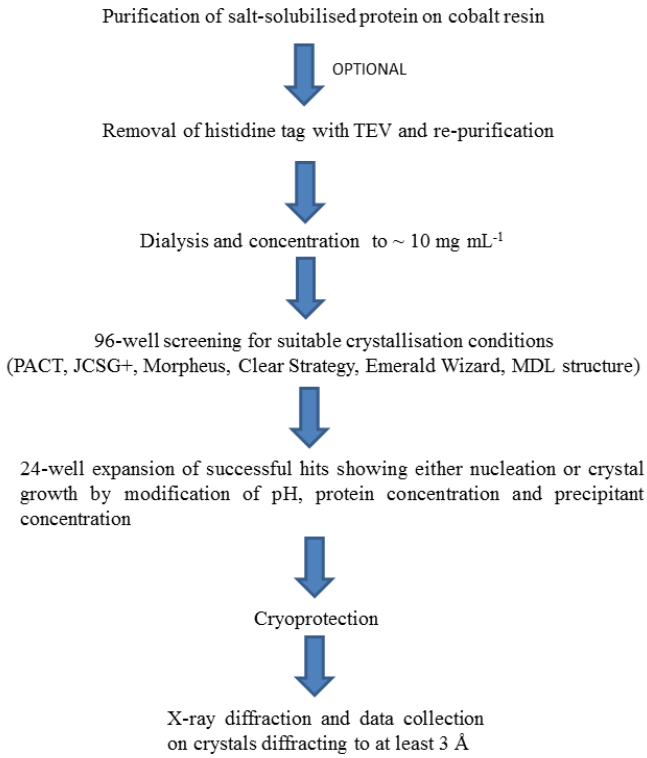

Figure 6.2: Schematic flow diagram showing the procedure followed for crystal formation, optimisation and refinement in this study. This process was applied to the *Streptococcus pneumoniae* MurM protein and the *Staphylococcus aureus* FemX and FemB proteins for which there are no existing crystallisation conditions or structures in the literature.

In addition to the above aims, work carried out in Chapter 4 lead to the requirement to repeat crystallisation of *S. aureus* FemA despite the availability of a 2.1 Å structure in the literature (Benson *et al*. 2002). This was to enable identification of the metal ion binding sites within the protein. All crystals were subjected to cryo-protection, as described in Chapter 2, section 2.6.3.6, prior to X-ray diffraction experiments. Unless otherwise stated, this process involved soaking each crystal for 1 min in mother liquor substituted with 30% (v/v) glycerol prior to immersion in liquid nitrogen.

6.3. Crystallisation of the MurM protein from *Streptococcus pneumoniae* strains R6, Pn16 and 159

6.3.1. 96-well crystallisation screening with MurM

During attempts to concentrate MurM to 10 mg mL^{-1} for the purpose of 96-well crystallisation screening, it was noted that the protein repeatedly precipitated out of solution when a concentration of 3.5 mg mL^{-1} was reached. This problem was alleviated by supplementation of the concentration buffer with 20% (w/v) glycerol. Glycerol has also been found to be a necessary component for maintenance of stability at high protein concentrations when *S. aureus* FemA was crystallised (Benson *et al*., 2002).

Initially, all three forms of MurM were concentrated to 10 mg mL^{-1} in buffer containing 50 mM HEPES pH 7.0, 100 mM NaCl and 20% (w/v) glycerol prior to use in 96-well crystallisation trials set up as described in Chapter 2, section 2.6.3.1. Regardless of whether or not the proteins were histidine-tagged, crystal formation was only observed for $MurM_{Pn16}$ and completion of crystal growth required

incubation of the trays at 18°C for two weeks. Therefore, all crystallisation images presented in this chapter were generated using dodeca-histidine tagged $MurM_{Pn16}$ at a starting concentration of 10 mg mL^{-1} and are intended to be representative of the results obtained with hexa-histidine tagged and untagged protein as well. The two successful mother liquors resulting in nucleation and crystal growth of $MurM_{Pn16}$ were identified as Emerald Wizard condition H4 (0.1 M imidazole pH 8.0, 0.2 M $Zn(OAc)_2$ and 20% w/v PEG 3 K) and MDL structure condition G3 (0.1 M MES pH 6.5, 0.01 M zinc sulphate heptahydrate and 25% v/v PEG monomethylether 550) as shown in Figure 6.3.

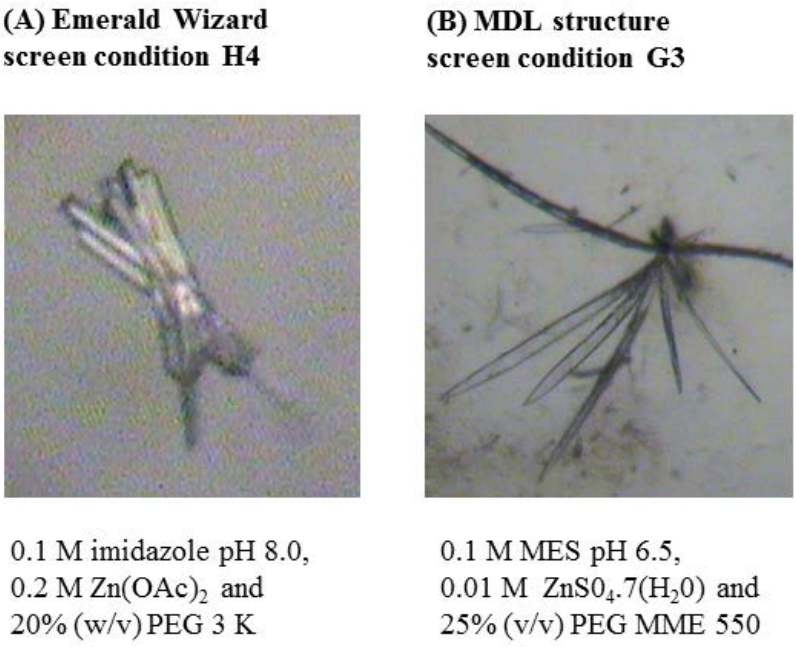

Figure 6.3: Results of 96-well crystallisation screens carried out on $MurM_{Pn16}$ concentrated to 10 mg mL^{-1} in 50 mM HEPES pH 7.0, 100 mM NaCl and 20% (w/v) glycerol. Despite the use of 6 different screens (PACT, JCSG+, Morpheus, Clear Strategy, Emerald Wizard and MDL Structure) and 3 different forms of the protein (un-tagged, hexa-histidine tagged and dodeca-histidine tagged) only two conditions were found to be successful. Pictures shown are for dodeca-histidine tagged $MurM_{Pn16}$. Complete removal of the tag or reduction of the length of the tag to 6 histidine residues had no effect on crystal morphology. Each crystal shown in this figure was approximately 20 µm in length.

As shown in Figure 6.3, initial 96-well screens carried out on $MurM_{Pn16}$ resulted in the growth of small crystal clusters in only two conditions, both of which contained zinc. Improvements in crystal size and morphology could not be achieved by replacement of dodeca-histidine tagged protein with either un-tagged or hexa-histidine tagged protein making 24-well refinement of the conditions essential.

6.3.2. 24-well refinement of suitable crystallisation conditions for $MurM_{Pn16}$

Refinement of MDL structure condition G3 was carried using the 24-well plate set-up described in Chapter 2, section 2.6.3.2. Minor adjustments were made to both the pH of the MES buffer and the final concentration of PEG MME 550. The final concentration of PEG MME 550 was varied across the plate from 20% to 30% in a total of six 2% increments. The pH of 0.1 M MES was increased going down the plate in 4 steps to give pH 5.5, pH 6.0, pH 6.5 and pH 6.8. The results of this process, after incubation of the tray at 18^{o}C for two weeks, are shown in Figure 6.4.

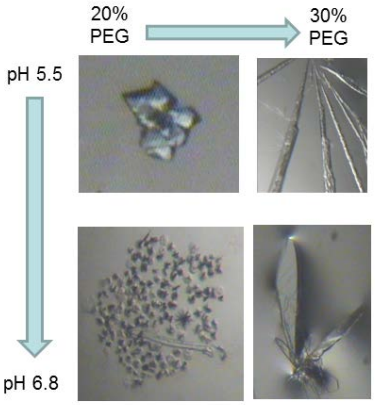

Figure 6.4: Results of refinement of MDL structure condition G3 using the 24-well plate set-up described in Chapter 2. The final concentration of zinc sulphate heptahydrate was kept constant at 0.01 M. The final concentration of MES was kept at 0.1 M but the pH was varied between 5.5 and 6.8. The final concentration of PEG MME 550 was varied between 20% and 30% across the plate in 2% increments. The length of the crystals shown in this figure varied from 5 µM for each small cluster on the left to 500 µm for those on the right.

As indicated in Figure 6.4, refinement of MDL structure condition G3 indicated that, when the concentration of PEG MME 550 was increased from the original 25% (v/v) to 30% (v/v), crystal growth to a size suitable for diffraction experiments was encouraged regardless of pH. In contrast to this, reduction in the final concentration of PEG MME 550 to 20% (v/v) caused an increase in nucleation either from a single point (pH 5.5) or from multiple points (pH 6.8) generating crystals that were unsuitable for diffraction. Unfortunately, the crystals grown in mother liquor consisting of either 0.1 M MES pH 5.5 or pH 6.8, 0.01 M zinc sulphate heptahydrate and 30% (v/v) PEG MME 550 (Figure 6.4) did not produce any diffraction upon exposure to X-rays. As a result of this, the small crystal clusters grown under the initial G3 condition were using in seeding experiments to improve crystal morphology.

6.3.3. Refinement of $MurM_{Pn16}$ crystal morphology and diffraction by seeding

To generate a $MurM_{Pn16}$ crystal seed stock, a single crystal from Figure 6.3 (B) was extracted from the cluster and placed into an Eppendorf tube containing 50 µL of mother liquor as described in Chapter 2, section 2.6.3.3. Liquid and horse hair crystal seeding were carried out in the 24-well format used for refinement of MDL structure condition G3. Variations in the concentration of PEG MME 550 were made across the plate and variations in the pH of 0.1 M MES were made down the plate as described before in section 6.3.2. The effects of seeding on the morphology of $MurM_{Pn16}$ crystals are shown in Figure 6.5.

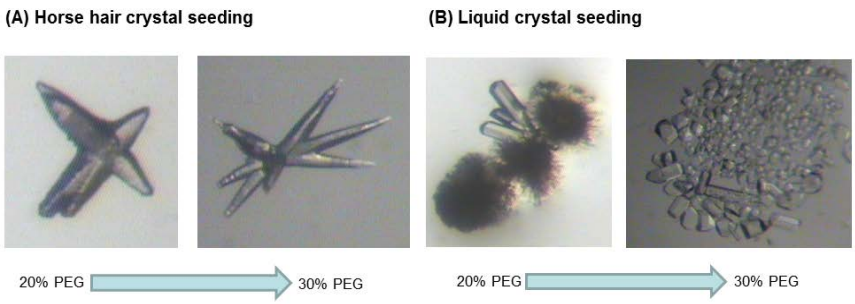

Figure 6.5: Changes in the crystal morphology of $MurM_{Pn16}$ induced by horse hair and liquid seeding. The crystals shown in this figure were obtained at pH 5.5. The length of crystal obtained after horse hair seeding was approximately 20 µm after removal of one crystal from the cluster. The length of crystal obtained after liquid seeding was between 50 µm and 100 µm. All crystals obtained by seeding were of a suitable size for diffraction using the I24 microfocus beamline at Diamond Light Source (Oxfordshire, UK).

As shown in Figure 6.5, seeding experiments resulted in an overall improvement in the size of $MurM_{Pn16}$ crystals which appeared to be independent of the pH of 0.1 M MES used. Liquid crystal seeding also resulted in the formation of single crystals as opposed to clusters. However, despite the vast improvements in morphology, none of the crystals shown in Figure 6.5 gave a diffraction pattern upon exposure to X-rays. Further attempts to improve diffraction were carried using two additive screens (Silver Bullets and Hampton Additive) and mother liquor equivalent to that of MDL structure screen condition G3.

6.3.4. Refinement of $MurM_{Pn16}$ crystal morphology and diffraction using additive screens

Both the Silver Bullets and the Hampton Additive screen (Hampton Research) were set up with $MurM_{Pn16}$ using mother liquor comprising 0.1 M MES pH 6.5, 0.01 M zinc sulphate heptahydrate and 25% (v/v) PEG MME 550 and the methodology described in Chapter 2, section 2.6.3.4. The Silver Bullets screen consists of a library of molecules that promote the formation of a well-structured crystal lattice by

stabilising the protein and encouraging the formation of lattice contact points. In comparison, the Hampton Additive screen is designed to improve crystal formation by modifying the solubility of the protein sample. Changes in $MurM_{Pn16}$ crystal morphology were only observed with the Silver Bullets screen (Figure 6.6).

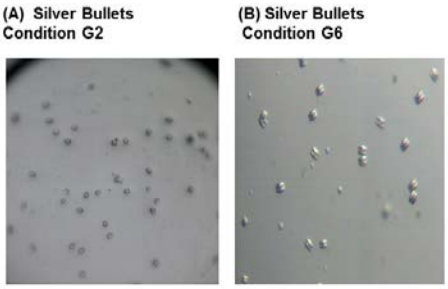

Figure 6.6: Silver Bullets screen refinement of the morphology of $MurM_{Pn16}$ crystals. Silver Bullets condition G2 consisted of 0.20% (w/v) 2-2'-Thiodiglycolic acid, 0.20% (w/v) Adipic acid, 0.20% (w/v) Benzoic acid, 0.20% (w/v) Anhydrous oxalic acid, 0.20% (w/v) Terephthalic acid and 0.02 M HEPES sodium pH 6.8. Silver Bullets condition G6 consisted of 0.16% (w/v) Glutaric acid, 0.16% (w/v) Mellitic acid, 0.16% (w/v), Anhydrous oxalic acid, 0.16% (w/v) Pimelic acid, 0.16% (w/v) Sebacic acid, 0.16% (w/v) Trans-cinnamic acid and 0.02 M HEPES sodium pH 6.8. The maximum length of crystals obtained using this technique was 10 µm.

The crystals obtained using the Silver Bullets screen were of a suitable size for diffraction analysis on the I24 microfocus X-ray beamline at Diamond Light Source (Oxfordshire, UK). However, no diffraction was detected from these crystals. Exhaustion of refinement methods lead to re-attempts at crystallisation of $MurM_{Pn16}$ after concentration of the protein to 10 mg mL^{-1} into the buffer system that enabled Benson *et al.* (2002) to obtain diffraction-quality crystals of *S. aureus* FemA.

6.3.5. Crystallisation screening and refinement for $MurM_{Pn16}$ after concentration of the protein to 10 mg mL^{-1} into buffer containing 50 mM ethanolamine pH 10.0, 100 mM NaCl and 20% (w/v) glycerol

In order to obtain other possible crystallisation conditions for $MurM_{Pn16}$, zinc chloride was added at the protein purification stage to a final concentration of 50 µM in the 50 mM and 200 mM imidazole wash buffers used during elution of the protein from cobalt resin (modification to the method described in Chapter 2, section 2.4.1 only used for the purpose of ensuring MurM was saturated with zinc prior to crystallisation attempts).

To maintain stability, purified protein was then dialysed against 50 mM ethanolamine pH 10.0, 100 mM NaCl and 20% glycerol prior to concentration to 10 mg mL^{-1} as described in Chapter 2, sections 2.4.5 and 2.4.8. 96-well screening using this protein resulted in the identification of two additional crystallisation conditions: 0.2 M magnesium formate, 20% (v/v) PEG 3350 (JCSG+ screen, condition A5) and 0.1 M Tris pH 8.5, 0.2 M calcium acetate, 25% (v/v) PEG 2 K MME (Clear Strategy pH 7.5-8.5 screen, condition G5). Images of crystals grown under these conditions are shown in Figure 6.7.

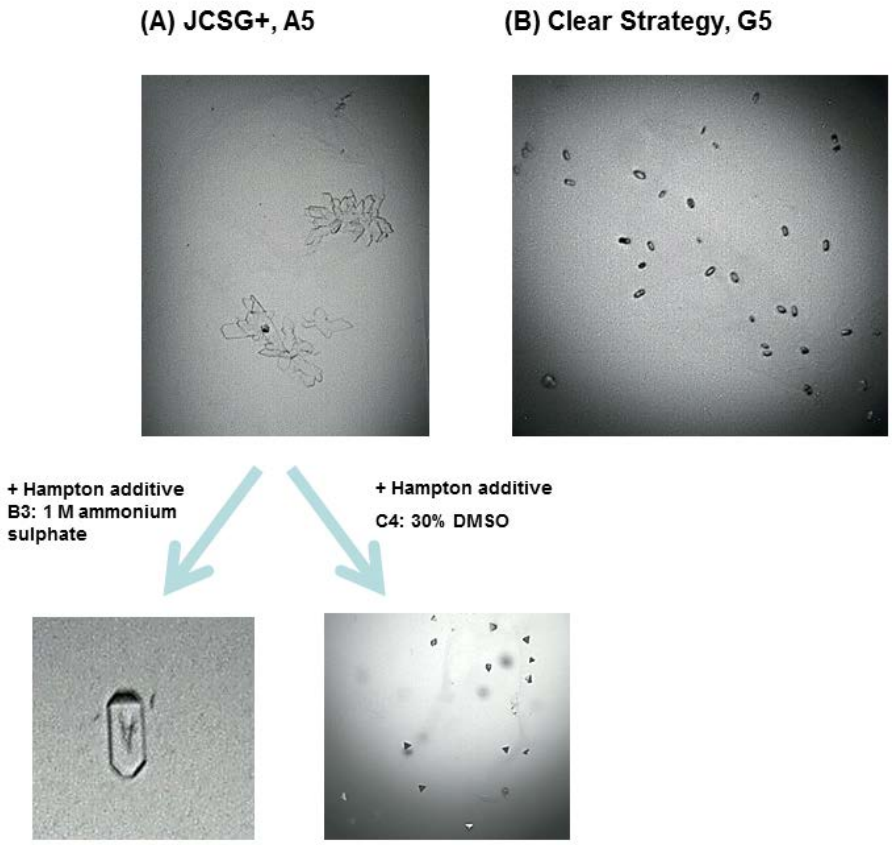

Figure 6.7: Results of 96-well crystallisation screens carried out on zinc-saturated $MurM_{Pn16}$ concentrated to 10 mg mL^{-1} in 50 mM ethanolamine pH 10.0, 100 mM NaCl and 20% (w/v) glycerol. Successful conditions were JCSG+ condition A5 consisting of 0.2 M magnesium formate and 20% (w/v) PEG 3350 and Clear Strategy condition G5 consisting of 0.1 M Tris pH 8.5, 0.2 M calcium acetate and 25% (w/v) PEG 2 K MME. Refinement of crystal morphology was achieved with the latter condition using the Hampton Additive screen. Pictures shown are for dodeca-histidine tagged $MurM_{Pn16}$. Complete removal of the tag or reduction of the length of the tag to 6 histidine residues had no effect on crystal morphology. The maximum length of crystals obtained using this technique was 20 µm.

As shown in Figure 6.7, concentration of $MurM_{Pn16}$ into the buffer system used for successful crystallisation of FemA resulted in identification of an additional two potential conditions supporting nucleation and crystal growth (Benson *et al.*, 2002). Condition A5 in the JCSG+ screen resulted in the formation of crystal plates which could be encouraged to form single crystals by the use of the Hampton Additive screen. Unfortunately, none of the crystals shown in Figure 6.7 gave a diffraction

pattern when tested on the I24 microfocus X-ray beamline at Diamond Light Source (Oxfordshire, UK). This led to the decision to undertake rational surface mutagenesis of MurM as a last resort for generating diffraction quality crystals of the enzyme in its un-liganded form (Derewenda, 2004; Derewenda and Vekilov, 2005).

6.3.6. Rational surface mutagenesis of the MurM protein from *Streptococcus pneumoniae* strains Pn16 and 159

It has been estimated that, on average, fewer than 30% of all the soluble proteins expressed by *E. coli* can be crystallised and, subsequently, only a small portion of these will diffract to a resolution of 2 Å or better (Dale *et al.*, 2003; Derewenda, 2004). In the case of proteins that will either not crystallise at all or produce crystals of poor quality, modification of the sample, usually by site-directed mutagenesis, is the only option.

Rational surface mutagenesis is specifically designed to reduce the overall entropy on the surface of a protein by replacing polar amino acids, such as lysine and glutamate, with other amino acids that have a smaller side chain, such as alanine. This can promote the development of contact-forming surface patches during protein folding that are homogeneous in terms of their conformation and which can subsequently aid crystal lattice formation (McElroy *et al.*, 1992; Derewenda, 2004). When applied to human RhoGDI protein, crystals formed using a double surface entropy mutant (K199-200R) exceeded the diffraction of crystals formed from the wild-type enzyme by approximately 1 Å. This resulted in the generation of a high resolution X-ray crystal structure for this protein (Czepas *et al.*, 2004).

Goldschmidt *et al.* (2007) have developed a server (SERp) that is designed to predict suitable residues within proteins whose mutation could facilitate crystallisation by causing reduction in surface entropy. The suggested residues for mutation are predicted by the server using an algorithm that takes into account conformational entropy, secondary structure predictions and sequence conservation. When the protein sequences of $MurM_{159}$ and $MurM_{Pn16}$ (see Chapter 3) were loaded onto the SERp server, five possible mutational clusters were identified in each case and these are shown in Figure 6.8 using the model of MurM as a guideline for their locations.

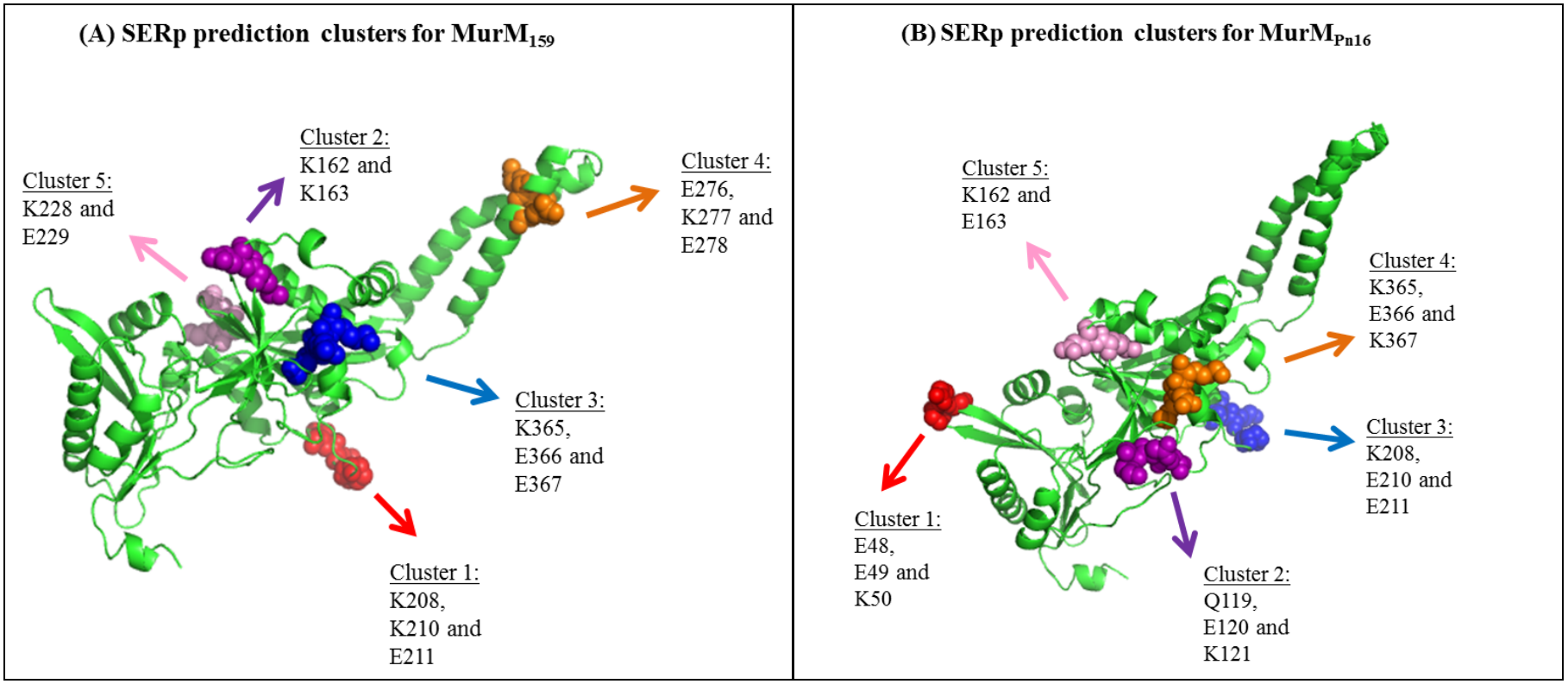

Figure 6.8: SERp predicted residue clusters within (A) $MurM_{159}$ and (B) $MurM_{Pn16}$. Mutation to alanine of every residue comprising a cluster is predicted to result in a reduction in surface entropy and therefore improvements to crystal lattice formation. The SERp score, indicating predicted success of the mutations, decreases moving from cluster 1 to cluster 5 and was as follows for $MurM_{159}$ and $MurM_{Pn16}$, respectively: Cluster 1: 6.15 and 7.12, Cluster 2: 5.49 and 6.13, Cluster 3: 5.44 and 6.03, Cluster 4: 4.85 and 5.43 and, Cluster 5: 4.83 and 5.34. The SERp server can be found at http://www.doe-mbi.ucla.edu/Services/SER (Goldschmidt *et al.*, 2007).

In the case of both $MurM_{Pn16}$ and $MurM_{159}$, the dodeca-histidine tagged pET22b::MurM expression constructs were used as templates for making two site-directed mutants of each protein: one mutated at each of the residues in cluster 1 and the other mutated at each of the residues in cluster 2. The methodology and primer sequences used in this process are shown in Chapter 2, section 2.2.9 and Table 2.3, respectively. Acquisition of expression constructs harbouring the correct mutations was determined by DNA sequencing as described in Chapter 2, section 2.2.11. Expression and purification of each mutant MurM protein were carried out as described in Chapter 3 for the wild-type enzymes with no significant differences in overall yield or purity.

After concentration of each MurM mutant to 10 mg mL^{-1} into buffer containing either 50 mM HEPES pH7.0, 100 mM NaCl and 20% (w/v) glycerol or 50 mM ethanolamine pH 10.0, 100 mM NaCl and 20% (w/v) glycerol, 96-well crystallisation screens were set up as described in Chapter 2, section 2.6.3.1. In the case of $MurM_{159}$, mutation of cluster 1 residues or cluster 2 residues to alanine still did not enable the protein to crystallise under any of the tested conditions. In the case of $MurM_{Pn16}$, the equivalent mutations of cluster 1 or cluster 2 residues to alanine resulted in no improvement to the morphology or size of crystals obtained. This suggested that acquisition of a high resolution crystal structure of MurM might require mutation of residues within multiple clusters at the same time or that inherent properties of the protein prevent successful crystallisation in an un-liganded form.

6.4. Crystallisation of the FemX protein from *Staphylococcus aureus* strain Mu50

Given the difficulties encountered in obtaining a high resolution X-ray crystal structure of MurM, attempts were made to crystallise the *S. aureus* equivalent of this protein, FemX. Prior to crystallisation, salt-solubilised FemX was purified and separated from its histidine tag as described in Chapter 4. Purified protein was dialysed against buffer containing 50 mM ethanolamine pH 10.0, 100 mM NaCl and 20% (w/v) glycerol, concentrated to 12 mg mL^{-1} and used in 96-well crystallisation screens as described for MurM. After incubation of the trays for 1 week at 18^{o}C, small rod clusters were identified in the Morpheus screen under condition A1 (0.1 M imidazole-MES buffer mix pH 6.5, 0.06 M $MgCl_2$; $CaCl_2$ divalent metal ion mix and 30% PEG MME 550_PEG 20 K mix) as shown in Figure 6.9.

Figure 6.9: Image of *Staphylococcus aureus* FemX crystals formed at 18^{o}C under condition A1 in the Morpheus screen (0.1 M imidazole-MES buffer mix pH 6.5, 0.06 M $MgCl_2$; $CaCl_2$ divalent metal ion mix and 30% PEG MME 550_PEG 20 K mix) after concentration of untagged protein to 12 mg mL^{-1} in 50 mM ethanolamine pH 10.0, 100 mM NaCl and 20% (w/v) glycerol. The maximum length of a single crystal within each rod cluster was approximately 5 µm.

In addition to this, quasi-crystals had formed under three conditions in the Emerald Wizard screen: E1 (0.1 M acetate pH 4.5, 0.2 M zinc acetate and 10% (w/v) PEG 3

K), H4 (0.1 M imidazole pH 8.0, 0.2 M zinc acetate and 20% (w/v) PEG 3 K) and F8 (0.1 M MES pH 6.0, 0.2 M zinc acetate and 15% (v/v) ethanol). All three of these conditions contained zinc. Development of micro-crystals from the quasi-crystals could only be achieved by mixing FemX with a molar equivalent of cardiolipin (Invitrogen) prior to 96-well screening as shown in Figure 6.10.

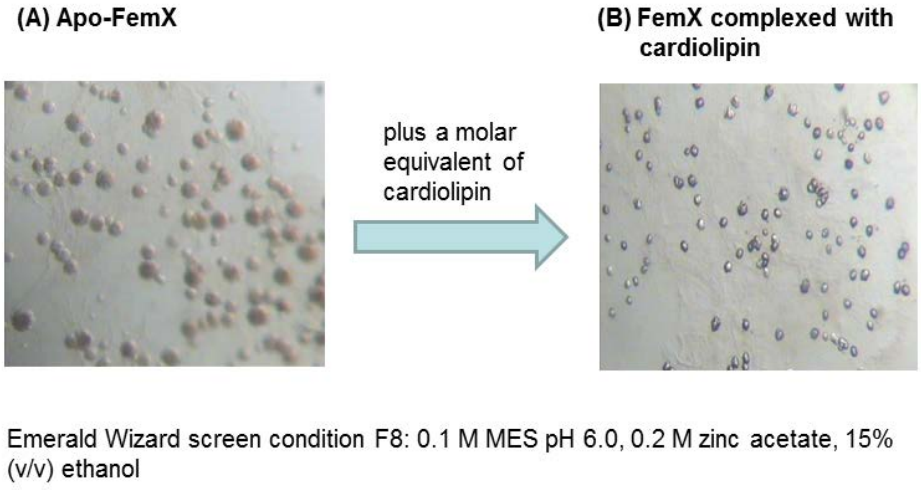

Figure 6.10: Image of *Staphylococcus aureus* FemX crystals formed at 18^{o}C under condition F8 in the Emerald Wizard I and II screen after concentration of untagged protein to 12 mg mL^{-1} in 50 mM ethanolamine pH 10.0, 100 mM NaCl and 20% (w/v) glycerol. The maximum length of the micro-crystals obtained after addition of a molar equivalent of cardiolipin to FemX prior to re-screening, was approximately 2 µm.

Due to the fragile natural and small size of the FemX crystals, it was not possible to carry out any diffraction experiments. However, the preliminary results presented in Figures 6.9 and 6.10 are promising and further screening using the 24-well plate setup described in Chapter 2, section 2.6.3.2 may be all that is necessary to improve crystal size and quality.

6.5. Crystallisation of the FemB protein from *Staphylococcus aureus* strain Mu50

Given the difficulties encountered during attempts to obtain a crystal structure of MurM and the formation of either quasi-crystals or small rod clusters in the case of FemX, it was decided that crystallisation of FemB should be trialled as a means of gaining more structure information about members of the Fem ligase family as a whole.

The X-ray crystal structure of the *S. aureus* FemA protein has already been solved by Benson *et al*. (2002) and, whilst FemX is only 36% homologous and 23% identical to this protein, FemB is 52% homologous and 39% identical to FemA. Therefore, FemB is proposed to have greater structural similarity to FemA than FemX. It was thus proposed that the levels of homology between the latter two proteins would increase the chances of successfully solving the structure of FemB by molecular replacement with the published structure of FemA (Benson *et al.*, 2002). This would avoid the need for multi-wavelength anomalous diffraction (MAD) phasing if good quality crystals of FemB could be produced, providing a major motivation for this work to be undertaken.

6.5.1. Cloning of *FemB* into pET28a

The *femB* gene from *S. aureus* strain Mu50 was cloned into the expression vector pET28a to encode a TEV-cleavable C-terminal hexa-histidine fusion tag for purification. PCR amplification of *femB* from chromosomal DNA was achieved using Accuprime *Taq* DNA polymerase (Invitrogen) and primer numbers 14 and 15 shown in Chapter 2, Table 2.2. After purification, the PCR product was digested

with *Bsa*I and *Xho*I prior to ligation into gel-extracted *Nco*I/*Xho*I restricted pET28a as described in Chapter 2, sections 2.2.4 to 2.2.7. After transformation into *E. coli* Top10 cells, plasmid DNA was extracted from a series of potential clones and those containing the *femB* insert were identified by *Xba*I/*Xho*I digestion, as shown in Figure 6.11.

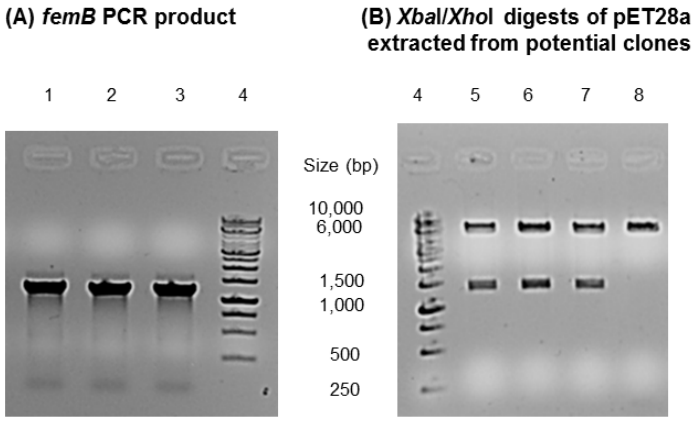

Figure 6.11: Summary agarose gels showing (A) PCR amplification of *femB* from *Staphylococcus aureus* Mu50 chromosomal DNA and (B) *Xba*I/*Xho*I digests of plasmid DNA extracted from 4 potential pET28a::FemB clones. The size of the pET28a vector is 5,369 bp. The size of the *femB* gene is 1,260 bp.

Lanes 1-3 - *femB* PCR product,
Lane 4 – 1 kb ladder,
Lanes 5-8 – *Xba*I/*Xho*I digests of plasmid DNA extracted from clones 1 to 4.

As shown in Figure 6.11, the *femB* gene had successfully inserted into pET28a in three out of the four potential clones tested by *Xba*I/*Xho*I digestion. Further confirmation of insertion of *femB* into pET28a was obtained by DNA sequencing using the T7 forward and T7 reverse primers, as described in Chapter 2, section 2.2.11.

6.5.2. Expression, salt-solubilisation and purification of FemB

For determination of optimal FemB expression conditions, the final construct was transformed into both *E. coli* B834 (DE3) and BL21 Star (DE3).placIRare2

expression strains. Levels of protein expression were investigated after IPTG-induction at 25^{o}C for 4 h, as described in Chapter 2, section 2.3.3. Crude extracts were obtained from these cultures by sonication at 10% power for 15 sec and centrifugation to obtain both soluble and insoluble fractions. Bradford reagent was used to determine the protein concentration of the crude extracts so that 25 µg of protein were loaded into each lane of a 12.5% SDS PAGE gel (Chapter 2, section 2.4.9). Results of this experiment are shown in Figure 6.12.

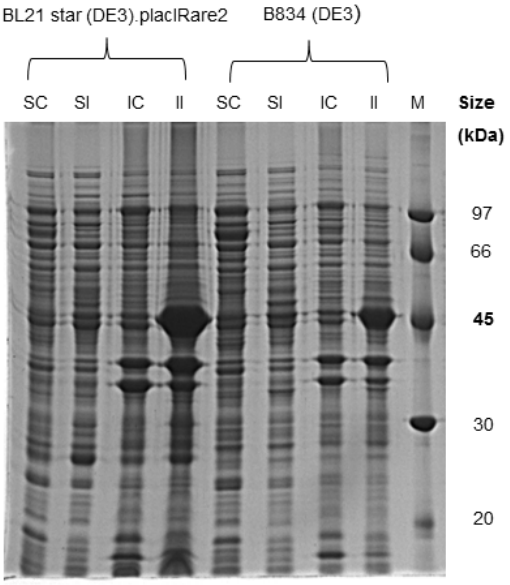

M - molecular weight standards,
SC - soluble proteins expressed by non-induced cells,
SI - soluble proteins expressed by induced cells,
IC - insoluble proteins expressed by non-induced cells,
II - insoluble proteins expressed by induced cells.

Figure 6.12: 12.5% SDS PAGE gel showing the crude extracts obtained from *E. coli* B834 (DE3) and *Escherichia coli* BL21 Star (DE3).placIRare2 cells transformed with pET28a::FemB and induced to express protein by IPTG-induction at 25^{o}C for 4 h. The molecular weight of FemB is 49,676 Daltons.

As shown in Figure 6.12, FemB was expressed in an insoluble form regardless of the *E. coli* expression strain used. However, out of the two *E. coli* expression strains tested, the overall yield of FemB was higher in BL21 Star (DE3).placIRare2 cells.

Therefore this strain was selected as the most suitable host for large-scale expression of the protein. Large-scale expression, salt-solubilisation, purification and removal of the histidine tag from FemB using TEV protease were carried out as described for FemA in Chapter 4, sections 4.5.4 to 4.5.6, with equal success. The overall purity of FemB protein used for crystallisation is shown in Figure 6.13.

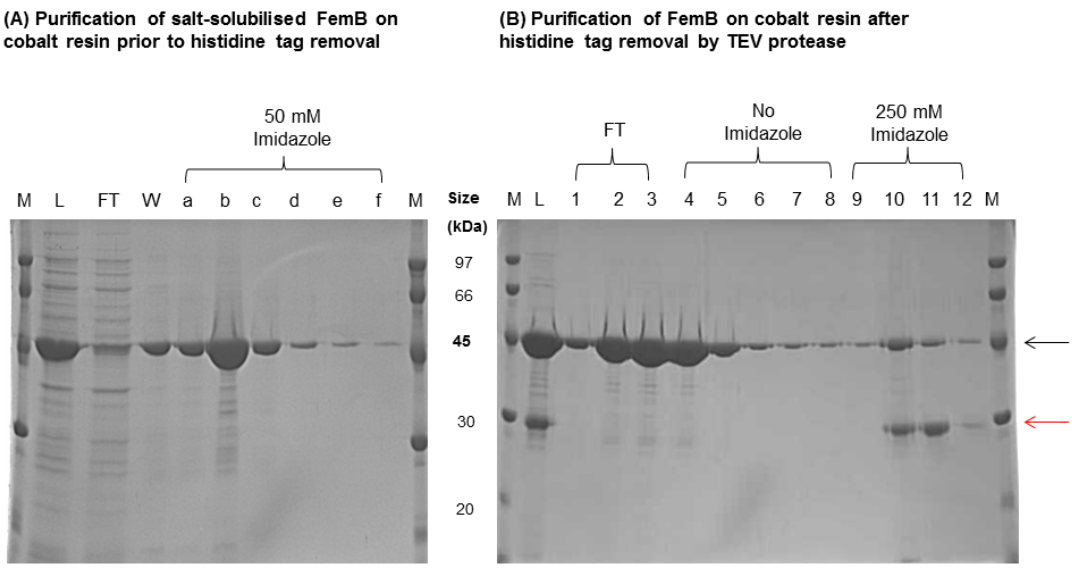

M - molecular weight standards,
L - a sample of the protein before loading onto the column,
FT - flow-through from the column as the protein is loaded onto it and,
W – protein eluted from the column during wash with equilibration buffer.

Figure 6.13: 12.5% SDS PAGE gels showing purification of (A) salt-solubilised FemB from 1 L of *Escherichia coli* BL21 Star (DE3).placIRare2 cells transformed with pET28a::FemB and induced to express protein by IPTG-induction at 25°C for 4 h on cobalt resin and, (B) FemB on cobalt resin after incubation with TEV protease to remove the C-terminal hexa-histidine tag. The position of eluted FemB is indicated with a black arrow. The position of hexa-histidine tagged TEV protease during wash with buffer containing 250 mM imidazole is indicated with a red arrow in (B).

As was the case with the *S. aureus* FemX and FemA proteins, hexa-histidine tagged FemB eluted from cobalt resin pre-equilibrated as described in Chapter 2, section 2.4.1, during wash with buffer supplemented with 50 mM imidazole. After purification of the FemB::TEV protease digest on cobalt resin, untagged FemB was

dialysed against 50 mM ethanolamine pH 10.0, 100 mM NaCl and 20% (w/v) glycerol and concentrated to 13 mg mL^{-1} as described in Chapter 2, section 2.4.8 for use in 96-well crystallisation screens.

6.5.3. 96-well crystallisation screening and 24-well refinement of suitable conditions for FemB: towards a high resolution X-ray crystal structure

96-well crystallisation screens were set up for FemB as described for MurM and FemX. After incubation of the trays at 18^{o}C for two weeks, crystals were found under three conditions: JCSG+ screen condition A5 (0.2 M magnesium formate and 20% (w/v) PEG 3350), Clear Strategy pH 7.5 - 8.5 screen condition G6 (0.1 M Tris pH 8.5, 0.2 M calcium acetate and 15% (w/v) PEG 4 K) and, PACT screen condition D10 (0.1 M Tris pH 8.0, 0.2 M magnesium chloride and 20% (w/v) PEG 6 K). Images of the FemB crystals formed as a result of these experiments are shown in Figure 6.14.

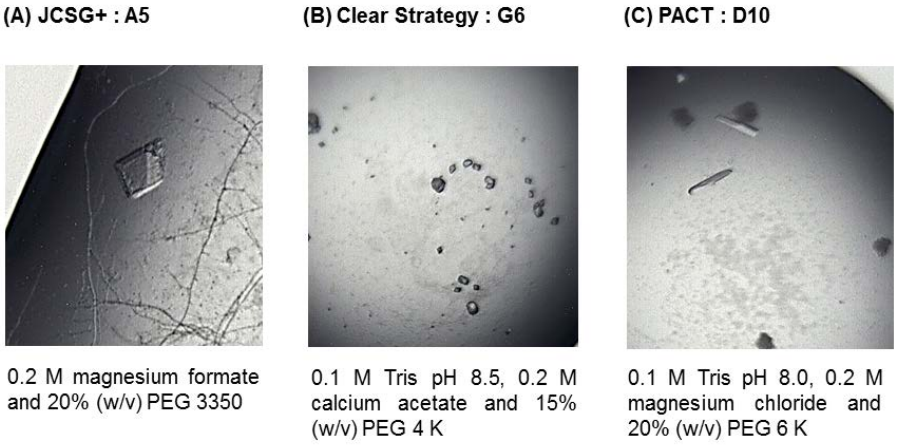

Figure 6.14: Images of FemB crystals obtained after 96-well screens were set up at 18^{o}C using untagged protein dialysed against 50 mM ethanolamine pH 10.0, 100 mM NaCl and 20% (w/v) glycerol and concentrated to 13 mg mL^{-1}. The maximum crystal length obtained under Clear Strategy condition G6 was 5 µm. In contrast to this, the maximum crystal length obtained under JCSG+ condition A5 and PACT condition D10 was 50 µm.

For the purpose of cryo-protection, each crystal shown in Figure 6.14 was subjected to a 1 min soak in mother liquor supplemented with 30% (v/v) glycerol prior to being frozen in liquid nitrogen. The diffraction qualities of all of the crystals were assessed using the I24 microfocus beamline at Diamond Light Source (Oxfordshire, UK). This indicated that the crystals formed under Clear Strategy condition G6 were likely to be salt. However, the single crystal grown under JCSG+ condition A5 diffracted to 3.5 Å and the two crystals grown under PACT condition D10 both diffracted to 3 Å allowing a complete dataset to be collected.

Unfortunately, the diffraction of the PACT D10 crystals weakened markedly with prolonged exposure to the X-ray beam even though 20% transmission was used for data collection. This resulted in the collection of a dataset that was only 60% complete. However, analysis of this dataset has established that the FemB structure could be solved by molecular replacement using the major globular domain of FemA (Benson *et al.*, 2002) as a search model in the first instance (Professor Vilmos Fulop, personal communication). Given the medium resolution and incomplete nature of this initial dataset it was decided to await further data collection experiments before proceeding. A 24-well screen to refine this condition has also resulted in the growth of larger FemB crystals which have not yet been tested on an X-ray beamline. An image of these refined crystals is shown in Figure 6.15.

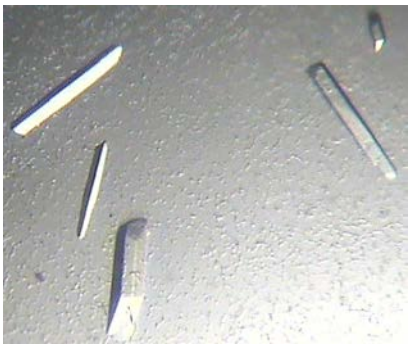

Figure 6.15: Image showing refinement of the FemB crystals grown under PACT screen condition D10. Improvements in crystal growth were obtained by increasing the protein to mother liquor ratio from 1:1 to 2:1. The maximum length of the crystals shown in this image was approximately 600 µm.

In order to optimise diffraction of the crystals shown in Figure 6.15, several different cryo-protectants should be trialled alongside the usual supplementation of mother liquor with 30% glycerol. Future work should also involve 24-well refinement of JCSG+ screen condition A5 with the ultimate aim of producing the best crystals for generation of the highest possible resolution structure of FemB.

6.6. Repetition of the crystal structure of *Staphylococcus aureus* FemA originally solved by Benson *et al*. (2002): structural identification of metal ion binding and the residues involved in this process

The structure of the FemA protein from *S. aureus* was originally solved to 2.1 Å by Benson *et al.* (2002) and no bound metal ions were visible in the electron density map generated by this study. However, biochemical evidence presented in Chapter 4 has proven that this enzyme binds both zinc and magnesium. Circular dichroism has suggested that the binding of these metal ions by FemA is essential for maintenance of the native structure of the enzyme. In addition to this, work carried out on MurM

in Chapter 4 has also led to the hypothesis that zinc may be important for the catalytic activity of FemA. Therefore, gaining an X-ray crystal structure of FemA with zinc and magnesium easily distinguishable in the electron density map is considered to be important both for confirmation of the residues involved in this process and for future drug-design against this enzyme and other members of the Fem ligase family.

In order to repeat crystallisation of FemA, the dodeca-histidine tagged version of the protein was purified as described in Chapter 4 and dialysed against 50 mM ethanolamine pH 10.0, 100 mM NaCl and 20% glycerol as described by Benson *et al.* (2002). The protein was concentrated to 12 mg mL^{-1} and used in a 24-well vapour diffusion based hanging drop crystallisation setup with the mother liquor composition kept the same as that reported to generate diffraction quality crystals by Benson *et al*. (2002). Unfortunately, despite the use of mother liquor of identical composition to that used previously (0.1 M Imidazole pH 8.0, 0.2 M calcium acetate and 10% (v/v) PEG 8 K) no crystals of FemA were seen after incubation of the tray at 18^{o}C for two weeks. Therefore, the stock protein solution was used to set up the six 96-well screens listed for MurM in an attempt to find similar conditions supporting crystal nucleation and growth. After incubation for 1 week at 18^{o}C, suitable crystals were found in the PACT screen under condition D11 (0.1 M Tris pH 8.0, 0.2 M calcium chloride and 20% PEG 6 K). An image of these crystals is shown in Figure 6.16.

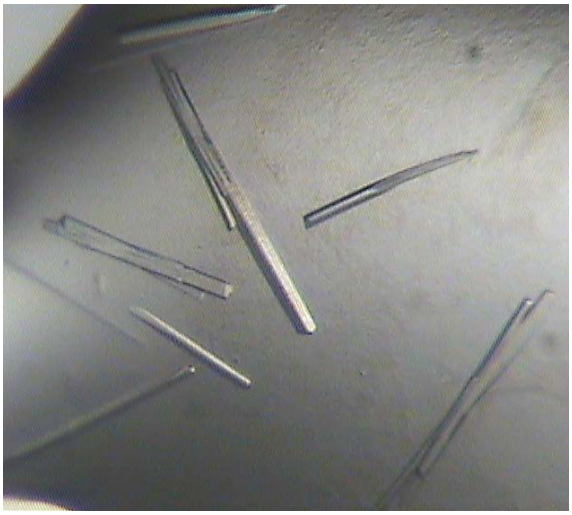

Figure 6.16: Image of FemA crystals formed under PACT condition D10 after dialysis of the protein against 50 mM ethanolamine, 100 mM NaCl and 20% glycerol and concentration to 12 mg mL^{-1}. Maximum length of crystals obtained under this condition was 1000 µm.

In the case of the crystals shown in Figure 6.16, cryo-protection using low viscosity oil (MiTeGen) allowed for collection of a dataset that could be resolved to 1.5 Å. In addition, each crystal was subjected to a fluorescence scan so that three sets of data could be collected at the zinc edge. Upon fluorescence scanning of each crystal, a peak specific for zinc was found. This allowed for collection of the high resolution dataset at a wavelength of 1.28 nm using the energies specific for the peak and inflection given by this metal ion (9674.00 eV, 9664.00 eV and 9824.00 eV). However, despite the high resolution of the structure obtained, it was not possible to locate zinc in the electron density map. Given that a peak was observed for this metal ion upon fluorescence scanning, there is clear evidence for the presence of zinc in the crystals. However, incomplete occupancy of the binding site may account for the lack of a defined zinc atom in the electron density map. Repetition of this experiment

is required and may be better achieved by dialysis of the protein against EDTA followed by incubation with a molar excess of zinc prior to crystallisation.

6.7. Discussion

The emergence of multidrug-resistant strains of bacteria has resulted in a requirement for the identification of novel antibiotic targets. Given that peptidoglycan is unique to prokaryotic cells, it is still an ideal target for antibiotic design and there is an increasing amount of interest in targeting the enzymes involved in the cytoplasmic and lipid linked stages of peptidoglycan biosynthesis.

Members of the Fem ligase family are responsible for the addition of amino acid cross bridges to cell wall precursors that subsequently results in indirect cross-linkage of peptidoglycan. At the present time, these enzymes are under-explored as targets for novel antibiotic design even though their inhibition has the potential to restore the activity of many clinically approved antibiotics including penicillin. There are only two structures of members of the Fem ligase family deposited in the protein data bank; *S. aureus* FemA and *W. viridescens* FemX, hindering rational structure-based drug design against these proteins (Benson *et al.*, 2002; Biarrotte-Sorin *et al.*, 2004).

One of the main hurdles in obtaining a high resolution crystal structure of the *S. pneumoniae* MurM protein has been maintaining the stability of the protein at concentrations greater than 3 mg mL^{-1}. The work of Benson *et al*. (2002) indicated that the stability of FemA at 10 mg mL^{-1} could be maintained by supplementation of the buffer the protein was presented to crystallisation screens in with 100 mM NaCl

and 20% glycerol. This methodology was applied with success for the first time to MurM in this study, allowing the protein to be concentrated to 10 mg mL^{-1} without any visible signs of precipitation or aggregation. In addition, concentration of MurM to 20 mg mL^{-1} was found to be possible if the buffer system contained at least 50 mM ethanolamine and the pH was kept at 10.0.

Despite exhaustive efforts, it was not possible to grow diffracting crystals of apo-MurM within the time frame of this study. In order to see whether this is attributable to a disorder in lattice formation or damage caused during crystal freezing, future work will require an extensive test of various different cryo-protectants with MurM crystals. In addition to this, examination of the ability of MurM crystals to diffract at room temperature would enable determination of whether poor diffraction is due to disorder within the lattice as opposed to problems encountered during the freezing process.

Rational surface mutagenesis of MurM across residues comprising more than one predicted cluster at the same time may also cause a significant reduction in surface entropy that allows for better formation of the crystal lattice. However, in the absence of this being successful, obtaining a structure of MurM might only be achieved by co-crystallisation of the enzyme with either one or both of its substrates. Co-crystallisation of *S. aureus* FemX with cardiolipin in this study was shown to cause progression from quasi-crystals to micro-crystals. Therefore, co-crystallisation of $MurM_{Pn16}$ with cardiolipin may result in the formation of diffraction quality crystals, especially given that the catalytic efficiency of the enzyme is increased by 36-fold in the presence of this phospholipid (see Chapter 5).

If enough material can be gathered, future work should also involve co-crystallisation of MurM with the stable aminoacylated 2'-amino mini-helix $tRNA^{Ala}$ species. This tRNA species was shown to be a potent inhibitor of MurM in the work carried out in Chapter 5. It is likely that the demonstrated inhibitory effect was a result of the stable amino-linkage between the tRNA and the amino acid which prevented transfer of alanine from the tRNA to Lipid II by MurM. Co-crystallisation with this tRNA species may cause MurM to adopt a more compact structure that ultimately results in better crystal lattice formation. Preliminary work has indicated that co-crystallisation of MurM with this inhibitory tRNA species results in the formation of single diamond-shaped crystals as opposed to the small clusters obtained with the apo-enzyme. However, further screening and refinement is required to optimise the quality of the crystals produced.

In the case of FemB, data collection on the refined crystals produced during this study may enable a high resolution crystal structure of this enzyme to be solved by molecular replacement with the published structure available for FemA (Benson *et al.*, 2002). Acquisition of this structure will be beneficial for future drug design. In addition to this, given that diffraction quality crystals of FemB can be readily produced, it will be possible to soak potential inhibitory compounds into the lattice structure in the future to gain additional information about the catalytic mechanism of this enzyme.

Identification of the metal ion binding sites within MurM and FemA would be aided by the acquisition of high resolution crystal structures where zinc and magnesium are

easily distinguishable in the electron density map. Future work to achieve this should involve dialysis of FemA against EDTA to remove bound metal ions and incubation with a molar excess of both zinc and magnesium prior to crystallisation. This should ensure that the metal ion binding sites within each molecule of FemA contain the correct metal ion rather than other metal ions that could potentially be picked up during the purification process.

Chapter 7

Final discussion and conclusions

Objectives of the project

The main objective of this project was to investigate the relationship between levels and types of amino acids used in indirect cross-linking within pneumococcal peptidoglycan across penicillin-resistant and penicillin-sensitive strains. In addition, the secondary aim of this work was to determine how differences between amino acid preference and the proportion of indirect cross-linkages in the cell wall relate to the structure and function of allelic variants of the MurM protein from these strains.

With the global increase in the prevalence of multidrug-resistant strains of bacteria, the need for the development of novel antibiotics and the identification of new antimicrobial targets is becoming much more urgent. Peptidoglycan is a key structural component of the bacterial cell wall providing protection against turgor pressure and osmotic stress. Since this structure is unique to bacteria, it is still a valuable target for the development of novel antibiotics. Currently the cytoplasmic and lipid-linked stages of peptidoglycan biosynthesis remain under-exploited (Gautam *et al.*, 2010).

In *S. pneumoniae*, the peptidoglycan structure comprises a combination of branched and linear muropeptides (Filipe *et al.*, 2000). The synthesis of branched muropeptides is catalysed by two aminoacyl-ligases called MurM and MurN. Selective inactivation of the genes encoding these ligases has indicated that the

protein products act within a specific sequence (Filipe *et al.*, 2000). MurM adds either L-alanine or L-serine to the stem peptide lysine of the pentapeptide side chain. MurN than invariably adds alanine as the second amino acid of the cross bridge. Even though selective inactivation of *murM* causes a reversion to penicillin sensitivity in strains that were previously resistant, the relationship between activity of MurM and penicillin resistance is complicated. It is also known that, in the absence of low affinity forms of penicillin-binding proteins, MurM activity is not sufficient to confer high level penicillin resistance (Filipe *et al.*, 2002).

Prior to this finding, Garcia-Bustos and Tomasz (1990) had investigated the link between the proportion of branched muropeptides in the pneumococcal cell wall and penicillin sensitivity. In these studies, the proportion of branched muropeptides across four penicillin-sensitive strains of *S. pneumoniae* was found to range from 16% to 27%. This contrasted with the proportion of branched muropeptides found across four penicillin-resistant strains of *S. pneumoniae* which ranged from 73% to 86%. In the same study, the proportion of branched muropeptides in strain R6 was found to be 60% despite being classed as penicillin-sensitive. Therefore, in order to further understand the relationship between penicillin resistance and MurM activity, the MurM protein from *S. pneumoniae* strain R6 was cloned, over-expressed and purified for biochemical characterisation in this study.

Kinetic characterisation of hexa-histidine tagged versions of $MurM_{Pn16}$ and $MurM_{159}$ had already been undertaken by Lloyd *et al.* (2008) prior to development of a means of producing a high yield of a single species of *S. pneumoniae* $tRNA^{Ala}$ and $tRNA^{Ser}$ in this study. However, structural work undertaken during this PhD project on

$MurM_{Pn16}$ had indicated that these proteins are zinc-dependent metallo-enzymes and, in order to test this dependence, it was necessary to re-clone all three variants of MurM such that the histidine tag could be removed from the protein after it had served its purpose in purification.

It was considered important to investigate the metal ion requirements of MurM due to findings made by Fiser *et al.* (2003) upon bioinformatics-based predictive modelling of the structure of MurM on the X-ray crystal structure of FemA. Distance matrix alignment, combinatorial extension and comparison of the predicted model of MurM to other proteins in the protein data bank suggests that the coiled-helical arm comprising domain II is similar to tRNA recognition domains in tRNA synthetase enzymes. This finding was reinforced by the identification of structural similarities between the coiled-helical arm of FemA and seryl-tRNA synthetase when the structure of the former was solved to 2.1 Å by X-ray crystallography (Benson *et al.*, 2002).

It is well documented in the literature that many tRNA synthetase enzymes require divalent metal ions for catalysis, maintenance of structure or a combination of the two. *E. coli* AlaRS requires zinc in order to recognise its cognate tRNA species and removal of this metal ion from the enzyme causes a loss in the secondary structure as has been seen in this study with MurM (Sood *et al.*, 1999). However, despite the similarity in structure between Fem Ligases and some tRNA synthetases, the dependence of the former on divalent metal ions has not been investigated before now.

Preliminary assessment of the requirement of MurM for divalent metal ions was made by dialysis of the protein against EDTA. EDTA is a strong metal ion chelating agent which binds zinc and magnesium with dissociation constants of approximately 10^{-16} M and 10^{-9} M, respectively (Nyborg and Peersen, 2004). Removal of metal ions from MurM caused inactivation of the protein and was also demonstrated to result in a 50% reduction in alpha helical content as determined by circular dichroism. Restoration of total activity required incubation of the protein with a molar equivalent of both zinc and magnesium. Whilst zinc alone could restore approximately 80% of total activity, magnesium alone could not.

The metal ion binding potential of MurM was characterised further by isothermal titration calorimetry (ITC). ITC data indicated that MurM had one binding site for magnesium with a K_d of 0.89 ± 0.06 µM. Zinc ion binding was found to be much more complex due to interaction of this metal ion with the magnesium ion binding site. Presentation of zinc to MurM after saturation of the protein with magnesium generated data indicative of the protein having one high affinity binding site for zinc with a K_d of 0.50 ± 0.04 µM (or 1 nM when the two site model was applied). Magnesium and zinc ion binding were shown to be a feature of two other members of the Fem ligase family, *S. aureus* FemX and FemA, in addition to MurM. This has demonstrated for the first time that divalent metal ions are involved in the catalytic mechanism of this family of enzymes which has far reaching implications for future drug design. In *S. pneumoniae*, peptidoglycan deacetylase has also been reported to require zinc for catalytic activity (Blair *et al.*, 2005).

In order to identify potential amino acid residues involved in metal ion binding within MurM, the predicted model of the enzyme was loaded on to the CHED server for prediction of transition metal ion binding sites within proteins (Babor *et al.*, 2008). This bioinformatics-based analysis identified one potential metal ion binding site in MurM comprising E229, E307 and D230. Both glutamate residues were found to be functionally conserved as either aspartate or glutamate across all sequenced variants of MurM and were, therefore, subjected to site directed mutagenesis in $MurM_{159}$.

When the X-ray crystal structure of FemA was loaded onto the CHED server, two amino acid clusters were identified supporting ITC results that were indicative of the presence of two metal ion binding sites. Double mutation of E229 and E307 in $MurM_{159}$ to alanine was shown to result in the abolition of an ITC signal for magnesium ion binding. This is a direct result of a significant decrease in the binding affinity of this mutant form of $MurM_{159}$ for magnesium. Complete abolition of magnesium ion binding to $MurM_{159}$ E229A:E307A cannot be confirmed due to the detection limits of ITC, however it is a possibility.

Whilst $MurM_{159}$ E229A:E307A was found to have an equal catalytic efficiency (k_{cat}/K_m) to the wild-type enzyme with respect to Lipid II, it could not be stimulated by cardiolipin. Given that the overall cardiolipin-induced improvement to apparent k_{cat}/K_m with wild-type $MurM_{159}$ was only 2-fold, it was considered necessary to investigate the effect of mutation at these two residues in $MurM_{Pn16,}$ where the cardiolipin-induced increase in k_{cat}/K_m with the wild-type enzyme was much more significant (37-fold). Unfortunately, the double mutant of $MurM_{Pn16}$ was found to be

inactive preventing further analysis of the involvement of magnesium in interaction of the enzyme with phospholipids. Thus, the conclusion drawn from this work is that magnesium ion binding to MurM is not essential for catalytic activity but is involved in the regulation of the activity of the enzyme by phospholipids. It is also possible that the MurM enzymes from penicillin-resistant strains of *S. pneumoniae* have evolved to become less responsive to phospholipids in order to achieve high levels of overall activity and indirect cell-wall cross-linkage. However, in order to confirm this hypothesis, the MurM enzymes from other penicillin-resistance strains of *S. pneumoniae* must be characterised in the same way as $MurM_{159}$. Magnesium-aided protein interaction with a lipid bilayer has already been reported for methanol dehydrogenase (Carver *et al.*, 1984).

The most pronounced finding from this study was a direct result of investigation into the substrate specificity of MurM by exploitation of the ability of AlaRS to mis-aminoacylate $tRNA^{Ala}$ with serine (Guo *et al.*, 2009). Generation of lethal amounts of mis-aminoacylated Ser-$tRNA^{Ala}$, which would disrupt the fidelity of protein synthesis, are usually prevented by a combination of the activity of the editing domain of AlaRS and free-standing genome-encoded homologues of the AlaRS editing domain called AlaXps proteins (Sokabe *et al.*, 2005). However, no homologues of AlaXps proteins have been identified in the genome of *S. pneumoniae.*

It is possible that genes encoding AlaXps proteins may have been lost from the *S. pneumoniae* genome during gene shuffling which occurs rapidly within the organism as a result of exposure to antibiotics (Croucher *et al.*, 2011). This loss would be

feasible in the presence of another conserved protein within the organism that is able to perform the same function. The ability of full-length *S. pneumoniae* AlaRS to generate and release mis-aminoacylated Ser-tRNA^{Ala} has been demonstrated in this study. In addition, the catalytic efficiencies of all three MurM enzymes were found to be much greater (at least 32-fold for MurM$_{159}$ and 60-fold for MurM$_{Pn16/R6}$) when mis-aminoacylated Ser-tRNA^{Ala} was presented as a substrate instead of Ala-tRNA^{Ala} and Ser-tRNA^{Ser}. This is the first evidence for the involvement of a member of the Fem ligase family in the maintenance of the fidelity of protein synthesis and provides an explanation for conservation of the functionality of MurM across all strains of *S. pneumoniae*.

The work undertaken in this study has also led to the hypothesis that the generation of Ser-tRNA^{Ala} and Ser-tRNA^{Thr} by AlaRS and ThrRS, respectively is promoted by hydrogen peroxide production during aerobic growth of *S. pneumoniae*. This is based on the work by Ling and Söll (2010) who demonstrated that the editing ability of *E. coli* ThrRS was severely hampered in the presence of hydrogen peroxide. In addition, it has been shown by Pesakhov *et al.* (2007) that expression of cardiolipin in the pneumococcal cell membrane is up-regulated during aerobic growth as a result of an increase in hydrogen peroxide concentration.

Unpublished data from Dr Adrian Lloyd (University of Warwick) and data acquired during this study have demonstrated that MurM activity is stimulated by cardiolipin. This effect was found to be more pronounced in the MurM proteins from penicillin-sensitive strains Pn16 and R6 compared to MurM from the penicillin-resistant strain 159. Hence it is likely that the up-regulation of cardiolipin expression during

exposure to hydrogen peroxide further stimulates MurM to utilise mis-aminoacylated Ser-tRNA^{Ala} and, potentially Ser-tRNA^{Thr}, to prevent the fidelity of protein synthesis from becoming compromised. However, further work is required to fully prove this hypothesis. If true, when combined with the confirmation obtained in this study that MurM accepts the amino acid from the 2' hydroxyl of the terminal adenine of its tRNA substrate, this knowledge could lead to the design of potent inhibitors of MurM enabling the success rate of current treatment regimens to be improved.

References

Adrian, P. V. and Klugman, K. P. (1997). Mutations in the dihydrofolate reductase gene of trimethoprim-resistant isolates of *Streptococcus pneumoniae*. *Antimicrob Agents Chemother* **41**: 2406-2413.

Allen, H. K., Donato, J., Wang, H. H., Cloud-Hansen, K. A., Davies, J. and Handelsman, J. (2010). Call of the wild: antibiotic resistance genes in natural environments. *Nat Rev Microbiol* **8**: 251-259.

Aravind, L., de Souza, R. F. and Iyer, L. M. (2010). Predicted class-I aminoacyl tRNA synthetase-like proteins in non-ribosomal peptide synthesis. *Biol Direct* **5**: 48.

Arnez, J. G. and Moras, D. (1997). Structural and functional considerations of the aminoacylation reaction. *Trends Biochem Sci* **22**: 211-216.

Austrian, R. (1981). Pneumococcus: the first one hundred years. *Rev Infect Dis* **3**: 183-189.

Avery, O. T., Macleod, C. M. and McCarty, M. (1944). Studies on the Chemical Nature of the Substance Inducing Transformation of Pneumococcal Types : Induction of Transformation by a Desoxyribonucleic Acid Fraction Isolated from Pneumococcus Type iii. *J Exp Med* **79**: 137-158.

Babor, M., Gerzon, S., Raveh, B., Sobolev, V. and Edelman, M. (2008). Prediction of transition metal binding sites from apo protein structures. *Proteins* **70**: 208-217.

Badet-Denisot, M. A., Fernandez-Herrero, L. A., Berenguer, J., Ooi, T. and Badet, B. (1997). Characterization of L-glutamine:D-fructose-6-phosphate amidotransferase from an extreme thermophile *Thermus thermophilus* HB8. *Arch Biochem Biophys* **337**: 129-136.

Badet, B., Vermoote, P., Haumont, P. Y., Lederer, F. and LeGoffic, F. (1987). Glucosamine synthetase from *Escherichia coli*: purification, properties, and glutamine-utilizing site location. *Biochemistry* **26**: 1940-1948.

Barreteau, H., Kovac, A., Boniface, A., Sova, M., Gobec, S. and Blanot, D. (2008). Cytoplasmic steps of peptidoglycan biosynthesis. *FEMS Microbiol Rev* **32**: 168-207.

Bellais, S., Arthur, M., Dubost, L., Hugonnet, J. E., Gutmann, L., van Heijenoort, J., Legrand, R., Brouard, J. P., Rice, L. and Mainardi, J. L. (2006). Asl_{fm}, the D-aspartate ligase responsible for the addition of D-aspartic acid onto the peptidoglycan precursor of *Enterococcus faecium*. *J Biol Chem* **281**: 11586-11594.

Benson, T.E., Walsh, C.T. and Hogle, J.M. (1997). X-ray crystal structures of the S229A mutant and wild-type MurB in the presence of the substrate enolpyruvyl-UDP-N-acetylglucosamine at 1.8-Å resolution. *Biochemistry* **36**: 806–811.

Benson, T. E., Prince, D. B., Mutchler, V. T., Curry, K. A., Ho, A. M., Sarver, R. W., Hagadorn, J. C., Choi, G. H. and Garlick, R. L. (2002). X-ray crystal structure of *Staphylococcus aureus* FemA. *Structure* **10**: 1107-1115.

Bertrand, J.A., Auger, G., Martin, L., Fanchon, E., Blanot, D., Le Beller, D., van Heijenoort, J. and Dideberg, O. (1999). Determination of the MurD mechanism through crystallographic analysis of enzyme complexes. *J Mol Biol* **289**: 579–590.

Beuning, P.J. and Musier-Forsyth, K. (1999). Transfer RNA recognition by aminoacyl-tRNA synthetases. *Biopolymers* **52**: 1-28.

Biarrotte-Sorin, S., Maillard, A. P., Delettre, J., Sougakoff, W., Arthur, M. and Mayer, C. (2004). Crystal structures of *Weissella viridescens* FemX and its complex with UDP-MurNAc-pentapeptide: insights into FemABX family substrates recognition. *Structure* **12**: 257-267.

Bilokapic, S., Maier, T., Ahel, D., Gruic-Sovulj, I., Söll, D., Weygand-Durasevic, I. and Ban, N. (2006). Structure of the unusual seryl-tRNA synthetase reveals a distinct zinc-dependent mode of substrate recognition. *EMBO J* **25**: 2498-2509.

Blair, D. E., Schuttelkopf, A. W., MacRae, J. I. and van Aalten, D. M. (2005). Structure and metal-dependent mechanism of peptidoglycan deacetylase, a streptococcal virulence factor. *Proc Natl Acad Sci U S A* **102**: 15429-15434.

Blencowe, D. K. and Morby, A. P. (2003). Zn(II) metabolism in prokaryotes. *FEMS Microbiol Rev* **27**: 291-311.

Blewett, A.M. (2005). The substrate specificity of peptidoglycan biosynthesis enzymes from *Streptococcus pneumoniae*. PhD Thesis, University of Warwick.

Bouhss, A., Josseaume, N., Severin, A., Tabei, K., Hugonnet, J. E., Shlaes, D., Mengin-Lecreulx, D., Van Heijenoort, J. and Arthur, M. (2002). Synthesis of the L-alanyl-L-alanine cross-bridge of *Enterococcus faecalis* peptidoglycan. *J Biol Chem* **277**: 45935-45941.

Bouhss, A., Mengin-Lecreulx, D., Blanot, D., van Heijenoort, J. and Parquet, C. (1997). Invariant amino acids in the Mur peptide synthetases of bacterial peptidoglycan synthesis and their modification by site-directed mutagenesis in the UDP-MurNAc:L-alanine ligase from *Escherichia coli*. *Biochemistry* **36**: 11556-11563.

Bouhss, A., Mengin-Lecreulx, D., Le Beller, D. and Van Heijenoort, J. (1999). Topological analysis of the MraY protein catalysing the first membrane step of peptidoglycan synthesis. *Mol Microbiol* **34**: 576-585.

Bouhss, A., Trunkfield, A. E., Bugg, T. D. and Mengin-Lecreulx, D. (2008). The biosynthesis of peptidoglycan lipid-linked intermediates. *FEMS Microbiol Rev* **32**: 208-233.

Brissette, J. L. and Pieringer, R. A. (1985). The effect of penicillin on fatty acid synthesis and excretion in *Streptococcus mutans* BHT. *Lipids* **20**: 173-179.

Brissette, J. L., Shockman, G. D. and Pieringer, R. A. (1982). Effects of penicillin on synthesis and excretion of lipid and lipoteichoic acid from *Streptococcus mutans* BHT. *J Bacteriol* **151**: 838-844.

Bugg, T. D. (1999). Bacterial peptidoglycan biosynthesis and its inhibition. In *Comprehensive Natural Products Chemistry*, Vol 3, pp. 241-294. Edited by M. Pinto. Oxford, United kingdom: Elsevier Science Ltd.

Bupp, K. and van Heijenoort, J. (1993). The final step of peptidoglycan subunit assembly in *Escherichia coli* occurs in the cytoplasm. *J Bacteriol* **175**: 1841-1843.

Buynak, J. D. (2007). Cutting and stitching: the cross-linking of peptidoglycan in the assembly of the bacterial cell wall. *ACS Chem Biol* **2**: 602-605.

Cabacungan, E. and Pieringer, R. A. (1980). Excretion of extracellular lipids by *Streptococcus mutans* BHT and FA-1. *Infect Immun* **27**: 556-562.

Cabeen, M. T. and Jacobs-Wagner, C. (2005). Bacterial cell shape. *Nat Rev Microbiol* **3**: 601-610.

Cafini, F., del Campo, R., Alou, L., Sevillano, D., Morosini, M. I., Baquero, F. and Prieto, J. (2006). Alterations of the penicillin-binding proteins and murM alleles of clinical *Streptococcus pneumoniae* isolates with high-level resistance to amoxicillin in Spain. *J Antimicrob Chemother* **57**: 224-229.

Caillet, J., Graffe, M., Eyermann, F., Romby, P. and Springer, M. (2007). Mutations in residues involved in zinc binding in the catalytic site of *Escherichia coli* threonyl-tRNA synthetase confer a dominant lethal phenotype. *J Bacteriol* **189**: 6839-6848.

Carrio, M.M. and Villaverde, A. (2001). Protein aggregation as bacterial inclusion bodies is reversible. *FEBS Lett* **489**: 29-33.

Carver, M. A., Humphrey, K. M., Patchett, R. A. and Jones, C. W. (1984). The effect of EDTA and related chelating agents on the oxidation of methanol by the methylotrophic bacterium, *Methylophilus methylotrophus*. *Eur J Biochem* **138**: 611-615.

Charpentier, E. and Tuomanen, E. (2000). Mechanisms of antibiotic resistance and tolerance in *Streptococcus pneumoniae*. *Microbes Infect* **2**: 1855-1864.

Chayen, N.E. (1998). Comparative studies of protein crystallisation by vapour-diffusion and microbatch techniques. *Acta Crystallogr D Biol Crystallogr* **54**: 8-15.

Chayen, N. E., Helliwell, J. R. and Snell, E. H. (2010). *Macromolecular Crystallization and Crystal Perfection*. Oxford, United Kingdom: Oxford University Press.

Chesnel, L., Carapito, R., Croize, J., Dideberg, O., Vernet, T. and Zapun, A. (2005). Identical penicillin-binding domains in penicillin-binding proteins of *Streptococcus pneumoniae* clinical isolates with different levels of beta-lactam resistance. *Antimicrob Agents Chemother* **49**: 2895-2902.

Chong, Y. E., Yang, X. L. and Schimmel, P. (2008). Natural homolog of tRNA synthetase editing domain rescues conditional lethality caused by mistranslation. *J Biol Chem* **283**: 30073-30078.

Cressina, E., Lloyd, A. J., De Pascale, G., James Mok, B., Caddick, S., Roper, D. I., Dowson, C. G. and Bugg, T. D. (2009). Inhibition of tRNA-dependent ligase MurM from *Streptococcus pneumoniae* by phosphonate and sulfonamide inhibitors. *Bioorg Med Chem* **17**: 3443-3455.

Cressina, E., Lloyd, A. J., De Pascale, G., Roper, D. I., Dowson, C. G. and Bugg, T. D. (2007). Adenosine phosphonate inhibitors of Lipid II: alanyl tRNA ligase MurM from *Streptococcus pneumoniae*. *Bioorg Med Chem Lett* **17**: 4654-4656.

Croucher, N. J., Harris, S. R., Fraser, C., Quail, M. A., Burton, J., van der Linden, M., McGee, L., von Gottberg, A., Song, J. H., Ko, K. S., Pichon, B., Baker, S., Parry, C. M., Lambertsen, L. M., Shahinas, D., Pillai, D. R., Mitchell, T. J., Dougan, G., Tomasz, A., Klugman, K. P., Parkhill, J., Hanage, W. P. and Bentley, S. D. (2011). Rapid pneumococcal evolution in response to clinical interventions. *Science* **331**: 430-434.

Czepas, J., Devedjiev, Y., Krowarsch, D., Derewenda, U., Otlewski, J. and Derewenda, Z. S. (2004). The impact of Lys-->Arg surface mutations on the crystallization of the globular domain of RhoGDI. *Acta Crystallogr D Biol Crystallogr* **60**: 275-280.

Dale, G. E., Oefner, C. and D'Arcy, A. (2003). The protein as a variable in protein crystallization. *J Structural Biology* **142**: 88-97.

Dantley, K. A., Dannelly, H. K. and Burdett, V. (1998). Binding interaction between Tet(M) and the ribosome: requirements for binding. *J Bacteriol* **180**: 4089-4092.

Davies, J. and Davies, D. (2010). Origins and evolution of antibiotic resistance. *Microbiol Mol Biol Rev* **74**: 417-433.

de la Campa, A. G., Garcia, E., Fenoll, A. and Munoz, R. (1997). Molecular bases of three characteristic phenotypes of pneumococcus: optochin-sensitivity, coumarin-sensitivity, and quinolone-resistance. *Microb Drug Resist* **3**: 177-193.

De Lencastre, H., Wu, S. W., Pinho, M. G., Ludovice, A. M., Filipe, S., Gardete, S., Sobral, R., Gill, S., Chung, M. and Tomasz, A. (1999). Antibiotic resistance as a stress response: complete sequencing of a large number of chromosomal loci in *Staphylococcus aureus* strain COL that impact on the expression of resistance to methicillin. *Microb Drug Resist* **5**: 163-175.

De Pascale, G. (2007). Molecular studies on tRNA dependent ligase MurN from penicillin-resistant *S. pneumoniae*. PhD Thesis, University of Warwick.

De Pascale, G., Lloyd, A. J., Schouten, J. A., Gilbey, A. M., Roper, D. I., Dowson, C. G. and Bugg, T. D. (2008). Kinetic characterization of Lipid II-Ala:alanyl-tRNA ligase (MurN) from *Streptococcus pneumoniae* using semisynthetic aminoacyl-Lipid II substrates. *J Biol Chem* **283**: 34571-34579.

del Campo, R., Cafini, F., Morosini, M. I., Fenoll, A., Linares, J., Alou, L., Sevillano, D., Canton, R., Prieto, J. and Baquero, F. (2006). Combinations of PBPs and MurM protein variants in early and contemporary high-level penicillin-resistant *Streptococcus pneumoniae* isolates in Spain. *J Antimicrob Chemother* **57**: 983-986.

Derewenda, Z. S. (2004). Rational protein crystallization by mutational surface engineering. *Structure* **12**: 529-535.

Derewenda, Z. S. and Vekilov, P. G. (2005). Entropy and surface engineering in protein crystallization. *Acta Crystallogr D Biol Crystallogr* **62**: 116-124.

Dessen, A., Mouz, N., Gordon, E., Hopkins, J. and Dideberg, O. (2001). Crystal structure of PBP2x from a highly penicillin-resistant *Streptococcus pneumoniae* clinical isolate: a mosaic framework containing 83 mutations. *J Biol Chem* **276**: 45106-45112.

Deva, T., Baker, E.N., Squire, C.J. and Smith, C.A. (2006). Structure of *Escherichia coli* UDP-N-acetylmuramoyl: L-alanine ligase (MurC). *Acta Crystallogr D Biol Crystallogr* **62**: 1466-1474.

Dramsi, S., Magnet, S., Davison, S. and Arthur, M. (2008). Covalent attachment of proteins to peptidoglycan. *FEMS Microbiol Rev* **32**: 307-320.

Ehlert, K., Tschierske, M., Mori, C., Schroder, W. and Berger-Bachi, B. (2000). Site-specific serine incorporation by Lif and Epr into positions 3 and 5 of the Staphylococcal peptidoglycan interpeptide bridge. *J Bacteriol* **182**: 2635-2638.

El Zoeiby, A., Sanschagrin, F. and Levesque, R. C. (2003). Structure and function of the Mur enzymes: development of novel inhibitors. *Mol Microbiol* **47**: 1-12.

Ernst, C. M. and Peschel, A. (2011). Broad-spectrum antimicrobial peptide resistance by MprF-mediated aminoacylation and flipping of phospholipids. *Mol Microbiol* **80**: 290-299.

Eschenburg, S., Priestman, M. and Schonbrunn, E. (2005). Evidence that the fosfomycin target Cys115 in UDP-N-acetylglucosamine enolpyruvyl transferase (MurA) is essential for product release. *J Biol Chem* **280**: 3757-3763.

Feng, Y., Li, M., Zhang, H., Zheng, B., Han, H., Wang, C., Yan, J., Tang, J. and Gao, G. F. (2008). Functional definition and global regulation of Zur, a zinc uptake regulator in a *Streptococcus suis* serotype 2 strain causing streptococcal toxic shock syndrome. *J Bacteriol* **190**: 7567-7578.

Fersht, A. R. (1977). Editing mechanisms in protein synthesis. Rejection of valine by the isoleucyl-tRNA synthetase. *Biochemistry* **16**: 1025-1030.

Filipe, S. R., Pinho, M. G. and Tomasz, A. (2000). Characterization of the murMN operon involved in the synthesis of branched peptidoglycan peptides in *Streptococcus pneumoniae*. *J Biol Chem* **275**: 27768-27774.

Filipe, S. R., Severina, E. and Tomasz, A. (2001a). Functional analysis of *Streptococcus pneumoniae* MurM reveals the region responsible for its specificity in the synthesis of branched cell wall peptides. *J Biol Chem* **276**: 39618-39628.

Filipe, S. R., Severina, E. and Tomasz, A. (2001b). The role of murMN operon in penicillin resistance and antibiotic tolerance of *Streptococcus pneumoniae*. *Microb Drug Resist* **7**: 303-316.

Filipe, S. R., Severina, E. and Tomasz, A. (2002). The murMN operon: a functional link between antibiotic resistance and antibiotic tolerance in *Streptococcus pneumoniae*. *Proc Natl Acad Sci USA* **99**: 1550-1555.

Filipe, S. R. and Tomasz, A. (2000). Inhibition of the expression of penicillin resistance in *Streptococcus pneumoniae* by inactivation of cell wall muropeptide branching genes. *Proc Natl Acad Sci USA* **97**: 4891-4896.

Finney, L. A. and O'Halloran, T. V. (2003). Transition metal speciation in the cell: insights from the chemistry of metal ion receptors. *Science* **300**: 931-936.

Fiser, A., Filipe, S. R. and Tomasz, A. (2003). Cell wall branches, penicillin resistance and the secrets of the MurM protein. *Trends Microbiol* **11**: 547-553.

Fonvielle, M., Chemama, M., Lecerf, M., Villet, R., Busca, P., Bouhss, A., Etheve-Quelquejeu, M. and Arthur, M. (2010). Decoding the logic of the tRNA regiospecificity of nonribosomal FemX(Wv) aminoacyl transferase. *Angew Chem Int Ed Engl* **49**: 5115-5119.

Fonvielle, M., Chemama, M., Villet, R., Lecerf, M., Bouhss, A., Valery, J. M., Etheve-Quelquejeu, M. and Arthur, M. (2009). Aminoacyl-tRNA recognition by the FemXWv transferase for bacterial cell wall synthesis. *Nucleic Acids Res* **37**: 1589-1601.

Francklyn, C. S. and Minajigi, A. (2010). tRNA as an active chemical scaffold for diverse chemical transformations. *FEBS Lett* **584**: 366-375.

Fraser, T.H., and Rich, A. (1973). Synthesis and aminoacylation of 3'-amino-3'-deoxy transfer RNA and its activity in ribosomal protein synthesis. *Proc Natl Acad Sci USA* **70**: 2671-2675.

Garcia-Bustos, J. and Tomasz, A. (1990). A biological price of antibiotic resistance: major changes in the peptidoglycan structure of penicillin-resistant pneumococci. *Proc Natl Acad Sci USA* **87**: 5415-5419.

Garcia-Bustos, J. F., Chait, B. T. and Tomasz, A. (1987). Structure of the peptide network of pneumococcal peptidoglycan. *J Biol Chem* **262**: 15400-15405.

Garcia-Bustos, J. F., Chait, B. T. and Tomasz, A. (1988). Altered peptidoglycan structure in a pneumococcal transformant resistant to penicillin. *J Bacteriol* **170**: 2143-2147.

Garg, R. P., Qian, X. L., Alemany, L. B., Moran, S. and Parry, R. J. (2008). Investigations of valanimycin biosynthesis: elucidation of the role of seryl-tRNA. *Proc Natl Acad Sci USA* **105**: 6543-6547.

Garrett, R.H. and Grisham, C.M. (2005). Enzymes – kinetics and specificity. In *Biochemistry*, 3rd edn, pp. 405-441. Edited by S. Kiselica and P. Williams. Belmont, USA: Thomson Brooks/Cole Press.

Gautam, A., Vyas, R. and Tewari, R. (2010). Peptidoglycan biosynthesis machinery: A rich source of drug targets. *Crit Rev Biotechnol* in press.

Giannouli, S., Kyritsis, A., Malissovas, N., Becker, H. D. and Stathopoulos, C. (2009). On the role of an unusual tRNAGly isoacceptor in *Staphylococcus aureus*. *Biochimie* **91**: 344-351.

Goldschmidt, L., Cooper, D. R., Derewenda, Z. S. and Eisenberg, D. (2007). Toward rational protein crystallization: A Web server for the design of crystallizable protein variants. *Protein science* **16**: 1569-1576.

Gordon, E., Flouret, B., Chantalat, L., van Heijenoort, J., Mengin-Lecreulx, D. and Dideberg, O. (2001). Crystal structure of UDP-N-acetylmuramoyl-l-alanyl-d-glutamate: meso-diaminopimelate ligase from *Escherichia coli*. *J Biol Chem* **276**: 10999–11006.

Grant, S. G., Jessee, J., Bloom, F. R. and Hanahan, D. (1990). Differential plasmid rescue from transgenic mouse DNAs into *Escherichia coli* methylation-restriction mutants. *Proc Natl Acad Sci USA* **87**: 4645-4649.

Grebe, T. and Hakenbeck, R. (1996). Penicillin-binding proteins 2b and 2x of *Streptococcus pneumoniae* are primary resistance determinants for different classes of beta-lactam antibiotics. *Antimicrob Agents Chemother* **40**: 829-834.

Guillerez, J., Lopez, P.J., Proux, F., Launay, H. and Dreyfus, M. (2005). A mutation in T7 RNA polymerase that facilitates promoter clearance. *Proc Natl Acad Sci USA* **102**: 5958-5963.

Guo, M., Chong, Y. E., Shapiro, R., Beebe, K., Yang, X. L. and Schimmel, P. (2009). Paradox of mistranslation of serine for alanine caused by AlaRS recognition dilemma. *Nature* **462**: 808-812.

Hakenbeck, R., Grebe, T., Zahner, D. and Stock, J. B. (1999). Beta-lactam resistance in *Streptococcus pneumoniae*: penicillin-binding proteins and non-penicillin-binding proteins. *Mol Microbiol* **33**: 673-678.

Hanahan, D. (1985). Techniques for transformation of *Escherichia coli*. In *DNA cloning: A practical approach*, 1st edn, pp. 109-135. Edited by D.M. Glover. Oxford, United Kingdom: IRL Press.

Healy, V. L., Lessard, I. A., Roper, D. I., Knox, J. R. and Walsh, C. T. (2000). Vancomycin resistance in enterococci: reprogramming of the D-ala-D-Ala ligases in bacterial peptidoglycan biosynthesis. *Chem Biol* **7**: 109-119.

Hegde, S. S. and Blanchard, J. S. (2003). Kinetic and mechanistic characterization of recombinant *Lactobacillus viridescens* FemX (UDP-N-acetylmuramoyl pentapeptide-lysine N6-alanyltransferase). *J Biol Chem* **278**: 22861-22867.

Hegde, S. S. and Shrader, T. E. (2001). FemABX family members are novel nonribosomal peptidyltransferases and important pathogen-specific drug targets. *J Biol Chem* **276**: 6998-7003.

Heydanek, M. G., Jr., Struve, W. G. and Neuhaus, F. C. (1969). On the initial stage in peptidoglycan synthesis. 3. Kinetics and uncoupling of phospho-N-acetylmuramyl-pentapeptide translocase (uridine 5'-phosphate). *Biochemistry* **8**: 1214-1221.

Hitchings, G. H. (1973). Mechanism of action of trimethoprim-sulfamethoxazole. I. *J Infect Dis* **128 (Suppl)**: 433-436.

Holt, R., Evans, T. N. and Newman, R. L. (1969). Tetracycline-resistant pneumococci. *Lancet* **2**: 545.

Hong, H. J., Hutchings, M. I., Hill, L. M. and Buttner, M. J. (2005). The role of the novel Fem protein VanK in vancomycin resistance in *Streptomyces coelicolor*. *J Biol Chem* **280**: 13055-13061.

Horne, D., Hakenbeck, R. and Tomasz, A. (1977). Secretion of lipids induced by inhibition of peptidoglycan synthesis in streptococci. *J Bacteriol* **132**: 704-717.

Hoskins, J., Alborn, W. E., Jr., Arnold, J., Blaszczak, L. C., Burgett, S., DeHoff, B. S., Estrem, S. T., Fritz, L., Fu, D. J., Fuller, W., Geringer, C., Gilmour, R., Glass, J. S., Khoja, H., Kraft, A. R., Lagace, R. E., LeBlanc, D. J., Lee, L. N., Lefkowitz, E. J., Lu, J., Matsushima, P., McAhren, S. M., McHenney, M., McLeaster, K., Mundy, C. W., Nicas, T. I., Norris, F. H., O'Gara, M., Peery, R. B., Robertson, G. T., Rockey, P., Sun, P. M., Winkler, M. E., Yang, Y., Young-Bellido, M., Zhao, G., Zook, C. A., Baltz, R. H., Jaskunas, S. R., Rosteck, P. R., Jr., Skatrud, P. L. and Glass, J. I. (2001). Genome of the bacterium *Streptococcus pneumoniae* strain R6. *J Bacteriol* **183**: 5709-5717.

Huang, H. W. and Cowan, J. A. (1994). Metallobiochemistry of the magnesium ion. Characterization of the essential metal-binding site in *Escherichia coli* ribonuclease H. *Eur J Biochem* **219**: 253-260.

Janoir, C., Zeller, V., Kitzis, M. D., Moreau, N. J. and Gutmann, L. (1996). High-level fluoroquinolone resistance in *Streptococcus pneumoniae* requires mutations in *parC* and *gyrA*. *Antimicrob Agents Chemother* **40**: 2760-2764.

Jasin, M., Regan, L. and Schimmel, P. (1983). Modular arrangement of functional domains along the sequence of an aminoacyl-tRNA synthetase. *Nature* **306**: 441-447.

Jedrzejas, M. J. (2001). Pneumococcal virulence factors: structure and function. *Microbiol Mol Biol Rev* **65**: 187-207.

Kamiryo, T. and Matsuhashi, M. (1972). The biosynthesis of the cross-linking peptides in the cell wall peptidoglycan of *Staphylococcus aureus*. *J Biol Chem* **247**: 6306-6311.

Kelly, S. M., Jess, T. J. and Price, N. C. (2005). How to study proteins by circular dichroism. *Biochim Biophys Acta* **1751**: 119-139.

Lanie, J. A., Ng, W. L., Kazmierczak, K. M., Andrzejewski, T. M., Davidsen, T. M., Wayne, K. J., Tettelin, H., Glass, J. I. and Winkler, M. E. (2007). Genome sequence of Avery's virulent serotype 2 strain D39 of *Streptococcus pneumoniae* and comparison with that of unencapsulated laboratory strain R6. *J Bacteriol* **189**: 38-51.

Leahy, D. J., Hendrickson, W. A., Aukhil, I. and Erickson, H. P. (1992). Structure of a fibronectin type III domain from tenascin phased by MAD analysis of the selenomethionyl protein. *Science* **258**: 987-991.

Lees, J. G., Miles, A. J., Janes, R. W. and Wallace, B. A. (2006a). Novel methods for secondary structure determination using low wavelength (VUV) circular dichroism spectroscopic data. *BMC Bioinformatics* **7**: 507-517.

Lees, J. G., Miles, A. J., Wien, F. and Wallace, B. A. (2006b). A reference database for circular dichroism spectroscopy covering fold and secondary structure space. *BMC Bioinformatics* **22**: 1955-1962.

Li, L. and Ismagilov, R. F. (2010). Protein crystallization using microfluidic technologies based on valves, droplets, and SlipChip. *Annu Rev Biophys* **39**: 139-158.

Ling, B. and Berger-Bachi, B. (1998). Increased overall antibiotic susceptibility in *Staphylococcus aureus* femAB null mutants. *Antimicrob Agents Chemother* **42**: 936-938.

Ling, J. and Söll, D. (2010). Severe oxidative stress induces protein mistranslation through impairment of an aminoacyl-tRNA synthetase editing site. *Proc Natl Acad Sci USA* **107**: 4028-4033.

Liu, J., Lin, S. X., Blochet, J. E., Pezolet, M. and Lapointe, J. (1993). The glutamyl-tRNA synthetase of *Escherichia coli* contains one atom of zinc essential for its native conformation and its catalytic activity. *Biochemistry* **32**: 11390-11396.

Lloyd, A. J., Gilbey, A. M., Blewett, A. M., De Pascale, G., El Zoeiby, A., Levesque, R. C., Catherwood, A. C., Tomasz, A., Bugg, T. D., Roper, D. I. and Dowson, C. G. (2008). Characterization of tRNA-dependent peptide bond formation by MurM in the synthesis of *Streptococcus pneumoniae* peptidoglycan. *J Biol Chem* **283**: 6402-6417.

Lloyd, A. J., Weitzman, P. D. and Soll, D. (1993). Incomplete citric acid cycle obliges aminolevulinic acid synthesis via the C5 pathway in a methylotroph. *Microbiology* **139**: 2931.

Lopez, P. J., Marchand, I., Joyce, S. A. and Dreyfus, M. (1999). The C-terminal half of RNase E, which organizes the *Escherichia coli* degradosome, participates in mRNA degradation but not rRNA processing *in vivo*. *Mol Microbiol* **33**: 188-199.

Lovering, A. L., de Castro, L. H., Lim, D. and Strynadka, N. C. (2007). Structural insight into the transglycosylation step of bacterial cell-wall biosynthesis. *Science* **315**: 1402-1405.

Macheboeuf, P., Contreras-Martel, C., Job, V., Dideberg, O. and Dessen, A. (2006). Penicillin-binding proteins: key players in bacterial cell cycle and drug resistance processes. *FEMS Microbiol Rev* **30**: 673-691.

Maillard, A. P., Biarrotte-Sorin, S., Villet, R., Mesnage, S., Bouhss, A., Sougakoff, W., Mayer, C. and Arthur, M. (2005). Structure-based site-directed mutagenesis of the UDP-MurNAc-pentapeptide-binding cavity of the FemX alanyl transferase from *Weissella viridescens*. *J Bacteriol* **187**: 3833-3838.

Manavathu, E. K., Fernandez, C. L., Cooperman, B. S. and Taylor, D. E. (1990). Molecular studies on the mechanism of tetracycline resistance mediated by Tet(O). *Antimicrob Agents Chemother* **34**: 71-77.

Maskell, J. P., Sefton, A. M. and Hall, L. M. (1997). Mechanism of sulfonamide resistance in clinical isolates of *Streptococcus pneumoniae*. *Antimicrob Agents Chemother* **41**: 2121-2126.

Mazmanian, S. K., Ton-That, H. and Schneewind, O. (2001). Sortase-catalysed anchoring of surface proteins to the cell wall of *Staphylococcus aureus*. *Mol Microbiol* **40**: 1049-1057.

McElroy, H., Sisson, G., Schoettlin, W., Aust, R. and Villafranca, J. (1992). Studies on engineering crystallizability by mutation of surface residues of human thymidylate synthase. *J Crystal Growth* **122**: 265-272.

Mellor, D. and Maley, L. (1948). Order of stability of metal complexes. *Nature* **161**: 436-437.

Miroux, B. and Walker, J. E. (1996). Over-production of proteins in *Escherichia coli*: mutant hosts that allow synthesis of some membrane proteins and globular proteins at high levels. *J Mol Biol* **260**: 289-298.

Mohammadi, T., van Dam, V., Sijbrandi, R., Vernet, T., Zapun, A., Bouhss, A., Diepeveen-de Bruin, M., Nguyen-Disteche, M., de Kruijff, B. and Breukink, E. (2011). Identification of FtsW as a transporter of lipid-linked cell wall precursors across the membrane. *EMBO J* **30**: 1425-1432.

Morar, M. and Wright, G. D. (2010). The genomic enzymology of antibiotic resistance. *Annu Rev Genet* **44**: 25-51.

Mordasini, T., Curioni, A. and Andreoni, W. (2003). Why do divalent metal ions either promote or inhibit enzymatic reactions? The case of *Bam*HI restriction endonuclease from combined quantum-classical simulations. *J Biol Chem* **278**: 4381-4384.

Naganuma, M., Sekine, S., Fukunaga, R. and Yokoyama, S. (2009). Unique protein architecture of alanyl-tRNA synthetase for aminoacylation, editing, and dimerization. *Proc Natl Acad Sci USA* **106**: 8489-8494.

Neuhoff, V., Arold, N., Taube, D. and Ehrhardt, W. (1988). Improved staining of proteins in polyacrylamide gels including isoelectric focusing gels with clear background at nanogram sensitivity using Coomassie Brilliant Blue G-250 and R-250. *Electrophoresis* **9**: 255-262.

Nyborg, J. K. and Peersen, O. B. (2004). That zincing feeling: the effects of EDTA on the behaviour of zinc-binding transcriptional regulators. *Biochem J* **381**: e3-4.

Parisi, A. F. and Vallee, B. L. (1969). Zinc metalloenzymes: characteristics and significance in biology and medicine. *Am J Clin Nutr* **22**: 1222-1239.

Payne, D. J. (2008). Microbiology. Desperately seeking new antibiotics. *Science* **321**: 1644-1645.

Pesakhov, S., Benisty, R., Sikron, N., Cohen, Z., Gomelsky, P., Khozin-Goldberg, I., Dagan, R. and Porat, N. (2007). Effect of hydrogen peroxide production and the Fenton reaction on membrane composition of *Streptococcus pneumoniae*. *Biochim Biophys Acta* **1768**: 590-597.

Ray, S. S., Bonanno, J. B., Chen, H., de Lencastre, H., Wu, S., Tomasz, A. and Burley, S. K. (2003). X-ray structure of an *M. jannaschii* DNA-binding protein: implications for antibiotic resistance in *S. aureus*. *Proteins* **50**: 170-173.

Reese, C.B. and Trentham, D.R. (1965). Acyl migration in ribonucleoside derivatives. *Tetrahedron Lett*: 2467-2472.

Ribeiro, S., Nock, S. and Sprinzl, M. (1995). Purification of aminoacyl-tRNA by affinity chromatography on immobilized *Thermus thermophilus* EF-Tu.GTP. *Anal Biochem* **228**: 330-335.

Rohrer, S. and Berger-Bachi, B. (2003a). Application of a bacterial two-hybrid system for the analysis of protein-protein interactions between FemABX family proteins. *Microbiology* **149**: 2733-2738.

Rohrer, S. and Berger-Bachi, B. (2003b). FemABX peptidyl transferases: a link between branched-chain cell wall peptide formation and beta-lactam resistance in gram-positive cocci. *Antimicrob Agents Chemother* **47**: 837-846.

Rohrer, S., Ehlert, K., Tschierske, M., Labischinski, H. and Berger-Bachi, B. (1999). The essential *Staphylococcus aureus* gene fmhB is involved in the first step of peptidoglycan pentaglycine interpeptide formation. *Proc Natl Acad Sci USA* **96**: 9351-9356.

Rupp, B. (2010). *Biomolecular crystallography: Principles, practice, and application to structural biology*, 1st edn. Edited by S. Scholl and A. Engels. New York, USA: Garland Science, Taylor & Francis Group.

Sampson, J. R. and Uhlenbeck, O. C. (1988). Biochemical and physical characterization of an unmodified yeast phenylalanine transfer RNA transcribed *in vitro*. *Proc Natl Acad Sci USA* **85**: 1033-1037.

Sangeetha, K., Morris, V. B. and Emilia Abraham, T. (2008). Stability and catalytic properties of encapsulated subtilisin in xerogels of alkoxisilanes. *Applied Catalysis A: General* **341**: 168-173.

Sankaranarayanan, R., Dock-Bregeon, A. C., Rees, B., Bovee, M., Caillet, J., Romby, P., Francklyn, C. S. and Moras, D. (2000). Zinc ion mediated amino acid discrimination by threonyl-tRNA synthetase. *Nat Struct Biol* **7**: 461-465.

Sarkar, B. (1995). Metal replacement in DNA-binding zinc finger proteins and its relevance to mutagenicity and carcinogenicity through free radical generation. *Nutrition* **11**: 646-649.

Sauguet, L., Moutiez, M., Li, Y., Belin, P., Seguin, J., Le Du, M. H., Thai, R., Masson, C., Fonvielle, M., Pernodet, J. L., Charbonnier, J. B. and Gondry, M. (2011). Cyclodipeptide synthases, a family of class-I aminoacyl-tRNA synthetase-like enzymes involved in non-ribosomal peptide synthesis. *Nucleic Acids Res* **39**: 4475-4489.

Sauvage, E., Kerff, F., Terrak, M., Ayala, J. A. and Charlier, P. (2008). The penicillin-binding proteins: structure and role in peptidoglycan biosynthesis. *FEMS Microbiol Rev* **32**: 234-258.

Schleifer, K. H. and Kandler, O. (1972). Peptidoglycan types of bacterial cell walls and their taxonomic implications. *Bacteriol Rev* **36**: 407-477.

Schneider, T., Senn, M. M., Berger-Bachi, B., Tossi, A., Sahl, H. G. and Wiedemann, I. (2004). *In vitro* assembly of a complete, pentaglycine interpeptide bridge containing cell wall precursor (Lipid II-Gly5) of *Staphylococcus aureus*. *Mol Microbiol* **53**: 675-685.

Skarzynski, Y., Mistry, A., Wonacott, A., Hutchinson, S.E., Kelly, V.A. and Duncan, K. (1996). Structure of UDP-N-acetylglucosamine enolpyruvyl transferase, an enzyme essential for the synthesis of bacterial peptidoglycan, complexed with substrate UDP-N-acetylglucosamine and the drug fosfomycin. *Structure* **4**: 1465–1474.

Smith, C. A. (2006). Structure, function and dynamics in the mur family of bacterial cell wall ligases. *J Mol Biol* **362**: 640-655.

Sokabe, M., Okada, A., Yao, M., Nakashima, T. and Tanaka, I. (2005). Molecular basis of alanine discrimination in editing site. *Proc Natl Acad Sci USA* **102**: 11669-11674.

Sood, S. M., Wu, M. X., Hill, K. A. and Slattery, C. W. (1999). Characterization of zinc-depleted alanyl-tRNA synthetase from *Escherichia coli*: role of zinc. *Arch Biochem Biophys* **368**: 380-384.

Soriano, F., Cafini, F., Aguilar, L., Tarrago, D., Alou, L., Gimenez, M. J., Gracia, M., Ponte, M. C., Leu, D., Pana, M., Letowska, I. and Fenoll, A. (2008). Breakthrough in penicillin resistance? *Streptococcus pneumoniae* isolates with penicillin/cefotaxime MICs of 16 mg/L and their genotypic and geographical relatedness. *J Antimicrob Chemother* **62**: 1234-1240.

Staudenbauer, W. and Strominger, J. L. (1972). Activation of D-aspartic acid for incorporation into peptidoglycan. *J Biol Chem* **247**: 5095-5102.

Staudenbauer, W., Willoughby, E. and Strominger, J. L. (1972). Further studies of the D-aspartic acid-activating enzyme of *Streptococcus faecalis* and its attachment to the membrane. *J Biol Chem* **247**: 5289-5296.

Stranden, A. M., Ehlert, K., Labischinski, H. and Berger-Bachi, B. (1997). Cell wall monoglycine cross-bridges and methicillin hypersusceptibility in a femAB null mutant of methicillin-resistant *Staphylococcus aureus*. *J Bacteriol* **179**: 9-16.

Studier, F. W. (2005). Protein production by auto-induction in high density shaking cultures. *Protein Expr Purif* **41**: 207-234.

Taiji, M., Yokoyama, S. and Miyazawa, T. (1983). Transacylation rates of (aminoacyl)adenosine moiety at the 3'-terminus of aminoacyl transfer ribonucleic acid. *Biochemistry* **22**: 3220-3225.

Tankovic, J., Perichon, B., Duval, J. and Courvalin, P. (1996). Contribution of mutations in *gyrA* and *parC* genes to fluoroquinolone resistance of mutants of *Streptococcus pneumoniae* obtained *in vivo* and *in vitro*. *Antimicrob Agents Chemother* **40**: 2505-2510.

Ton-That, H., Labischinski, H., Berger-Bachi, B. and Schneewind, O. (1998). Anchor structure of staphylococcal surface proteins. III. Role of the FemA, FemB, and FemX factors in anchoring surface proteins to the bacterial cell wall. *J Biol Chem* **273**: 29143-29149.

Trombe, M. C., Laneelle, M. A. and Laneelle, G. (1979). Lipid composition of aminopterin-resistant and sensitive strains of *Streptococcus pneumoniae*. Effect of aminopterin inhibition. *Biochim Biophys Acta* **574**: 290-300.

Tschierske, M., Mori, C., Rohrer, S., Ehlert, K., Shaw, K. J. and Berger-Bachi, B. (1999). Identification of three additional femAB-like open reading frames in *Staphylococcus aureus*. *FEMS Microbiol Lett* **171**: 97-102.

van Heijenoort, J. (2007). Lipid intermediates in the biosynthesis of bacterial peptidoglycan. *Microbiol Mol Biol Rev* **71**: 620-635.

Villet, R., Fonvielle, M., Busca, P., Chemama, M., Maillard, A. P., Hugonnet, J. E., Dubost, L., Marie, A., Josseaume, N., Mesnage, S., Mayer, C., Valery, J. M., Etheve-Quelquejeu, M. and Arthur, M. (2007). Idiosyncratic features in tRNAs participating in bacterial cell wall synthesis. *Nucleic Acids Res* **35**: 6870-6883.

Vollmer, W., Blanot, D. and de Pedro, M. A. (2008). Peptidoglycan structure and architecture. *FEMS Microbiol Rev* **32**: 149-167.

von Ehrenstein, G. (1967). Isolation of sRNA from intact *Escherichia coli* cells. *Methods Enzymol* **12**: 588-596.

Waldron, K. J. and Robinson, N. J. (2009). How do bacterial cells ensure that metalloproteins get the correct metal? *Nat Rev Microbiol* **7**: 25-35.

Waldron, K. J., Rutherford, J. C., Ford, D. and Robinson, N. J. (2009). Metalloproteins and metal sensing. *Nature* **460**: 823-830.

Weber, B., Ehlert, K., Diehl, A., Reichmann, P., Labischinski, H. and Hakenbeck, R. (2000). The *fib* locus in *Streptococcus pneumoniae* is required for peptidoglycan crosslinking and PBP-mediated beta-lactam resistance. *FEMS Microbiol Lett* **188**: 81-85.

Weinger, J. S., Parnell, K. M., Dorner, S., Green, R. and Strobel, S. A. (2004). Substrate-assisted catalysis of peptide bond formation by the ribosome. *Nat Struct Mol Biol* **11**: 1101-1106.

Whitmore, L. and Wallace, B. A. (2004). DICHROWEB, an online server for protein secondary structure analyses from circular dichroism spectroscopic data. *Nucleic Acids Res* **32**: W668-673.

Widdowson, C. A. and Klugman, K. P. (1999). Molecular mechanisms of resistance to commonly used non-Beta-lactam drugs in *Streptococcus pneumoniae*. *Semin Respir Infect* **14**: 255-268.

Yan, Y., Munchi, S., Leiting, B., Anderson, M.S., Chrzas, J. and Chen, Z. (2000). Crystal structure of *Escherichia coli* UDPMurNAc-tripeptide d-alanyl-d-alanine-adding enzyme (MurF) at 2.3 A resolution. *J Mol Biol* **304**: 435–445.

Zighelboim, S. and Tomasz, A. (1980). Penicillin-binding proteins of multiply antibiotic-resistant South African strains of *Streptococcus pneumoniae*. *Antimicrob Agents Chemother* **17**: 434-442.

Zubay, G. (1962). The isolation and fractionation of soluble ribonucleic acid. *J. Mol. Biol* **4**: 347-356.